Understanding the Molecular Factors Governing Inhibitor Potency and Oxygen Activation in Copper Amine Oxidases

by

Eric Michael Shepard

A dissertation submitted in partial fulfillment
of the requirements for the degree

of

Doctor of Philosophy

in

Biochemistry

MONTANA STATE UNIVERSITY
Bozeman, Montana

April 2006

APPROVAL

of a dissertation submitted by

Eric Michael Shepard

This dissertation has been read by each member of the dissertation committee and has been found to be satisfactory regarding content, English usage, format, citations, bibliographic style, and consistency, and is ready for submission to the Division of Graduate Education.

David M Dooley

Approved for the Department of Chemistry and Biochemistry

David J. Singel

Approved for the Division of Graduate Education

Joseph J. Fedock

STATEMENT OF PERMISSION TO USE

In presenting this dissertation in partial fulfillment of the requirements for a doctoral degree at Montana State University, I agree that the Library shall make it available to borrowers under rules of the Library. I further agree that copying of this dissertation is allowable only for scholarly purposes, consistent with "fair use" as prescribed in the U.S. Copyright Law. Requests for extensive copying or reproduction of this dissertation should be referred to ProQuest Information and Learning, 300 North Zeeb Road, Ann Arbor, Michigan 48106, to whom I have granted "the exclusive right to reproduce and distribute my dissertation in and from microform along with the non-exclusive right to reproduce and distribute my abstract in any format in whole or in part."

Eric M. Shepard

April 17th, 2006

ACKNOWLEDGEMENTS

I would like to thank my family for all of their love and support over the years. I wouldn't be where I am today if it weren't for them. This thesis is dedicated to the life of my best friend Trevor Jessie Seaman (1977 – 2005), and to the memory of his son Trent Jeremy Seaman (2005 – 2006).

TABLE OF CONTENTS

TABLE OF CONTENTS CONTINUED

TABLE OF CONTENTS CONTINUED

TABLE OF CONTENTS CONTINUED

LIST OF TABLES

Table Page

LIST OF FIGURES

LIST OF FIGURES CONTINUED

LIST OF FIGURES CONTINUED

LIST OF FIGURES CONTINUED

ABSTRACT

Copper amine oxidases (CuAOs) catalyze the oxidative deamination of primary amines to the corresponding aldehydes, with the concomitant reduction of O_2 to H_2O_2. CuAOs are known to have a multitude of physiological roles, and activity levels are upregulated in several pathological states. With the potential for therapeutic applications, substantial efforts were made to determine the molecular factors governing inhibitor selectivity. As such, several mechanism-based inhibitors were screened against CuAOs from bacterial, yeast, plant, and mammalian sources. The results provided vast insight into the molecular factors governing inhibitor potency in a bacterial (AGAO) and a plant (PSAO) CuAO. This was the defining work in establishing how certain aromatic residues in the substrate channel of AGAO directly control inhibitor potency. Furthermore, this work details the cross-reactivity between CuAOs and monoamine oxidase (MAO) enzymes using the antidepressant MAO-directed inhibitor tranylcypromine, and describes the characterization of a class of compounds which selectively inhibit only CuAOs. In addition to the studies aimed at understanding the molecular factors governing inhibitor binding in CuAOs, this work probes the role of copper during enzymatic reoxidation. Binding and inhibition studies of CuAOs were performed with the monodentate copper ligands cyanide and azide. Studies with cyanide provided the first spectroscopic evidence for cyanohydrin derivitization of TPQ in PSAO and led to the proposal of a detailed mechanism for inhibition of CuAO catalysis by cyanide. Azide studies in PSAO clearly revealed that azide was a competitive inhibitor towards substrate dioxygen, thereby supporting the viability of a redox role for copper. However, azide studies with a yeast CuAO were much more difficult to interpret, as azide was found to significantly inhibit the reaction velocity of both half-reactions. Lastly, temperature jump relaxation measurements of the internal redox equilibrium in AGAO were performed, allowing for the calculation of the electron transfer rate between reduced TPQ and copper(II). The results unequivocally establish that the copper(I)-semiquinone state is a viable catalytic intermediate in the reoxidation reaction of AGAO. Collectively, the results presented in this thesis provide evidence for a redox role of copper during the oxidative half-reaction, although further experimentation is necessary to confirm this.

INTRODUCTION

Amine oxidases catalyze the oxidative deamination of primary amines to the corresponding aldehydes, with the concomitant reduction of O_2 to H_2O_2. The two classes of amine oxidases present in mammals are the flavin-dependent monoamine oxidases (MAO enzymes; EC 1.4.3.4) and the quinone and copper-containing amine oxidases. MAO enzymes are exclusively found in the outer mitochondrial membrane of virtually all mammalian cell types and can oxidize primary, secondary, and tertiary amine compounds. MAOs act either through a single electron transfer mechanism or through a concerted covalent catalysis mechanism, both involving the FAD cofactor [1]. In contrast, quinone copper-containing amine oxidases principally oxidize primary amine compounds. Copper-containing amine oxidases are the first examples of enzymes in which a post-translationally modified amino acid side chain is present in the active site and plays a redox role in catalysis [2-5]. Copper-containing amine oxidases can currently be divided into two subclasses based on the type of cofactor present in the enzyme active site: 2,4,5–trihydroxyphenylalanine quinone (TPQ; E.C. 1.4.3.6) or lysyl tyrosylquinone (LTQ; E.C. 1.4.3.13). The work presented in this thesis will focus solely on the characterization of the TPQ-containing copper amine oxidases (CuAOs).

Post-Translationally Modified Amino Acid Cofactors

It is now widely recognized that some proteins contain chemical modification(s) of amino acid side-chains that may serve to diversify the biological functionality of these

residues. This process, referred to as post-translational amino acid modification, requires the alteration of an intrinsic, encoded amino acid residue. Typically, these modifications are required for catalytic activity and can either be self-processing events or may require the participation of chaperone proteins. Numerous enzymes including copper amine oxidases, galactose oxidase, lysyl oxidase, methylamine dehydrogenase, cytochrome oxidase, catechol oxidases, and nitrile hydratases are now known to contain such post-translationally modified amino acids in their active sites [6]. In many of these cases, the crosslinking of amino acid side chains generates redox active cofactors, such as in galactose oxidase (Y–C), lysyl oxidase (Y–K), amine dehydrogenase (W–W), and catechol oxidase (H–C) [6]. Cytochrome *c* oxidase contains a Y–H linkage, which could either function as a new type of cofactor [7], or simply have a structural role within the heme a_3-Cu_B site, given the fact that the crosslinked His residue is a Cu_B ligand [8]. Examination of the structural and functional consequences of such post-translational modifications is an area of intense current interest in protein biochemistry.

Among the family of post-translationally modified amino acid cofactors is a quinone subset, which are specifically derived from oxidation of either tyrosine or tryptophan residues. The identification of the TPQ cofactor in 1990 [9], thought to be the noncovalently associated cofactor pyrroloquinoline quinone (PQQ) for nearly 20 years, raised great interest, eventually resulting in the identification of a series of these quinone cofactors. Accordingly, four covalently attached amino acid derived quinone cofactors have now been identified (Figure 1): (1) TPQ of the copper amine oxidases; (2) LTQ found in copper lysyl oxidases; (3) tryptophan tryptophylquinone (TTQ) present in

bacterial methylamine dehydrogenase (MADH; EC 1.4.99.3); and (4) cysteine tryptophyl quinone (CTQ) of the bacterial quinohemoprotein amine dehydrogenase.

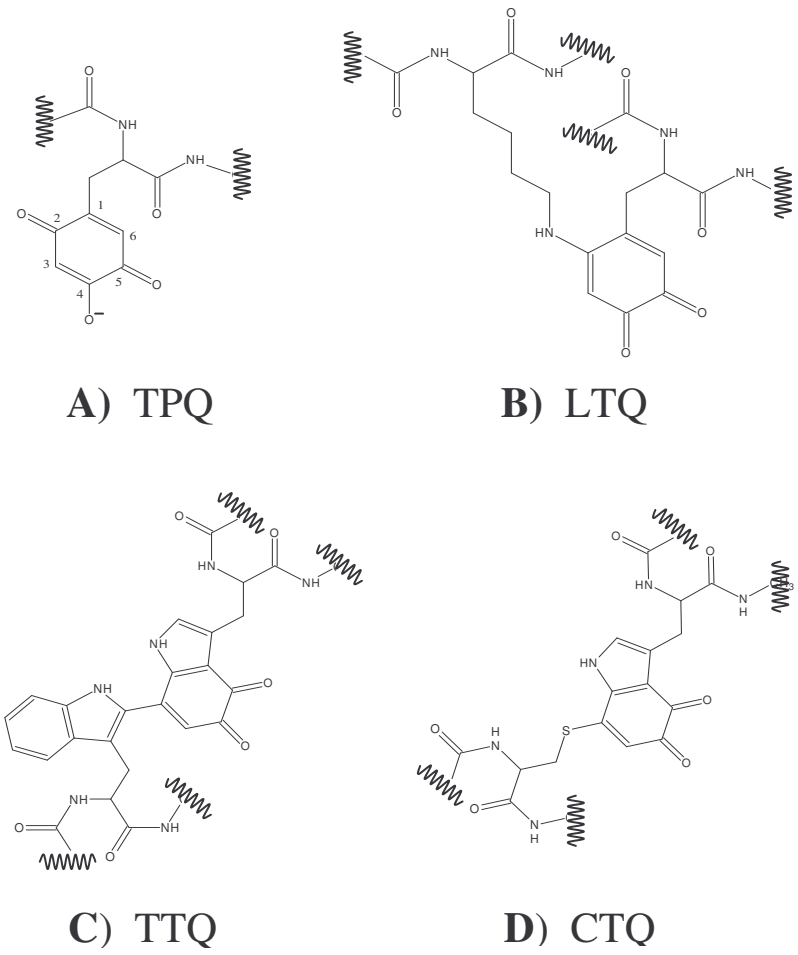

Figure 1: Tyrosine and tryptophan derived quinone cofactors. A) 2,4,5-trihydroxyphenylalanine quinone, TPQ; B) lysyl tyrosylquinone, LTQ; C) tryptophan tryptophylquinone, TTQ; D) cysteine tryptophyl quinone, CTQ.

The formation of TPQ and LTQ occurs through self processing events, requiring only apo-unprocessed enzyme, copper, and molecular oxygen [5,10-13]. For TTQ biogenesis to occur, the expression of the *mauDEF* and *G* gene products, and the α and β

subunit structural genes of MADH are needed [14]. Formation of the CTQ cofactor is less understood, as it is not known whether biogenesis is a self processing event or if chaperone proteins are needed [15].

Amine Oxidase Physiology

CuAOs have long been known to be widely distributed in nature and have been purified from mammals, plants, and microorganisms, including *Archea* [16-19]. Amine oxidases frequently have a nutritional role in the utilization of primary amines as the sole source of nitrogen or carbon in microorganisms [16,20]. The role of these enzymes in higher organisms is considerably more complex and diverse. CuAO substrate specificities depend on the enzyme source but nearly all biogenic primary amines can be substrates, e.g. histamine, cadaverine, putrescine, agmatine, tyramine, tryptamine, dopamine, serotonin, norepinephrine, mescaline, spermine, and spermidine. Due to the observation that the physiological function of many amine oxidases is the breakdown or transformation of biologically active amines, these enzymes likely act as regulators of physiological amine concentrations and may therefore participate in several biological processes. Along these lines, it is not surprising that CuAOs are widely distributed in mammalian tissues, e.g. brain, plasma, kidney, placenta, and throughout the cardiovascular and gastrointestinal systems, with expression levels varying dramatically, either as a function of disease states or pregnancy [21].

Biogenic amines are involved in a multitude of biological processes. For example, polyamines are implicated in the stimulation and control of cell proliferation, protein and

nucleic acid synthesis, growth, and development [22]. Polyamines may also be involved in enzyme regulation as their oxidation products are implicated as inhibitors of cell proliferation [23]. Polyamine and diamine oxidation and interconversion in the brain are involved in both normal functions and during injury in direct response to several kinds of deleterious stimuli [24,25]. Agmatine, a compound produced *in vivo* via the enzymatic decarboxylation of arginine, has been identified in mammalian plasma, brain, kidney, and liver tissues, and is now known to be an endogenous neuromodulator and/or neurotransmitter [26]. The ability of recombinant human diamine oxidase (rhDAO) to oxidize agmatine *in vitro* (B.O. Elmore and D.M. Dooley, unpublished results), coupled with the known expression of DAO in human kidney, liver, and certain regions of the brain, points to a possible role of *in vivo* agmatine metabolism by hDAO. Specifically, a model has recently been put forth for the interregulation of arginine pathways by arginine decarboxylase metabolites. In this model, agmatine coordinates between early and repair phase pathways during inflammation by gating the transition between the inducible nitric oxide synthase (iNOS)/NO and arginase/ornithine decarboxylase/polyamine pathways [27]. A key aspect of this proposal relates to the ability of agmatine to induce both antizyme and spermine/spermidine N-acyltransferase and to suppress iNOS through conversion of agmatine to γ-guanidinobutyraldehyde via DAO [27,28]. In addition to agmatine, diamine oxidase can also oxidize histamine. Histamine is a potent effector of the cardiovascular and gastrointestinal systems, and is directly involved in inflammatory, allergic, and ischemic phenomena [29,30]. Furthermore, histamine has been linked to anaphylaxis, ulcerative colitis, and Crohn's disease [31-33]. Histamine degradation occurs through the actions of diamine oxidase and histamine *N*-methyltransferase (E.C.2.1.1.8) [34,35]. The

observation that histamine and 1-methylhistamine are the preferred substrates for rhDAO strongly suggests that hDAO may play a central role in histamine metabolism [18]. In addition, the role of DAO may also include the alleviation of product inhibition of histamine *N*-methyltransferase. It is likely that diamine oxidase is the enzyme primarily responsible for controlling extracellular histamine levels *in vivo*, given that histamine *N*-methyltransferase is localized intracellularly [36-38].

In addition to diamine oxidase, semicarbazide-sensitive amine oxidases (SSAOs) have been detected or described in numerous mammalian tissues [39,40]. SSAOs have been implicated in the pharmacology and toxicology of biogenic and exogenous amines and their oxidation products. In addition to the biogenic amines listed previously, methylamine and aminoacetone are now recognized to be possible physiological substrates for SSAO. SSAO activity levels are upregulated in several pathological states, including diabetes mellitus, congestive heart failure, hepatic cirrhosis, uremia, and Alzheimer's disease [41-43]. The increased formation of potentially cytotoxic products of amine oxidation by SSAO may contribute to endothelial injury, resulting in the early development of severe atherosclerosis [43]. Furthermore, it has been speculated that SSAOs may participate in the regulation of physiological processes through generation of the well known signaling molecule H_2O_2 [41,44]. Along these lines, SSAO has been shown to stimulate glucose uptake in adipocytes, thought to be controlled by the generation of H_2O_2 during amine oxidation [42-45]. Lastly, human vascular adhesion protein (HVAP-1), which mediates L-selectin dependent lymphocyte adhesion to endothelial cells, has been recently identified as an SSAO [45-47]. In spite of these suggestions for numerous and diverse roles of this protein, a recent mouse knockout study concluded that in a pathogen

free environment, AOC3 (VAP-1) deficient animals showed no overt phenotypes, were completely healthy, and had no overt macroscopic or microscopic changes in any tissues or organs [48]. AOC3 was concluded to be unnecessary for normal development; VAP-1's role in immunity is the only function incapable of substitution by other protein(s).

Amine Oxidase Structure

Seven copper-containing amine oxidase structures have been solved to-date: *Arthrobacter globiformis* phenylethylamine oxidase (AGAO) [16], pea seedling amine oxidase (PSAO) [49], *Hansenula polymorpha* amine oxidase (HPAO) [50], *Escherichia coli* amine oxidase (ECAO) [51], *Pichia pastoris* "lysyl" oxidase (PPLO; Figure 2) [52], bovine plasma amine oxidase (BPAO) [53], and human vascular adhesion protein [54].

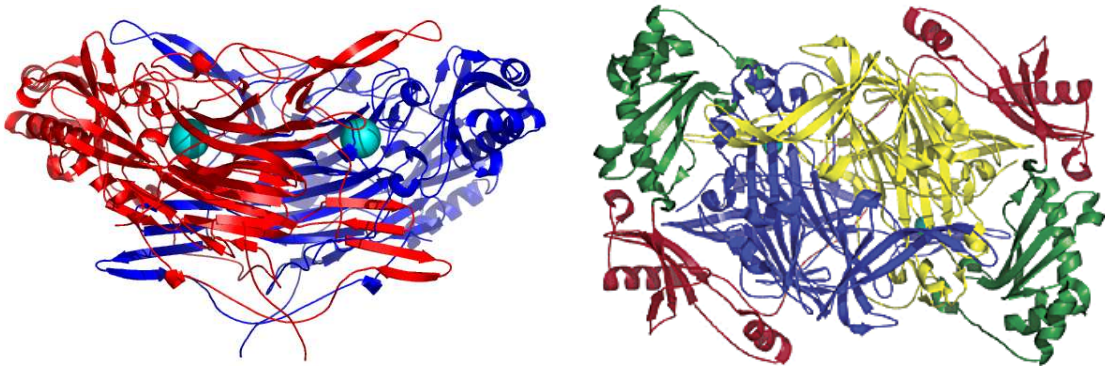

Figure 2: PPLO secondary structure rendition. The "front" view (left) shows each monomer (red and blue) and copper (cyan sphere). The "top" view (right) shows each domain: D2 (maroon), D3 (green), and D4 (yellow and blue).

Collectively, the native enzymes share considerable structural homology. All CuAOs are homodimeric and contain one active site per monomer. Each monomer is

composed of three or four domains with a large, C-terminal β-sandwich catalytic domain, designated as domain 4 (Figure 2) [16,51]. A β-ribbon from one monomer, comprising between two and four β-strands, extends to the active site channel in the opposite monomer to varying extents. Residues at the end of these strands form part of the active site channel entrance and vary considerably in size and polarity among amine oxidases (Figure 3) [50]. Of particular interest is the presence of one or two negatively charged residues at the end of the β-arm, e.g., E359 and E365 in PSAO. In PPLO, the second hairpin of the β-arm contains five such residues (D738, D739, E740, E742, and E743). The functional significance of these residues may be either recruitment of positively charged amines to the channel entrance (ECAO, PSAO, AGAO, HPAO) or stabilization of the second charged amino group of long-chained polyamines (BPAO, HVAP, PPLO). In addition, a second-metal binding site exists in CuAO structures, located ~ 33 Å from the copper site. These sites are believed to be occupied by Ca(II), Mg(II), Mn(II), or Zn(II) under physiological conditions. While some CuAOs contain two second-metal binding sites per monomer, only one of these sites is conserved. Its function(s) has largely remained elusive, although recent results with AGAO indicate that the site may play a role in either proper protein folding or dimer integrity. A point mutation of one of the second-metal site ligands in AGAO (D440A) results in expression of insoluble protein, as overexpression of this site-directed variant in an *E. coli* host showed recombinant AGAO to be located in inclusion bodies (K.M. Okonski, G.A. Juda, and D.M. Dooley, unpublished results).

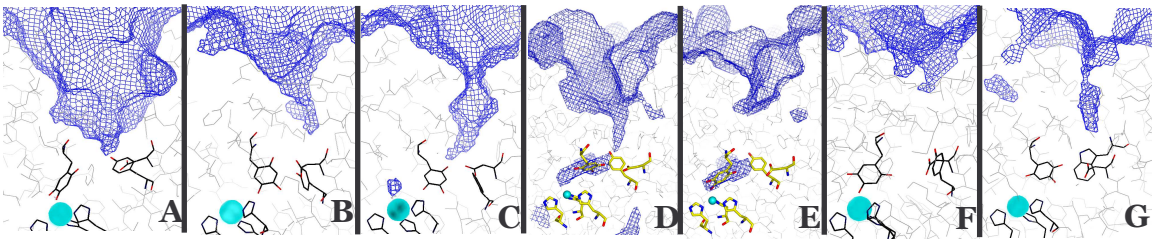

Figure 3: Solvent accessibility calculations (blue mesh) of CuAO crystal structures. (A) PPLO. (B) AGAO. (C) PSAO. (D) BPAO. (E) HVAP. (F) ECAO. (G) HPAO. These calculations were performed by Anthony Duff, University of Sydney, Australia, as described in [52].

Each CuAO active site is located ~10 – 12 Å from the protein surface (Figure 3) and contains a single Type II copper ion and the TPQ cofactor [55-57]. The Cu(II) ion is 5-coordinate (3 equatorial His ligands and 2 H_2O molecules, one equatorial, one axial) in distorted square pyramidal geometry (Figure 4A). TPQ is in close proximity to the Cu(II) ion and has been observed to exist in two states, differing by a ~180° rotation: "on"-copper (Figure 4C), and "off"-copper (Figure 4A) [58]. Only the productive conformation of TPQ can bind substrate amine.

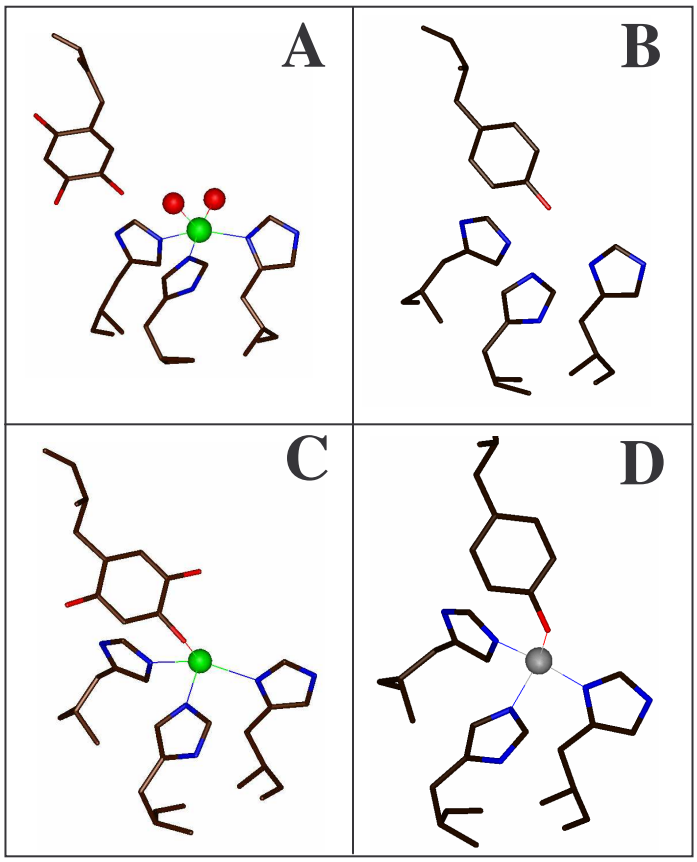

Figure 4: Active site representations of AGAO. (A) Productive AGAO. (B) Apo-AGAO. (C) Nonproductive AGAO. (D) Zinc-substituted HPAO. Panels A, B, C adapted from [16], panel D was taken from [59]. Red spheres represent H_2O molecules, while green and grey spheres correspond to Cu(II) and Zn(II), respectively.

Significant similarity exists among CuAOs in regards to both the Cu(II) environment and the overall protein topology. As mentioned previously, significant structural homology exists among the known CuAO structures and is expressed by the low root mean square difference (1.4 Å) between the 1178 Cα main chain atoms in PSAO and ECAO [49]. However, in spite of the close structural similarity in the tertiary folds of these enzymes [50], a sequence alignment of the catalytic domain from plant and bacterial sources showed sequence identity of less than 35% for all known sequences

[60]. Several sequence trends are, however, apparent. For instance, the plant enzymes share greater than 50% identity and the plasma and SSAO enzymes across species are quite similar, *e.g*. BPAO and human VAP-1 protein display 83% sequence identity [60]. Significant distinctions exist among mammalian CuAOs, whereby DAO sequences share roughly 45% identity with the plasma and SSAO enzymes [60,61]. A consequence of the overall low sequence identity among all CuAOs can be extended to variations in active site dimensions, TPQ accessibility, and in the presence or absence of amino acids which may or may not act as "gate" residues to the active site [50,58] (Figure 3). Variances in channel dimensions and TPQ accessibility are believed to be the governing factors in determining substrate and inhibitor specificity [62,63].

The presence of a large active site funnel confers relatively broad substrate specificity to both PPLO and BPAO (Figure 3A and 3D). However, differences in charge distribution and architecture lead to significant distinctions in substrate specificity. For example, K_M values for lysine, spermine, spermidine, and putrescine between these enzymes differ by two-to-three orders of magnitude, and unique variances in inhibitor recognition and potency have been observed (see Chapters 2 and 3) [20,62-64]. This may in part be explained by the presence of a "hydrophobic wall" in BPAO's channel formed by ten residues from domain 4, a feature not present in PPLO's active site channel. These intriguing structural variances can be extended to the pea seedling diamine oxidase, which preferentially oxidizes diamines of 4 – 7 carbon atoms (putrescine, cadaverine, etc.) and contains a very narrow channel leading to a buried active site (Figure 3C) [49,65]. The relative inaccessibility of the active sites of AGAO (Figure 3B), ECAO (Figure 3F), and HPAO (Figure 3G), may partly explain why these enzymes

preferentially oxidize smaller amines like β-phenylethylamine (AGAO and ECAO) and methylamine (HPAO), respectively.

TPQ Cofactor Biogenesis

The 2,4,5-trihydroxyphenylalanine quinone (TPQ) cofactor was identified in 1990 through mass spectral analysis in BPAO [9] and subsequently confirmed for a number of CuAOs through resonance Raman spectroscopy [66]. TPQ is currently known to be derived from a conserved tyrosine residue present in the consensus sequence T/S–X–X–N–Y(TPQ)–D/E–Y/N. The biogenesis process requires only apo-unprocessed enzyme, copper, and molecular oxygen [5,10-12]. TPQ generation in AGAO was shown to be a 6 electron oxidation process, consuming 2 moles of O_2 for every mole of H_2O_2 and mole of TPQ formed, and yielding the net stoichiometry of: $2\ O_2 + \text{E-Tyr} \rightarrow \text{E-TPQ} + H_2O_2$ [67]. Additionally, the rate of H_2O_2 production was shown to be approximately equal to the rate of TPQ formation.

In metal-free, unprocessed apo-AGAO, the precursor tyrosine (Y382) is poised to bind Cu(II) and serve as an axial ligand (Figure 3B) [16]. This hypothesis is further substantiated through two subsequent reports detailing the structures of both Zn(II)-substituted HPAO (Figure 3D) [59] and Co(II)-substituted AGAO [68], in which the precursor tyrosine is observed to ligate the respective metal centers. Collectively, these results corroborate the initial hypothesis put forth by Dooley and coworkers in 1997, whereby the precursor tyrosine is activated for biogenesis by binding to Cu(II) [12,16].

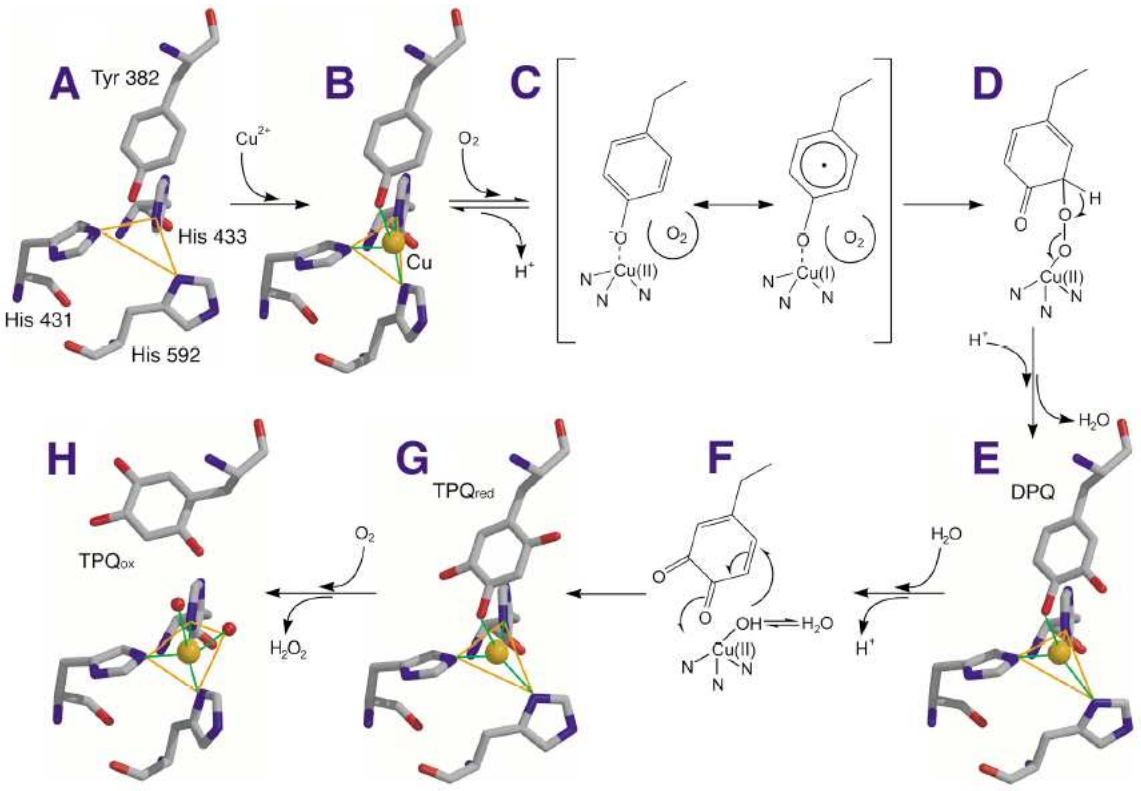

Figure 5: Proposed mechanism of TPQ biogenesis. Figure taken from [69]. Stages A, B, E, G, and H represent intermediates that were isolated in this time-resolved crystallographic study. The Cu(I)-tyrosyl radical (equilibrium at stage C) has never been observed in solution studies, indicating that this resonance form must be present at very low concentrations.

Definitive evidence for precursor tyrosine ligation to Cu(II) was experimentally observed in a recent study performed by Kim *et al*. (2002) through the characterization of freeze-trapped intermediates via X-ray crystallography in AGAO (Figure 5) [69]. The initial structure clearly shows the Y382/TPQ precursor–Cu(II) complex (Figure 5B). Of particular interest is the relatively long phenolic O···Cu(II) bond length of 2.5 Å, which is not expected to yield intense LMCT transitions. As such, this bond length suggests that the hydroxyl group of Y382 remains protonated. The observation that Y382 remains protonated is in agreement with prior biogenesis reports utilizing HPAO, which

concluded that deprotonation of the precursor tyrosine and formation of the LMCT complex are O_2 initiated events [70-73]. This previous work identified an O_2-dependent intermediate with λ_{max} = 350 nm, which decayed with the isosbestic formation of the 480 nm TPQ absorbance feature. The two possibilities for this intermediate were either a Cu(II)-tyrosinate species (Figure 5C, left species) or a Cu(II)-aryl-peroxide species (Figure 5D). Recent results ruled out the peroxide species giving rise to the 350 nm absorbance feature, as the rate of biogenesis was found to be identical when using ring-3,5-[$^2H_2$]-tyrosine substituted protein, indicating that there was no isotope effect on the rate of C3-H bond cleavage (Figure 5, D $\rightarrow$ E) [74]. Given the results from this latest work, it appears that the initial reaction between enzyme and O_2 occurs in a two-step process. Initially, the precursor tyrosine and O_2 form a "collision complex", which is linearly dependent upon the dissolved O_2 concentration. The "collision complex" then undergoes isomerization to form the 350 nm Cu(II)-tyrosinate complex [68,74]. This O_2-dependent process indicates that dioxygen binding promotes a conformational change in the active site that aids in the formation of this complex, although the detailed basis of this structural change is currently unknown. Two possible O_2 binding sites have been explored: either at the vacant equatorial site of the copper center [16] or at an off-metal site involving Met634, that is adjacent to the Tyr(TPQ) precursor [72]. A theoretical study has concluded that the O_2 binding energy to the equatorial copper position is more favorable by 11.7 kcal/mol [75].

Regardless of where O_2 actually binds, the event triggers activation of the phenol ring towards nucleophilic attack by O_2. Either full or partial charge-transfer from the tyrosinate to copper may occur, with the result being the activation of the carbon ring

atoms [16,76]. It is then believed that O_2 is reduced to $O_2^{\bullet-}$ through the facile reaction with Cu(I), thereby generating dopaquinone [16], although it should be stated that Cu(I) may not actually be the reactant species, simply given the presence of the Cu(I)-$Y^{\bullet}$ resonance form. One of the early freeze-trapped intermediate structures revealed 3,4-dihydroxyphenylalanine quinone, or dopaquinone (DPQ), coordinated to copper via the O4 atom (Figure 5E) [69]. The water/hydroxide species bound in the equatorial position (Figure 5E, 2.1 Å from copper) would be expected to readily exchange with solvent [16], thereby permitting solvent oxygen incorporation into TPQ, as consistent with resonance Raman results [77]. Following ~ 180° rotation and nucleophilic attack by copper-bound hydroxide at the C2 position, topa is generated. Indeed, the late intermediate structure (Figure 5G) reveals the cofactor to be 2,4,5-trihydroxyphenylalanine (reduced form of TPQ; TPQ_{red}). In the presence of O_2, TPQ_{red} is rapidly oxidized to TPQ, which then dissociates from Cu(II) [16]. The final stage structure clearly shows the oxidized cofactor in the productive conformation, with the copper center in five-coordinate distorted square-pyramidal geometry (Figure 5H).

Until very recently, Cu(II) has been the only metal believed to support TPQ biogenesis, as neither Mn(II), Co(II), Ni(II), Cd(II), Be(II), Mo(II), Mg(II), Ba(II), Ca(II), nor Zn(II) were found to promote biogenesis [11]. In a current, more thorough study, Okajima *et al*. retested these metals, as well as Ag(I), Cr(II), Fe(II), Hg(II), Pd(II), Rb(I), Sn(II), and Sr(II), for their ability to generate TPQ [68]. Only Co(II) and Ni(II) ions support formation of TPQ in AGAO, although at rates that were 1200-fold slower than with Cu(II) [68]. Metal-substitution studies were also recently performed in HPAO and only Ni(II) was discovered to support biogenesis at a rate 120-fold slower than Cu(II)

[78]. The drastically reduced k_{obs} rates for biogenesis with Co(II) and Ni(II) in AGAO most likely explain why these ions were not identified in the initial study as being able to support TPQ formation. Furthermore, the latest study discovered that out of all the metals listed above, only Cu(II), Co(II), Ni(II), and Zn(II) can tightly bind to the enzyme active site. These results raise some interesting issues in terms of the proposed biogenesis mechanism (Figure 5), as these four metals share different Lewis acid and redox properties.

When assessing Lewis acidity in terms of metal-coordinated water molecules, Cu(II) ion has a pK_a value two pH units lower (pK_a = 7.5) than that of Co(II) (pK_a = 9.6), Ni(II) (pK_a = 9.4), and Zn(II) (pK_a = 9.6) [68]. At neutral pH, Cu(II)-coordinated H_2O is 100-fold more dissociated than those of the other metals. This higher Lewis acidity of Cu(II) may be advantageous for the activation of the tyrosine precursor phenol ring (Figure 5C) and may therefore explain the rate enhancement observed with Cu(II). Another possibility comes from the ability of transition metals to promote O–O bond heterolysis of coordinated alkyl peroxides by enhancing the electrophilicity of the departing oxygen atom [78]. Thus, replacement of Cu(II) with metals that are weaker Lewis acids could be expected to have a detrimental effect on this metal-assisted cleavage step (Figure 5D). However, this alone does not explain the kinetic behavior observed with these metals, as Zn(II) fails to support biogenesis to any measurable extent. In terms of redox chemistry, if full electron transfer to Cu(II) indeed occurs (Figure 5C, right species), then the facile reaction of Cu(I) with O_2 would be expected to occur, with superoxide then readily reacting with $Tyr^{\bullet}$. This chemistry, however, is only feasible with Cu(II), as Zn(II) is not capable of redox chemistry, and the one-electron

reduction of Co(II) and Ni(II) is unlikely given the respective low reduction potential of these metals. It therefore seems that a much less efficient and completely different mechanism may be operative in the cases of Co(II) and Ni(II).

The mechanism recently put forth for Ni(II)-substituted HPAO provides further insight into this alternate chemistry [78]. Nickel was found to substantially affect the rate of the Michael addition step of the metal-bound hydroxide to DPQ (Figure 5F), in a manner which made this step partially rate-limiting. This effect was attributed to the depressed Lewis acidity of this metal. The principal rate-limiting step in Ni(II)-biogenesis was proposed to be the initial electron transfer event to O_2. Due to the low reduction potential of Ni(II) complexes with N/O ligands (~ -1.1 V) [78,79], it is highly unlikely that a Ni(I)-tyrosine radical species could be generated to react with O_2, or that this specis would be a significant resonance form. As such, the authors propose that the coordination of tyrosine to Ni(II) facilitates in the removal of an electron from the phenolate complex, which then is involved in the initial outer-sphere electron transfer to O_2. Due to the fact that the Ni(II)-tyrosinate complex would remain a poor one-electron reductant, this step would be expected to be largely rate-limiting [78].

Taken in a broad context, these results indicate that Zn(II) may be inert due to its closed shell properties. The observation that Co(II) does not support biogenesis in HPAO is an interesting distinction from AGAO and speaks volumes about the perplexing aspects of metal specificity in these enzymes (see Amine Oxidase Mechanism section). Of course, this result may simply reflect a difference in the thoroughness of the two recent studies, as AGAO is a much easier protein to purify in vast amounts in order to perform such detailed spectroscopic and kinetic analyses. Only further, more careful

experimentation will definitively show if Co(II) is indeed unable to support biogenesis in HPAO.

In addition to examining the effect of different metals on TPQ formation, several site-directed mutagenesis studies have been performed in an attempt to understand the role that certain consensus sequence (T/S–X–X–N–Y(TPQ)–D/E–Y/N) residues play during biogenesis. In AGAO, the variants N401D/Q, D403E/N, and Y404F were generated [80]. Changing Asn401 to either an aspartate or glutamine residue resulted in a 10^3-10^4 fold decrease in the rate of biogenesis, illustrating the requirement of this residue for rapid TPQ formation. Similarly, the D403N mutant produced a marked decrease in the biogenesis rate, whereas the D403E variant processed TPQ at rates comparable to wild-type enzyme. These latter results indicate that D403 is necessary to maintain the structural integrity of the active site during TPQ formation, most likely through hydrogen bonding. Mutation of Y404 to Phe showed no effects during biogenesis; however, substantial effects on substrate preference were observed during catalytic turnover. Mutations of the amino acids immediately flanking TPQ in HPAO (E406Q and N404D) suggested that these residues not only play a key role in determining the rate of biogenesis but are required for the proper positioning of the mature cofactor during catalysis [81,70]. Furthermore, altering Y305 to an alanine resulted in an ~ 800-fold decrease in k_{obs} for TPQ formation, implying that this amino acid orients the precursor tyrosine in a conformation that promotes biogenesis [82]. Interestingly, mutation of the corresponding amino acid in ECAO to phenylalanine was discovered to principally affect k_{cat} during amine oxidation [83]. Rates of TPQ biogenesis were not measured in this latter study, but TPQ was reported to be fully processed [83]. Collectively, the results

summarized above show the critical importance of the consensus sequence residues not only during biogenesis, but in catalysis.

Amine Oxidase Mechanism

Much of the following discussion is taken from an NIH grant proposal jointly written by myself, Gregory A. Juda, and David M. Dooley (P.I.) [84].

CuAOs utilize the TPQ cofactor to bind and oxidize primary amine compounds. CuAOs from various sources preferentially oxidize a multitude of primary amines, from short to long chain aliphatic mono- and diamines, including several arylalkylamines [18,50,85]. The two-electron oxidation of amine compounds, with the subsequent reduction of O_2 to H_2O_2, proceeds through a Ping-Pong Bi Bi mechanism divided into two half reactions:

$$E_{ox} + RCH_2NH_2 \leftrightarrow E\text{-}RCH_2NH_2 \rightarrow E_{red} + RCHO \quad (1)$$

$$E_{red} + O_2 + H_2O \rightarrow E_{ox} + H_2O_2 + NH_3 \quad (2)$$

The first half-reaction (Eq. 1) is known as the reductive half reaction and is detailed in Figure 6, A $\rightarrow$ D. The decisive step is the conversion of the initial quinoneimine "substrate Schiff base" (B, TPQ_{SSB}) to a quinolaldimine "product Schiff base" (C, TPQ_{PSB}), facilitated by proton abstraction from the α carbon of amine substrate by an

absolutely conserved aspartate residue acting as a general base [86,58]. Product aldehyde is then released by hydrolysis generating the reduced cofactor (TPQ_{AMQ}).

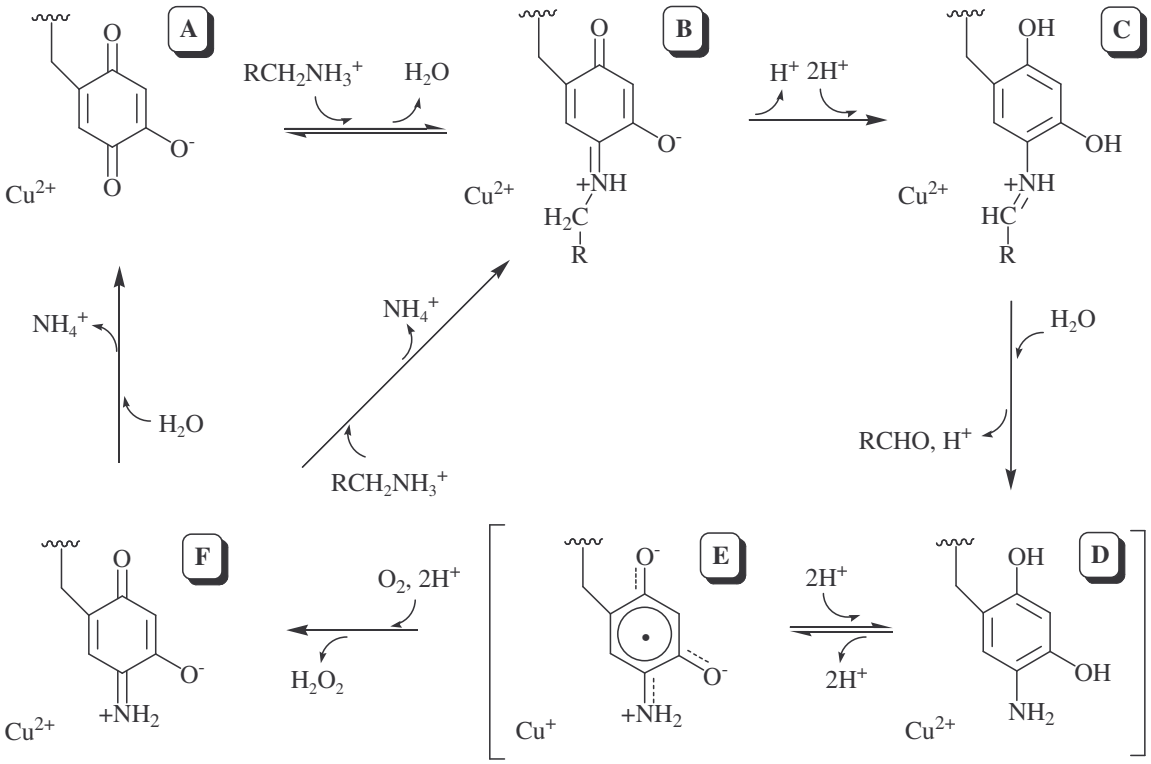

Figure 6: The proposed catalytic reaction mechanism for CuAOs.

The second half-reaction involving reoxidation of the organic cofactor is known as the oxidative half-reaction, and is diagrammed in steps D → A (Figure 6). Upon release of aldehyde, the reduced enzyme exists as an equilibrium between a Cu(II)-aminoquinol (D, TPQ_{AMQ}) and a Cu(I)-semiquinone (E, TPQ_{SQ}) state, with the magnitude of K_{eq} being highly dependent upon the source of the enzyme [87]. Reduction of O_2 to H_2O_2 yields an iminoquinone species (F, TPQ_{IMQ}), which hydrolyzes to liberate NH_3 and the resting cofactor (A, TPQ_{OX}) [16]. Model chemistry has suggested the release of NH_3

may also occur through a transimination reaction between substrate and the iminoquinone, generating the substrate Schiff base (F → B) [88,89]. The rate-limiting step (r.l.s.) during catalysis depends upon the enzyme source. In lentil seedling AO (LSAO), formation of TPQ_{AMQ} and release of aldehyde product is rate limiting [90], while examination of ^{18}O isotope effects on catalysis in BPAO concluded that ~60% of the r.l.s. could be attributed to proton abstraction during the reductive half reaction, with the remaining ~40% ascribed to the first electron transfer to O_2 during the oxidative half reaction [91]. The species observed to accumulate under single turnover conditions in AGAO was the deprotonated iminoquinone, suggesting that either hydrolysis of this species (yielding ammonia and the charge delocalized, oxidized TPQ) or dissociation of metal-bound peroxide is rate-limiting [92]. Conversely, the r.l.s. in HPAO has been proposed to be formation of cationic TPQ_{SQ} and metal bound superoxide [82,93].

Several key studies on the reductive half-reaction have been reported. While no enzyme-substrate complex has been structurally characterized to-date, a substrate analog has been utilized to trap the enzyme at the substrate Schiff-base stage (Figure 6, B) to probe active site changes accompanying substrate binding [58]. In the case of the substrate analog 2-hydrazinopyridine (2-HP), a nitrogen is adjacent to the amine group (as opposed to a carbon), thereby preventing proton abstraction from occurring and trapping the enzyme in a covalent complex. This structure provides a "snapshot" of the initial catalytic intermediate and reveals several significant details, most importantly that TPQ must be in the "productive" conformation to facilitate proton abstraction from the α carbon of amine substrate (Figure 7). Furthermore, the absolutely conserved tyrosine residue (Tyr369) is observed to form a short hydrogen bond (less than 2.5 Å) with O4 of

TPQ and the active site "gate" residue, Tyr381, is seen to rotate out of the substrate channel thereby permitting access to the active site [58]. Interestingly, the tip of the pyridine ring in the TPQ-2-HP complex is at the edge of the interface between domains 3 and 4, providing some of the first evidence of the substrate channel in ECAO (Figure 7). In addition to this structure, the structures of AGAO adducts with benzylhydrazine and tranylcypromine, two compounds that are also trapped at stage B have been more recently solved. Collectively, these structures have shed light on the structural changes that occur upon substrate binding.

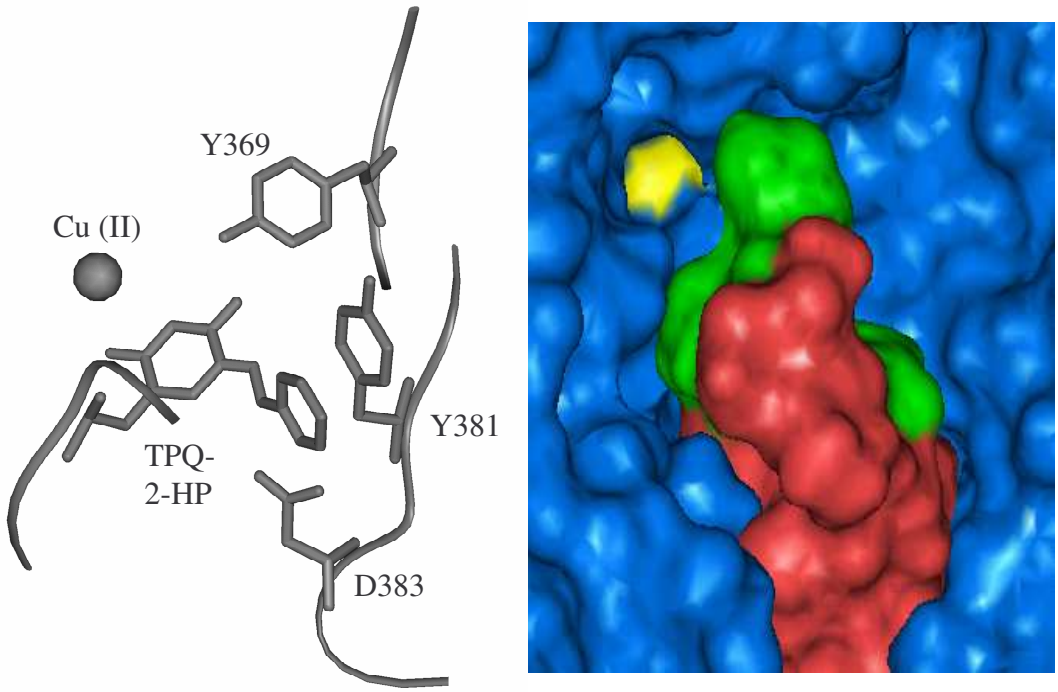

Figure 7: The ECAO 2-hydrazinopyridine structure. The left panel depicts those residues which are described in text. The right panel shows the solvent accessibility calculation for this structure as described in [62]. Blue: monomer 1. Red: β arm of monomer 2. Green: residues of β arm forming entrance to channel. Yellow: TPQ-2-hydrazinopyridine complex.

As the ECAO 2-HP structure revealed, the C5 atom of TPQ must be oriented towards the catalytic base in order for substrate to bind and proton abstraction to occur. Several studies have shown that proton abstraction in most CuAOs by the active site base is stereospecific, with stereospecificity varying depending on the enzyme source, and in some cases the identity of the substrate [58,94-96]. For example, CuAOs isolated from pea seedling, soybean seedling, chickpea seedling and pig kidney are specific for *pro-S* Cα hydrogen abstraction from tyramine, however, CuAOs from pig and horse plasma are *pro-R* specific for proton abstraction from tyramine [94,95]. In contrast, the oxidative deamination of benzylamine involves removal of the *pro-S* hydrogen for all enzymes studied [95].

Evidence from the crystal structures and kinetics studies of the site-directed variants of D383 (D383A, D383N, D383E) in ECAO, have conclusively shown that the catalytic base performs the key step of proton abstraction during catalysis, in addition to assisting substrate binding [86,97]. Another residue implicated in positioning TPQ-derived intermediates during turnover is the conserved Tyr residue (Y284 in AGAO; Y369 in ECAO; Y305 in HPAO), seen to hydrogen bond with O4 of TPQ in the ECAO-2-HP structure (Figure 7) [58]. Mutational studies of this residue in ECAO proved quite informative. In the crystal structure of ECAO Y369F, TPQ was found to predominantly adopt a "non-productive" conformation, substantiating the belief that Y369 positions TPQ for optimal interaction with substrate [83]. Kinetics studies of this mutant displayed significant reduction in catalytic efficiency below pH 7.0 (k_{cat}/K_M dropped 140-fold at pH 6.0) [83]. This was attributed to a rise in K_M for the substrate as a result of an increased pK_a (5.75 – 6.5) for the catalytic base Asp383 (typically pK_a ~ 5). Mutagenesis

experiments of this residue in HPAO (Y305A) showed an ~ 800-fold decrease in k_{obs} for TPQ biogenesis versus WT-HPAO, indicating that this residue also coordinates biogenesis intermediate(s) in an orientation(s) that is more favorable for biogenesis [82].

The principal unresolved issue in CuAO catalysis is the precise role of copper during enzymatic reoxidation (Eq. 2). Two possible reoxidation mechanisms are outlined in Figure 8. Based on the detection of appreciable quantities of Cu(I)-TPQ_{SQ} present in substrate reduced CuAOs from various sources [87], our laboratory suggested that the first electron reduction of O_2 occurs by reaction with Cu(I) (Figure 8B) resulting in a Cu(II) bound superoxide species (Figure 8C) [87,98]. This proposal circumvents the well-known spin conversion problem associated with two-electron reductions of oxygen [99] and is supported by the ample precedence for the reactivity of three-coordinate Cu(I) sites with O_2 in copper-containing metalloproteins [100-103]. This hypothesis was supported by temperature jump relaxation measurements on PSAO [104] and APAO [105], which showed that the electron transfer rate between the reduced TPQ cofactor and the copper center ($k_{ET} \cong 20{,}000\ s^{-1}$ in PSAO; $k_{ET} \cong 75\ s^{-1}$ in APAO) was significantly faster than respective k_{cat} values, thereby indicating that the Cu(I)-TPQ_{SQ} moiety could be a kinetically competent intermediate during catalytic turnover. Despite this evidence, an obligatory role for a Cu(I)-semiquinone intermediate has not been established, and other viable mechanisms have been suggested [75,91].

Substantial research on the CuAO from *Hansenula polymorpha* (HPAO) has led to the proposal that copper reduction is not essential for regeneration of the resting cofactor, giving rise to the suggestion of an alternative reaction pathway (Figure 8, A2 $\rightarrow$ C2) [72,106,107]. Based on the observation that Co(II)-substituted HPAO was active

and displayed a k_{cat} close to that of the native Cu(II) enzyme near pH 7.0, Klinman and coworkers argued that the first electron transfer to O_2 occured directly from TPQ_{AMQ} and suggested that copper reduction was not essential for catalysis. The differences in the kinetics of the Co(II)-enzyme compared to the Cu(II) enzyme were attributed to a much larger K_M for O_2 [106,107]. This difference in oxygen binding affinity for the nonmetal site (see discussion below) was believed to arise from an increase in pK_a of the axial H_2O molecule in the cobalt-substituted enzyme relative to the wild-type copper enzyme, resulting in an active site net charge increase from +1 (with Cu(II)-OH^-) to +2 (with Co(II)-H_2O) [106,107]. These studies suggest that O_2 receives the first electron directly from TPQ_{AMQ} (A2 $\rightarrow$ B2; rate limiting step), with the superoxide species subsequently migrating to Cu(II) (B2 $\rightarrow$ C2) [89]. An essential feature of this mechanism is the proposal that the copper-bound axial water serves as a proton source in TPQ reduction, resulting in a Cu(II)-OH^- species (A2). It is believed that following the first electron transfer to O_2, the pK_a of TPQ_{SQ} is perturbed in a way to allow for rapid proton transfer back to the metal bound hydroxide species forming H_2O. The metal bound water would then be expected to undergo rapid substitution with superoxide anion [89]. Further support of a non-redox role for copper comes from a theoretical study utilizing density functional theory, which implicates the paramagnetic copper center in the spin transitions necessary to produce singlet TPQ from the reaction of singlet TPQ_{AMR} with triplet O_2 [108]. However, this report was premised on the rate-limiting step being the first electron transfer to O_2, which is not the case for all CuAOs (see above).

Besides the different proposal in regards to the redox role of copper, the two mechanisms outlined in Figure 8 differ in the location of oxygen binding. This directly

arises from studies aimed at examining the nature of O_2 reactivity during the oxidative half reaction. An examination of solvent viscosity effects in BPAO showed no effect on the rate of enzymatic reoxidation [91], suggesting that O_2 prebinds to the enzyme prior to its reduction [91,109]. Oxygen prebinding in HPAO and BPAO was subsequently hypothesized to take place in a proteinaceous, hydrophobic pocket near TPQ comprised of the residues Y407, L425, and M634 (HPAO numbering) [109]. This pocket was identified by comparing native and zinc substituted HPAO structures. Such analysis revealed that L425 and M634 were closer together in the unprocessed enzyme, in a manner that could preclude O_2 binding, thereby explaining the higher $K_M(O_2)$ observed for biogenesis relative to catalysis (233 μM versus 15 μM, respectively) [59].

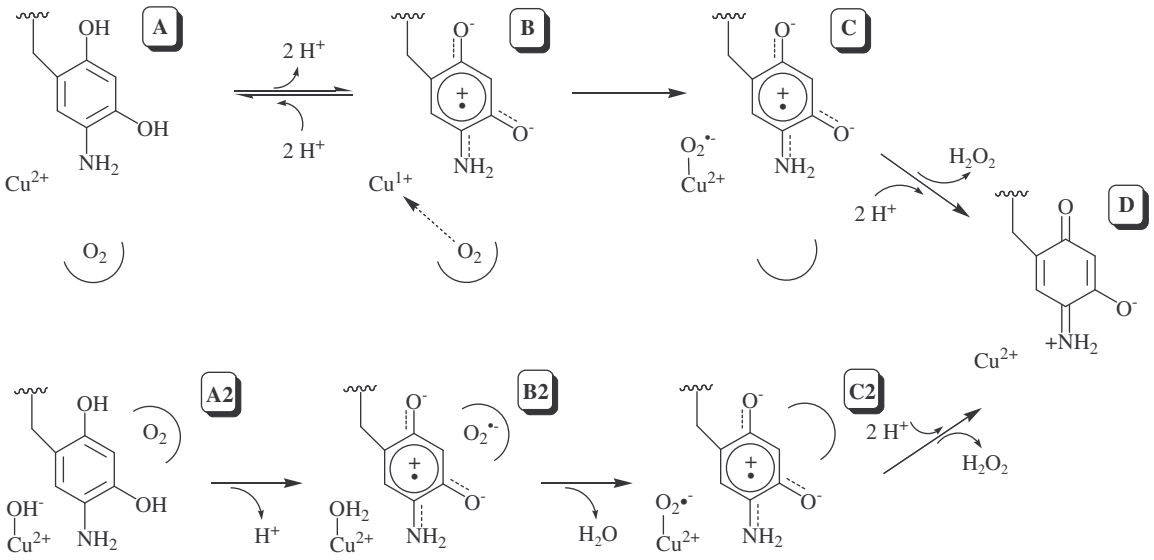

Figure 8: The two proposed CuAO reoxidation mechanisms. Each mechanism starts at the TPQ_{AMQ} species (Figure 6D). A→D represents the pathway proposed by Dooley and coworkers. A2→D represents the catalytic steps proposed by Klinman and coworkers.

Oxygen binding to the copper center has been directly probed through the use of the exogenous ligand azide, which is known to bind equatorially to the copper site in CuAOs [110-112]. Azide was found to exhibit noncompetitive inhibition with respect to O_2 in HPAO, which was interpreted in terms of prebound O_2 reacting directly with TPQ_{AMQ} [72]. This result supports the mechanism put forth by Klinman, whereby O_2 binds off metal. In contrast, two earlier studies concluded that azide displayed competitive inhibition with respect to substrate O_2 in the CuAO from porcine plasma (PPAO), which is consistent with O_2 reacting initially with the copper center [113,114].

A highly influential study designed to trap and structurally characterize intermediates in the oxidative half-reaction, Wilmot *et al.* report the structures of the anaerobic substrate-reduced nitric oxide complex and an aerobic equilibrium turnover species in ECAO [115]. With the goal of capturing the proposed initial dioxygen binding site, the authors exposed anaerobic substrate-reduced enzyme to nitric oxide, a presumed dioxygen mimic. The electron density reveals NO bound close to copper, replacing the axial water, at 2.4 Å and an angle of 117° [115]. The oxygen atom of NO is hydrogen bonded to O-2 of the cofactor. The authors suggest this is consistent with Cu(II)-NO-aminoquinol, with the aminoquinol O-2 being protonated. The structure of an equilibrium turnover species was revealed when ECAO crystals were aerobically exposed to excess substrate (Figure 9). Electron density attributed to a dioxygen species was seen in the position analogous to that occupied by NO in the anaerobic reduced NO structure. This moiety was bound in a side-on conformation and was assigned as peroxide, with TPQ in the iminoquinone state. Given the ligand binding site in the peroxide and NO complexes, electron transfer from either Cu(I) or TPQ_{AMQ} are both plausible mechanisms

(Figure 8). There was no evidence for dioxygen binding in the hydrophobic site proposed by Klinman [72].

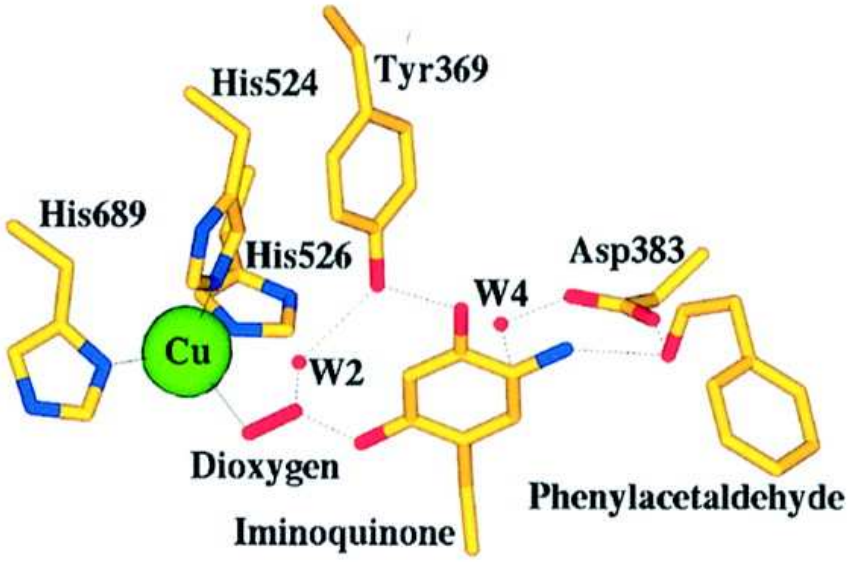

Figure 9: Aerobic steady-state ECAO intermediate. Figure taken from [115].

In an effort to experimentally probe whether a cavity suitable for O_2 binding existed near the active site of CuAOs prior to its reduction, our laboratory, in collaboration with Professor Hans C. Freeman and coworkers (University of Sidney, Australia), collected X-ray diffraction data at 1.7-2.2 Å resolution for crystals of three CuAOs under a high pressure of xenon gas [116]. Xenon has been used in this manner as a probe for potential hydrophobic binding pockets since 1965 when myoglobin crystals were found to form stable adducts when exposed to Xe gas under pressure [117]. Furthermore, xenon is an appropriate probe for potential O_2 binding sites because Xe atoms have similar van der Waals diameters as O_2 molecules (4.3 Å versus 3.0 – 4.3 Å)

[116]. Electron-density and anomalous electron-density difference maps provided evidence for multiple Xe binding sites, with only one of these sites being common to all three proteins. The consensus site has several distinguishing features (Figure 10A): it is the Xe site closest to the Cu/TPQ center in each structure; the Xe atom is ~7.5 Å from Cu(II) and ~9.5 Å from the C2 carbonyl of TPQ; five of the six nearest-neighbor residues of the Xe atom are homologous; and potential access from the interior solvent-filled cavity in each structure would require only minor fluctuations in side-chain orientation. Electron transfer from either the copper atom or the TPQ cofactor would require substantial migration of the O_2 molecule (4-6 Å), however, the most direct trajectory towards the active site would require an initial close approach to copper. Interestingly, a subsequent study identified the same Xe binding site in BPAO [53].

In the case of HPAO, no experimental evidence has been obtained to date delineating xenon binding sites. Through model building, however, a xenon atom could be placed in the site identified in the Xe-AGAO, Xe-PPLO, and Xe-PSAO structures with minor movement of two side-chains (Figure 10B) [116]. Modeling also confirmed that a xenon atom could be placed in the hydrophobic pocket initially proposed by Klinman *et al*. [59,109]. The difference in location between these two sites is easily observed when comparing the gold and magenta spheres in Figure 10B. The second Xe-binding site is much closer to TPQ and Cu(II) than the site experimentally observed (Figure 10A), with Xe-TPQ and Xe-Cu(II) distances of ~3.5 Å, respectively. Despite the attractive location of this second site, it is a fact that xenon is not observed to bind at this location in any of the four Xe-structures determined [53,109]. This may simply be due to the fact that the site is not as hydrophobic as initially believed, as a water molecule is

present in this cavity in the native HPAO structure. This water molecule is part of a chain of H_2O molecules extending between the copper center and the interior, solvent-filled cavity. Similar solvent molecules are observed to exist in other native CuAO structures. Therefore, it is reasonable to assume that xenon is not observed to bind in this second site because the cavity is too hydrophilic [116].

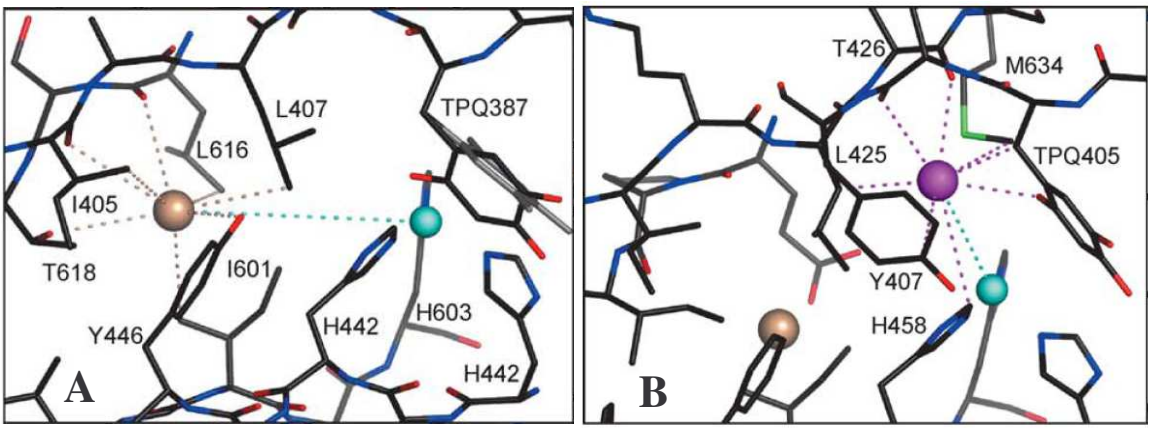

Figure 10: Xenon binding sites. (A) The consensus Xe binding site using PSAO as an example. (B) Xe-HPAO. Small spheres represent the Xe atom (gold) and the copper atom (cyan). In (B), the magenta sphere represents a Xe atom placed in the hydrophobic pocket initially proposed by Klinman (see text). This figure was taken from [116].

Understanding the nature and location of O_2 binding is intrinsic to comprehending the role of copper during the oxidative half-reaction. As mentioned above, several metal-substitution studies have been performed attempting to determine the effects on O_2 binding, and have led to the proposal that copper does not play a redox role during catalysis (Figure 8) [72,107]. These studies are partly problematic, however, as they rely on the CuAO from *Hansenula polymorpha*. HPAO is complicated because it does not fully process TPQ (~ 40%) and there are significant zinc contamination issues with the

purification procedure [118]. Therefore, it is absolutely critical to compare metal-substitution studies using CuAOs from different sources. Along these lines, two recent studies of metal-substituted AGAO have provided valuable insight into the role of copper in the oxidative half-reaction [92,119].

Stopped-flow studies of substrate reduced AGAO showed that reduced AGAO reacted very rapidly with O_2 (< 1 ms), forming a Cu-peroxy species (λ_{max} = 410 nm). The results were consistent with either Cu(I)-TPQ_{SQ} or Cu(II)-TPQ_{AMQ} reacting rapidly with O_2, or with rapid $1e^-$ transfer from TPQ_{AMQ} to Cu(II). Formation of the charge delocalized, oxidized TPQ was proposed to be the rate-determining step in the oxidative half-reaction of AGAO [119]. In marked contrast to the reports on HPAO [106,107], Co(II) and Ni(II) reconstituted forms of AGAO had K_M values for amine and O_2 substrates that were essentially identical to the native enzyme; however, k_{cat} values for Co(II)- and Ni(II)-AGAO were ~ 1 sec^{-1}, as compared to 110 sec^{-1} for Cu(II)-AGAO [92]. Metal substituted AGAO and HPAO differ in two critical aspects: (1) compared to other metal ion substituted enzymes, the Co(II) forms display the most activity in both AGAO and HPAO, but the levels of recovery vary substantially (2% in AGAO and 19% in HPAO, relative to the native copper enzymes); (2) the major cause of the reduced activity in HPAO was the large increase in K_M for O_2, whereas it is the substantial decrease in k_{cat} in AGAO, with $K_M(O_2)$ remaining unchanged. X-ray crystal structures of Co(II)- and Ni(II)-AGAO established that the hydrogen-bonding network in the active site was preserved [92]. The coordination of both Co(II) and Ni(II) was octahedral, with the addition of another H_2O molecule as a ligand. The results indicate that the low catalytic activities of Co(II)- and Ni(II)-AGAO were associated with impaired efficiency

of the oxidative half-reaction. Rate constants for reoxidation (measured by decay of the TPQ_{AMQ}) were 0.18 s^{-1} and 0.17 s^{-1} for Co(II)-and Ni(II)-AGAO, respectively, *and conclusively show that the initial reaction with O_2 is substantially slower in the metal substituted enzymes*. These reported k_{obs} values probably underestimate the true rate constants; nonetheless, it is clear that oxidation of TPQ_{AMQ} and subsequent formation of TPQ_{IMQ} occurs over 20 seconds, a rate which is at least two orders of magnitude slower than the Cu(II) enzyme. The rate acceleration of the initial reaction of substrate-reduced enzyme with O_2 observed for the native copper enzyme was regarded as consistent with the participation of a reactive Cu(I) semiquinone, but cannot be regarded as conclusive. Kishishita *et al*. propose that copper plays an essential role in catalyzing electron transfer between TPQ_{AMQ} and O_2, at least in part by acting as a binding site for reduced dioxygen species to be efficiently protonated and released [92].

In lentil seedling amine oxidase (LSAO), neither Ni(II) nor Zn(II) substituted LSAO displayed any catalytic activity, while Co(II)-LSAO displayed minor (7%) activity relative to the wild-type enzyme [120]. Detailed mechanistic studies of LSAO concluded that the reoxidation of the reduced enzyme at pH 7 proceeded mainly through the reaction of the Cu(I)-TPQ_{sq} with O_2, with a rate constant of 1.56 x 10^7 $M^{-1}s^{-1}$ [121]. This rate constant is consistent with the rapid intramolecular electron transfer rate of 20,000 s^{-1} from TPQ_{AMQ} to Cu(II) obtained from the closely related enzyme PSAO [104].

Taken collectively, the mechanistic results summarized above do not conclusively prove or disprove the role of the Cu(I)-TPQ_{SQ} moiety during the oxidative half-reaction. However, these data do suggest that *CuAOs from different sources may utilize distinct mechanisms to reoxidize the reduced quinone species*. This would certainly be a

remarkable finding, given the similarity between TPQ and copper coordination environments among the enzymes studied. It also must be acknowledged that the fundamental difference between the proposed mechanisms for the oxidative half-reaction (Figure 8) may ultimately be a relatively subtle one concerning the timing between the electron-transfer step relative to the migration of O_2 from its initial binding site to the metal ion. Nevertheless, these mechanistic issues are important ones, with implications for dioxygen reactivity in other enzyme systems, and warrant further investigation.

Research Goals

There are two main goals to the work described in this thesis. The first objective of this research was to determine if selective mechanism-based inhibitors of CuAOs could be developed. In the process of screening several compounds against copper amine oxidases from bacterial, yeast, plant, and mammalian sources, a selective inhibitor was indeed discovered. Extensive kinetics and spectroscopic studies, coupled with structural results from computer modeling and X-ray analysis provided vast insight into the molecular factors governing inhibitor potency in AGAO and PSAO. Additionally, a heretofore uncharacterized mechanism of inactivation involving the reduced quinone species was revealed. This work was critical to illustrating how certain aromatic residues in the substrate channel in a bacterial CuAO directly control inhibitor potency.

In a broader context, the development of selective copper amine oxidase inhibitors takes on an elevated sense of importance due to the fact that certain compounds can react with both CuAOs and monoamine oxidase (MAO) enzymes. In particular, this

work details the cross-reactivity for the antidepressant MAO-directed inhibitor tranylcypromine (TCP), which inhibits CuAOs from both bacterial and mammalian sources. The ability of certain compounds like TCP to react with CuAOs and MAOs arises because both these enzyme families carry out the same overall chemistry ($RCH_2NH_2 \rightarrow RCHO$). This work also details the spectroscopic characterization of a class of compounds (3-aryl-3-pyrrolines) which selectively inhibit only the copper containing amine oxidase family, while acting as pure substrates for MAO-B.

In addition to the studies aimed at developing selective inhibitors and understanding the molecular factors governing substrate and inhibitor binding in CuAOs, this work examines the oxidative half-reaction of CuAO catalysis. Specifically, the second objective of this thesis was to probe the role of copper during enzymatic reoxidation. Two mechanistic proposals have been put forth, whereby O_2 is reduced to $O_2^{\bullet-}$ by either Cu(I) or TPQ_{AMQ}. In order to investigate these possibilities, binding and inhibition studies of CuAOs were performed with the monodentate copper ligands cyanide and azide. Additionally, this thesis details temperature jump relaxation measurements for the internal redox equilibrium TPQ_{AMQ}-Cu(II) $\leftrightharpoons$ TPQ_{SQ}-Cu(I) in AGAO, as well as the pH dependence of kinetic activity, and the pH and temperature dependence of K_{eq} for the intramolecular electron-transfer reaction. Collectively, the results provide insights into the catalytic viability of the Cu(I)-TPQ_{SQ} moiety in O_2 reduction.

TOWARDS THE DEVELOPMENT OF SELECTIVE AMINE OXIDASE INHIBITORS: MECHANISM-BASED INHIBITION OF SIX COPPER-CONTAINING AMINE OXIDASES

Introduction

The copper-containing amine oxidases play a crucial role in metabolic oxidative deamination of primary amines to the corresponding aldehydes through the action of the TPQ cofactor. As would be expected for any enzyme relying on a carbonyl cofactor, arylhydrazines form catalytically inactive derivatives of these enzymes, which are also inhibited by chelating agents that remove or bind to the copper. Our interest here, however, is in mechanism-based inhibitors, also called "suicide" inhibitors, which undergo turnover-dependent conversion to electrophilic products capable of covalent binding to the enzyme. Not only can they display binding selectivities based on active-site fit, as with competitive inhibitors, but they offer a second level of distinction on the basis that irreversible inhibition will occur only when the electrophilic product is capable of accessing an active-site nucleophile. Hence, two different enzymes may have similar binding pockets but could quite likely have distinct spatial presentations of modifiable side-chains.

The basic approach in designing suicide inhibitors for amine oxidases has been to incorporate a moiety into an amine substrate that allows for creation of an electrophile upon the imine shift accompanying C_α proton abstraction during the initial phase of oxidation (Figure 6, B $\rightarrow$ C). Two strategies that have been utilized include either the

incorporation of a halogen group or of unsaturation at the β position, examples being β-bromoethylamine [122-127] and propargylamine [124]. The former case results in an S_N2-activated α-haloaldehyde as turnover product, whereas the latter case results in an electrophilic α,β-unsaturated aldehyde. Propargylamine derivatives have been studied as inhibitors of plasma amine oxidase [124], semicarbazide-sensitive amine oxidase (SSAO) [128,129], and monoamine oxidase [130-132].

At the time of this study, only four CuAO crystal structures had been solved: AGAO, PSAO, HPAO, and ECAO. Identification of the active site channel was a relatively recent finding. Even given just these four structures, it was clear at the time that substantial differences existed with respect to the apparent dimensions and electrostatic properties of the active site channel (Figure 3), including whether access to the channel was "gated" and the degree of accessibility to the TPQ cofactor. These observations led us to believe that these differences must contribute to the molecular basis for substrate specificity among these enzymes, and therefore observed preferences among mechanism-based inhibitors should be attributable to structural differences in a manner that may eventually become systematically predictable. Along these lines, our initial hypothesis was formulated: could these differences be exploited by altering substrate analog substituent groups in a systematic manner with the ultimate goal being the development of selective CuAO inhibitors?

To initiate such analysis, we tested the inhibitory effects of four different inactivators with six different CuAOs from mammalian (equine plasma amine oxidase (EPAO) and BPAO), plant (PSAO), yeast (PPLO), and bacterial (AGAO) sources in collaboration with Dr. Lawrence M. Sayre (Case Western Reserve University, Cleveland,

OH). Our choice of the four compounds, 4-(2-naphthyloxy)-2-butyn-1-amine (**1**), 1,4-diamino-2-chloro-2-butene (**2**), 1,6-diamino-2,4-hexadiyne (**3**), and 2-chloro-5-phthalimidopentylamine (**4**) (Figure 11), was based on promising preliminary results from screening a larger set of synthetic inhibitors against BPAO [133,134]. In addition, 1,4-diamino-2-butyne (DABY) was tested against selected enzymes. Comparative data were obtained wherever possible in terms of rates of inactivation, partition ratios, and degree of reversibility. This was the first systematic comparison among a broad collection of copper amine oxidases to critically explore the extent to which selective inhibition might be possible. Moreover, these data point to examples of especially potent and selective inhibition that were amenable to further studies. Along these lines, a subsequent report presented herein details the in-depth investigation of the structural and mechanistic basis of inhibition of a family of compounds derived from inhibitor **1**.

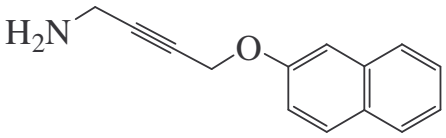

4-(2-naphthyloxy)-2-butyn-1-amine (**1**)

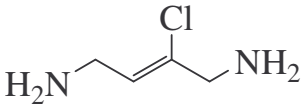

1,4-diamino-2-chloro-2-butene (**2**)

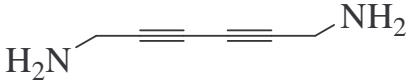

1,6-diamino-2,4-hexadiyne (**3**)

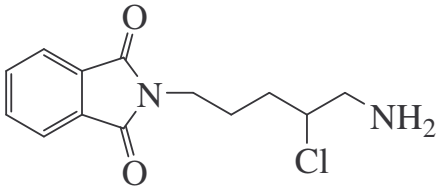

2-chloro-5-phthalimidopentylamine (**4**)

Figure 11: Initial inhibitor compounds.

Materials and Methods

Enzyme Isolation and Purification

Purified enzyme for these studies was provided by Jennifer Smith (AGAO, BPAO, and PSAO), Bradley O. Elmore (EPAO), and Jason Kuchar (PPLO). ECAO was a generous gift from Mike McPherson, University of Leeds (U.K.), and was purified as described previously [51]. PSAO was purified from pea seedling as described previously [19]. BPAO was purified from bovine plasma using minor modifications of a published procedure [135]. EPAO was purified by a revised protocol [21], based on that initially specified in [17]. PPLO was purified as initially described in [136]. AGAO was purified as described previously [12], with slight modifications specified below. Buffer contained no metal chelators, and induction occurred with IPTG and copper supplement to a final concentration of 30 μM. Cell lysate was incubated in 50 mM HEPES, pH 6.8, 0.1 mg/ml PMSF, 1 mg/ml TCPK, and 0.8 mM $CuSO_4$ (final concentration) for 2 hours at 30 °C.

Inhibitor Compounds

The five compounds used in this study (Figure 11), 4-(2-naphthyloxy)-2-butyn-1-amine hydrochloride (**1**), 1,4-diamino-2-chloro-2-butene dihydrochloride (**2**), 1,6-diamino-2,4-hexadiyne dihydrochloride (**3**), 2-chloro-5-phthalimidopentylamine hydrochloride (**4**), and 1,4-diamino-2-butyne dihydrochloride (DABY) were synthesized and characterized by Dr. Lawrence M. Sayre's laboratory, as described in [133,134].

Absorption Spectra and Steady-State Kinetics Assays

Absorption spectra and kinetic assays were recorded at 25 °C using a Hewlett Packard 8453 diode array spectrophotometer equipped with a thermostatted cell chamber connected to an Endocal RTE-5 circulating water bath. Protein concentrations were calculated using extinction coefficients at 280 nm as previously reported for ECAO [137], AGAO [138], EPAO [17], PSAO [19], BPAO [139], and PPLO [85]. Stock inhibitor solutions were prepared by dissolving required amount of compound in doubly-deionized H_2O to yield a final concentration of 1 mM. Experiments were run with freshly thawed protein aliquots from the same enzyme stock. All solutions were stirred during assays, with benzylamine used as a control substrate. Enzyme activity is reported as spectroscopic units per mg of protein.

Method A. To analyze general compound effectiveness, enzymes were incubated with varying concentrations of inhibitor for 30 min at 4 °C. Amine oxidase activity was determined using benzylamine as substrate and monitoring benzaldehyde production for 3 min at 250 nm using an extinction coefficient of 12,800 M^{-1} cm^{-1} [140]. Excess inhibitor was not removed before assaying but was diluted by at least a factor of 30 in the final assay mixture. Assays were run in triplicate for each inhibitor concentration. A control was prepared by incubating equivalent concentrations of enzyme and doubly-deionized H_2O at 4 °C for 30 min. All assays were performed at 25 °C in 100 mM phosphate buffer, pH 7.2.

Method B. Inactivation of amine oxidases over time by selected inhibitors was measured using the assay described above. Buffered enzyme and inhibitor mixtures were

prepared at 4 °C. Upon addition of inhibitor, time was noted and an aliquot was correspondingly taken from the mixture and diluted 30-fold into the assay cuvette. This was repeated until no activity remained or decreases in activity leveled off (both typically achieved within 30 minutes). Partition ratios were calculated from this data by plotting the percent residual activity versus [inhibitor]/[active site]. The error associated with the partition ratio was obtained from the linear fit of this plot using Origin 6.0 software (Microcal, MA, USA).

Method C. Determination of inhibitor oxidation was monitored using a horseradish peroxidase (HRP)-ABTS (2,2'-azino-bis(3-ethyl)benzthiazoline-6-sulfonic acid) coupled assay. The peroxidase-catalyzed reduction of H_2O_2 to H_2O is coupled to the $1e^-$ oxidation of ABTS, forming a metastable radical cation with λ_{max} of 414 nm [11,141]. Assays were performed at 30 °C in 100 mM phosphate buffer, pH 7.0. Total assay volume was 1 ml, and substrate (or inhibitor) concentration was adjusted accordingly to yield a final concentration of 300 μM. Benzylamine was used as a control substrate, and all assays were run in triplicate.

Method D. In order to test the results of Shimizu *et al*. (1997), who reported no benzylamine oxidation by AGAO, 4-aminoantipyrine assays were run using β-phenylethylamine as a control substrate [142]. The 4-aminoantipyrine/2,4-dichlorophenol coupled assay of Holt *et al*. forms an easily detectable quinoneimine dye with λ_{max} at 498 nm and ε_{498} of 6000 $M^{-1}cm^{-1}$ [67,143]. To test the possibility that 2,4-dichlorophenol was possibly inactivating AGAO, thereby explaining why Shimizu *et al*. (1997) reported no turnover of benzylamine, a comparative set of assays were run using

vanillic acid in place of phenol [67]. Reactions were done at 30 °C, and the ΔA_{498} was monitored.

Nitroblue Tetrazolium (NBT) Assay for TPQ Redox Competency

Purified BPAO or AGAO was incubated with a given molar excess of inhibitor determined to achieve loss of 92-97% activity in 2 h at 30 °C. SDS-PAGE analysis of the inactivated and control enzyme and incubations were performed by standard methods on a polyacrylamide slab gel (6% acrylamide with 0.16% bis-acrylamide). Control samples run were both native and phenylhydrazine-inactivated enzyme. Inhibited and control enzyme samples (40 μL) were mixed with 20 μL of standard denaturing buffer (10% SDS with 0.5 M 2-mercaptoethanol) and the mixture was heated at 100 °C for 6 min before application in duplicate to two halves of the gel. After running the gel (at 0.02 amp constant current, voltage near 200 V), the gel was cut in half and the two halves were stained with either Coomassie blue (0.25% Coomassie in 50% methanol, 7% acetic acid) or 0.24 mM nitroblue tetrazolium (NBT) in 2M potassium glycinate pH 10 for 120 min (BPAO) or 180 min (AGAO) in the dark [144]. No alteration of the electrophoretic properties of the enzyme or the intensity of Coomassie staining was observed for any inhibitor. The intensity of the NBT staining relative to the control was judged to the nearest decade percentage by the naked eye by three independent observers, and the value listed was the average of the three estimates. NBT staining assays were performed by Dr. Gang Sun (L.M.S. lab).

Phenylhydrazine Titration

Reactive TPQ can be quantified by its titration with phenylhydrazine, which forms a stable, intensely yellow-colored adduct with λ_{max} ~ 450 nm [135]. In order to determine possible modification of the cofactor by inhibitors, respective samples were titrated with phenylhydrazine. AGAO (32.1 μM protein) was incubated with 0.47 mM **1** for 1 hour at 4 °C in 100 mM phosphate buffer, pH 7.2. Incubation of AGAO (18.3 μM protein) with 5 mM **3** was carried out for 21 hours at 4 °C in 100 mM phosphate buffer, pH 7.2. Samples were then assayed according to Method A and titrated with sub-stoichiometric additions of freshly prepared phenylhydrazine at 25 °C. A control experiment of native enzyme from the same protein stock was also titrated. Adduct formation was monitored by following the change in absorbance at 442 nm.

Data Analysis

K_M and V_{max} values were obtained by graphing rates (ΔA/min) versus benzylamine concentration and non-linear curve fitting to the Michaelis-Menten equation. Catalytic constants (k_{cat}) for benzylamine were found by dividing V_{max} by ε_{250} for benzaldehyde and accounting for protein concentration [145]. Inactivation constants (k_{inact}) and inhibition constants (K_I) were determined by Kitz and Wilson plots of the 4 °C incubation [146]. The software program Origin 6.0 (Microcal, MA) was used to analyze data.

Computer Modeling

Solvent accessibility models for PSAO (1KSI.pdb), AGAO (1AV4.pdb), ECAO (1SPU.pdb), and PPLO [85] were determined using a Connolly surface calculation with a probe radius of 1.4 Å (Insight98, MSI, CA). AGAO coordinates were appropriately modified to create a dimer. Heteroatoms were not included in calculations, with the exception of the ligating equatorial copper water molecule.

Modeling **1** into the active site of AGAO and PSAO used the same protein coordinates utilized for solvent accessibility calculations. TPQ was rotated about the Cα - Cβ bond in both PSAO and AGAO such that C5 was in close proximity to the active site base (productive conformation). Inhibitor **1** was bound to TPQ at the substrate Schiff base stage, to mimic the initial enzyme-inhibitor complex. The model was based on the crystal structure of the 2-HP derivative of ECAO (Figure 7). In this structure, the O4 position of TPQ forms a short hydrogen bond with Tyr369. For computer modeling, TPQ(O4) was protonated to account for this hydrogen bond. Although the ECAO-2-HP adduct is believed to exist as a hydrazone derivative [58], it is conceivable that it may tautomerize into the azo form. Minimization calculations were run using Steepest Descent and Conjugate algorithms until RMS derivatives were 0.041 kcal mol^{-1} $Å^{-1}$ for PSAO and 0.0099 kcal mol^{-1} $Å^{-1}$ for AGAO (Insight98, MSI, CA).

Results

Standard Substrate Observations

In order to examine general trends of inhibition, benzylamine was chosen as the substrate for all enzymes. Analysis of benzylamine kinetics (Table 1) enabled us to

obtain a basis for comparison of oxidation rates for different amine oxidase enzymes. Contrary to previous results [142], we report benzylamine turnover by AGAO. The turnover rate of benzylamine is only about 3% that of phenethylamine using method D. Due to the relatively low k_{cat} value (Table 1), it is quite likely that benzylamine turnover was simply not detected by Shimizu *et al*. [142]. Comparisons to ECAO could not be made as only a small amount of this protein was available for inhibitor studies.

Table 1: Benzylamine Kinetics

Enzyme	k_{cat} (min^{-1})	K_M (μM)	k_{cat}/K_M ($min^{-1}\mu M^{-1}$)
EPAO	13 ± 0.5	87 ± 8	0.15
AGAO	32 ± 0.5	34 ± 1	0.94
PSAO	131 ± 3	215 ± 10	0.609
BPAO	69 ± 5	1500 ± 200	0.046
PPLO	46 ± 1	29 ± 2	1.6

Concentration Dependencies and Time-Based Inhibition

To determine the relative effectiveness of the inhibitors, concentration-dependent inhibition data were obtained according to methods A and B. Activities in Table 2 are reported as percentages relative to control assays. Inhibitor excesses reported are relative to monomer protein concentrations, i.e. the number of active sites. Concentrations of the enzymes are given in the legend. In some cases, the rate of loss of enzyme activity over time slowed, and the activity eventually plateaued at a level that was successively lower

with increasing starting concentration of inhibitor. This behavior signifies a partitioning of the non-covalent enzyme and reactive product complex between covalent attachment and release of the product into bulk solvent, allowing for maintenance of enzyme activity as long as the inhibitor is completely metabolized before all enzyme becomes inactivated. In these cases, a plot of the plateaued activity vs. the stoichiometric ratio of inhibitor concentration to enzyme concentration permitted an estimate of the partition ratio. Inspection of the data reveal the following general selectivity trends: (1) inhibitor **1** significantly inhibits all enzymes with the exception of PSAO; (2) compounds **2** and **3** extensively decrease activity of all enzymes, but PSAO, PPLO and EPAO are significantly more susceptible to inhibition by **2** than other AOs; (3) compound **4** inhibits only BPAO and EPAO.

Inhibitor Turnover

The ability of CuAOs to oxidize inhibitor compounds was determined through the use of a coupled assay, based on the production of H_2O_2 (method C). Table 3 displays turnover of inhibitor compounds relative to that of benzylamine. Oxidation rates can be seen to vary quite dramatically among respective enzymes.

Table 2: Inhibition of Six CuAOs Using Compounds in Figure 11

Enzyme	Compound	Inhibitor: Protein[a]	% Activity[b]	Enzyme	Compound	Inhibitor: Protein[a]	% Activity[b]
AGAO[c]	**1**	1	0	PSAO[c]	**1**	14	100
	2	1.6	63		**2**	1.3	6
		9	22			2.6	0
		17	8		**3**	14	74
	3[d]	1.5	42			27	17
		5	25		**4**	14	100
		8	18			27	92
	4	17	95	BPAO[c]	**1**	1	86
		34	90			8	38
ECAO[e]	**1**	1	100			16	12
		2.5	86		**2**	5	56
		5	67			10	32
	2	1	95			15	7
		3	69		**3**	1	27
		15	20			9	8
	3	2	63		**4**	7	81
		7	20			17	73
		19	6			34	53
	4	4	100			85	25
		7	100	EPAO[g]	**1**	2	89
		19	100			10	77
PPLO[f]	**1**	3	70			19	66
		7	14		**2**	2	2.5
		14	6		**3**	2	78
	2	1	5			20	70
	3	9	77			38	53
		19	65		**4**	2	62
		37	13			4	62
	4	9	100			11	50
		45	100				

[a] Reported as excess inhibitor relative to active site concentration. [b] Percent activity remaining relative to control rates (rounded to nearest integer), following a 30 min incubation. Numbers shown are averages of 3 assays. [c] Active site concentrations ranged between 4 and 7 μM. [d] Percent activity after a 60 min incubation. [e] Active site concentrations ranged between 20 and 33 μM. [f] Active site concentrations were at 5 μM, but compound **4** studies were done at 11 μM. [g] Active site concentrations ranged between 5 and 6 μM, but compound **4** studies were carried out at 47 μM.

Table 3: Oxidation Rates of Inhibitor Compounds[a]

Enzyme	Benzylamine Rate[c]	**1**[c]	**2**[c]	**3**[c]	**4**[c]
EPAO[d]	0.066	0.014 (0.21)[b]	0.034 (0.52)	0.018 (0.27)	0.0165 (0.25)
AGAO[e]	0.26	0.0 (0.0)	ND[j]	0.008 (0.031)	0.031 (0.12)
PSAO[f]	0.58[h]/0.74[i]	1.60[h] (2.8)	0.57[i] (0.77)	1.74[h] (2.4)	0.11[i] (0.19)
PPLO[g]	0.48	0.20 (0.42)	0.16 (0.33)	0.31 (0.65)	0.33 (0.69)

[a] Reported rates are recorded as μmoles of product per minute per mg of protein. [b] Numbers in parentheses represent compound turnover rate relative to benzylamine rate. [c] Substrate concentration was 300 μM. [d] Active site concentration was 0.78 μM. [e] Active site concentration was 0.67 μM. [f] Active site concentrations ranged between 0.53 and 0.6 μM. [g] Active site concentration was 0.47 μM. [h and i] Two different grades of enzyme were employed; both purified as described previously [19]. [j] Not determined.

Phenylhydrazine Titration and Determination of TPQ Cofactor Redox Integrity

In selected cases, the nature of irreversible inhibition was investigated in two different ways. First, the inactivated enzyme preparation was titrated against phenylhydrazine, which reacts stoichiometrically with the TPQ quinone C5 carbonyl in the unmodified enzymes, forming a stable hydrazone complex intensely absorbing at 450 nm [135]. Secondly, the redox integrity of the TPQ cofactor was measured by running the inactivated enzyme samples on a denaturing SDS polyacrylamide gel and then staining the enzyme band according to the redox cycling NBT assay [144], which assesses the ability of the exposed TPQ cofactor to mediate O_2-dependent redox cycling oxidation of glycinate. Table 4 summarizes the latter results.

Table 4: Nitroblue Tetrazolium Results

Enzyme	Inhibitor	Inhibited enzyme stained with NBT (% of control)
BPAO	**1**	100%
	2	6%
	3	85%
	4	100%
	1,4-diamino-2-butyne	10%
AGAO	**1**	100%
	2	10%
	3	100%
	1,4-diamino-2-butyne	100%

Observations With 4-(2-Naphthyloxy)-2-butyn-1-amine (**1**)

This compound displays potent and rapid time-dependent inhibition with AGAO; stoichiometric concentrations completely abolish enzymatic activity. Consistent with this observation, no turnover oxidation of **1** by AGAO could be detected (Table 3). Although AGAO inhibited by **1** displayed no detectable reactivity towards phenylhydrazine, NBT staining of the inactivated enzyme on the SDS polyacrylamide gel was indistinguishable from the control enzyme preparation.

Compared to AGAO, complete inhibition of PPLO requires greater amounts of **1**, but inhibition occurs almost immediately by a 45-fold excess of inhibitor. The inhibitory potency of **1** on the other enzymes diminishes further, with the overall trend being: AGAO > PPLO > BPAO > ECAO > EPAO >> PSAO. Both EPAO and BPAO displayed unusual behavior with this compound, in that following the initial drop in activity there was partial recovery: for a 38-fold excess of **1** the activity of EPAO increased from 48% at 10 min to a plateau at 75% activity over 2 h; for a 10-fold excess

of **1** the activity of BPAO increased from 35% at 10 min to a plateau at 45% over 60 min. The most likely explanation for this behavior is that there is potent reversible competitive inhibition superimposed on turnover-dependent inactivation: the enzyme activity is permanently diminished over time due to the latter, but eventual complete metabolism of the inhibitor by the active enzyme still present eliminates the competitive inhibition. With increasing amounts of **1**, there is an increasing fraction of enzyme that suffers inactivation before **1** is completely metabolized, and a high concentration of **1** was able to completely inactivate BPAO. Nonetheless, the NBT assay run at this point revealed no loss of the redox viability of the TPQ cofactor in this denaturing assay.

In contrast to the other enzymes, PSAO activity is unaffected by a 14-fold excess of **1** (Table 2) and even by a 1-hour incubation with a 62-fold excess of **1**, though a 135-fold excess results in 17% inhibition after 1 hour. At the same time, turnover of **1** by PSAO demonstrates that this compound is oxidized much faster than is benzylamine, while oxidation of **1** by PPLO and especially by EPAO was 2.5-5 times lower than oxidation of benzylamine by these enzymes (Table 3). Taken together, these inhibitory and substrate data suggest first that **1** is an excellent substrate for turnover by PSAO, with inactivation occurring only infrequently, whereas the decreased inactivation of EPAO and PPLO by **1** reflects in part weaker recognition.

The interaction of **1** with AGAO and PSAO was further investigated by UV/Vis spectroscopy, with the hope of revealing the basis of divergent substrate vs. inhibitor behavior. Since the inhibitor alone absorbs at 322 nm (Figure 12), with a calculated extinction coefficient of 1003 M^{-1} cm^{-1} due to the naphthyl group, absorption in this region can serve as a crude reporter of the stoichiometry of binding of the inhibitor.

Concentrated solutions of PSAO and **1** showed no noticeable color change from native state (pink), whereas those of AGAO and **1** were a faint yellow. Samples of both enzymes inactivated by exposure to a large excess (140 equiv) of **1** were prepared and run over a Sephadex G-25 column, clearly separating excess **1** from AGAO and PSAO. Spectra of the enzymes at this point were not changed by subsequent extensive dialysis against 100 mM phosphate buffer, pH 7.2. It can be seen that the spectrum for AGAO and **1** (Figure 12a) displays a small shoulder at 328 nm corresponding to a ΔA of ~0.005 (see inset), which, assuming that the bound form of **1** has the same ε as that of free **1**, suggests that there is ~5 μM of **1** bound to the 5 μM of AGAO in this sample. In contrast, the spectrum for PSAO and **1** (Figure 12b) displays a more prominent shoulder at 328 nm corresponding to a ΔA of ~0.05, which, assuming that the bound form of **1** has the same ε as that of free **1**, suggests that there is ~50 μM of **1** bound to the 3.5 μM of PSAO in this sample. Post-dialysis assays were run according to methods A (no incubation) and C, confirming that AGAO is inhibited completely by **1**, whereas PSAO still retained 75% of the control activity, despite the substantially higher amount of bound inhibitor.

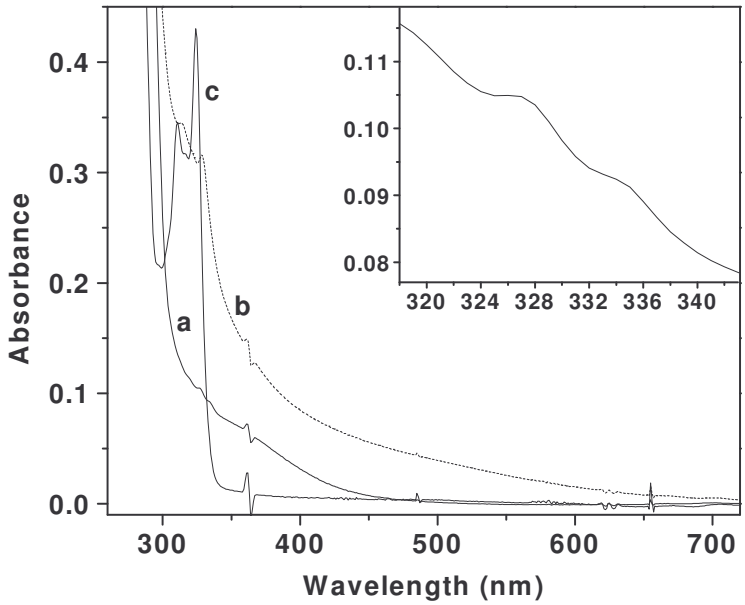

Figure 12: Postdialysis spectral analysis of samples incubated with **1**. a: AGAO (5 μM); b: PSAO (3.4 μM); c: **1** (370 μM). Graph inset depicts a magnified spectrum a.

Observations With 1,4-Diamino-2-chloro-2-butene (**2**)

This compound is the most broadly effective inhibitor against the amine oxidases examined in this study. A stoichiometric quantity of **2** results in 95% inhibition of PPLO, and 1.3 and 2 equivalents of **2** inhibit PSAO and EPAO by 94% and 97.5%, respectively (Table 2). However, the finding that all three enzymes exhibit turnover with this compound (Table 3) suggests that there is some partitioning between product release and inactivation, but with low partition ratios. Interpolation of the data listed in Table 2 for the other three enzymes reveals that whereas 50% inhibition of AGAO requires ~3.5 equivalents of **2**, 50% inhibition of BPAO and ECAO requires a 6.5-7.0-fold excess of **2** over active sites. Time-dependent studies reveal that a 2-fold excess of **2** effects 50% inhibition of PPLO in 0.5 min. Inhibition of the other enzymes occurs more slowly: PSAO has a $t_{1/2}$ value of 7.5 min using a 3-fold excess of **2**, AGAO has a $t_{1/2}$ value of 15

minutes at a 4.6-fold excess, while EPAO has a $t_{1/2}$ value of 6 min at a 9-fold excess of inhibitor. Whereas a 10-fold excess of **2** over BPAO active sites results in a rapid drop ($t_{1/2}$ of 3 min) to a 32% activity plateau, suggesting substantial turnover, a 20-fold excess of inhibitor brings the plateau level of activity down to 5% (with a $t_{1/2}$ of 2.5 min).

More extensive data obtained in the case of AGAO and BPAO permitted both the construction of partition ratio plots and the determination of kinetic parameters by Kitz and Wilson analysis [146]. Accordingly, the calculated partition ratios were 60 ± 9 and 43 ± 5, while K_I values were 12.0 ± 0.8 μM (k_{inact} = 0.188 ± 0.003 min^{-1}) and 220 ± 40 μM (k_{inact} = 1.26 ± 0.11 min^{-1}), respectively, for AGAO and BPAO. For both these enzymes, inhibitor **2** caused ≥ 90% reduction of the NBT signal, consistent with an inactivation mechanism that results in cofactor modification. Interestingly, for the related compound, 1,4-diamino-2-butyne (DABY), loss of cofactor redox competence as indicated by the NBT assay occurred in the case of BPAO but not AGAO.

UV/Vis spectroscopic analysis of the nature of inhibition induced by **2** was pursued with BPAO as a representative enzyme (Figure 13). Immediately upon the addition of **2** to the protein, a short-lived band is observed at 600 nm in place of the starting cofactor absorption at 480 (Figure 13b), which is most likely attributed to a highly conjugated derivative of the TPQ cofactor. This complex then decays into another species with a strong absorbance in the 390 nm region (Figure 13b → f). Assays of the 3 hour sample revealed no remaining kinetic activity.

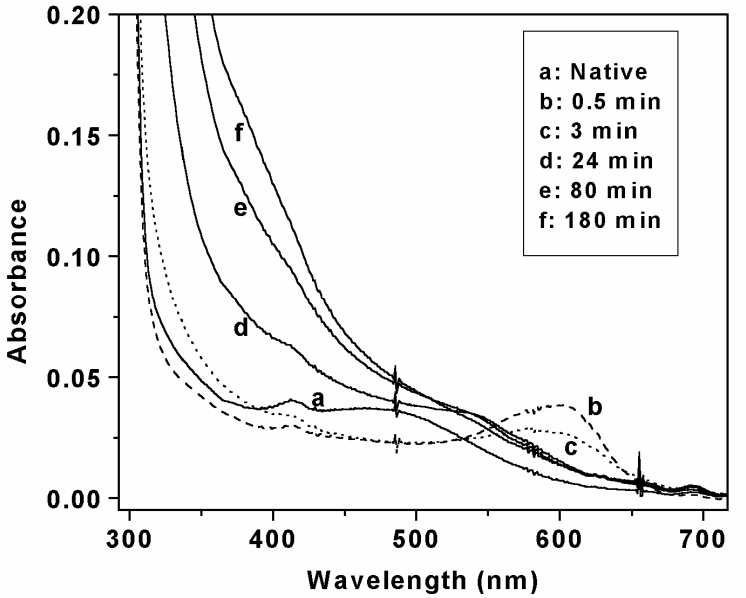

Figure 13: BPAO (8.5 μM) inhibition with compound **2** (150 μM). Feature at 410 nm is likely a trace amount of catalase.

Observations With 1,6-Diamino-2,4-hexadiyne (**3**)

Considerable inhibition is seen for all enzymes with **3**, though with differing potencies. A stoichiometric concentration of **3** inhibits BPAO by 73%, with 1.5 equivalents of inhibitor reducing AGAO by 58% and 2 equivalents reducing ECAO by 37%. For the other three enzymes, significantly higher concentrations were needed to effect inhibition (Table 2), with the overall rank order being BPAO > AGAO > ECAO > EPAO > PSAO ≥ PPLO. Partition ratio plots for AGAO and PSAO gave values of 36 ± 6 and 78 ± 6 (Figure 14), respectively.

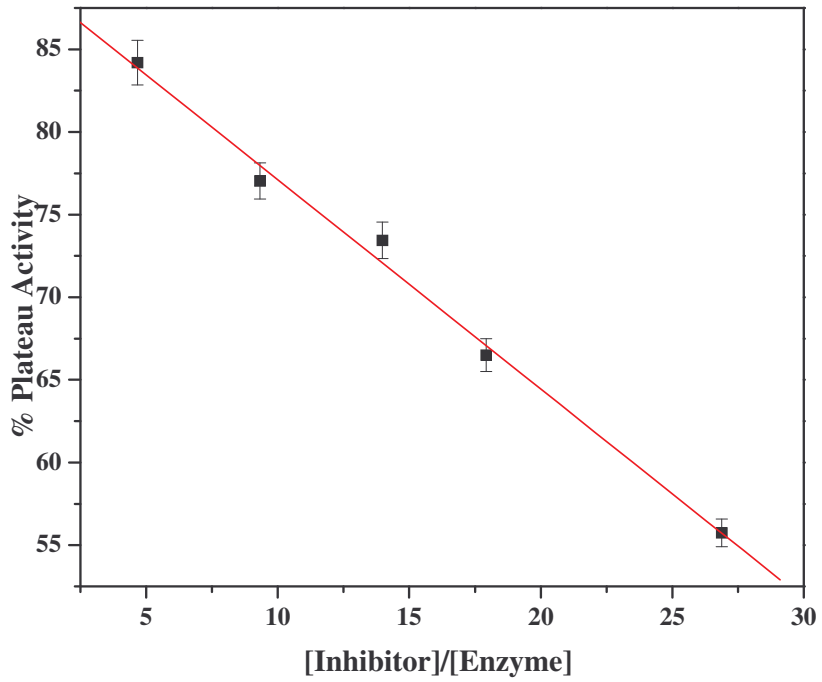

Figure 14: Partition ratio plot for 1,6-diamino-2,4-hexadiyne and PSAO. The partition ratio is calculated by solving for the x-intercept.

Although phenylhydrazine titration of a preparation of AGAO inactivated with **3** by 96% was accompanied by a 92% loss of the ability to form the cofactor phenylhydrazone, the NBT assay on the completely inactivated preparation indicated no loss of cofactor redox competence. A 15% reduction in the NBT signal was seen for a preparation of BPAO completely inactivated by **3** (Table 4).

Time-course studies reveal interesting differences among the enzymes in the rates of inactivation by **3**. Inactivation of AGAO and PSAO exhibit marked plateau behavior within the 30 min time course of the data reported in Table 2. Using $t_{1/2}$ values as the time needed to decrease activity by half that observed at the plateau, Kitz and Wilson plots yield a k_{inact} of 0.244 ± 0.032 min^{-1} and K_I of 143 ± 22 μM for AGAO and a k_{inact} of 0.46 ± 0.01 min^{-1} and K_I of 14.8 ± 1.2 μM for PSAO. For PPLO, although increasing

amounts of **3** resulted in increasing extents of inhibition (Table 2), an even more prominent plateau behavior precluded a Kitz and Wilson analysis: the time taken to reach 50% of the eventual loss of activity did not vary much (~8 min) over an inhibitor concentration range of 10 to 35-fold in excess over active sites. Inhibition of BPAO by **3** displayed very similar behavior, with an average $t_{1/2}$ value of 4 min for inhibitor concentrations ranging from 2 to 10-fold in excess over active sites, spanning a plateaued activity from 26% down to 13%, respectively.

Spectral analysis of amine oxidase inhibition with **3** resulted in remarkably similar spectra for all enzymes. Upon immediate addition of **3** to PSAO, an adduct with λ_{max} at 440 nm appears (30 s – 12 min, data not shown), accompanied by a change of the solution color from pink to yellow, but by 2 h, a species with a strong absorbance in the 360 nm region develops, resulting in a shoulder off the strong absorption below 300 nm. The absorbance in the 360 nm region continues to increase over time, yielding the characteristic spectra seen for all enzymes inactivated by **3** (data not shown). After overnight incubation of either AGAO or PSAO with **3** at 4° C, the solutions become deep reddish brown. This, however, may well reflect the buildup in solution of a chromophoric product derived from this highly conjugated molecule, rather than the inactivated enzyme, since substantial turnover occurs in both cases.

Observations With 2-Chloro-5-phthalimidopentylamine (**4**)

AGAO, ECAO, PPLO, and PSAO display no significant loss of activity when incubated with varying amounts of this compound. However, both BPAO and EPAO activities are significantly reduced by **4** (Table 2). A sample of BPAO completely

inhibited by **4** exhibited no loss of the NBT signal, indicative of retention of cofactor redox competence in the inactivated enzyme. Time-based studies were not performed with this compound. Spectral studies of enzymes inactivated with 4 displayed a slight shoulder off the 280-nm peak (data not shown), but this may simply be indicative of a generic interaction with **4**, which itself has a strong absorbance at 300 nm. EPAO and BPAO spectral features in the visible range, including that of TPQ, did not appear affected, and thus further analysis of spectral changes seemed unwarranted.

Observations With 1,4-Diamino-2-butyne (DABY)

The relatedness of the chloro inhibitor **2** to DABY (they differ by the elements of HCl), led us to examine the interaction AGAO and BPAO with this compound. Whereas AGAO inactivated (97%) by DABY was found to retain full TPQ redox competence in the NBT staining assay, inactivation of BPAO (99%) by DABY was accompanied by ~90% loss of TPQ redox competence (Table 4).

Computer Modeling

The crystal structure obtained for ECAO derivatized by 2-HP (Figure 7) [58], provided the basis for modeling the interaction of the inhibitors in the current study with other crystallographically defined amine oxidases. As described by Wilmot *et al*. [58], the hydrazone derivative of ECAO is analogous to the substrate Schiff base (Figure 6B). Asp383 is positioned perfectly to carry out deprotonation of Cα of the substrate Schiff base (Figure 7). Tyr369 is suggested to stabilize the inhibited complex through a

hydrogen bond with O4 on the quinone ring. Tyr381, located at the bottom of the channel to the active site, acts as a "gate" and is in an "open" position.

To investigate if differences in the active-site structures of PSAO and AGAO contribute to the striking differences in behavior observed with the naphthyloxy compound **1**, the compound was modeled into the respective active sites of the native enzyme crystal structures as a Schiff base TPQ derivative in order to mimic the initial enzyme-inhibitor complex. Each respective structure was then energy minimized using Steepest Descent and Conjugate Gradient algorithms (Insight98, MSI, CA). The C5=N moiety is seen to be planar, as expected for the substrate Schiff base. In the PSAO-**1** structure (Figure 15), the only active site residues that come into close proximity with the inhibitor are Val384 and Gly385. The active site base, Asp300, is in an excellent position to abstract a Cα proton from the compound (2.49 Å away). The conserved tyrosine residue (Tyr286 in PSAO) is hydrogen bonded (2.0 Å) to O4 of TPQ, reminiscent of Tyr369 in the ECAO-2-HP crystal structure. The active site "gate", Phe298, is in the "open" position, much as Tyr381 is in Figure 7.

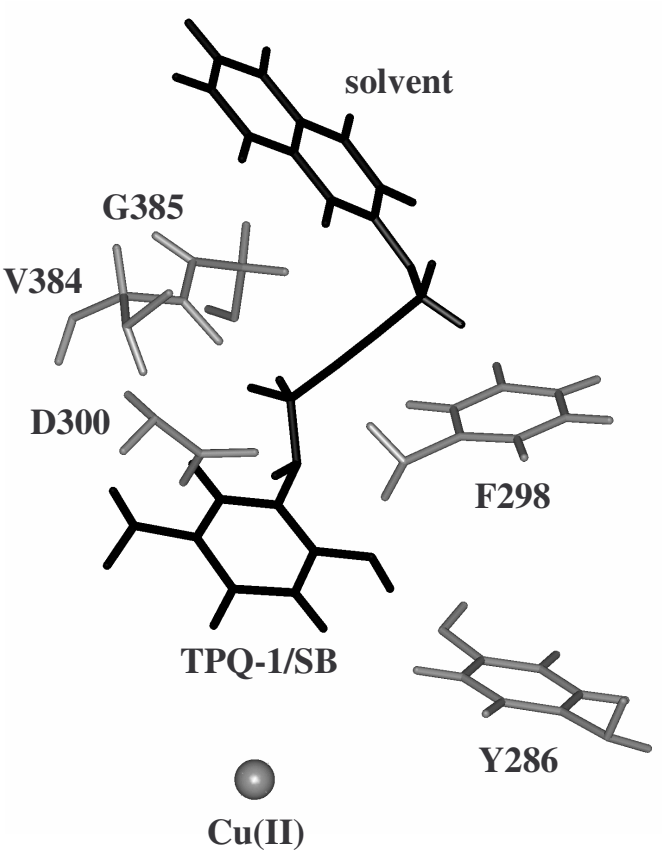

Figure 15: Minimized structure of PSAO and **1**. Hydrogen bonds are not shown for clarity. TPQ-**1**/SB: compound **1** bound to TPQ as a substrate Schiff base moiety.

Figure 16 displays the calculated structure for the AGAO-**1** Schiff base. Asp298, the active site base, is in a suitable position for proton abstraction from Cα (2.68 Å). The active site "gate", Tyr296, is in the "open" position. Interestingly, the conserved tyrosine, Tyr284, is hydrogen bonded (2.13 Å) to O2 of TPQ, and Tyr384 is hydrogen bonded (1.54 Å) to Asp298 (Figure 16A). The most notable difference between Figures 15 and 16 is the depiction of several residues that may directly interact with **1** in the latter case. Tyr296, Tyr302, and Asn381 (N381 not shown in figure) all lie in close proximity (~ 3 Å) to the inhibitor, although no direct interactions were detectable in the model.

Residues Trp359 (from β ribbon on Arm I, at entrance to channel), Trp168, Phe105, Tyr302 and Tyr307 (Figure 16B) appear to outline a hydrophobic pocket, which is observed to easily accommodate the naphthyl ring. In addition, it appears that Phe105 and Tyr302 are in a good position to form π-stacking interactions with the naphthyl ring of **1**. The AGAO-**1** model was minimized to a greater degree than that of the PSAO-**1** model in order to determine if the apparent π-stacking interactions would be more clearly observed in a highly-refined structure. The average distance of these residues from the naphthyl ring is approximately 4.0 Å. Although clear π-stacking interactions are not resolved in the model, given the proximity of these aromatic residues to the naphthyl ring, such interactions may be present in the enzyme-inhibitor complex in solution [147]. Figure 17 depicts the AGAO-TPQ-**1**/SB energy minimized complex in two additional views to further illustrate the packing of residues around the inhibitor in the active site channel. Both of these views (Figure 17A and B) are from the surface of the protein, as if looking downward on the active site channel. The tight packing of residues around **1** observed in Figure 17A does not occur in the PSAO-TPQ-**1**/SB model.

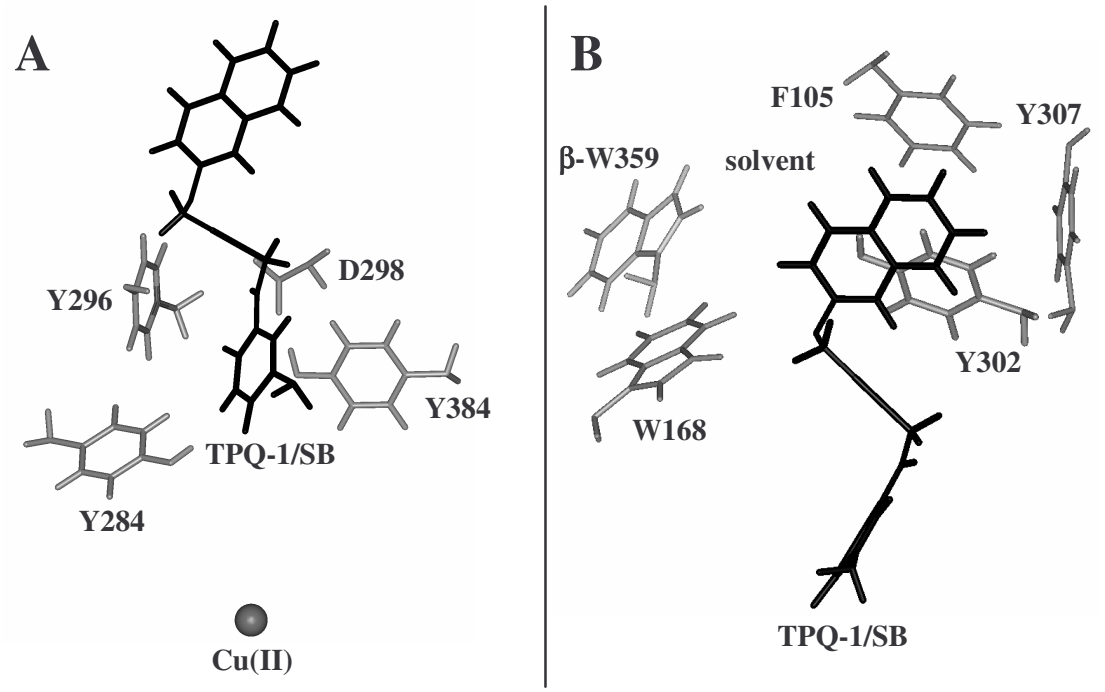

Figure 16: Minimized structure of AGAO and **1**. TPQ-**1**/SB: compound **1** bound to TPQ as a substrate Schiff base moiety. (A) Key interactions with TPQ-**1**/SB as described in text. (B) Hydrophobic pocket accommodating the naphthyl ring of **1**. The TPQ-**1**/SB moiety is rotated counterclockwise to illustrate the planarity of the Schiff base species. Residues in panel A are not shown for clarity.

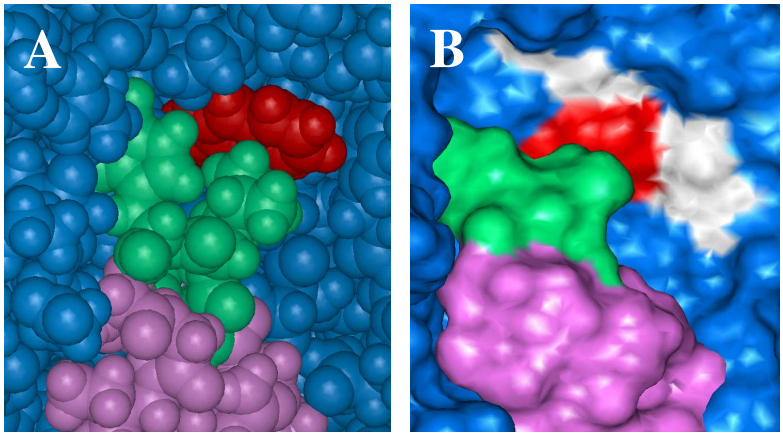

Figure 17: Surface accessibility views of the AGAO-TPQ-**1**/SB complex. (A) CPK representation of the packing of active site channel residues around the TPQ-**1**/SB complex. (B) Solvent accessibility (Connolly surface) calculation of panel A using a probe radius of 1.4 Å (Insight98, MSI, CA). Blue: monomer 1. Purple: β arm of monomer 2. Green: residues of β arm forming entrance to channel. Red: the naphthyl ring of the TPQ-**1**/SB complex. White: F105 and β-W359, respectively.

To test the hypothesis that TPQ accessibility may be important in determining compound selectivity, solvent accessibility calculations were performed for two known enzyme structures (PSAO and AGAO), one homology structural model (PPLO), and one enzyme inhibitor complex (ECAO-2-HP, Figure 7). Active site accessibility varies quite dramatically among these species. Although active site channel sizes for PSAO and AGAO are comparable, TPQ is more clearly visible from the surface in PSAO when respective gate residues are omitted from the model (data not shown). The TPQ accessibility among these four enzymes qualitatively follows the rank order PPLO > PSAO ≥ AGAO > ECAO. The open accessibility of Tyr/TPQ478 in PPLO, as predicted by the amino acid sequence based model [85], may help explain why PPLO can oxidize substrates ranging from short chain amines to pentapeptides [85,148]. As previously reported for the ECAO 2-HP structure, the tip of the pyridine ring can be seen protruding into the active site channel (Figure 7), and TPQ was determined to be basically inaccessible to solvent without substantial movement of several side chains [16,58]. In contrast, due to the small size of the active-site "gate" in HPAO (Ala317), our calculations (data not shown) indicate that both TPQ and the active-site base (Asp319) are solvent accessible in the crystal structure [50]. It should be noted that subsequent to our initial report on TPQ accessibility [62], more detailed solvent accessibility calculations were performed on the seven CuAO crystal structures in order to further explore the relationship between substrate specificity and active site channel dimensions (Figure 3). These calculations are in excellent agreement with our original results.

Discussion

Amine oxidase inhibition has been extensively studied, but no systematic comparison among different amine oxidases has been conducted to determine if selective inhibition is feasible. Using six different CuAOs, four compounds that were shown in preliminary studies to inactivate BPAO [133] were found here to inhibit the various enzymes with significantly different potencies and selectivities.

As a first approximation, one might expect some correlation between the efficiency of substrate activity (k_{cat}/K_M) (Table 1) and the efficiency of inactivation (k_{inact}/K_I), although little or no substrate turnover is observed when partition ratios approach zero. Differences in the turnover efficiency will reflect in part the differences noted among the active-site channels that govern accessibility to TPQ as a function of substrate/inhibitor size and shape. There are also crucial stereochemical issues governing turnover in terms of the orientation of the catalytic base with respect to that of the substrate/inhibitor when bound in Schiff base linkage to the TPQ cofactor. For any given enzyme-inhibitor Schiff base complex, the catalytic base will likely be positioned for preferential removal of either the *pro*-R or *pro*-S Cα proton. Likewise, if there is a Cα methyl group, only one of the two enantiomers will be processed. The finding that different amine oxidases display opposite stereochemical preferences for the same substrates [149] is strong evidence that the respective active-sites engender significant differences in binding modes, consistent with our observations of rank order reversals in the inhibitory activity of the four compounds studied.

Mechanism-based inactivation can result either from covalent derivatization of the TPQ cofactor in a manner that precludes reoxidation, or from covalent attachment to residues in or near the active site that block access of substrate. In the latter regard, inactivation of *Aspergillus niger* AO [150] and grass pea AO [151] by DABY is proposed by Frebort *et al*. to reflect conjugate addition of the aminoynal turnover product to a nucleophilic residue near the entrance to the channel, resulting in an adduct that cyclizes to a pyrrole. This residue has been implicated as Lys356 in *Aspergillus niger* AO [150] and glutamate in grass pea AO [151], and homology modeling suggests that Lys113 would be the target in PSAO [151]. Further evidence that covalent modification of residues close to the substrate channel can result in inactivation was obtained in the case of the recombinant phenethylamine oxidase from AGAO, where a lysine chemical modification agent (NBD-F) was found to selectively modify the channel residues Lys184 and Lys354 [152].

With this background, we can begin to interpret the findings of the current study. Compound **1** will be presented last, as further studies by our laboratory with a family of compounds derived from **1** were performed based on the unique selectivity differences reported above. Results obtained with the chloro inhibitor **2** show that it is readily processed by all six amine oxidases studied, with good substrate activities relative to benzylamine in the three cases measured (Table 3) and highly efficient inactivation occurring in the cases of PPLO ~ PSAO ≥ EPAO > AGAO > BPAO ~ ECAO (Table 2). The NBT assay performed for preparations of AGAO and BPAO inactivated nearly completely by **2** reveals a level of TPQ redox competence consistent only with the small fraction of active cofactor remaining (Table 4). Figure 13 supports modification of the

cofactor, as the transient chromophore at 600 nm is attributed to a conjugated complex formed between TPQ and **2**. Despite the NBT result, we cannot exclude the possibility that inactivation may also involve an active site residue, in line with Abeles' proposal of alkylation by an allenic intermediate generated upon expulsion of chloride following C_α-proton abstraction [122,123].

Despite the relatedness of **2** to DABY (by the elements of HCl), our finding that AGAO inactivated by DABY retains full TPQ redox competence in the NBT assay supports a side-chain modification mechanism of inhibition in this case, with little or no reaction with TPQ. Inactivation likely involves cyclocondensation onto a nucleophilic residue at or near the active site channel, as demonstrated by Frebort *et al*. for DABY inactivation of *Aspergillus niger* AO and grass pea AO [150]. However, inactivation of BPAO by DABY was accompanied by loss of TPQ redox competence, in agreement with what was found for **2** with both BPAO and AGAO. These results are most compatible with two different mechanisms of inactivation by DABY. The mechanism of TPQ modification by DABY in BPAO may be related to how **2** modifies the cofactor for both BPAO and AGAO, since one could envision loss of HCl at a stage subsequent to TPQ Schiff base formation with **2** to give the same intermediate arising from DABY. Even if the mechanisms of inactivation by **2** and DABY do converge in the case of BPAO, this cannot be the case at least for AGAO.

The diyne inhibitor **3** is generally less potent than the chloro inhibitor **2**, though the selectivities among the six amine oxidases follow a markedly different trend: BPAO > AGAO > ECAO > EPAO > PSAO ≥ PPLO (Table 2 and kinetics). Substrate turnover for **3** is particularly low with AGAO and particularly high with PSAO, consistent with

the lower partition ratio measured in the former case (36) and higher in the latter case (78; Figure 14). Despite the inactivated preparation of AGAO being incapable of reaction with phenylhydrazine, the NBT staining results for both AGAO and BPAO (Table 4) indicate respectively full or nearly full redox competence of the TPQ cofactor following this denaturing assay. Although one might be inclined to interpret the dramatic spectral changes observed in terms of TPQ modification, especially the initial absorbance at 440 nm seen with PSAO (data not shown), a unified mechanism for the various enzymes would then require hydrolytic regeneration of redox-active TPQ in the NBT assay, at least in the case of AGAO and BPAO. Thus, a more conservative interpretation is that inactivation reflects covalent modification of active-site or channel residues, with the spectral changes arising from chromophores generated upon rearrangement of the diyne moiety.

The phthalimide inhibitor **4** shows significant turnover by all enzymes tested (Table 3), though significant inhibition was seen only with the two mammalian plasma amine oxidases (Table 2). The mechanism of inactivation by this compound most likely involves alkylation of a protein side-chain by the 2-chloroaldehyde turnover product, based on the result of the NBT assay with BPAO indicating no permanent cofactor modification. The selective vulnerability of the mammalian enzymes suggests that they may contain active site features that differ considerably from the other amine oxidases.

By far the most intriguing results of this study were observed with the naphthyloxy compound **1**. In the case of AGAO, stoichiometric inactivation is obtained (Table 2), and compound turnover does not occur (Table 3). The findings that the inactivated enzyme complex cannot be derivatized by phenylhydrazine and that its

spectrum lacks the 480 nm TPQ absorption band (Figure 12a), suggests a modification of the TPQ cofactor and occupation of the active site cavity. However, since subjection of the inactivated enzyme to the NBT assay (Table 4) revealed that TPQ is not permanently damaged, it appears that derivatization of TPQ by **1** represents a form that becomes subject to hydrolysis upon denaturation of the protein in the NBT assay. It is possible that the inactive AGAO-**1** complex represents merely either (i) a substrate Schiff base that cannot be transformed because of a misorientation between the catalytic base and the αC, or (ii) a product Schiff base that cannot be hydrolyzed because of inaccessibility of solvent water to the imine linkage. Alternatively, the observed result may reflect rearrangement of the product Schiff base to a more stable, yet ultimately hydrolysable derivative of TPQ that may or may not also involve an active site residue. Structural information on the inactivated enzyme will be needed to resolve these ambiguities.

In the case of PSAO, the naphthyloxy compound **1** is an excellent substrate (Table 3) as well as an inactivator. Inhibition thus most likely reflects partitioning of an electrophilic aldehyde turnover product toward alkylation of the active site channel. Assuming the covalently-bound form of **1** has the same extinction coefficient as free **1**, one calculates from the spectrum (Figure 12b) that there are ~14 molecules of **1** bound to this preparation of PSAO that still has 75% activity. It appears that the reactive turnover product can bind to surface side-chains, such as the 32 solvent accessible Lys residues suggested by Frebort *et al*. [151], in a manner that does not interfere with enzyme function unless there is modification of a side-chain within or at the entrance to the active site.

The computer modeling results on the PSAO-**1** Schiff base (Figure 15) suggest that **1** is an excellent substrate for PSAO because the only residues in close proximity to the bound inhibitor are Val384 and Gly385, and there are no unfavorable non-bonded interactions. The "gate" residue, Phe298, is rotated out of the way leaving room for the aldehyde product to exit after conversion of the substrate to product Schiff base and hydrolysis of the latter. In contrast, computer modeling of the AGAO-**1** Schiff base (Figure 16) reveals several intriguing differences. The hydrogen bond between conserved Tyr284 and O2 of TPQ is curious because the hydrogen bond of the conserved tyrosine in ECAO [115] and HPAO [82] is purported to involve O4 of TPQ during normal turnover. We can infer that this hydrogen bond also exists for other AO species, as Figure 15 suggests. The significance of the hydrogen bond with O2 instead of O4 is not known, nor is the significance of the hydrogen bond between Tyr384 and the active site base, Asp298. It may just be that these are artifacts of the minimization process. The close proximity of nucleophiles Asn381, Tyr296, and Tyr302 may implicate these residues in trapping an intermediate species during turnover. The most striking difference between the AGAO-**1** and PSAO-**1** models is the presence of several aromatic residues near the naphthyl ring in the former case that may potentially be a source for stabilization due to π-stacking interactions, though this was not definitive in the static model depicted in Figure 16B.

The work reported herein has been published in the *European Journal of Biochemistry* [62]. The importance of this comparative screening study comes to light when considering the development of selective inhibitors of the copper-containing amine oxidases. This report was one of the first to demonstrate such practical selectivity.

Furthermore, this was the first evidence put forth that substantiated the belief that distinctions among the active sites were responsible for differentiating the chemical interactions between the inhibitors and selected enzymes. The unique difference in behavior with the naphthyloxy compound **1** seen between AGAO and PSAO can be understood at least in part from the differences in active-site interactions revealed by the computer modeling studies. This speaks directly to the importance of subtle differences in the active sites of these enzymes, as channel sizes are quite comparable between AGAO and PSAO (Figure 3).

In addition to the unique differences noted with compound **1**, several other interesting observations can be made with the other compounds studied. For example, if we compare inhibitor potency for the chloro compound **2**, we find that PSAO and PPLO are both substantially more sensitive to this compound than are AGAO and ECAO, whereas the reverse is true for the diyne compound **3**. Furthermore, these four enzymes all display similar behavior with the phthalimide **4**. It is clear that these trends depart from what would be predicted based strictly on TPQ accessibility (Figure 3). In addition, in some cases, gate residues must move in order for the inhibitor to bind, as was observed in the ECAO-2-HP crystal structure (Figure 7) and is further indicated by the AGAO and PSAO model structures with the naphthyloxy compound **1** (Figures 15 and 16). These observations indicate that factors such as the dynamics of "gate" residues, the dimensions/shape of the substrate channel and binding pocket, as well as the orientation of residues that can be alkylated, play at least as important a role in determining inhibitor selectivity as does TPQ accessibility.

The results presented here for DABY illustrate the point that various amine oxidases may interact with mechanism-based inhibitors by multiple mechanisms: although inhibition of BPAO by DABY is associated with TPQ modification, it appears that AGAO, PSAO, grass pea AO, and *Aspergillus niger* AO are inhibited by a mechanism distinct from cofactor alteration. This is even more fascinating considering that the closely related chloro inhibitor **2** appears to inactivate both AGAO and BPAO by a similar cofactor modification mechanism. Thus, subtle differences between the inhibitors and between the respective active sites can not only underlie differences in selectivity but also differences in the mechanism of inhibition.

In an attempt to more clearly understand the molecular factors that govern inhibitor potency, we subsequently pursued the particularly striking example of selective irreversible inhibition seen in AGAO by screening a family of compounds derived from inhibitor **1**. One of the intrinsic aspects of this latter report was to focus specifically on the in depth kinetic analysis (partition ratios) of AGAO with this family of inhibitors. This analysis, coupled with crystallographic studies performed in collaboration with Dr. Hans C. Freeman (University of Sydney), allowed us to experimentally probe the role of the hydrophobic pocket identified from the computer modeling studies in determining inhibitor potency for this enzyme. The main results from this latter paper will be presented below.

Differential Inhibition by a Family of 4-(Aryloxy)-2-butynamines

Through our continued collaboration with Dr. Lawrence M. Sayre (Casewestern Reserve University, Cleveland, OH), a series of 4-aryloxy analogues of **1** were

synthesized in hopes of achieving potent and selective inhibition of the various copper amine oxidases.

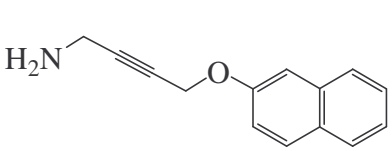

4-(2-naphthyloxy)-2-butyn-1-amine (**1**)

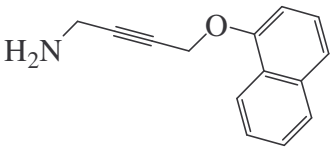

4-(1-naphthyloxy)-2-butyn-1-amine (**1a**)

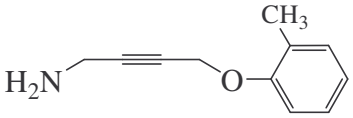

4-(2-methylphenyloxy)-2-butyn-1-amine (**1b**)

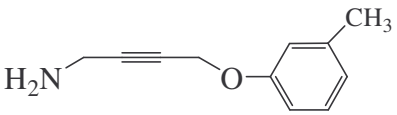

4-(3-methylphenyloxy)-2-butyn-1-amine (**1c**)

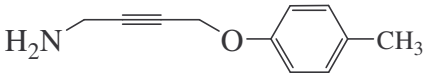

4-(4-methylphenyloxy)-2-butyn-1-amine (**1d**)

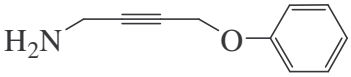

4-(1-phenyloxy)-2-butyn-1-amine (**1e**)

Figure 18: A series of 4-aryloxy inhibitors.

In depth kinetic screening on AGAO, BPAO, EPAO, rhDAO, PPLO, and PSAO with these five additional compounds (Table 5) was performed by Kimberly M. Hilmer (O'Connell) under my guidance. Based on the data in this report [63], each compound effectively inhibited select amine oxidases to varying extents but were always most potent against AGAO. The α-naphthyl isomer **1a** was about half as potent against AGAO as the β-naphthyl isomer **1**. As in the case of compound **1**, no detectable oxidation of compound **1a** by AGAO was observed. The *ortho*- (compound **1b**), *meta*- (compound **1c**), and *para*- (compound **1d**) methylphenoxy analogs and the unsubstituted

phenoxy compound **1e** were all at least ten times less effective than compound **1a** toward AGAO. However, **1c**, **1d,** and **1e** were considerably more potent than **1b**. Therefore, the inhibitory potency of the compounds for AGAO followed the trend: **1 > 1a > 1c ≈ 1d ≈ 1e > 1b** (Table 5).

Table 5: Potency of CuAO Inhibition

Enzyme	Inhibitor	$IC_{50}(\mu M)$	Partition Ratio
AGAO	1	-	0[a]
AGAO	1a	7	1[b]
AGAO	1b	97	28 ± 5[b]
AGAO	1c	47	12 ± 2[b]
AGAO	1d	48	12 ± 1[b]
AGAO	1e	50	12 ± 1[b]

[a] Value reported in initial paper [62]. [b] Values reported in subsequent paper [63].

To gain an insight into the structural basis of the inactivation of AGAO by this class of inhibitors**,** crystal structures of AGAO derivatized by compounds **1** and **1d** were refined at high resolution (Figures 19 and 20). These structures identify a novel and completely unexpected modification of the TPQ cofactor. From the bent geometry of the electron density corresponding to the TPQ-inhibitor moiety (Figure 19), it is clear that the TPQ is covalently attached to the middle position of the inhibitor. The new bond joined what was originally the O5 atom of the TPQ to the third carbon along the chain from the original amine group of the inhibitor (Figure 18). Subsequently, the atom types of the linking atom and the terminal atom of the inhibitor were changed to nitrogen and oxygen, respectively, to be consistent with the proposed mechanism of inhibition (see below). In both complexes, the TPQ cofactors are in the "off"-copper conformation. In both cases, the "gate" Tyr296 is in the "open" conformation (Figure 20). The naphthyloxy- and

methylphenoxy-groups have identical orientations with respect to the protein and the two inhibitors bind in an almost identical fashion (Figure 20). If the structures of the two complexes are superimposed, the chemically equivalent atoms of the inhibitors and the TPQ cofactors have a root mean square difference of 0.32 Å (Figure 19B). Furthermore, comparing the AGAO-**1** and AGAO-**1d** structures shows that there is no significant shift of any active-site residue. The terminal amino (aldehyde) groups of the inhibitors make a short contact (~ 2.5 Å) with one of carboxyl oxygen atoms of the catalytic base, Asp298. If the inhibitors have been converted to the equivalent aldehyde, as we propose below, then the close contact is consistent with a hydrogen bond. In this case, the carboxyl group of Asp298 must be protonated.

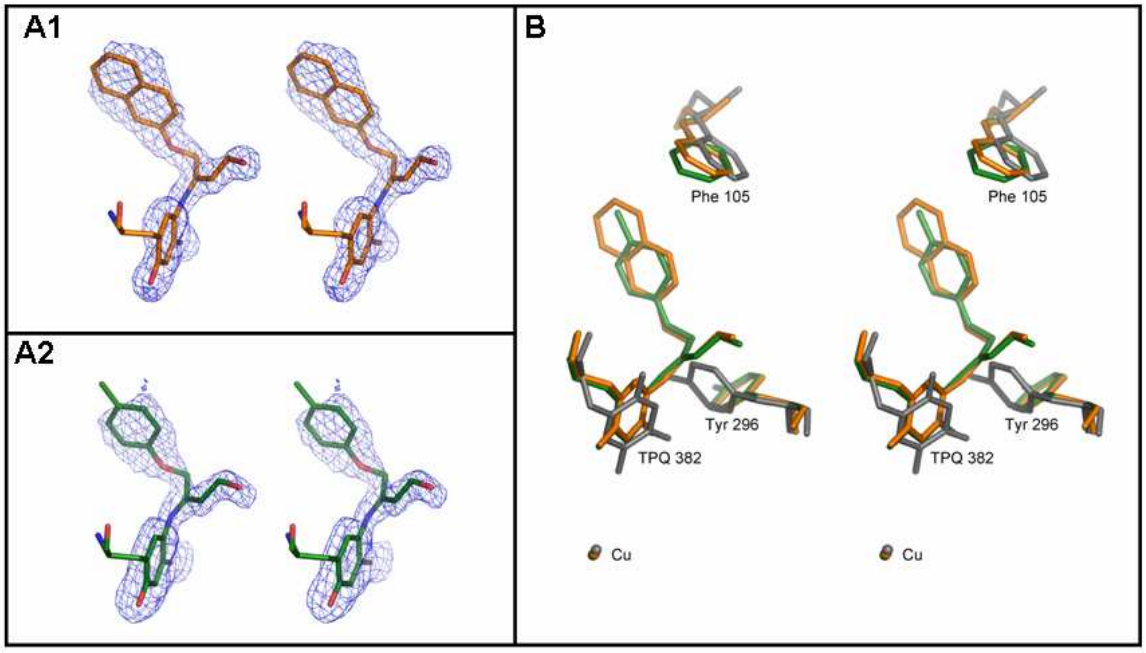

Figure 19: Electron density and stereo overlay of the TPQ/inhibitor moieties. (A1) TPQ_{AMQ}-4-(2-naphthyloxy)-2-butenal moiety. (A2) TPQ_{AMQ}-4-(4-methylphenoxy)-2-butenal moiety. Both structures have been solved to 1.7 Å resolution. (B) Stereo view of the overlayed structures of native AGAO (grey), TPQ_{AMQ}-4-(2-naphthyloxy)-2-butenal moiety (orange), and TPQ_{AMQ}-4-(4-methylphenoxy)-2-butenal moiety (green). Figure taken from [63].

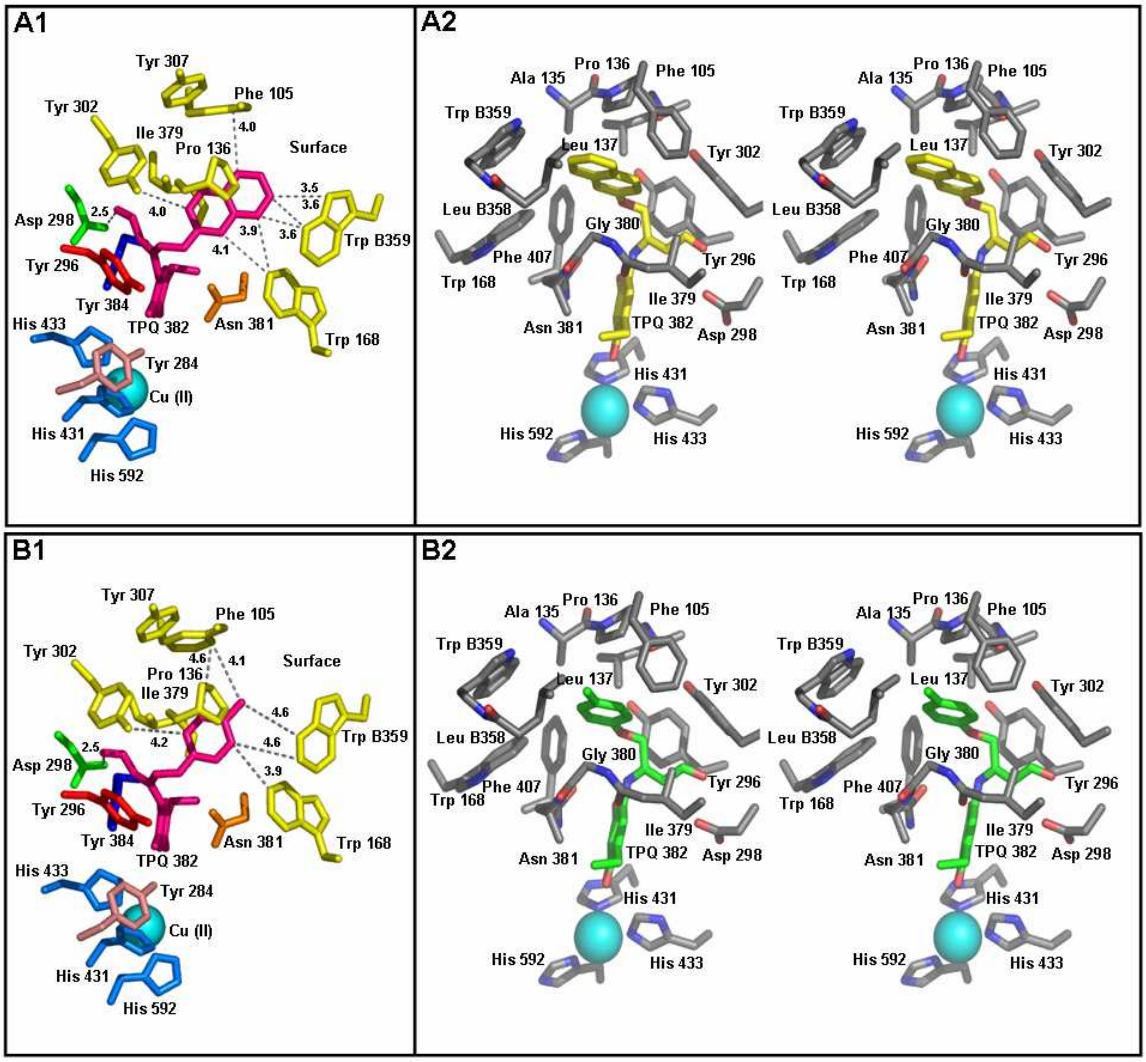

Figure 20: TPQ derivatized with two 4-(aryloxy)-2-butynamines. (A1) TPQ_{AMQ}-4-(2-naphthyloxy)-2-butenal positioned in the active site of AGAO. (A2) Stereo view of the active site of the AGAO-TPQ_{AMQ}-4-(2-naphthyloxy)-2-butenal structure. (B1) TPQ_{AMQ}-4-(4-methylphenoxy)-2-butenal moiety positioned in the active site of AGAO. (B2) Stereo view of the active site of the AGAO-TPQ_{AMQ}-4-(4-methylphenoxy)-2-butenal structure. Views shown in panels A2 and B2 are oriented differently then the views shown in A1 and B1. In panels A1 and B1, the residues composing the hydrophobic pocket are colored yellow and the TPQ/inhibitor moiety is magenta. Distances shown are from residues in the hydrophobic pocket to each respective substituent group of the 4-(aryloxy)-2-butenal moieties. In panels A1 and B1, "surface" indicates the interface between bulk solvent and the protein derived substrate channel. In panels A2 and B2, residues are colored by atom (gray, carbon; blue, nitrogen; red, oxygen) with the exception of the TPQ/inhibitor moieties in which carbon atoms are colored yellow and green, respectively. Figure taken from [63].

The naphthyloxy and methylphenoxy groups of **1** and **1d** are indeed similarly positioned within the hydrophobic binding pocket suggested previously [62] (Figures 16B and 20). Residues comprising the hydrophobic cleft, which accommodates the hydrophobic naphthyloxy and methylphenoxy moieties, can be classified according to their approximate position with respect to the common plane of the aromatic rings. Gly380, Ile379 and Trp168 lie on the "TPQ-side" of this ring plane and Ala135, Pro136, Leu137 and Tyr296 lie on the other side. Tyr302 and Phe407 lie on the edges of the aromatic rings (Figure 20). Phe105 and two hydrophobic residues, Leu358 and Trp539 (from the β-arm of the adjacent subunit), lie at the end of the channel near the inhibitors, consistent with what was observed from the computer modeling studies (Figure 16B). The positions of the residues on the β-arms of the native and complex structures are identical within the limits of precision.

Although the carbon-carbon triple bond in the reactants **1** and **1d** (Figure 18) is unreactive, the observed electron density is consistent with an adduct that would result from nucleophilic attack by the amino group of the reduced aminoquinol cofactor (TPQ_{AMQ}) at C3 of the propargyl aldehyde turnover products of **1** and **1d**. A reaction mechanism that accommodates these findings is shown in Figure 21. The initial steps in the catalysis of the inhibitor are the same as for a normal amine substrate. First, the "substrate Schiff base" is converted to the "product Schiff base" (**B→C**) facilitated by a conserved aspartate acting as a general base and abstracting a proton from the α carbon of the inhibitor. Following hydrolysis of the "product Schiff base", the highly electrophilic (at C3) α,β-unsaturated aldehyde is generated within the active site.

Subsequently, nucleophilic attack by the amino group of TPQ_{AMQ} at the C3 position (**E→F**) completed by proton transfer to C2 (**F→G**) results in formation of the final TPQ_{AMQ}-4-(aryloxy)-2-butenal derivatives observed in the respective crystal structures (Figures 19 and 20). Although the observed electron density would also be consistent with adduction of the α,β-unsaturated aldehyde turnover product to the triol form of the reduced cofactor rather than TPQ_{AMQ} (we cannot distinguish -O- from -NH-), it is not clear what scenario would lead to such an alternate adduct.

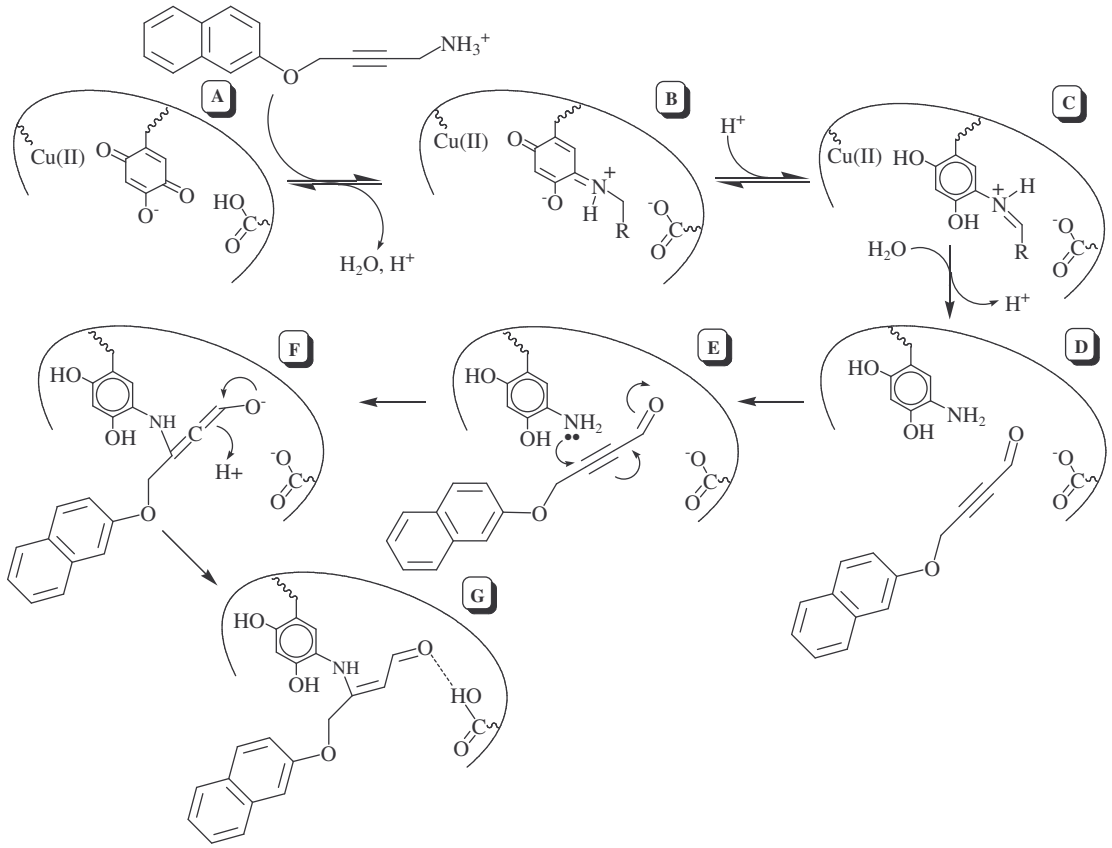

Figure 21: Proposed mechanism of inhibition for 4-(2-naphthyloxy)-2-butyn-1-amine (**1**) and related compounds.

In order to permit the C3 of the product aldehyde to get within a reasonable distance for reaction with TPQ, some active-site rearrangement must occur. This might simply involve the aldehyde product moving ~ 3.5 Å down the channel until the nucleophile and its target are in suitable proximity (Figure 22). Whatever the mechanism, it is particularly efficient for compound **1**, for which the product of every turnover event then forms an inactivation event adduct.

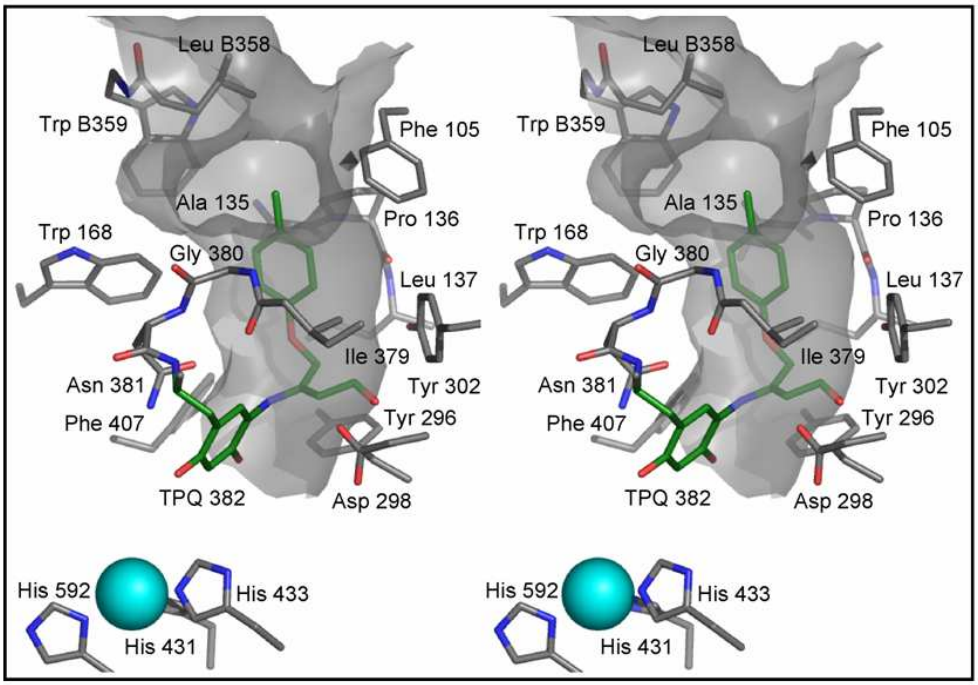

Figure 22: Stereo view of the active site channel in the AGAO-TPQ$_{AMQ}$-4-(methylphenoxy)-2-butenal structure. Atoms are colored as described in Figure 20. The active site channel is shown in gray. Figure taken from [63].

Given the relationship of each 4-(aryloxy)-2-butenal compound to the hydrophobic pocket in AGAO (Figures 20A, 20B, and 22), it is plausible that the extent of van der Waals interactions between pocket and inhibitor may be the main determinant of inhibitor effectiveness. The inhibitors that contain the largest substituents (**1** and **1a**)

are also the most potent against AGAO. Compared with the phenoxy and methylphenoxy substituents, the naphthyloxy group makes more extensive van der Waals interactions with the hydrophobic pocket. The 2-fold weakening of the α-naphthyloxy relative to β-naphthyloxy inhibitor might simply reflect a better steric fit of the more linearly extended β-naphthyl substituent (Figure 18). This suggests that the interactions of the substituent group with residues in the active site channel, namely those in the hydrophobic binding pocket, may play a key role in determining overall potency of inhibition for AGAO by a wide range of structurally diverse inhibitors.

While the phenoxy- and methylphenoxy- analogs (compounds **1c, 1d, 1e**) were not stoichiometric in their potency, they displayed decreasing potency in the order **1c ~ 1d ~ 1e > 1b**. Presumably, the product aldehydes can diffuse from the active site with varying probability. The greater potency of the unsubstituted phenoxy and the *meta*- and *para*-methylphenoxy analogs with respect to the *ortho*-methylphenoxy (**1b**) compound suggests that a more or less linearly extended methyl substituent group can project into the hydrophobic pocket in AGAO in a manner that makes more favorable van der Waals contacts for the phenoxy family of inhibitors. Yet, when comparing **1b** to **1a**, it appears that the phenyl ring interacts more favorably with residues in the hydrophobic pocket (Trp168 and Trp359) than does the *ortho*-methyl substituent.

In terms of the other structurally characterized amine oxidases, a similar hydrophobic pocket was not identified in the modeling studies of **1** with PSAO [62]. This may explain why the 4-(aryloxy)-2-butynamine inhibitors induce only infrequent inhibition of PSAO. PSAO inhibition is proposed to arise by turnover-product aldehyde modification of surface exposed Lys residues, obstructing access of substrate to the active

site [62,151]. Likewise no such hydrophobic binding pocket exists in PPLO, as the channel in this enzyme is extremely open [52] and any substrate analog from this family of compounds interacting with TPQ is likely to be in contact with solvent, as opposed to any residues in the active site channel. However, the lack of a hydrophobic binding pocket in PPLO does not explain the effectiveness of these compounds towards this enzyme in terms of the relatively low partition ratios and IC_{50} values observed [63]. BPAO also lacks a hydrophobic pocket, and contains a relatively large channel (Figure 3). Unlike PPLO, however, structural analysis shows the presence of a wall, extending from the active-site to the protein surface, formed mainly by hydrophobic residues belonging to the D4 domain (F388, L468, M467, F393, A394, P396, L424, W412, F414, Y392) [53]. Despite the presence of this hydrophobic wall, BPAO displays radically different inhibitor potency with the compounds in Figure 18 [63].

Along these lines, interactions between respective enzymes and inhibitors may not be explained solely by contacts within the active site channel. Despite the observations that for AGAO there exists a likely correlation between an inhibitor's capacity to fill the hydrophobic pocket and its potency, it is clear that these same distinctions do not apply to other CuAOs. As observed in the cases of two amine oxidases lacking this hydrophobic binding pocket, PSAO and PPLO behave very differently when treated with 4-(aryloxy)-2-butynamines. The relatively potent inhibition of PPLO may actually arise as a *direct result* of its relatively solvent-accessible TPQ cofactor, although the true nature of substrate binding interactions within this enzyme remains unclear at this time. Furthermore, if the same TPQ_{AMQ}-4-(aryloxy)-2-butenal adduct observed in AGAO (Figure 21) is responsible for inactivation of PPLO, it is not

clear why it is resistant to either oxidation or hydrolysis (see below), given that it is most likely directly exposed to solvent. The observation of ~ 35% phenylhydrazine reactivity of the fully inhibited denatured PPLO may suggest a unique mode of inactivation for this enzyme [63].

The covalent modification of TPQ by **1** and **1d** supports the lack of phenylhydrazine reactivity of fully inhibited samples of AGAO, as well as the fact that extensive dialysis did not result in any restoration of activity. However, it does not explain why full redox competency of the TPQ moiety, as indicated by the NBT assay, was restored when the inactivated enzymes were denatured [62,63]. Two possible reaction mechanisms could explain the reversibility of inhibition observed upon enzyme denaturation (Figure 23). Mechanism A involves the oxidation of the TPQ_{AMQ}-4-(aryloxy)-2-butenal moiety to a Schiff base which is then hydrolyzed in a similar manner as the TPQ_{IMQ} (Figure 6, **F**→**A**) yielding TPQ_{OX} and 3-amino-4-(aryloxy)-2-butenal. In contrast to mechanism A, where hydrolysis follows oxidation, mechanism B involves an initial enamine hydrolysis (releasing 4-(aryloxy)-3-oxobutanal) followed by oxidation of the resulting TPQ_{AMQ}. The similar structural evidence obtained with compounds **1** and **1d** in AGAO suggests that the same mechanisms for both inhibition and denaturation-dependent reversibility occur for all the 4-(aryloxy)-2-butynamine compounds studied (Figures 21 and 23). A possible source for stabilization of the modified quinone in the native folded enzyme is the formation of a hydrogen bond between the aldehyde functional group of each TPQ-inhibitor adduct and the catalytic base Asp298 (Figures 20 and 21). Such stabilization might protect the modified cofactor against the mechanisms proposed in Figure 23.

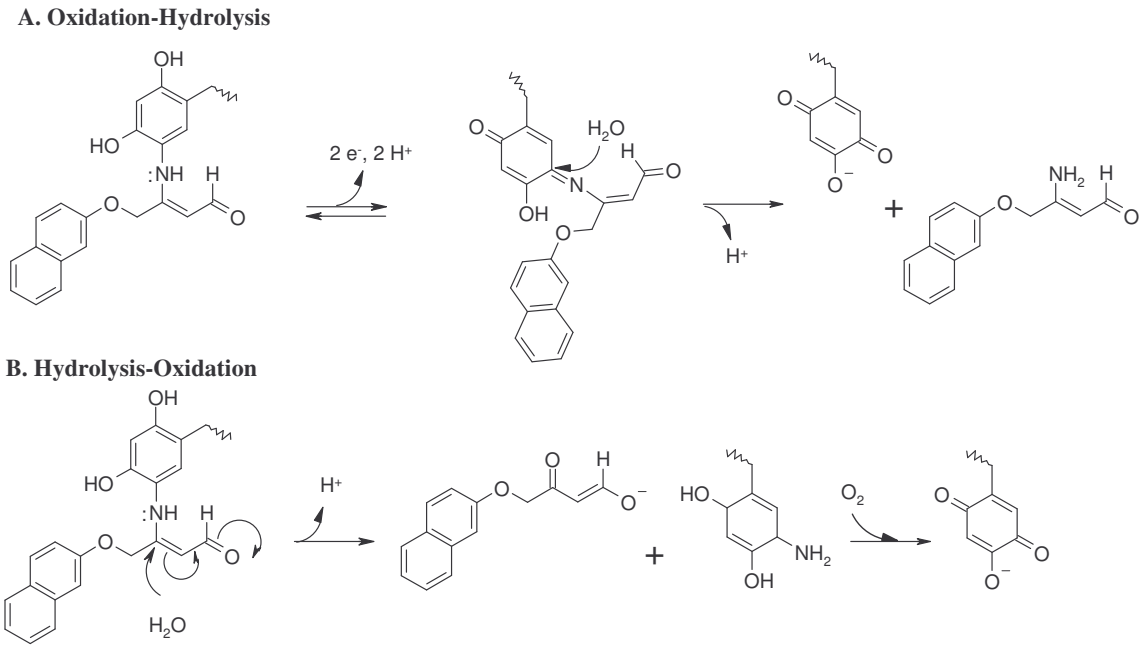

Figure 23: Proposed mechanisms for recovery of TPQ redox integrity.

Conclusions

The importance of this comparative screening study comes to light when considering the development of selective inhibitors of the copper-containing amine oxidases. The clear advantage of mechanism-based inhibitors is that selectivity can arise both from variations in the initial non-covalent binding of the inhibitors with the enzymes, as well as from variations in the ensuing chemistry [153]. Our initial report was one of the first to demonstrate such practical selectivity. Furthermore, this was the first evidence put forth that substantiated the belief that distinctions among the active sites were responsible for differentiating the chemical interactions between the inhibitors and selected enzymes. These observations indicated that factors such as the dynamics of

"gate" residues, the dimensions/shape of the substrate channel and binding pocket, as well as the orientation of residues that can be alkylated, play at least as important a role in determining inhibitor selectivity as does TPQ accessibility. The structural analysis of AGAO complexed with inhibitors **1** and **1d** provided strong support for these conclusions. Moreover, the remarkable distinctions between AGAO and PSAO observed with this family of compounds provided the first example of a substrate analog that could serve as a potent mechanism-based inhibitor for one CuAO and a substrate for another.

The observation that the TPQ_{AMQ} species can itself act as an effective nucleophile in the covalent adduct formation described herein is unprecedented and suggests that the enzyme inactivation by other inhibitors turned over to electrophilic products may involve the TPQ cofactor rather than nucleophilic side-chains of active site or substrate channel residues. The hydrophobic binding pocket identified from computer modeling studies in AGAO was confirmed by crystal structure analysis of inhibited enzyme samples. Additionally, this binding pocket was shown to play a direct role in determining inhibitor potency with the compounds in Figure 18. This hydrophobic binding pocket was also subsequently shown to play a role in binding other compounds completely structurally unrelated to the 4-(aryloxy)-2-butynamine family. For example, the small aliphatic amine tranylcypromine (see following chapter), and molecular wires comprised of either a Ru(II)- or Re(I)-complex head group, an aromatic tail group, and an alkane linker were found to lie in the same plane within the active site as compounds **1** and **1d** [154]. Structural analysis reveals that the inhibitor is capable of making contacts of 3–5 Å with up to nine residues in the active-site channel and pocket, including the five near-neighbor residues identified in the computer simulations of AGAO and compound **1** [62]. These

reversible inhibitors bind to AGAO with nanomolar affinity, and it can be surmised that the interactions between these molecular wires and the hydrophobic binding pocket serve as the predominant forces for such potent binding. Furthermore, the position of the dimethylaniline group in relation to TPQ was found to be the same as that of the methylphenoxy moiety in the covalent adduct of AGAO with the inhibitor **1d** [154]. In other complexes of AGAO with covalently bound aromatic inhibitors, the aromatic ring is found to lie in the same position (D.B. Langley, A.P. Duff, H.C. Freeman, and J.M. Guss, University of Sydney, unpublished results). Thus it is apparent that the hydrophobic binding pocket in this enzyme plays a crucial role in determining inhibitor potency for a broad range of amine analogues. The role of this pocket in normal substrate amine recognition is unknown, although it may be expected that interactions between the substrate and residues comprising this pocket may allow for the oxidation of certain aromatic amines, such as the preferred substrate β-phenylethylamine.

CROSS REACTIVITY BETWEEN THE COPPER AMINE OXIDASE AND MONOAMINE OXIDASE FAMILIES AND THE DEVELOPMENT OF SELECTIVE MECHANISM-BASED INHIBITORS

Introduction

As stated in the previous chapter, a significant aspect of our interest in CuAOs is the development of selective mechanism-based amine oxidase inhibitors. The major advantage with mechanism-based inhibitors is two-fold: (1) *in vivo* inhibition is often long acting because recovery of activity requires new protein synthesis; and (2) these types of compounds offer a second level of selectivity through their ability to reversibly inhibit several enzymes, with long-lasting effects occurring only on the specific enzyme that is irreversibly inactivated [146]. Mechanism-based inhibition of copper amine oxidases has been extensively studied based on the strategy of creating substrate analogues that contain either unsaturation or halogen substitution at the β position. This approach enables the formation of an electrophile formed upon Cα proton abstraction from the substrate Schiff base species, and has been quite successful in designing several selective AO inhibitors, as summarized in the previous chapter [62,125,127]. The problem with designing such primary amine analogues concerns is the potential for cross-reactivity with enzymes that carry out the same overall chemistry ($RCH_2NH_2 \rightarrow RCHO$), such as the monoamine oxidase flavoenzymes A and B, located on the outer mitochondrial membrane. Previous examples of the cross-reactivity between these two families of amine oxidases have been discovered (propargylamine derivatives) [124,128-

132]. MAO enzymes catalyze the oxidative deamination of several biogenic amines, including dopamine, serotonin, norepinephrine, and tyramine, which are also oxidized by at least some CuAOs. Substantial evidence indicates that MAO-A and MAO-B oxidize amines either through a single electron transfer mechanism or through a concerted covalent catalysis mechanism, both involving the FAD cofactor [1]. Regardless of which mechanism MAOs actually utilize, it is quite clear that these enzyme reactions do not utilize an imine shift (transamination) mechanism. Therefore, amine compounds capable of effecting a *transamination-specific* irreversible modification should potentially inactivate only the quinone-dependent copper amine oxidase family. Such compounds would be considered excellent probes for evaluating the physiological functions of these enzymes and may even have therapeutic potential as selective inhibitors.

Due to their role in degrading neurotransmitters, MAOs have been a target for inhibition in patients suffering from depression [155]. Tranylcypromine (TCP, brand name Parnate) is a reversible MAO inhibitor administered as a racemic mixture of the two trans enantiomers 1S,2R-(+)-trans-2-phenylcyclopropylamine (Figure 24) and 1R,2S-(-)-trans-2-phenylcyclopropylamine [156,157], although (+)-TCP is ten times more potent a MAO inhibitor than (-)-TCP *in vivo* [156,158,159], and (-)-TCP causes ~ 3 times greater inhibition of synaptic catecholamine uptake [156,160]. Moises and Beckmann (1981) [159], in a study involving the efficacy of both enantiomers, showed that side effects including agitation, gastrointestinal symptoms, and loss of weight were more pronounced only in those patients treated with the (+)-isomer. TCP was also discovered to inhibit the copper amine oxidase from *Escherichia coli* [161]. Subsequent studies have resulted in utilizing TCP as a CuAO substrate analogue to examine the

reductive half reaction during catalysis in ECAO, as well as the recent determination of the ECAO-TCP crystal structure [162]. The (+)-enantiomer was only found to bind to the enzyme, and the ECAO-TCP structure was discovered to be quite similar to the ECAO-2-hydrazinopyridine structure, with both TPQ-inhibitor adducts resembling the substrate Schiff base moiety (Figure 24) [162].

The focus of this chapter is the kinetic and spectrospopic characterization of the MAO inhibitor TCP with three mammalian AOs, (EPAO, BPAO, and HKAO), one plant AO, (PSAO), one bacterial AO, (AGAO), and a yeast amine oxidase (PPLO). Furthermore, this chapter presents the exciting results of our continued collaborative efforts with Dr. Lawrence M. Sayre (Case Western Reserve University, Cleveland, OH) with the spectroscopic characterization of a class of compounds (3-aryl-3-pyrrolines, Figure 24) which were discovered to selectively inhibit only the copper containing amine oxidase family, while acting as pure substrates for MAO-B purified from beef liver.

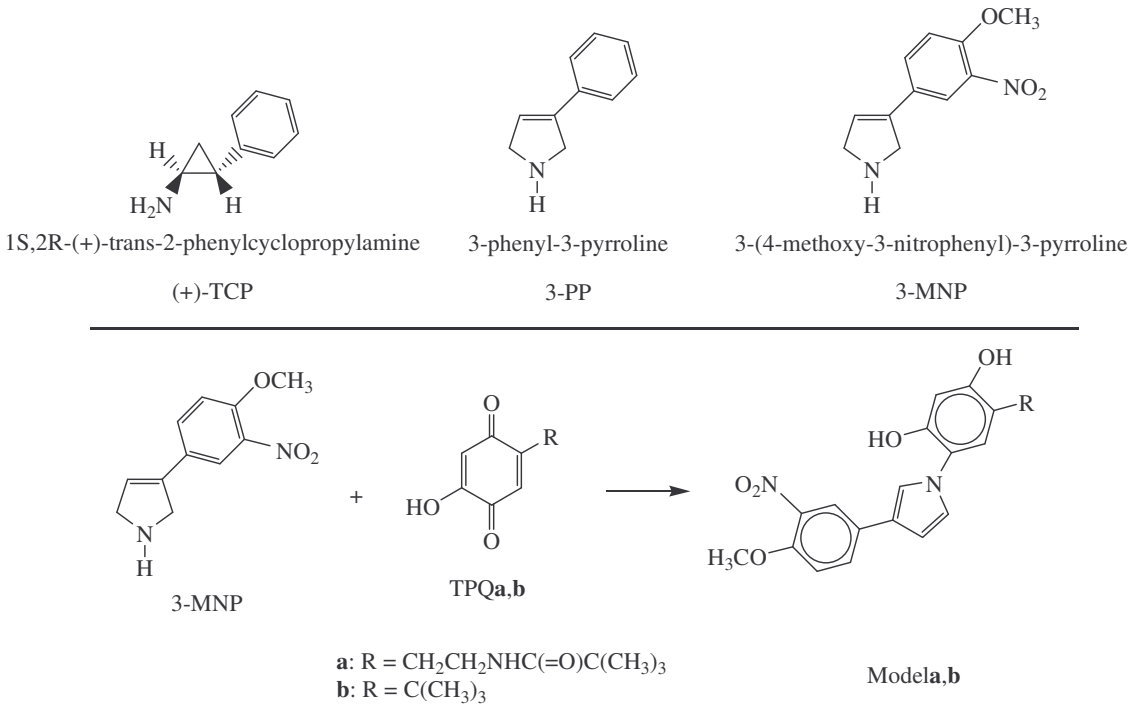

Figure 24: Amine compounds with copper amine oxidase and monoamine oxidase significance (top) and model compounds used in resonance Raman studies (bottom).

Materials and Methods

Enzyme Isolation and Purification

Purified enzyme for these studies was provided by Jennifer Smith (BPAO and PSAO), Bradley O. Elmore (EPAO and rhDAO), Jason Kuchar (PPLO), and Gregory A. Juda (AGAO). PSAO was purified from pea seedling as described previously [19]. BPAO was purified from bovine plasma using minor modifications of a published procedure [135]. EPAO was purified by a revised protocol [21], based on that initially specified in [17]. PPLO was purified as initially described in [136]. AGAO was purified as described in [163], and rhDAO was purified as described in [18].

Inhibitor Preparation

Tranylcypromine hydrochloride obtained from Aldrich was used with no further purification. Stock inhibitor solutions were prepared by dissolving required amount of compound in 100 mM phosphate buffer, pH 7.2 to yield a final concentration between 1 and 10 mM. Solutions of TCP were found to be stable at 25 °C for at least 24 hours, and remained stable for over 96 hours at 4 °C, consistent with previous reports [164]. Solutions were made up fresh directly prior to use. Due to the report by Saysell *et al*. (2002) [164], which indicates that only the (+)-TCP enantiomer reacts with ECAO, calculated TCP excess reported in Table 6 is listed relative to the (+)-isomer.

The synthesis of 3-PP and several 3-PP analogs was carried out by Dr. Lawrence M. Sayre's lab and detailed descriptions can be found in reference [165]. The nitro-containing analogue of 3-PP was synthesized for spectroscopic studies on the interaction of the inhibitor with BPAO. Synthesis of 3-(4-nitrophenyl)-3-pyrroline was unsuccessful due to internal oxidation-reduction yielding 3-(4-nitrosophenyl)-3-pyrrole. In this regard, placing the nitro group in a meta position, as opposed to a para position, would yield a compound resistant to internal redox, and as such the 3-MNP analog was synthesized [165]. A description of the synthesis of the TPQ**a** and TPQ**b** model compounds, as well as the reaction of these compounds with 3-MNP (Figure 24, bottom), can be found in [165].

TCP Spectroscopic Analysis and Steady-State Kinetics

Absorption spectra and kinetic data were collected at 25 °C using a Hewlett Packard 8453 diode array spectrophotometer equipped with a thermostatted cuvette

holder connected to an Endocal RTE-5 circulating water bath. Protein concentrations were calculated utilizing ε_{280} as previously reported for AGAO [163], EPAO [17], PSAO [19], BPAO [139], PPLO [85], and rhDAO [18]. All solutions were stirred during assays, with benzylamine used as a control substrate. Experiments were run with freshly thawed protein aliquots from the same enzyme stock. Enzyme activity is reported as spectroscopic units per mg of protein (Table 6).

To analyze the general effectiveness of TCP against the six CuAO enzymes, enzyme samples were incubated with varying amounts of TCP for 30-min at 30 °C. Activity was then monitored spectroscopically using benzylamine as substrate at 25 °C in 100 mM phosphate buffer, pH 7.2 as described in [62]. Assays were run in triplicate for each inhibitor concentration listed in Table 6. Time-based kinetic analysis of TCP inhibition of AGAO was performed as described in [62]. Samples subjected to gel filtration were run over a Sephadex G-25 column (Pharmacia, PD-10), clearly separating excess TCP from enzyme.

Time-dependent spectroscopic inhibition of AGAO by TCP involved adding a 200-fold excess of racemic TCP to an 11.8 μM sample of AGAO in 100 mM phosphate buffer, pH 7.2. The sample was mixed and a spectrum was immediately recorded. Subsequent spectra were recorded at different time intervals out to 3.5 hours. Kinetic assays were then performed as described above. While the stock solution of TCP was found to have a λ_{max} at 260 nm, absorbance at 280 nm was found to be negligible.

Spectroscopic Characterization of Pyrrole Models**a**,**b** and BPAO Modified by 3-MNP

A solution of highly purified BPAO (~25 μM dimer, ~50 μM TPQ) was incubated with 1 or 4 equivalents of 3-MNP based on TPQ content at 30 °C for 3.5 or 1 hour, respectively. The protein sample was assayed and found to have no remaining activity. The sample was subsequently run over a Sephadex G-25 column (Pharmacia, PD-10) in 0.1 M phosphate buffer, pH 7.2, and then concentrated to ~400 μM TPQ, reassayed, and found to contain no activity. Optical spectra of appropriate dilutions of native and inactivated enzyme were then recorded.

Raman spectra on the undiluted samples were collected at room temperature after 413.1 nm excitation. Raman spectra were collected on a Spex Triplemate 1877 (1800 groove setting), using a liquid-N_2 cooled Spex Spectrum One CCD detector, and Coherent Kr-ion laser. The collection times were 5 min (at 30 mW) for pyrrole Model**b** in 100% acetonitrile, 8 min (at 70 mW) for pyrrole Model**a** in 75% deuterated methanol and 25% D_2O, 15 min (at 30 mW) for pyrrole Model**b** in 100% deuterated methanol, and 60 min (at 50 mW) for BPAO inactivated by 3-MNP. Pyrrole Model**b** in 100% chloroform was only collected for 0.5 min (at 20 mW) due to the formation of a precipitate. Raman spectra were also collected for pyrrole Model**b** in 63% CD_3OD and 37% D_2O (8 min at 75 mW), 3-MNP in H_2O (30 min at 20 mW), and a denatured sample of BPAO inactivated by 3-MNP (13 min at 28 mW). Preparation of the latter sample involved adding 55.5 μM 3-MNP to a solution of BPAO (52.6 μM in TPQ). Time point aliquots were removed and assayed for activity. At 3.5 hour, 1.6% activity remained and the sample was subsequently run over a Sephadex column as described above. The

concentrated sample (~400 μM TPQ) was reassayed and found to contain 2.1% activity. The sample was then thoroughly mixed with 0.45% SDS and 0.1 mM dithiothreitol before being placed into a thermocycler programmed to heat the sample to 55 °C for 6 min with subsequent cooling to 25 °C. Raman data were then immediately collected.

Reversibility of TCP Binding

Reactive TPQ can be quantified by its titration with phenylhydrazine, which reacts stoichiometrically with the C5 carbonyl of TPQ, forming a stable, intensely yellow-colored adduct with λ_{max} ~ 450 nm and extinction coefficient of ~ 32000 $M^{-1}cm^{-1}$ [66,135]. In order to determine if TCP binding to the quinone cofactor of AGAO was completely reversible, a sample of AGAO was prepared and titrated with phenylhydrazine. The AGAO sample was prepared by incubating TCP with enzyme, as described above, until only ~ 5% activity remained. This sample was then subjected to gel filtration utilizing a Sephadex G-25 column. The sample was then extensively dialyzed (3 exchanges against 1 L of 100 mM phosphate buffer, pH 7.2) for ~ 20 hrs at 4 °C, concentrated, and then titrated with phenylhydrazine. A phenylhydrazine stock solution was prepared immediately prior to use. Due to the instability of phenylhydrazine, the stock solution was kept anaerobic by gently bubbling Ar gas through it. Phenylhydrazine was added to the 5.8 μM enzyme solution in 2 μL increments, yielding 1.14 μM additions, or 0.2 increments of reactive TPQ. The titration was carried out at 25 °C in 100 mM phosphate buffer, pH 7.2, and was repeated three times. A control experiment of native enzyme from the same protein stock was also

titrated. Adduct formation was monitored by following the change in absorbance at 442 nm.

The reversibility of TCP binding in AGAO was further examined by the anaerobic titration of the substrate benzylamine. A 4.3 μM sample of AGAO inhibited by a 100-fold excess of (+)-TCP was prepared as described above in 100 mM phosphate buffer, pH 7.2. The sample was then made anaerobic by gently blowing Ar gas over the enzyme-inhibitor mixture in a tightly sealed cuvette for 2 hours. Anaerobic benzylamine (100 mM stock solution) was then added to the sample in substoichiometric increments gradually building to a large excess (~ 150-fold). The absorbance at 350 nm was monitored.

Determination of TCP Oxidation by AGAO

Determination of TCP oxidation was measured by monitoring H_2O_2 production using a HRP-ABTS coupled assay. This assay is described in the previous chapter. Assays were performed at 30 °C in 100 mM phosphate buffer, pH 7.2. Total assay volume was 1 ml, and substrate concentration was adjusted accordingly to yield a final concentration of 300 μM. Protein concentration in the assay was 0.293 μM, yielding ~ 250-fold excess of each TCP enantiomer over active sites. Benzylamine was used as a control substrate, and assays were run in triplicate. A small blank rate was obtained using ABTS, HRP, TCP, and buffer, which was nearly identical to those blank rates obtained with ABTS, HRP, and buffer. No significant side reactions between ABTS and TCP were observed to occur, in disagreement with that reported in reference [164].

Results

TCP Inhibition

As seen in Table 6, only the two mammalian plasma enzymes EPAO and BPAO and the bacterial enzyme AGAO displayed significant levels of inhibition with TCP following a 30-min incubation. The inhibitory potency of TCP on these enzymes follows the trend AGAO > BPAO > EPAO >> PPLO > PSAO > rhDAO. Time-based studies performed with a 200-fold excess of TCP revealed that AGAO activity dropped to less than 5% almost immediately. This concurs with the time-based spectroscopic analysis of TCP binding, which indicates that TCP binds rapidly to the enzyme based on the observation that the TPQ-TCP complex in AGAO (see below) shows no significant change in absorbance at 350 nm over a period of 3.5 hours (data not shown). Activity at this time was identical to that reported in Table 6.

Table 6: TCP Inhibition Results

Enzyme	TCP: Active Sites[a]	% Activity[b]
EPAO	1[c]	90
	20[c]	86
	100	57
BPAO	1[c]	91
	20	81
	50	68
	100	38
AGAO	1	94
	20	57
	100	4
PSAO	100	93
PPLO	100[d]	86
rhDAO	1	100
	20	98
	50	99
	100	98

[a] Reported as excess (+)-TCP relative to active site concentration. [b] Percent activity remaining following a 30-min incubation. Numbers shown are averages of three assays. [c] Active site concentrations ranged between 23 and 25.5 μM. [d] Active site concentration was 1 μM. All other active site concentrations ranged between 2 and 5.5 μM.

TCP Spectroscopic Analysis

AGAO and BPAO samples were incubated with a given molar excess of TCP determined to yield greater than 75% inactivation following a 30-min incubation at 30 °C. TCP binding to AGAO was shown to form a complex with a λ_{max} at 350 nm (Figure 25) and binding to BPAO was shown to form a complex with a λ_{max} ~ 370 nm; both representing slight shifts from the ECAO-TCP complex which was shown to have a λ_{max} at 365 nm [164]. BPAO inhibited by TCP was subjected to gel filtration and despite clearly separating excess TCP from the enzyme, a significant amount of TCP was still bound to BPAO indicating that this compound has fairly high affinity for the active site.

The same sample was then extensively dialyzed and the native spectrum of BPAO was seen to return with a λ_{max} at 480 nm due to the unmodified TPQ chromophore (data not shown). Activity assays confirmed the full restoration of BPAO activity, similar to what is reported for TCP inhibition of ECAO [162,164].

Interestingly, complete removal of TCP bound to AGAO did not occur following either gel filtration or dialysis, suggesting inhibition with TCP is not readily reversible (Figure 25). Utilizing the 1.2 titrateable TPQs per enzyme (see below), the protein concentrations in Figure 25 correlate to 48.9 μM and 24.4 μM reactive TPQs, respectively. Based on the absorbance at 480 nm and using an extinction coefficient of ~ 3200 $M^{-1}cm^{-1}$ for TPQ [89], this indicates that ~ 64% of reactive TPQ in the post gel filtration spectrum are modified, whereas ~ 45% of reactive TPQ are modified in the post dialysis spectrum. This is consistent with the measured increase in levels of activity between these samples; post gel filtration assays indicated ~ 25% of full activity whereas post dialysis assays revealed 60% of full activity. A different sample of AGAO prepared in the aforementioned manner was allowed to dialyze for 60 hours, with measured activity increasing to 76%, with an estimated 30% of reactive TPQ modified.

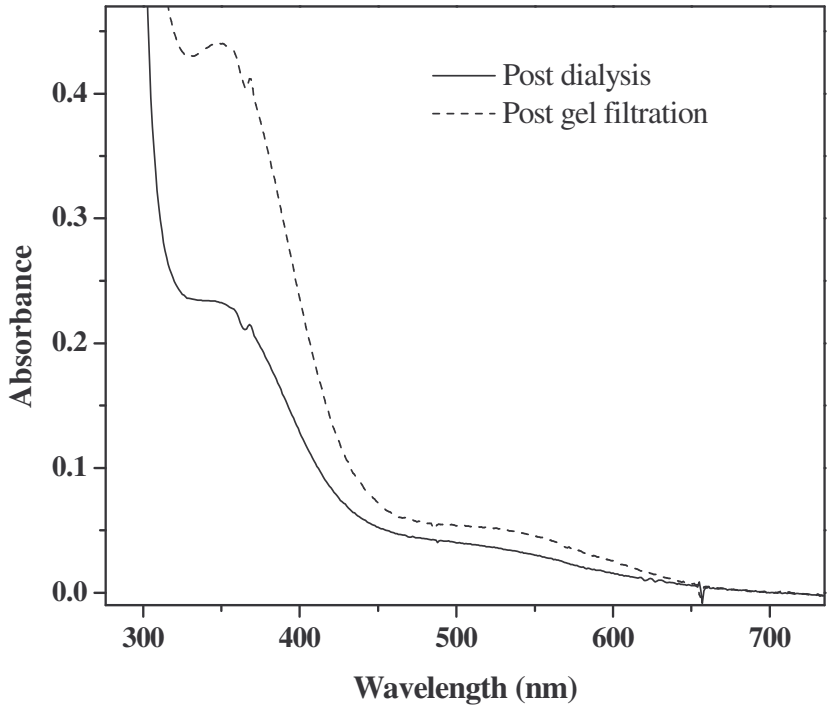

Figure 25: Post-gel filtration (40.7 μM) and post-dialysis (20.4 μM) spectra of AGAO inhibited by TCP.

Reversibility of TCP Binding

The potential reactivity of the post-dialysis TCP-AGAO adduct (λ_{max} 350 nm; Figure 25) towards carbonyl reagents was examined via phenylhydrazine titration (Figure 26). Absorbance at 350 nm is seen to decrease with increasing equivalents of phenylhydrazine, indicating that phenylhydrazine displaces TCP from TPQ to form the phenylhydrazone derivative of the quinone cofactor with λ_{max} at 442 nm. The initial sample contains 11.6 μM potential reactive TPQ (based on ~ 1 reactive cofactor per monomer). The absorbance at 480 nm is 0.0153 and using an extinction coefficient of 3200 $M^{-1}cm^{-1}$ for the native cofactor, there is approximately 4.8 μM unmodified TPQ in this sample. Absorbance of the 442 nm adduct reached a maximum at 1.2 equivalents of phenylhydrazine, suggesting that there are 1.2 reactive TPQs per dimer, consistent with

control titrations (data not shown) and that previously reported [163]. This measurement is also comparable to the 1.3 reactive cofactors per protein dimer reported for titration of ECAO with TCP [164]. Due to the lack of a significant decrease in absorbance at 350 nm for the first two equivalents (1.14 μM additions) of phenylhydrazine, it appears that phenylhydrazine preferentially reacts with the cofactors that are unmodified by TCP. However, by the third addition of phenylhydrazine, substantial loss of absorbance at 350 nm is observed. Subsequent additions of phenylhydrazine resulted in continued loss of absorbance at 350 nm with concurrent increase in absorbance at 442 nm, until all bound TCP was displaced (Figure 26).

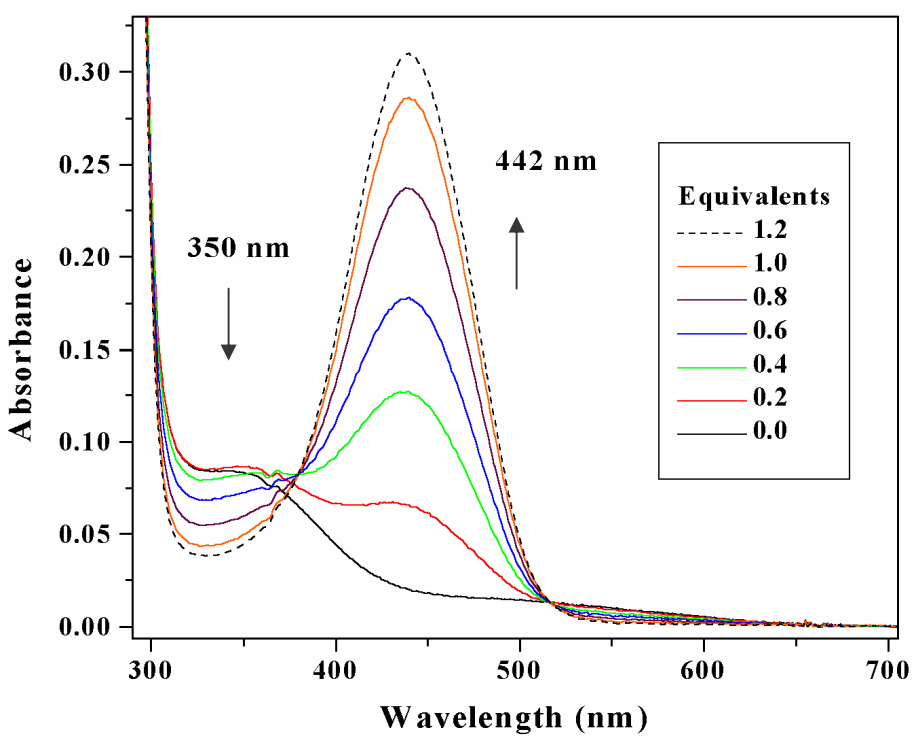

Figure 26: Phenylhydrazine displacement of bound TCP in AGAO.

To examine if benzylamine could also displace bound TCP from the active site of AGAO, an anaerobic titration was performed. Under these conditions, TPQ is prevented from reoxidizing, trapping the cofactor in the $TPQ_{AMQ} \leftrightharpoons TPQ_{SQ}$ equilibrium. The semiquinone can easily be observed to form given its characteristic absorption spectra (λ_{max} = 360, 434, and 464 nm) [87,121]. In this case, substoichiometric additions of benzylamine were found to decrease the absorbance at 350 nm, with the slow accumulation of the semiquinone species (data not shown). This experiment substantiates the result obtained from the phenylhydrazine titration indicating that both a substrate and a substrate analog can displace TCP bound to TPQ.

Determination of TCP Oxidation

Based on the observation that only (+)-TCP binds to ECAO, Wilmot and coworkers examined whether (-)-TCP was acting as a substrate for ECAO by monitoring oxygen consumption. No oxidation of (-)-TCP was observed indicating that this enantiomer cannot form a substrate Schiff base with the TPQ cofactor [162]. Similar results were obtained in this study with AGAO by monitoring H_2O_2 production, indicating that no detectable oxidation of the racemic TCP mixture occurs. We conclude that neither TCP enantiomer is oxidized by AGAO.

Spectroscopic Analysis of BPAO Inactivated by 3-MNP

Absorption data of 3-MNP in methanol showed a λ_{max} at 340 nm (355 nm in H_2O) with ε = 1960 M^{-1} cm^{-1} (2160 M^{-1} cm^{-1} in H_2O), while Model**b** was found to have λ_{max} at

371 nm with $\varepsilon = 570\ M^{-1}\ cm^{-1}$ (data not shown) [165]. Figure 27 shows the spectra for native BPAO and for a sample of enzyme inactivated by 3-MNP. The inactivated enzyme spectrum exhibits loss at 480 nm and a shoulder near 370 nm. Resolving the shoulder at 370 nm in the inhibited enzyme spectrum is difficult given the strong background absorbance in this region. The estimated difference spectrum displays a shoulder at 371 nm more prominently. Calculation of the difference spectrum required precise knowledge of the concentration of both native and inactivated enzyme cofactor. Whereas this could be calculated in the former case from the known extinction coefficient of enzyme-bound TPQ, this was estimated for the BPAO-3-MNP TPQ derivative by assuming that the shoulder at 370 nm represented the proposed pyrrole and that the displacement of the shoulder over the background rise in absorbance in this region could be converted by use of the same extinction coefficient as exhibited by Model**b** at 370 nm. The concentration estimated in this way agreed reasonably well with that based on dilution of the sample obtained following gel filtration.

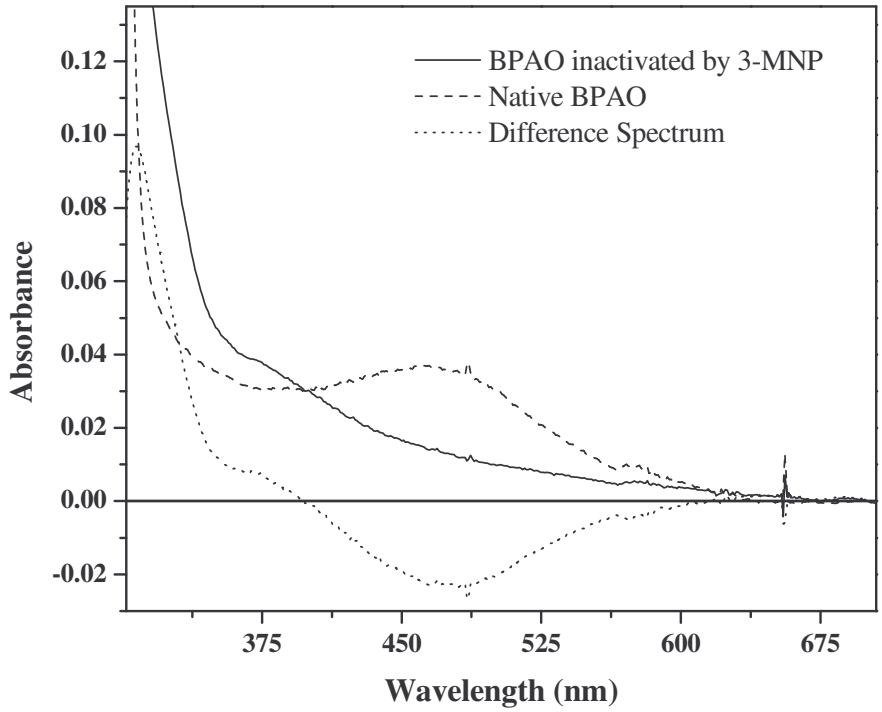

Figure 27: Spectral analysis of BPAO inactivated by 3-MNP.

Additional spectroscopic data on the interaction of 3-MNP with BPAO was obtained through comparison of resonance Raman (rR) data (Figure 28) on the inactivated enzyme and respective 3-MNP derived Model**a** and Model**b** compounds (Figure 24). In native BPAO, the region from 1450 to 1690 cm^{-1} is dominated by TPQ ring stretches, with the C5=O stretching mode at 1678 cm^{-1} and a protein mode at 1450 cm^{-1} [77]. Given the observation that the amide I vibration is between 1650 and 1660 cm^{-1} [166], we tentatively assign the 1652 cm^{-1} stretch as a protein mode, in agreement with previous reports [167,168]. Analysis of the rR data for the inactivated enzyme reveals the presence of the 1450 and 1652 cm^{-1} modes and the absence of the C5=O stretch. The latter suggests that the C5=O bond has been altered upon modification with 3-MNP.

Comparison of the rR spectra of the inactivated enzyme and respective model compounds reveals similar vibrational patterns, with the 1565 and 1620 cm^{-1} modes matching exactly. We propose that the 1344 cm^{-1} mode in the inactivated enzyme spectrum relates to the 1350-1358 cm^{-1} modes seen in the model rR data in solution. The variation of the latter mode over the range 1350-1358 cm^{-1} in the model spectra shown is presumably due to different solvent interactions. The data obtained for Model**b** in 63% CD_3OD and 37% D_2O (not shown) revealed a shift from 1358 cm^{-1} (in 100% deuterated methanol) to 1355 cm^{-1}. Additionally, a shift from 1344 to 1350 cm^{-1} was observed in the rR spectrum of a denatured preparation of BPAO inactivated by 3-MNP (data not shown). Except for this shift, which we believe to be solely due to interactions with solvent, the rR spectrum for the denatured sample was identical to that shown in Figure 28 for the nondenatured enzyme. We can tentatively assign the 1344-1358 cm^{-1} frequency (inactivated enzyme and models) to the nitro aromatic stretch (aryl-NO_2) originating from 3-MNP, as stretching modes for such groups range from ~1330 to 1360 cm^{-1} [166]. This assignment is also in agreement with the 1357 cm^{-1} mode seen in the Raman spectrum for 3-MNP itself in H_2O (data not shown) and with our previous rR analysis of BPAO inactivated by 4-nitrobenzylamine, where a 1344 cm^{-1} mode was observed [153]. It should be noted that the apparent shift of the mode at 1565-1567 cm^{-1} observed for Model**b** to 1556 cm^{-1} for Model**a** in 75% CD_3OD and 25% D_2O is not a solvent shift and must reflect subtle differences between the two quinone model compounds, since this mode in the rR spectrum of Model**b** in 63% CD_3OD and 37% D_2O still occurs at 1565 cm^{-1}.

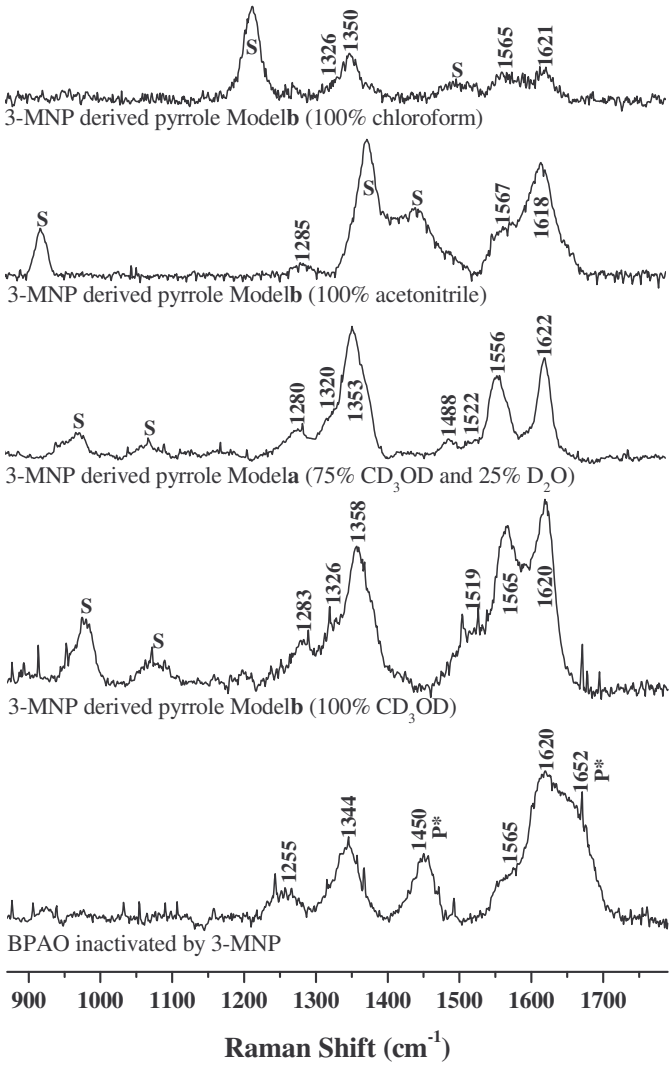

Figure 28: Resonance Raman spectra of 3-MNP derived pyrrole model compounds and of BPAO inactivated by 3-MNP. "P*" denotes protein mode and "S" signifies solvent peak.

Discussion

Tranylcypromine

Tranylcypromine is an antidepressant administered clinically as a racemic mixture of the 1S,2R-(+)- and 1R,2S-(-)- trans enantiomers [156,157]. TCP is a reversible MAO

inhibitor and the (+)-enantiomer has been shown to induce numerous severe side effects in patients [159]. Recent structural and kinetic studies have extensively characterized the molecular nature of the interaction between TCP and ECAO, revealing that (+)-TCP binds to C5 of the quinone cofactor as the substrate Schiff base species with λ_{max} of 365 nm [162,164].

AGAO oxidation of TCP was not detected in this study, consistent with that observed for ECAO [162]. In the latter case, failure of ECAO to abstract a proton from Cα of (-)-TCP is expected based on the pro-S stereospecificity of this enzyme [169]. Modelling studies support the conclusion that (-)-TCP cannot access the active site of ECAO due to steric exclusion [162]. Stereospecificity for Cα proton abstraction for other CuAOs depends upon the source of enzyme. For example, pig and horse plasma amine oxidase are pro-R specific for proton abstraction from tyramine [94,95], whereas pea seedling, chick pea seedling, soybean seedling and pig kidney have been shown to be pro-S specific for proton abstraction from tyramine [94,170]. Along these lines it is possible that other CuAOs could bind both enantiomers or specifically bind (-)-TCP rather than (+)-TCP. Oxidation of either (-)-TCP or (+)-TCP may also occur in select cases and the formation of a ketone could be a potential source of side reactions with excess TCP.

Given the disparity among amine oxidases in processing different enantiomers, it is also plausible that AGAO binds both (+)- and (-)-TCP. The inability to completely remove bound TCP from AGAO following gel filtration and dialysis (Figure 25) may indicate a mixed population of modified cofactor. Each enantiomer could interact with AGAO in a slightly different manner, due to distinct orientations of the cyclopropyl and

phenyl rings. This could result in one enantiomer being easier to remove than another. The lack of a clean isosbestic point at ~ 375 nm (Figure 26) may be evidence in support of a mixed population of TPQ adducts modified by both TCP enantiomers.

Additional studies of interest have utilized TCP to examine the effect upon activation of semicarbazide sensitive amine oxidase (SSAO) following long term MAO inhibition [171,172]. SSAO levels were found to increase substantially, suggesting that SSAO can to some extent compensate for loss of MAO activity. Furthermore, the IC_{50} value for SSAO inhibition by tranylcypromine in rat heart homogenates was calculated to be 88 μM [172]. However, no significant inhibition of SSAO was observed at TCP concentrations between 0.2 and 1 μM, which afforded between 65 – 90% inhibition of MAO-A and MAO-B [172].

The observation of SSAO inhibition by tranylcypromine is comparable to the results obtained in this study relating to TCP inhibition of the mammalian plasma enzymes EPAO and BPAO (Table 6). Extrapolating the data in Table 6 and calculating the exact molar (+)-TCP concentration yields 212 μM inhibitor for the 100-fold excess EPAO data (57% activity). This suggests that the IC_{50} at 30-min for TCP inhibition of EPAO is slightly greater than 212 μM. In the case of BPAO, TCP concentrations are 137 μM for the 50-fold excess (68% activity) and 196 μM for the 100-fold excess (38% activity), indicating that the IC_{50} is between these respective concentrations. The inability to completely remove bound TCP from BPAO following gel filtration suggests that TCP displays significant affinity for the active site. AGAO was found to be the most sensitive to inhibition by TCP with the estimated IC_{50} calculated to be slightly greater

than 38 μM. PSAO and PPLO did not display any significant levels of inhibition with TCP. It is of particular interest that TCP did not inhibit rhDAO to any measurable extent. Thus we may infer that the side effects associated with TCP therapies are not associated with inhibition of human diamine oxidase.

The relatively low IC_{50} calculated for TCP inhibition of AGAO is consistent with the rapid loss of activity measured in the time-based kinetic experiment and the rapid binding of TCP as observed in the time-based spectroscopy experiment. Furthermore, the observation that activity levels of AGAO inhibited by TCP increased successively following gel filtration and dialysis, respectively, also indicates that TCP has a fairly high affinity (low K_d) for the active site of AGAO. If this complex had a high K_d (or a higher k_{off}), then nearly complete removal of TCP would most likely result following either gel filtration or dialysis. The results obtained for the post dialysis sample point to approximately 50% active site occupation by TCP (Figure 25). Slightly greater removal of bound inhibitor was obtained by allowing the sample to dialyze for an extremely long period of time. It is of interest that the most effective way of removing bound TCP from AGAO samples is through chemical displacement via titration with either benzylamine or phenylhydrazine (Figure 26). This confirms the premise that TCP has substantial affinity for approximately half the active sites. The ability of substrate analogs and/or substrate to displace bound TCP signifies that the C5 of the cofactor still contains enough electrophilic character in the substrate Schiff base moiety to undergo nucleophilic attack by the primary amine. As anticipated, the displacement of TCP does not occur instantaneously, because levels of activity in a 3-min benzylamine assay would then be expected to be much greater than those reported. In addition, the time noted for the

absorbance at 442 nm to stop changing following each addition of phenylhydrazine between 0.4 and 1.2 equivalents was ~ 15 minutes, as compared to the control where the absorbance stopped changing following each addition at ~ 5 minutes. The K_i for the ECAO-TCP adduct was calculated to be ~ 1.2 μM and dialysis completely removed bound TCP [164]. Taken collectively, the results presented here support the notion that while inhibition of AGAO by TCP is fully reversible, the AGAO-TCP adduct must have a low dissociation constant. This is consistent with the formation of a substrate Schiff base adduct that is not processed further by the enzyme.

In an effort to substantiate this conclusion, our collaborators at the University of Sydney pursued an AGAO-TCP crystal structure. TCP was soaked with crystals of native AGAO and a structure was solved to 1.65 Å resolution (Figure 29). TCP was concluded to bind to TPQ as the substrate Schiff base adduct (A.P. Duff, D.B. Langley, H.C. Freeman, and J.M. Guss, University of Sydney, unpublished results). Interestingly, the phenyl substituent group of the cyclopropyl ring was found to lie in the center of the hydrophobic pocket, in the same plane as the naphthyloxy and methylphenoxy groups of compounds **1** and **1d** (detailed in the previous chapter, see Figures 19 and 20).

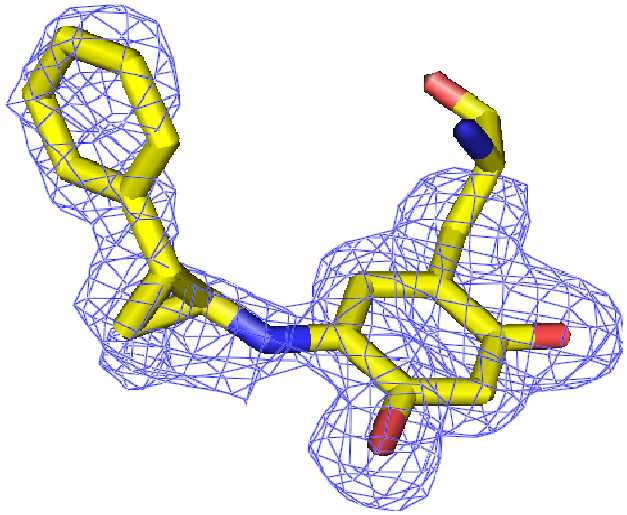

Figure 29: The electron density of the AGAO-TCP substrate Schiff base adduct (A.P. Duff, D.B. Langley, H.C. Freeman, and J.M. Guss, University of Sydney, unpublished results).

3-Aryl-3-Pyrrolines

Early results of pyrrole model study reactions from Dr. Sayre's laboratory suggested that the mechanism of inactivation of BPAO by 3-pyrroline and its 3-aryl analogues involved condensation with the TPQ cofactor and transamination to give, following loss of proton, the corresponding pyrrolylated cofactor [173]. The availability of chromophoric inhibitor 3-MNP suggested that direct evidence for the nature of enzyme inactivation might be obtained by comparing the spectral properties of the 3-MNP inactivated enzyme with those of small molecule adducts generated by reaction of 3-MNP with TPQ models. From the spectroscopic results of 3-MNP and Model**b** (data not shown, see [165]), it was expected that derivatization of the native TPQ cofactor to a pyrrole through reaction with 3-MNP would result in an inactivated enzyme spectrum with a loss of the native 480 nm quinone chromophore and a gain of absorbance near 370 nm. The inactivated enzyme spectrum seen in Figure 27 indeed exhibits the expected

loss at 480 nm and a shoulder near 370 nm, clearly consistent with the proposed enzymatic oxidation of 3-MNP to give the respective TPQ-pyrrole derivative.

Additional evidence to support enzymatic transformation of 3-MNP to the TPQ-pyrrole derivative was obtained through comparison of resonance Raman (rR) data on the inactivated enzyme and respective 3-MNP derived Models**a** and **b** (Figure 28). As seen in Figure 28, comparison of the rR spectra of the inactivated enzyme and respective model compounds reveals similar vibrational patterns. Analysis of some of these vibrations provides insight into the potential structure of the enzyme-3-MNP adduct. For instance, three or more coupled C=C stretches have a characteristic vibration between 1540 and 1620 cm^{-1} [166], so it is possible that the 1565 and 1620 cm^{-1} modes are due to the aryl conjugation present in the adduct. Since there are modes at 1570 and 1620 cm^{-1} in the Raman spectrum of 3-MNP (data not shown), it is plausible that the frequencies at 1565 and 1620 cm^{-1} are due to the coupled deformation of ring modes in the TPQ-3-MNP derivative.

In the rR spectrum of the BPAO-methylamine adduct, an intense mode at 1616 cm^{-1} was assigned to the N=C stretch of the product Schiff base [167]. The absence of a stretching frequency at 1616 cm^{-1} in the spectrum of the inactivated enzyme (Figure 28) is consistent with resonance delocalization in a pyrrolylated cofactor, rather than any derivative containing a localized imine. Overall, the similarities in the spectra of Models**a** and **b** and the inactivated BPAO-3-MNP derivative indicate that the pyrrole structure seen to form in the model reaction is a good candidate for the structure of the adduct formed enzymatically.

Conclusions

This chapter reports the kinetic and spectrospopic characterization of the MAO inhibitor TCP with six CuAOs and presents the results on the spectroscopic characterization of a class of compounds (3-aryl-3-pyrrolines, Figure 24) which selectively inhibit only the copper containing amine oxidase family, while acting as pure substrates for monoamine oxidases. The TCP results have been published in the journal *Biochimica et biophysica acta: Protein Structure and Molecular Enzymology* [174], and the 3-pyrroline data has been published in the *Journal of the American Chemical Society* [165].

Copper amine oxidase inhibition with TCP displayed interesting selectivity, with only BPAO, EPAO, and AGAO showing significant losses of activity. The absence of TCP affects on rhDAO argues against the inhibition of diamine oxidase as a potential source for some of the deleterious side effects occurring in patients treated with TCP. TCP inhibition of BPAO was shown to be completely reversible, with restoration of full activity following dialysis. AGAO inhibition also proved to be completely reversible, however, dialysis could not extract all bound compound. TCP could be removed upon chemical displacement either with a substrate or a substrate analogue, suggesting that TCP has very high affinity for the active site of AGAO. Our assignment of the 350 nm absorbance peak as being characteristic of the substrate Schiff base was confirmed by structural characterization of the AGAO-TCP complex by our collaborators at the University of Sydney. Just as in the case with the structural characterization of AGAO inactivated with two 4-(aryloxy)-2-butynamines, the hydrophobic pocket identified from

our initial modeling studies was observed to cradle the phenyl substituent of TCP. It is quite possible that this group forms π-stacking interactions with some of the aromatic residues in this pocket (Figure 20), which confers the observed stability to this Schiff base complex.

The observation that 3-pyrroline [173] and 3-aryl-3-pyrrolines [165] inactivated bovine plasma amine oxidase was quite unexpected, considering that secondary amines were previously thought to be nonsubstrates for this enzyme. Prior model studies [173], coupled with the spectroscopic studies on the inactivated enzyme presented in this chapter, suggest a mechanism involving a unique conversion of the quinone cofactor to a reduced pyrrolylated form that cannot be reoxidized to the starting quinone. Cofactor pyrrolylation would correspond to mechanism-based inactivation with a partition ratio of zero. In contrast, for bovine liver mitochondrial monoamine oxidase B, 3-phenyl-3-pyrroline is an excellent substrate, being dehydrogenated to 3-phenylpyrrole [165]. The identification of these compounds as pure inactivators of one enzyme class and pure substrates for another enzyme class is novel, permitting us to refer to the 3-pyrrolines as transamination-specific mechanism-based inactivators.

This is the first example of a class of compounds which can selectively inhibit one amine oxidase enzyme family, while acting as substrates for the other amine oxidase family. Essentially, the origin of the novel reactivity arises from the ability of the TPQ-containing AOs to bind secondary amines, further inhibitory selectivity within the CuAO class may be achieved through appropriate substitution of the parent 3-pyrroline. This is evident when comparing inhibitory potency of the parent compound 3-pyrroline against a series of CuAOs. Whereas 1 equivalent of this compound effected 50% loss of activity in

EPAO, PPLO, and BPAO, 40 equivalents were needed to effect 80% inhibition of AGAO, while 40 equivalents only effected ~ 15% inhibition of PSAO and rhDAO. Thus, in addition to selective inhibition of the quinone-dependent amine oxidases on the basis of mechanism, a further level of discrimination can be achieved by fine tuning preferential recognition by the enzyme substrate binding cavity.

Overall, the development of highly selective inhibitors should be possible, and such compounds should aid in unraveling the complex physiological roles of the various mammalian quinone-dependent amine oxidases. In addition, the ability to design specific and selective inhibitors of one amine oxidase class would be highly beneficial in terms of current pharmaceutical drugs which have pronounced side effects. The potential of this approach can be understood by simply examining what we now know about the anti-depressant drug tranylcypromine. TCP is administered as an MAO inhibitor, however, this compound is found to also inhibit mammalian SSAO, which may serve as the source for many of this drug's deleterious side effects. In terms of selectivity, it should be feasible to add a substituent group onto the cyclopropyl amine end of TCP which would preclude its binding by human CuAO enzymes, thereby alleviating some of the inadvertent side reactions caused by this drug. Appropriate screening of multiple candidates would reveal a structure which would still inhibit the monoamine oxidase enzymes with similar potency.

CYANIDE AS A COPPER AND QUINONE-DIRECTED INHIBITOR OF AN AMINE OXIDASE FROM *Pisum sativum*: EVIDENCE FOR BOTH COPPER COORDINATION AND CYANOHYDRIN DERIVATIZATION OF THE QUINONE COFACTOR

Introduction

The previous two chapters have dealt with the first objective of my research, namely the contribution made towards fully understanding the molecular factors governing substrate specificity and recognition, as well as inhibitor selectivity among CuAOs. The final three chapters of this thesis are concerned with probing the role of copper during enzymatic reoxidation. The role of copper is investigated by three methods, which form the topics of the remaining chapters. The first two methods examine the effects of the monodentate ligands cyanide and azide, respectively, on amine catalysis and O_2 reduction in PSAO. The final technique deals with the determination of the electron transfer rate between TPQ_{AMQ} and Cu(II) in AGAO, as a function of pH.

The ligands CN^- and N_3^- replace the equatorial water ligand of copper and have been described as inhibitors of both the reductive and oxidative half-reactions of CuAOs [110-113]. These ligands preferentially bind copper, and their monodentate coordination is advantageous because removal of copper from the enzyme does not typically occur. For this reason, investigation of the electronic and mechanistic effects of such ligand-substitution reactions can provide critical information regarding active site structure and the catalytic mechanism of CuAOs [111,112,175,176].

Inhibition of CuAO amine oxidation by cyanide has been described as mixed or uncompetitive [113,175], while cyanide's inhibition towards O_2 reduction has been described as competitive [114], non-competitive [113], and mixed [175]. In terms of the effects of this ligand on O_2 reduction, the observed inhibition patterns should be interpreted in terms of the two proposed O_2 binding sites. For example, if O_2 binds to the copper center, then competitive inhibition should be observed. However, if O_2 binds in an off-metal, proteinaceous site [72], then non-competitive inhibition will likely be observed. Previously, our laboratory has demonstrated that the effects of azide and cyanide during the oxidative half-reaction can be rationalized in terms of their effects on the internal redox equilibrium TPQ_{AMQ}-Cu(II) ⇆ TPQ_{SQ}-Cu(I), with N_3^- preferentially binding Cu(II) and CN^- preferentially binding Cu(I) [111]. Yet, inhibition due to cyanide may be more complex, as inhibition has also been suggested to arise from TPQ-cyanohydrin formation [113,175,176]. Cyanide binding to quinones is known to readily occur and has been observed for pyrroloquinoline quinone (PQQ), where cyanohydrin derivatization in glucose dehydrogenase resulted in competitive inhibition versus substrate glucose [177]. Despite this, no direct spectroscopic evidence for cyanohydrin derivatization of TPQ has been documented for CuAOs [111,178], even though a report indicated slight perturbations in the absorption spectrum of PKAO upon addition of CN^- [175].

This work details the spectroscopic and kinetic effects of cyanide binding on *Pisum sativum* amine oxidase. PSAO is an especially attractive enzyme for such binding studies because it is the most catalytically efficient copper amine oxidase enzyme [179], and it forms the most semiquinone under standard conditions (i.e. this enzyme has the

largest K_{eq} value for the TPQ_{AMQ}-Cu(II) ⇆ TPQ_{SQ}-Cu(I) equilibrium, [87]). The first direct spectroscopic evidence is provided for cyanohydrin derivatization of TPQ, which is further substantiated by model chemistry. Furthermore, K_d values for Cu(II)-CN^- and Cu(I)-CN^-, as well as the K_i for cyanide inhibition versus substrate amine are reported. Based on our results, a mechanism for CN^- inhibition against substrate amine is presented.

Materials and Methods

Protein Preparation

Pea seedling amine oxidase was purified as described previously [19]. Only protein of the highest quality was utilized for experimentation (1.8 TPQ/dimer for PSAO). Protein concentrations were calculated using extinction coefficients at 280 nm as previously reported for PSAO [19], and using an extinction coefficient of 2,500 $M^{-1}cm^{-1}$ for TPQ [89]. All PSAO used for cyanide and azide (see next chapter) binding studies was purified by E.M. Shepard.

Spectroscopic Characterization

UV and visible absorption data were acquired utilizing a Cary 6000i UV/vis/NIR spectrophotometer (Varian, Australia) connected to a Cary dual cell Peltier accessory for temperature control. All spectroscopic data were collected at 25 °C in 100 mM phosphate buffer, pH 7.2, and analyzed using Origin 7.0 software (Microcal, MA, USA).

A sample of PSAO (14.5 μM) was titrated with NaN_3 (Fisher) stock solution (1.5 M NaN_3 in 0.1 M KPO_4, pH 7.2) and the absorbance was monitored at 389 nm to determine the K_d value for the Cu(II)-N_3^- LMCT band. Following addition and thorough mixing of each aliquot, five minutes was allowed for equilibration before recording spectra. Longer incubation times yielded no significant increase in the LMCT band. The ΔA at 389 nm was plotted versus azide concentration and the data were fit to a second order equation in order to determine the K_d value for the Cu(II)-N_3^- complex.

In order to determine the K_d for the Cu(II)-CN^- complex in PSAO, a sample of enzyme preequilibrated with near saturating amounts of N_3^- was titrated with a stock solution of NaCN (Fluka Biochemika) using the method as described by He *et al*. (1995) [175]. All cyanide stock solutions (0.025 – 1.0 M) were prepared prior to each experiment using NaCN in 100 mM KPO_4, pH 7.2, and were kept anaerobic during the course of experimentation. PSAO (6.3 μM) was incubated with 196 mM N_3^- for 30 minutes at 25 °C in the dark prior to the first addition of NaCN. NaCN was then added in small aliquots to a final concentration of 31.5 mM, allowing 10 minutes between subsequent additions, and the ΔA at 389 nm was monitored as azide was displaced from Cu(II) by cyanide. The ratio of the two equilibrium constants (K_{CN^-} to K_{N3^-}) was then determined by linear least squares analysis according to the equation [175]:

$$-(A - A_O)/(A - A_Z) = (K_{CN^-}/K_{N3^-}) \bullet ([CN^-]/[N_3^-])$$

where A is the absorbance at 389 nm, and A_O and A_Z are the absorbance values at the beginning and end of the experiment, respectively.

Buffered samples (0.1 M KPO_4, pH 7.2) of wild-type PSAO were titrated with cyanide in order to determine if any spectroscopic alterations of the native TPQ chromophore occurred. Samples of PSAO (14 μM and 16.2 μM) were titrated with ~1 – 2 mM additions of CN^- up to final concentrations of 30 and 50 mM, respectively, allowing 5 minute equilibration time between additions. Spectroscopic changes were monitored at both 345 nm and 500 nm.

In order to examine pH effects upon the titration of PSAO with cyanide, two parallel experiments were performed. The first experiment involved incubating a 14.7 μM PSAO sample with 17.4 mM cyanide. The cyanide was added from a stock prepared in the aforementioned manner, yielding a pH in the cuvette of 7.8. In the second experiment, the NaCN stock was made up as described above; however, it was transferred to a vial and sealed to prevent any loss of HCN as a gas when HCl was added to establish a pH of 7.2. An aliquot of NaCN from this stock was then added to a 12.4 μM PSAO sample, yielding a cyanide concentration of 16.9 mM (final pH = 7.2). For both experiments, visible spectra were taken over the course of 50 minutes.

Samples of PSAO (10-20 μM) were reduced with benzylamine under anaerobic conditions and titrated with NaCN stock solution to determine a K_d for the Cu(I)-CN^- complex [111]. Anaerobic conditions were established by purging the protein sample with Ar gas passed through a vanadium bubbler, HCO_3, H_2O setup [180] for 3 hours. A catalase (~300 units), glucose (3.4 M), glucose oxidase (6 mg/ml) solution was added to the protein sample 30 minutes prior to experimentation to ensure that anaerobic conditions were maintained during the titration [135]. Protein samples were reduced with

2 – 5 fold excess benzylamine over TPQ. NaCN (25 mM stock) was added in aliquots ranging from 60 – 200 μM to a final concentration of approximately 1.5 mM, allowing 5 minutes for equilibration prior to recording spectra. Mixing was accomplished by inverting the cuvette. The absorbance maxima characteristic of TPQ_{SQ} were monitored [87,181].

The effect of cyanide on the binding of the substrate analog phenylhydrazine to TPQ was also investigated. Reactive TPQ can be quantified by its titration with phenylhydrazine, which reacts stoichiometrically with the C5 carbonyl of the quinone cofactor, forming a stable, intensely yellow-colored adduct with a λ_{max} at ~450 nm and extinction coefficient of ~ 32,000 $M^{-1}cm^{-1}$ [135]. A sample of PSAO (14.7 μM) was first equilibrated with 17.44 mM CN^- (final pH ~7.8) and then titrated with a freshly prepared phenylhydrazine solution. A control titration using the same enzyme stock (11.8 μM) was performed in the absence of CN^-. Phenylhydrazine stock (0.558 mM, Sigma) was kept anaerobic throughout the duration of the experiment to avoid decomposition of the reagent.

Kinetic Characterization

The effect of cyanide on enzymatic catalysis was investigated for PSAO. All kinetic data were collected at 25 °C in 100 mM phosphate buffer, pH 7.2. Kinetic analysis involved first equilibrating enzyme with a given amount of cyanide for 5 minutes under magnetic stirring, followed by addition of substrate benzylamine to initiate each assay. Amine oxidase activity was determined by monitoring benzaldehyde

production over the course of 3 minutes at 250 nm using an extinction coefficient of 12,800 $M^{-1}cm^{-1}$ [140]. Assays were at least run in duplicate, most often triplicate at varying cyanide concentrations and data were fit to the Michaelis-Menten equation using Origin 7.0 software (Microcal, MA, USA). Error bars on each plot represent the standard deviation of the rate at a particular substrate concentration. All steady-state kinetic data were collected on a Hewlett-Packard 8453 diode-array spectrophotometer equipped with a thermostatted cell chamber connected to an Endocal RTE-5 circulating water bath.

Results

Cyanide as a Cu(II)-Directed Ligand

The K_d for Cu(II)-N_3^- was found to be 53 ± 3 mM (K_{eq} = 18.7 ± 0.9 M^{-1}; ε_{389} = 3090 $M^{-1}cm^{-1}$) for PSAO as determined by monitoring the formation of the LMCT band at 389 nm (data not shown). This value represents the average obtained from a second order fit and a reciprocal plot of $1/\Delta A_{389}$ vs $1/[N_3^-]$ utilizing the raw data. The value for K_{eq} agrees quite well with that previously reported [111]. Determining a K_d value for the Cu(II)-CN^- complex is more difficult given that there exists no LMCT band in the visible region. PSAO was therefore titrated with cyanide following preincubation with near saturating amounts of azide, as established by He *et al*. [175]. Upon addition of azide, a λ_{max} shift from 500 to 509 nm of the TPQ chromophore was observed to occur in PSAO (Figure 30), most likely due to a perturbation of the electrostatic environment of the cofactor [111]. As seen in Figure 30, CN^- binding to Cu(II) was indirectly determined by monitoring the decrease in absorbance at 389 nm due to displacement of N_3^-. Linear

least-squares analysis of the ΔA versus cyanide concentration (Figure 31) produced a K_d value of 3.4 ± 0.3 mM (K_{eq} = 300 ± 24 M^{-1}) for PSAO. Spectroscopic and kinetic analysis following extensive dialysis of the protein sample (four exchanges against 1 L of 100 mM KPO_4, pH 7.2) showed complete recovery of the native TPQ_{OX} absorbance feature and full restoration of activity.

As observed in Figure 30, azide was not cleanly titrated off. A spectral feature with absorbance near 345 nm was observed to begin forming with the initial addition of cyanide, concurrent with a decrease at both 389 nm (Cu(II)-N_3^-) and 509 nm (TPQ_{OX}). This trend continued throughout the titration until the absorbance decrease at 389 nm was minimal. A blue shift of the λ_{max} of TPQ_{OX} was also observed to occur at higher cyanide concentrations (26 – 31 mM). When analyzing this data according to linear least squares analysis (Figure 31), it was necessary to utilize points where the Δ345 nm was negligible, since the 345 nm moiety has some absorbance at 389 nm. Therefore, in order to minimize the effects of the species growing in at 345 nm, only cyanide concentrations from 0 to 11.9 mM were linearly fit, despite using the final absorbance value (A_Z, see above) at 389 nm corresponding to a cyanide concentration of 24.4 mM. The red data points seen in Figure 31 show the deviation from linearity caused by the species growing in with absorbance ~ 345 nm. For comparative purposes, Δ420 nm was used to produce a similar plot providing a K_d of 4.6 ± 0.3 mM (data not shown). Utilizing absorbance at this wavelength eliminated much of the spectral contribution due to the formation of the 345 nm chromophore. The average calculated K_d from both plots was 4.0 ± 0.6 mM.

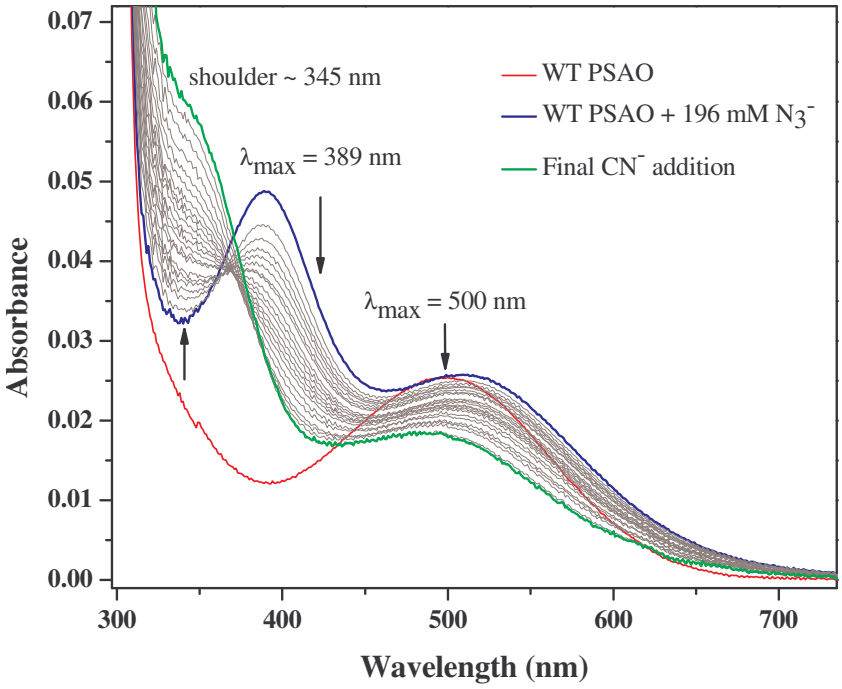

Figure 30: Cyanide as a Cu(II)-directed ligand in PSAO. CN^- displacement of azide bound to copper monitored via the decrease in the Cu(II)-N_3^- LMCT band. Final spectrum represented in green is 31.5 mM CN^-.

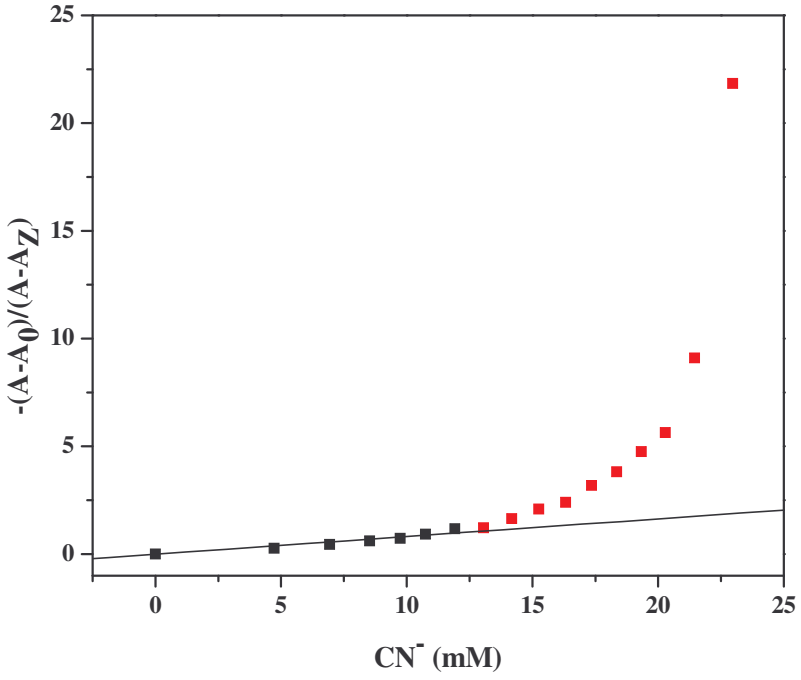

Figure 31: Linear least squares analysis of the displacement of N_3^- from Cu(II) by CN^-. Data points in red represent the deviation from linearity caused by the species growing in with absorbance ~ 345 nm, and as such were masked for this analysis.

Cyanide as a Cu(I)-Directed Ligand

As previously reported [87,111,175,176], cyanide preferentially binds to Cu(I), stabilizing the Cu(I)-TPQ_{SQ} moiety against reaction with O_2. In order to determine a K_d for CN^- binding to Cu(I), PSAO was reduced with benzylamine under stringent anaerobic conditions, producing the Cu(II)-TPQ_{AMQ} ⇆ Cu(I)-TPQ_{SQ} equilibrium [87,111,175]. Addition of cyanide will be reflected in a shift in this equilibrium to the right, resulting in an increase in the amount of TPQ_{SQ} present. Plotting changes in semiquinone absorbances at 363 nm and 409 nm versus cyanide concentration yielded apparent K_d values of 270 ± 40 μM and 333 ± 42 μM, respectively, for the Cu(I)-CN^- complex (Figure 32). The average K_d value calculated from these quantities is 302 ± 82 μM. The high degree of error obtained is reflective of the inherent difficulties of this experiment related to the formation of a precipitate. The titration was subsequently repeated several times with consistent results. In order to partly overcome the problems caused by the precipitate, spectra were corrected for baseline drift at 700 nm preceding data analysis. It is also worth noting that upon completion of the experiment, the sample required approximately 1 hour to reoxidize from TPQ_{SQ} to TPQ_{OX} once exposed to O_2 under stirring, in agreement with previous reports [111].

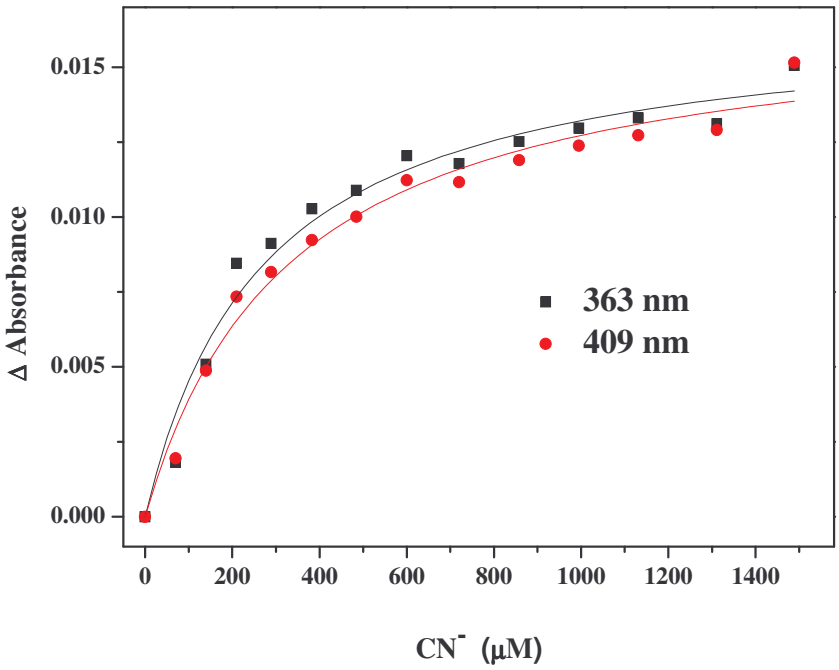

Figure 32: Cyanide as a Cu(I)-directed ligand in PSAO. Additions of cyanide cause a shift in the Cu(II)-TPQ_{AMQ} ⇆ Cu(I)-TPQ_{SQ} equilibrium to the right. Data fit with a binding curve in order to determine K_d values.

Addition of cyanide to the substrate reduced form of the enzyme led to the formation of a small amount of precipitate. The nature of this precipitate was examined using atomic absorption spectroscopy and found to contain trace copper. One possibility is that CN^- complexes Cu(I), which is 3-coordinate in the substrate reduced enzyme [182], thus removing it as CuCN(s). This explanation is consistent with the methodology for removing copper from CuAOs, which entails reducing the enzyme under anaerobic conditions and dialyzing against a substantial excess of CN^- [92,106]. It is more likely that the precipitate was protein, which would account not only for the trace copper observed in the atomic absorption results but also for the turbidity of the sample. Furthermore, it was noted that over the duration of the experiment (~3 – 4 hours), TPQ_{OX}

was consistently observed to reform in trace amounts. Initially it was believed this was due to slight O_2 contamination, leading to the implementation of the strict anaerobic conditions described above. However, even under these conditions, TPQ_{OX} was observed to slowly reform, implicating disproportionation of TPQ_{SQ} according to the relationship: 2 Cu(I)-TPQ_{SQ} + H_2O + H^+ ↔ Cu(I)-TPQ_{AMQ} + Cu(I)-TPQ_{OX} + NH_4^+ [87]. Precipitation [176] and loss of TPQ_{SQ} [176,183] could also be explained by trace levels of H_2O_2, formed from O_2 contaminant upon initial reduction with benzylamine, reacting with TPQ_{SQ} to produce $OH^\bullet$ according to the following equation:

$$TPQ_{SQ} + H_2O_2 \rightarrow TPQ + OH^\bullet + H_2O$$

In BPAO, addition of catalase provided no protection against the formation of $OH^\bullet$ [183], suggesting reaction of TPQ_{SQ} with H_2O_2 before it diffuses from the active site. The observation that precipitation occurred in the presence of CN^- would be consistent with stabilization of Cu(I)-TPQ_{SQ}, thereby yielding more TPQ_{SQ} to react with trace H_2O_2.

Cyanohydrin Derivatization of the Native Quinone Cofactor

To focus more directly on the spectroscopic feature near 340 nm (Figure 30) and eliminate the complexity associated with the azide displacement methodology, wild-type PSAO was titrated with cyanide. Figure 33 illustrates the results obtained with 14 μM PSAO up to a final cyanide concentration of 30 mM. It was determined that pH did not remain constant in this experiment even in the presence of 0.1 M KPO_4, pH 7.2. The pH of the 100 mM cyanide stock was measured to be 9.5, with the pH in the enzyme titration experiment gradually shifting to a more basic pH (final pH ~8.5). When the pH change is

slight (7.2 – 7.6; corresponding to a cyanide concentration of 0 – 13.3 mM), a clean isosbestic point ~410 nm can be seen between TPQ_{OX} (λ_{max} = 500 nm) and the new species with λ_{max} = 345 nm and ε_{345} ~8.4 x 10^3 $M^{-1}cm^{-1}$, indicating that this new moiety is a derivative of the quinone cofactor. Furthermore, a slight blue shift of the native TPQ_{OX} chromophore occurred as the pH became more alkaline at high cyanide concentrations, as observed in Figure 30. A separate PSAO sample (16.2 μM) was also titrated with cyanide to a final concentration of 50 mM in order to determine the general solvent effects upon the spectroscopic properties of TPQ. The λ_{max} of TPQ_{OX} was observed to blue shift by ~25 nm, while the absorbance at 345 nm (described above) slightly decreased concurrent with an overall broadening in this absorbance feature (data not shown). Formation of the ~345 nm species was observed to be rapid (less than 3 minutes). Protein samples were extensively dialyzed following titrations (four exchanges against 1 L of 100 mM KPO_4, pH 7.2) and kinetically and spectroscopically analyzed. The native TPQ_{OX} chromophore was observed to return and activity was fully restored to control levels.

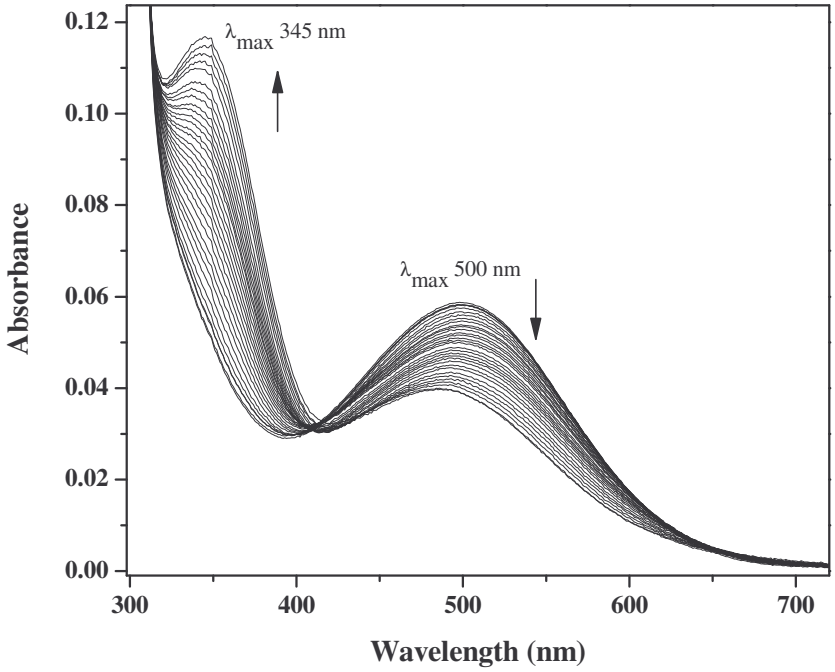

Figure 33: Cyanohydrin derivatization of the native quinone cofactor in PSAO. NaCN added in ~ 1 mM additions to a final CN^- concentration of 30 mM.

Interaction of Cyanide With a TPQ Model Compound

Analysis of the interaction of cyanide with a TPQ model compound (5-*tert*-butyl-2-hydroxy-1,4-benzoquinone; **1**) under a variety of conditions was performed by Dr. Ke-Qing Ling (Lawrence M. Sayre laboratory, Case Western Reserve University) and is presented in much greater detail in [98]. The following is a very brief synopsis of these results, in order to aid the analysis of what is observed in PSAO.

Model chemistry confirmed that addition of excess solid KCN resulted in a rapid conversion of **1** to a new product **2**, assigned as the C5 cyanohydrin (Figure 34). This conversion was discovered to be pH dependent, and Figure 34 shows the conjugate acid (**1H** and **2H**) and conjugate base forms ($\mathbf{1}^-$ and $\mathbf{2}^-$). The apparent sensitivity of the equilibrium to pH arises because addition of CN^- to the C5 carbonyl of **1** to give

cyanohydrin **2** requires completion by protonation. Furthermore, the pK_a of **2H** in water should be in the range of 4-5, thus, the 346 nm band observed upon addition of CN^- to **1** at neutral pH represents $\mathbf{2}^-$. From a titration experiment performed at pH 7.2, the extinction coefficient of the 346 nm absorption for $\mathbf{2}^-$ was calculated to be $4.8 \times 10^3\ M^{-1}\ cm^{-1}$, which compares favorably with that observed for the interaction of PSAO with cyanide. Interestingly, irreversible formation of a new chromophore around 335 nm was shown to occur to a small extent at high pH (>10) and higher [CN^-]. This 335 nm species was identified as the C1 conjugate adduct of $\mathbf{1}^-$ (K.-Q. Ling and L.M. Sayre, unpublished results).

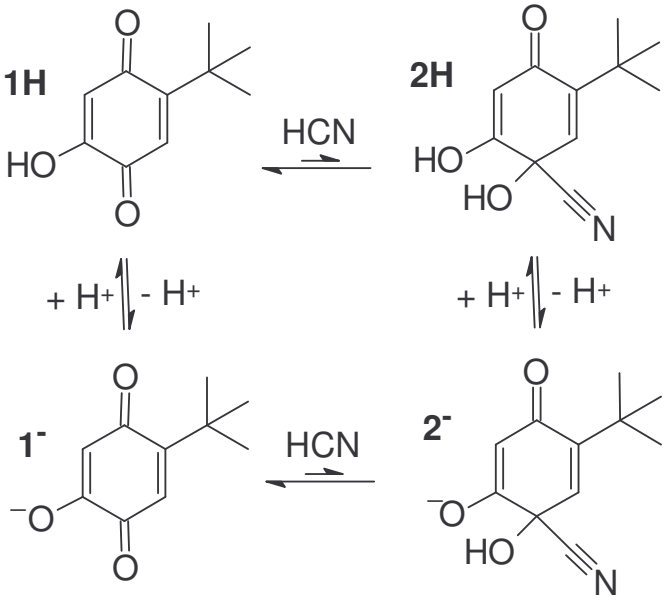

Figure 34: TPQ model chemistry with cyanide. (**1H**) TPQ model 5-*tert*-butyl-2-hydroxy-1,4-benzoquinone and ($\mathbf{1}^-$) its enolate form. (**2H**) The C5 cyanohydrin form of the TPQ model compound and ($\mathbf{2}^-$) its enolate form.

pH Effects on Cyanohydrin Formation in PSAO

To investigate the observed shifts in pH during the aforementioned cyanide titration experiments, and the pH effects observed in the model chemistry, samples of PSAO were incubated with ~17 mM CN^- from a stock solution that had been adjusted to a pH of 7.2 prior to addition. Comparatively, another sample of PSAO was incubated with a similar amount of cyanide from a stock that was not adjusted to a pH of 7.2, meaning that the pH in the cuvette was ~7.8 after addition of cyanide. Initial (~3 minutes) and final (~50 minutes) spectra between the two experiments were compared in order to quantitatively compare cyanohydrin formation (data not shown). Quantitation of TPQ_{OX} modification was determined by monitoring the ΔA_{500}, using an ε_{500} of 2500 $M^{-1}cm^{-1}$. It was determined that at pH 7.2 at 50 minutes, 13.5% of the native chromophore was modified, while at pH 7.8, 16% modification occurred. However, accounting for the slight difference in concentration of PSAO and cyanide in these experiments, it can be concluded that cyanohydrin formation occurred approximately to the same extent at both pH values. Interestingly, the majority (~65%) of TPQ_{OX} modification occurred within 3 minutes in both experiments, while the remaining ~35% was observed to occur steadily over the course of 50 minutes (data not shown). Moreover, it was observed in both experiments that modification continued beyond 50 minutes, as absorbance at 500 nm continued to decrease.

Reactivity of TPQ-Cyanohydrin With Phenylhydrazine

A sample of PSAO derivatized with cyanide was titrated with phenylhydrazine to determine the reactivity (i.e. reversibility) of the TPQ-cyanohydrin towards substrate

analog (Figure 35). PSAO was derivatized with 17.4 mM CN^-, which modified 4.3 µM TPQ out of 26.6 µM present (16%). Additions of phenylhydrazine reacted rapidly (~5 minutes) up to 1.2 equivalents, with subsequent additions requiring ~15 to 20 minutes to react. Complete reactivity was observed relative to the control sample (11.8 µM), as shown in Figure 35, inset. In contrast to a previous report [111], the λ_{max} of the topa-phenylhydrazone adduct in the presence of cyanide was identical to the control λ_{max} (445 nm) and 100% reactivity with phenylhydrazine was obtained.

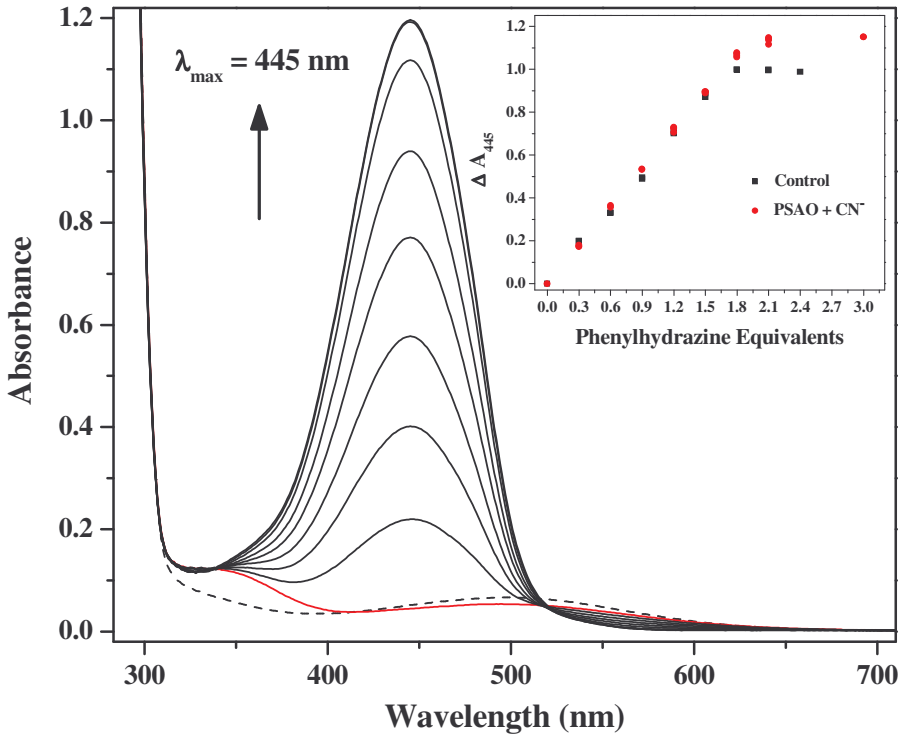

Figure 35: Reactivity of TPQ-cyanohydrin with phenylhydrazine in PSAO. Dashed line (-----) represents WT PSAO prior to addition of CN^-; solid red line represents PSAO spectrum after addition of 17 mM CN^-. Inset: Plot of ΔA_{445} vs phenylhydrazine equivalents for WT (11.8 µM; ■) and cyanide-derivatized PSAO (14.7 µM; ●).

The Effect of Cyanide on Amine Oxidation

The effects of cyanide on enzymatic catalysis were examined for PSAO. Data analysis revealed that V_{max} and K_{Mapp} decreased as cyanide concentration increased, indicating that cyanide was an uncompetitive inhibitor versus substrate amine (Figure 36). Interestingly, minor inhibition of PSAO was observed at higher substrate levels at a 1.35 mM cyanide concentration. This same kinetic effect has been observed for PSAO with azide (see next chapter). Standard substrate inhibition models do not describe this data, as fits yield implausible values for kinetic parameters (data not shown). The nature of this inhibition is currently not understood, but is deemed to be largely insignificant given that activity levels are only slightly affected (~10%) for three data points in the 1.35 mM cyanide curve. Yet, in order to exclude the complicating effects of this non-specific inhibition, the kinetic fit for the 1.35 mM cyanide curve was obtained by utilizing only the points where inhibition was not observed (Figure 36). The $1/K_{Mapp}$ versus CN^- concentration plot generated from the data fit in this manner (Figure 37), as explained by Segel (1975) [145], yielded a line with a regression value greater than 0.99 and a K_i value of 648 ± 77 μM.

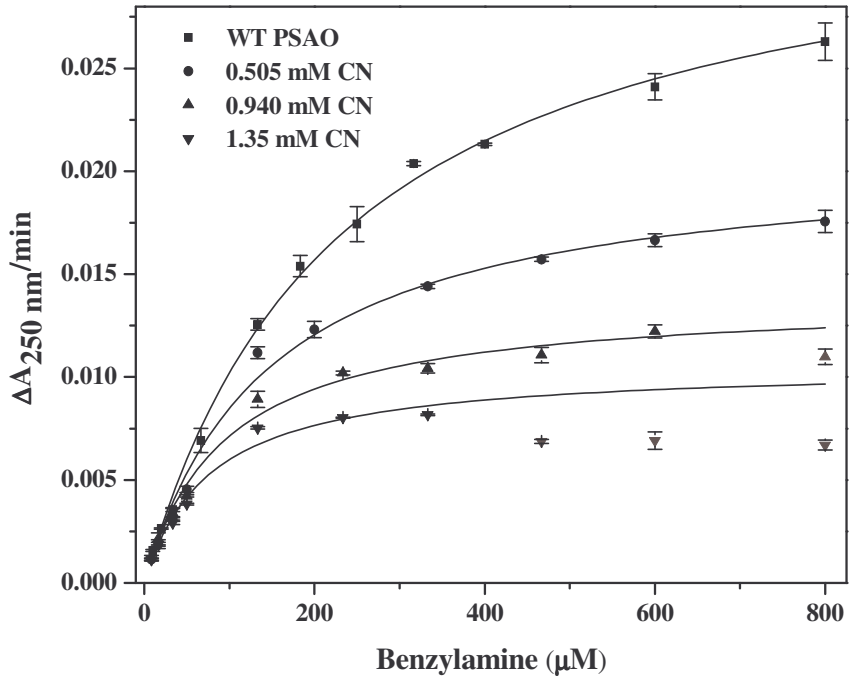

Figure 36: The effect of cyanide on amine oxidation in PSAO. Plot shows initial velocity versus substrate benyzlamine concentration for various concentrations of cyanide. All data curves were fit to the Michaelis-Menten equation.

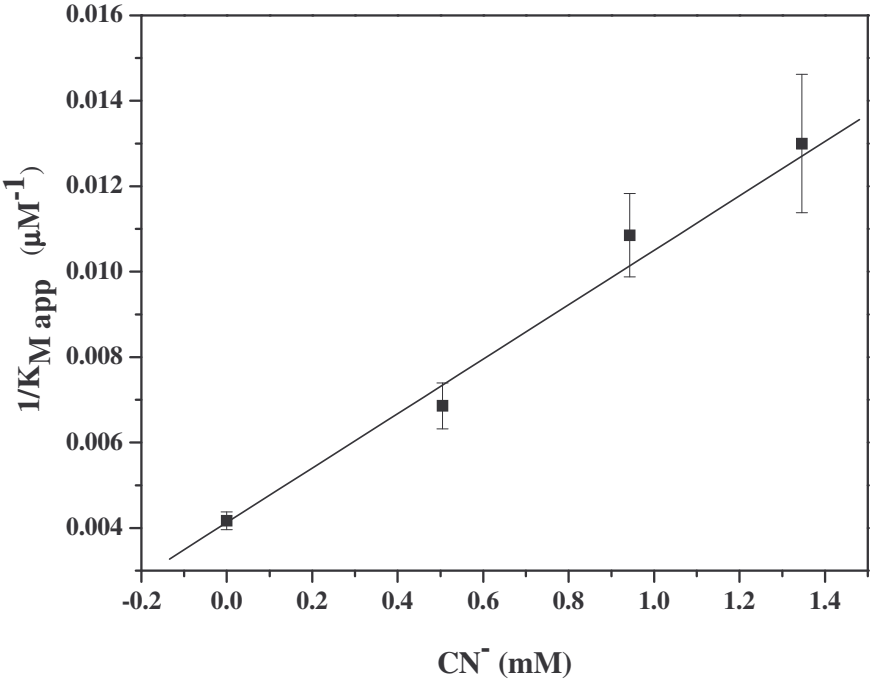

Figure 37: The reciprocal plot of $1/K_{Mapp}$ vs $[CN^-]$ for PSAO. Plot represents standard treatment of the data in Figure 36 for an uncompetitive inhibitor in order to calculate K_i.

Discussion

Given the ability of cyanide to coordinate both Cu(II) and Cu(I), this ligand has traditionally been used to probe the electronic environment in both the oxidized and substrate reduced forms of CuAOs [111,113,114,175,178]. This research has been primarily concerned with determining cyanide's affects on amine oxidation and O_2 reduction, respectively. The ligand substitution chemistry of cyanide is comparable among CuAOs, preferentially displacing a water molecule at the equatorial, as opposed to the axial position [112,113]. Consequences are reflected in the reactivity of the quinone cofactor and the copper ion, however, variability in observed modes of inhibition exists among CuAOs from different sources [113,114,175]. An early report with PPAO interpreted the uncompetitive mode of inhibition towards benzylamine and the noncompetitive mode of inhibition against O_2 as CN^- ligating copper and reacting with active site carbonyl groups [113]. This was substantiated in a subsequent study with BPAO and PKAO [175]. Despite this, no direct evidence for cyanohydrin formation in CuAOs has been presented [111,175]. Consequently, the main mechanism of inhibition by cyanide has been proposed to be the stabilization of Cu(I) by CN^-, which would prevent reaction of Cu(I) with O_2 during reoxidization [111]. This chapter presents the first direct spectroscopic evidence for cyanohydrin derivatization of the quinone cofactor in PSAO, and puts forth a mechanism for CN^- inhibition against substrate amine. This work has been published in the *Journal of Biological Inorganic Chemistry* [98], where the effects of cyanide on AGAO and a thorough analysis of cyanohydrin formation using TPQ model chemistry can be found.

TPQ-Cyanohydrin Formation

Interaction of CN^- with PSAO is featured by a reversible conversion of the native TPQ chromophore to a moiety with an absorbance at 345 nm in PSAO (Figure 33). Cyanide addition to TPQ in PSAO was concluded to occur exclusively at TPQ(C5) by virtue of its reversibility (dialysis resulted in return of the TPQ_{OX} absorbance band and full recovery of activity) and the match of the chromophore with that for the C5 cyanohydrin for the TPQ model **1** (Figure 34). The observation in the model chemistry that addition of CN^- could also occur at C1, rather than C5, of TPQ under basic conditions was surprising given the steric bulk (*tert*-butyl group) at this position, and raises the question as to whether this could occur in an enzyme system [98]. Although no evidence was obtained for addition of CN^- to C1 for PSAO, addition at TPQ(C1) might occur in other CuAOs if the steric and conformational consequences of C1 addition can be accommodated by the active site.

Certainly, there should be differences between CuAOs also in the likelihood of cyanohydrin formation at C5. The finding in the model system that cyanide adduction is favored more in DMSO than in water indicates that the equilibrium is quite sensitive to environmental effects, and this must explain the substantial difference in the reactivity of TPQ_{OX} towards CN^- observed between AGAO and PSAO, with TPQ-cyanohydrin formation in AGAO requiring cyanide concentrations an order of magnitude greater (~26 mM) than in PSAO (~700 μM) [98]. Although one might surmise that the active site of PSAO is more hydrophobic and that the active site of AGAO is more hydrophilic, the much greater ease of cyanohydrin formation in PSAO may also arise from specific

hydrogen-bonding or other non-covalent interactions within the active site that stabilize the adduct relative to the starting carbonyl.

Cyanohydrin derivatization of TPQ was examined by EPR and resonance Raman spectroscopies for APAO and PKAO in a previous report by Dooley and coworkers [111], concluding that CN^- was not bound to either TPQ_{SQ} or TPQ_{AMQ}. For the EPR experiments, CN^- isotopes were added *following* anaerobic substrate reduction of the enzymes, yet it is now clear that CN^- can interact only with TPQ_{OX}. The lack of any observed effects suggests that APAO, like AGAO, does not readily form the TPQ-CN adduct.

The complexity of TPQ in the enzymes regarding microenvironmental effects and interactions with active site residues may also explain the "biphasic" behavior observed for TPQ-CN formation in PSAO. Binding of CN^- to both TPQ_{OX} and Cu(II) is quite rapid, so the observation that TPQ-CN formation occurs in two apparent phases is unexpected. Although this might result from the co-existence of two orientations of TPQ within the active site [16,50,184], no biphasic reactivity was observed in control titration experiments with phenylhydrazine, indicating that TPQ is predominantly in one orientation. Recently, TPQ was reported to be found exclusively in the productive orientation in PSAO at physiological pH [184]. If binding of CN^- to either TPQ_{OX} or Cu(II) is rapid and random, a population of enzyme will accumulate with CN^- bound only to TPQ, just as a population of enzyme will exist where cyanide is bound to Cu(II) that contains free TPQ_{OX}. Slower cyanohydrin formation for this latter population of enzyme relative to the native enzyme could then explain the observed biphasic kinetics. Ligand substitution at the Cu(II) center could affect the reactivity of TPQ_{OX} towards CN^-.

Substantial evidence exists concerning how either ligand substitution at copper or TPQ modification influences the reactivity and spectroscopic properties of the other cofactor [111,175,185-188].

The reactivity of TPQ-CN was examined by titrating phenylhydrazine into a sample of PSAO preincubated with CN^-. As shown in Figure 35, 100% TPQ-phenylhydrazone was obtained relative to control; however, reactivity slowed from ~5 minutes between subsequent additions (WT) to ~20 minutes in the presence of cyanide, due to competition between phenylhydrazine and CN^- for the same binding site on the quinone cofactor. The effect of CN^- upon the rate of reactivity of phenylhydrazine is in agreement with previous accounts [111,175]. In the previous report by Dooley and coworkers, phenylhydrazine reactivity in the presence of CN^- was reported to decrease for PKAO, PPAO, BPAO, and PSAO to varying degrees (80–95% of control), with 90% reactivity occurring at 49 mM CN^- in PSAO [111]. He *et al*. (1995) [175] reported that cyanide affected phenylhydrazine binding to PKAO in a manner that depended upon the concentration of cyanide, yet obtained complete reactivity for BPAO and PKAO at 15 mM CN^-.

The results reported here are in very good agreement with our previous work with PSAO as reported in [111]. The slight disparity (10%) in the levels of phenylhydrazone formation can be reconciled by differences in protocol. In previous experiments [111], PSAO was incubated with ~50 mM CN^- (yielding a pH in the cuvette of ~10), adjusted to a pH ~8.0, and titrated with phenylhydrazine. Addition of HCl to the sample caused formation of a precipitate and the resulting λ_{max} of the phenylhydrazone adduct was blue shifted by 4 nm. In this study, the spectroscopic properties of WT – PSAO were

examined upon titration of CN^- to a final concentration of 50 mM. The absorbance of the TPQ-CN moiety (345 nm) was discovered to decrease slightly concurrent with an overall broadening in this absorbance feature (data not shown). These observations are undoubtedly due to the coupled effects of pH and ionic strength and may explain why only 90% phenylhydrazine reactivity was previously obtained. As seen in Figure 35, no shift of the TPQ-phenylhydrazone λ_{max} was observed relative to control and 100% reactivity was achieved. Additionally, both full activity and the TPQ_{OX} absorption feature returned to control amounts following extensive dialysis for AGAO and PSAO samples subsequent to titration with CN^-. This indicates that CN^- reversibly binds in the active sites of both these enzymes at CN^- concentrations up to 50 mM (PSAO) and 100 mM (AGAO) [98].

Mechanism of CN^- Interaction With PSAO and AGAO

Cyanide displays uncompetitive inhibition towards turnover of amine substrate in both PSAO (Figures 36 and 37) and AGAO (data not shown, [98]) with K_i values of 648 ± 77 μM and 1.05 ± 0.13 mM, respectively, meaning that inactivation arises when CN^- binds to the substrate reduced form of the enzyme (ES complex and/or E_{RED}) [189]. Although CN^- interacts with both TPQ_{OX} and Cu(II) in the resting enzymes (Figures 30 and 33), uncompetitive inhibition suggests that cyanohydrin formation, which would result in competitive inhibition of substrate turnover, is not responsible for the observed inhibition. The finding that inhibition arises when CN^- interacts with E_{RED} is consistent with the previous report by Dooley and coworkers [111], where stabilization of Cu(I) against reaction with O_2 was attributed to be the source of inactivation. If this were

indeed the case, then the K_d value for this complex should be in agreement with the K_i value. In order to directly test this hypothesis, the K_d value for the Cu(I)-CN^- complex in PSAO was calculated to be 302 ± 82 μM. However, due to the precipitation difficulties with this experiment (see Results section), it is only appropriate to put forth the following qualitative statements: (1) the affinity (K_d) of CN^- for Cu(I) is an order of magnitude greater than the K_d of CN^- for Cu(II) in PSAO; and (2) the value of K_d for the Cu(I)-CN^- complex in PSAO is of similar magnitude to the calculated inhibition constant (K_i) for CN^- inhibition of amine oxidation relative to substrate amine. Higher affinity of CN^- for Cu(I) over Cu(II) is expected owing to metal to ligand π* back bonding [190], which is more extensive for the electron rich d^{10} Cu(I) relative to d^9 Cu(II).

This evidence aside, it seems that classical uncompetitive inhibition does not provide a complete description of the interaction of CN^- with these enzymes, given the disparity between the K_i values for AGAO and PSAO with substrate amine and the K_d for the Cu(I)-CN^- complex in PSAO, as these values should be approximately equal if the sole mechanism of inhibition was due to Cu(I) complexation. A possible explanation for the difference in these values could arise from the difficulty in obtaining an accurate K_d for the Cu(I)-CN^- complex. A more likely explanation, however, is that the K_i is a result of Cu(I) complexation as well as TPQ-cyanohydrin formation, a result more consistent with noncompetitive inhibition where I binds to E and ES and S binds to E and EI [189]. This behavior may help to explain why cyanide has been classically described as a mixed and/or uncompetitive inhibitor with respect to substrate amine for several CuAOs, especially at relatively high CN^- concentrations. It is understandable why it may be difficult to discern the true mode of inhibition towards substrate amine for a set of

CuAOs, especially owing to the finding that cyanohydrin formation occurs in such varying affinities between PSAO and AGAO.

In the current report, only a small subset of the quinone cofactors present would be modified at the concentrations of CN^- used in the kinetic analysis. Examining Figure 33, 1.38 mM CN^- (second addition) causes only 2.2% modification of TPQ_{OX} at 5 minutes, meaning that ~2% of the cofactors would be modified in the kinetic experiments for PSAO, with even less in the case of AGAO. Substantial inhibition is observed at 1.35 mM CN^- in the kinetic experiments (Figure 36), an effect which is inconsistent with the level of TPQ-CN formation. These results taken collectively lend support to the idea that the dominant mode of inhibition towards amine oxidation is indeed uncompetitive with CN^- stabilizing Cu(I) (Figure 38). The observation of the slow reoxidation of TPQ_{SQ} to TPQ_{OX} in the presence of CN^- (see Results) is consistent with this scheme and concurs with previous reports [87,111,175,176,178]. Substrate analogs (phenylhydrazine) and presumably substrates react with unmodified TPQ cofactors at similar rates in the presence and absence of CN^-. TPQ cofactors modified by cyanide, however, cannot react directly with substrate amine. Therefore, conversion back to TPQ_{OX} through perturbation of the TPQ-CN $\leftrightarrows$ TPQ_{OX} equilibrium, as mediated by binding of amine to TPQ_{OX}, becomes the determining factor for reactivity with amine substrate. This is supported by the observation that complete phenylhydrazine reactivity is slowed by a factor of ~4 when CN^- is present during the titration. Consequently, preequilibration with CN^- yields a group of derivatized cofactors which do not rapidly react with substrate amine (Figure 38).

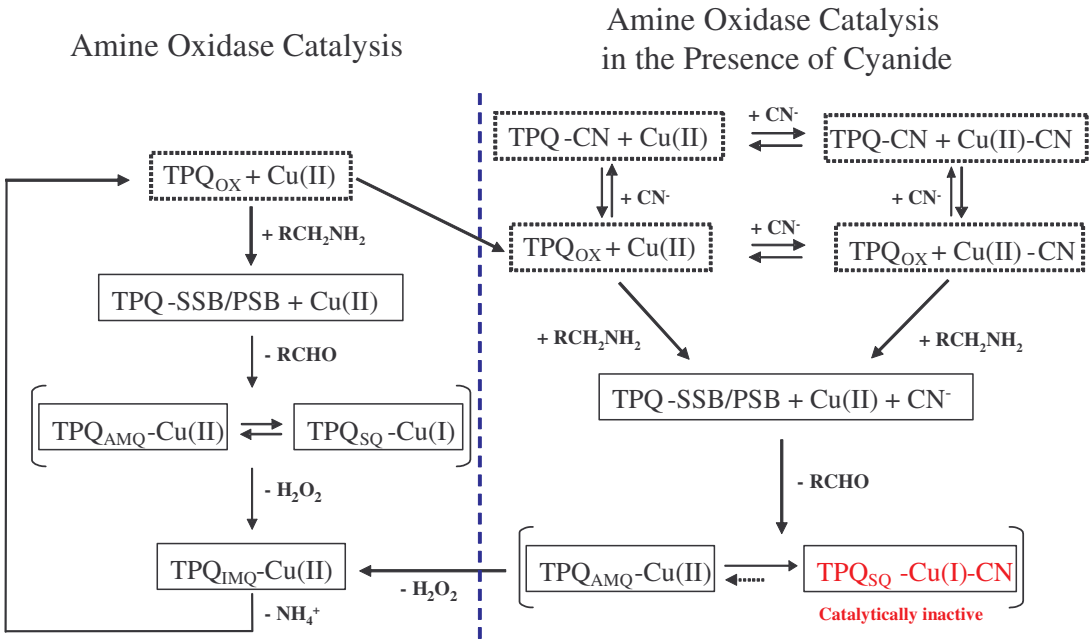

Figure 38: The proposed mechanism for CN^- inhibition of CuAO catalysis. The left panel indicates standard amine catalysis, also represented in Figure 6 (Chapter 1). The abbreviations used in this figure are given in Chapter 1.

Conclusions

In summary, the results summarized above in conjunction with those presented in reference [98], provide the first unequivocal spectroscopic evidence for cyanohydrin derivatization of the quinone cofactor. Cyanide addition to TPQ in both AGAO and PSAO was concluded to occur exclusively at TPQ(C5). The observation in the model chemistry that addition of CN^- can also occur at TPQ(C1) at high cyanide concentrations raises the question as to whether this addition might occur in other CuAOs if the steric and conformational consequences could be accommodated by the active site. The finding that cyanohydrin formation occurs so much more readily in PSAO than in AGAO is remarkable and suggests there are profound differences in the dielectric

microenvironment and/or the availability of nearby active site residues with non-covalent interaction potential, in the vicinity of the TPQ(C5) carbonyl between the two enzymes. Nonetheless, this type of interaction does not play a significant role in the mechanism of inhibition towards substrate amine. Stabilization of Cu(I) by CN^- appears to act as the dominant mode of inhibition, presumably acting in direct competition with O_2 for binding to Cu(I), thereby preventing reoxidation of the reduced enzyme [111,175]. It has been argued that the TPQ_{SQ}-Cu(I) species is off-pathway (Figure 8). In this case, CN^- ligation of Cu(I) would then perturb the equilibrium with the on-pathway, TPQ_{AMQ}-Cu(II) moiety. Furthermore, cyanide complexation to copper may disrupt electrostatic interactions between copper and reduced dioxygen species, as implicated as being potentially significant in O_2 affinity [107]. However, given the greater similarity between the K_i value for inhibition of substrate amine (648 ± 77 μM) and the K_d for the Cu(I)-CN^- complex (302 ± 82 μM), relative to the K_d for the Cu(II)-CN^- complex (4.0 ± 0.6 mM), the data suggest that Cu(I)-TPQ_{SQ} is likely a catalytically competent intermediate in PSAO.

A COMPARATIVE STUDY OF THE BINDING AND INHIBITION OF TWO COPPER CONTAINING AMINE OXIDASES BY AZIDE: IMPLICATIONS FOR THE ROLE OF COPPER DURING THE OXIDATIVE HALF-REACTION

Introduction

CuAO catalysis proceeds through a Ping-Pong Bi Bi mechanism divided into two half-reactions (see chapter 1):

$$E_{ox} + RCH_2NH_2 \leftrightarrow E\text{-}RCH_2NH_2 \rightarrow E_{red} + RCHO \quad (1)$$

$$E_{red} + O_2 + H_2O \rightarrow E_{ox} + H_2O_2 + NH_3 \quad (2)$$

The first half-reaction involving oxidation of primary amine compounds to aldehydes (Eq. 1) is known as the reductive half reaction and is detailed in Figure 6, A $\rightarrow$ D. The second half-reaction involving reoxidation of the organic cofactor is known as the oxidative half-reaction (Eq. 2), and is diagrammed in Figure 6, D $\rightarrow$ A. The foremost unresolved issue in CuAO catalysis concerns the precise role of copper during the oxidative half-reaction. Two potential reoxidation mechanisms are detailed in Figure 8. Initially, we suggested that the first electron reduction of O_2 occurred by direct reaction with Cu(I) (Figure 8, B), resulting in a Cu(II) bound superoxide species (A $\rightarrow$ C) [87,104,105]. This proposal circumvents the spin conversion problem related with two-electron reduction reactions of oxygen [99], and is corroborated by the ample precedence for the reactivity of three-coordinate Cu(I) sites with dioxygen in copper-containing metalloproteins [100-102]. A thorough kinetic study of the catalytic intermediates in

lentil seedlings amine oxidase (LSAO) strongly supported this mechanism [121,191]. Additional support for a redox role of copper comes from a recent report describing the effects of metal substitution in the CuAO from *Arthrobacter globiformis* [92]. The rate enhancement for reoxidation in the native, copper-containing enzyme, compared to metal-substituted forms, was proposed to be consistent with reduction of Cu(II) to Cu(I), thereby implicating the Cu(I)-TPQ_{SQ} species as a viable intermediate [92].

Results obtained using the amine oxidase enzymes from *Hansenula polymorpha* (HPAO) and bovine plasma (BPAO) have led to the proposal that Cu(II) reduction is not essential for enzymatic reoxidation, thereby providing the alternative reaction pathway shown in Figure 8, A2 $\rightarrow$ C2 [72,91,106,107]. These studies propose that O_2 binds in an off-metal hydrophobic pocket and the first electron transfer event to O_2 comes from TPQ_{AMQ} (A2 $\rightarrow$ B2; rate limiting step). The superoxide anion that is generated then migrates to the Cu(II) center (B2 $\rightarrow$ C2) [89]. A key feature of this mechanism is that the copper-bound axial water ligand serves as a proton source in TPQ reduction, resulting in a Cu(II)-OH^- species (A2). It is believed that once O_2 is reduced to $O_2^{\bullet -}$ by TPQ_{AMQ}, the pK_a of the resulting TPQ_{SQ} is perturbed in a manner allowing for rapid proton transfer back to the metal bound hydroxide species, thereby forming H_2O. This metal bound water molecule is then expected to undergo rapid substitution with superoxide anion [89]. Further support of a non-redox role for copper comes from a theoretical study utilizing density functional theory, which implicates the paramagnetic copper center in the spin transitions necessary to produce singlet TPQ from the reaction of singlet TPQ_{AMQ} with triplet O_2 [108].

Finally, Wilmot *et al*. determined the structure of a steady-state intermediate that accumulates in *Escherichia coli* amine oxidase (ECAO) upon aerobic exposure to excess β-phenylethylamine [115]. A reduced dioxygen species was resolved, replacing the axial water ligand of copper in a side-on fashion, and was assigned as the peroxide product (Figure 9) [73,115]. The observed peroxide species bridges the copper and TPQ cofactor, consistent with electron transfer occurring from either TPQ or copper [73,115]. It is clear that additional kinetics and spectroscopic experiments of structurally characterized CuAOs is necessary to clearly delineate the role of copper during the oxidative half-reaction.

As mentioned in the previous chapter, the monodentate ligands cyanide and azide replace the equatorial H_2O ligand of copper and are effective inhibitors of multiple CuAOs [110-113]. Their effects on catalysis can primarily be rationalized in terms of the internal redox equilibrium TPQ_{AMQ}-Cu(II) $\leftrightarrows$ TPQ_{SQ}-Cu(I), with N_3^- preferentially binding Cu(II) and CN^- preferentially binding Cu(I) [111]. The effects of these ligands can vary substantially from enzyme to enzyme, as the magnitude of K_{eq} for the above equilibrium is highly dependent upon the source of the enzyme [87].

Although these ligands have been used previously for the study of CuAOs, significant variations in the methodology, as well as the quality and reproducibility of the data, have led to ambiguities in interpretation. Furthermore, systematic and direct comparisons among CuAOs are necessary, as it has become increasingly clear that significant differences may exist in the interaction of CuAOs with these ligands [98,111,175]. For example, the inhibition of PPAO by azide with respect to substrate amine has previously been described as uncompetitive [192,193], while inhibition

patterns for BPAO have been reported as mixed at low amine concentrations with a shift to uncompetitive at higher substrate concentrations [112]. As far as the oxidative half-reaction, azide has been described as both a competitive inhibitor [113,114] and a noncompetitive inhibitor [72] with respect to O_2.

It may be anticipated that if substrate dioxygen interacts directly with the copper site during enzymatic reoxidation, inhibition by azide should appear competitive with respect to O_2. Although the results from inhibition experiments conducted under turnover conditions are not unambiguous, such data provide an important foundation for assessing possible mechanisms, and in this case can provide an informative test of hypotheses for the role of copper in the reaction of reduced CuAOs with O_2. The present chapter details the electronic and mechanistic effects of N_3^- binding on each half-reaction for *Pisum sativum* amine oxidase (PSAO) and *Pichia pastoris* amine oxidase (PPLO). PSAO is an especially attractive enzyme for such analysis because this enzyme has the largest K_{eq} value for the TPQ_{AMQ}-Cu(II) $\leftrightarrows$ TPQ_{SQ}-Cu(I) equilibrium [87]. PPLO, on the other hand, forms very little TPQ_{SQ}-Cu(I), even in the presence of cyanide (E.M. Shepard, D.M. Dooley, unpublished results). Therefore, comparison of the effects of azide between these two enzymes should provide valuable information in regards to the mechanism of O_2 reduction.

Materials and Methods

Enzyme Purification and Isolation

PSAO [19] and PPLO [194] were purified as described previously. Only protein of the highest quality was utilized for experimentation (1.8 TPQ/dimer). Protein concentrations were calculated using extinction coefficients at 280 nm as previously reported [19,194], and using an extinction coefficient of 2,500 $M^{-1}cm^{-1}$ for TPQ [89]. All experiments for PSAO were carried out in 100 mM potassium phosphate buffer, pH 7.2, while those for PPLO were performed in 50 mM HEPES buffer, pH 7.0.

Azide Titrations of Oxidized Amine Oxidases

A sample of PSAO (15.3 μM) was titrated with a 1.5 M stock of NaN_3 (Fisher Chemicals, NJ, USA) and the LMCT band for the Cu(II)-N_3^- complex was monitored at 389 nm. Samples of AGAO, PPLO, and rhDAO were also titrated with respective NaN_3 stocks and LMCT bands were monitored. All sodium azide stocks were made fresh immediately prior to use and were adjusted to the respective experimental pH values as listed above. UV and visible absorption data were acquired utilizing a Cary 6000i UV/vis/NIR spectrophotometer (Varian, Australia) connected to a Cary dual cell Peltier accessory for temperature control. Absorbance data were analyzed using Origin 7.0 software (Microcal, MA, USA). The ΔA of the respective LMCT bands were plotted versus azide concentration and the data were fit to a titration curve in order to determine respective K_d values for the Cu(II)-N_3^- complex. Titrations of PSAO, AGAO, and PPLO were performed at 30 °C, while rhDAO was performed at 37 °C.

Azide Mediated Inhibition of HRP

Since azide is a known H_2O_2 dependent mechanism-based inhibitor of HRP with a k_{inact} of 0.69 min^{-1} [195], it was critical to show that azide mediated inactivation of HRP was not occurring during the time frame of the coupled assays (≤ 1 min), as described below. A series of control assays performed with PSAO (the CuAO that exhibits the fastest turnover) at 250 mM azide indicated there was no azide mediated effect on the ability of HRP to turnover the H_2O_2 that was generated during the oxidation of putrescine. In addition, control assays with PPLO showed that there was no difference between the experimentally determined rate of benzylamine oxidation using the direct assay and the ABTS/HRP coupled assay in the presence of 40 mM azide (data not shown). Experiments were performed by E.M. Shepard and G.A. Juda.

Azide Inhibition of the Reductive Half-reaction

In order to determine the effects of azide upon the first half-reaction (Eq. 1), kinetic characterization was determined at three different azide concentrations for PPLO and PSAO. Substrate O_2 was kept at near saturating amounts (~ 185 μM dissolved O_2) while substrate amine was varied below and above respective K_M values for each enzyme. The preferred amine substrate varied depending on the enzyme source, with putrescine being used for PSAO and benzylamine for PPLO. Ionic strength was controlled for all kinetic assays (both those for the reductive and oxidative half-reactions) by addition of KCl. KCl was determined to have no inhibitory affect on respective CuAO activity, as determined through a series of control assays conducted prior to experimentation [98]. Assays (including those described below for the oxidative half-

reaction) were performed at controlled ionic strengths by varying the ratio of azide to salt (PPLO, 150 mM; PSAO, 540 mM). The factor controlling ionic strength was determined by the amount of azide required to achieve adequate levels of inhibition.

For PPLO, amine oxidase activity was determined by monitoring benzaldehyde production over the course of 3 min at 250 nm using an extinction coefficient of 12,800 $M^{-1}cm^{-1}$ [140]. PSAO catalytic activity was monitored via the 4-aminoantipyrine/vanillic acid coupled assay of Holt *et al*. utilizing an extinction coefficient of 6000 $M^{-1}cm^{-1}$ at 498 nm for the quinoneimine dye [67,143].

Kinetic analysis involved first equilibrating each enzyme with a given amount of azide for two min under magnetic stirring, followed by addition of substrate amine to initiate each assay. Assays were at least run in duplicate, most often triplicate, at a particular substrate concentration. Error bars on each plot represent the standard deviation of the rate at a particular substrate concentration (Origin 7.0 software, Microcal, MA, USA). Steady-state kinetic data were collected on a Hewlett-Packard 8453 diode-array spectrophotometer equipped with a thermostatted cell chamber connected to an Endocal RTE-5 circulating water bath.

Azide Inhibition of the Oxidative Half-reaction

In order to determine the effects of azide on the oxidative half-reaction of amine oxidation (Eq. 2), levels of substrate amine were kept at saturating amounts (at least $10 \times K_M$) while substrate O_2 was varied. Rates of oxygen uptake in the presence of varying amounts of azide were determined using an Instech (Plymouth Meeting, PA) model 125/05 Clark-type oxygen electrode interfaced to a single channel Instech model 103

oxygen electrode amplifier. All assays were conducted in a thermostatted, 680 μL sealed batch cell equipped with an Instech model 103 magnetic stirring mechanism. The ionic strength of all assays was kept consistent as described above. Concentrations of amine substrates varied given the respective K_M values for the different enzymes with 460 μM benzylamine utilized for PPLO and 6 mM putrescine used for PSAO. In addition, rates of oxygen consumption were measured for PSAO at 1 mM putrescine (~$2 \times K_M$).

The following procedure was used for each enzyme. Buffer was made at the appropriate ionic strength and allowed to equilibrate overnight in a 30 °C H_2O bath. Substrate amine was then freshly added to the temperature and air-equilibrated buffer, which was subsequently divided into two flasks. The first flask was left exposed to air while the second flask was purged with argon passed through a vanadium bubbler, HCO_3, H_2O setup [180] for at least 1 hour. Mixtures of air-equilibrated and anaerobic buffer were then injected into the cell chamber via gas tight syringes to achieve a desired level of dissolved O_2, as monitored using the calibrated Clark-type oxygen electrode. When desired levels of dissolved O_2 were reached, the cell chamber was sealed and the output reading was monitored for a period of 10 seconds to ensure there was no electrode drift. Assays were then initiated by addition of 2 – 3 μL of respective enzyme via a gas tight syringe (Figure 39). Initiation of kinetic assays by addition of enzyme could be accomplished due to the fact that azide binding in CuAOs has been shown to be rapid [72,98,111].

Substantial efforts were made in order to ensure the reproducibility of experimental rates. For each kinetic curve, a minimum of 14 – 20 data points were

collected. Each data point represents the rate of oxygen depletion from the assay chamber, determined from a linear fit of the change in dissolved oxygen levels over time (Figure 39). Reported error bars arise from the standard error associated with the linear fits to the initial reaction rate data (Origin 7.0 software, Microcal, MA, USA). In several cases, rates of O_2 consumption were obtained on consecutive days at the same concentrations of dissolved oxygen, and in each case examined the respective rates were within error.

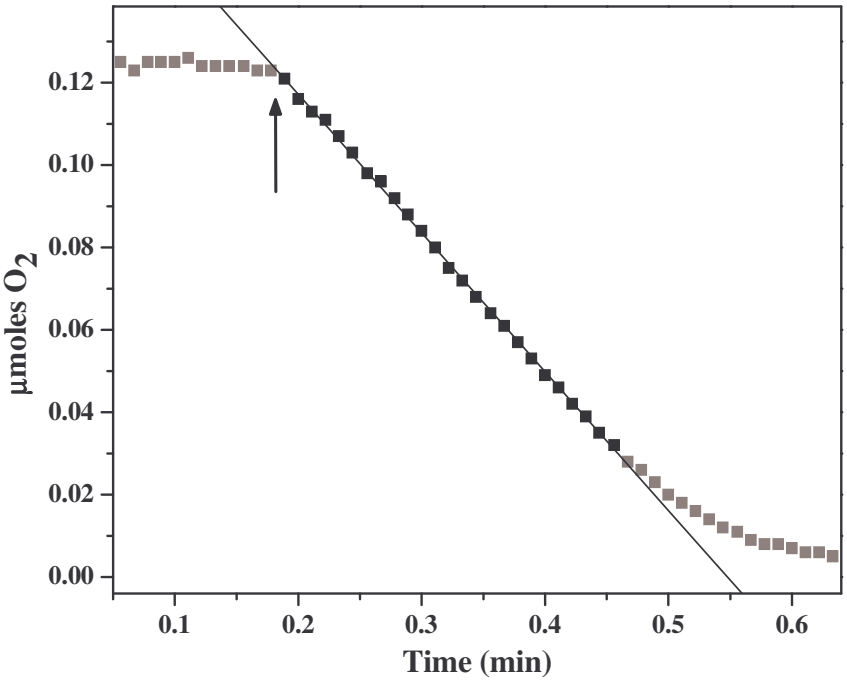

Figure 39: Representative oxygen consumption kinetics followed in the assay chamber. Trace represents PSAO control assay initiated at 181 µM O_2. Arrow indicates the point at which enzyme was injected into the chamber. Black squares (■) represent data points used to calculate rates of oxygen consumption. Grey squares (■) represent data points not included in linear fits.

Data Analysis

For each enzyme, kinetics data for both the reductive and oxidative half-reaction were analyzed using a statistical software package (GraphPad Prism version 4.03, GraphPad Software, San Diego CA, http://www.graphpad.com). Data were fit using global nonlinear regression analysis. Competitive, uncompetitive, noncompetitive, and mixed type ($1 < \alpha < \infty$ and $\beta = 0$) inhibition models were entered into the GraphPad program as user defined models according to Segel [145]. In each case, the appropriate mode of inhibition was judged by the model that best fit the experimental data as determined by analysis of the statistical parameters built into the GraphPad program (R^2, absolute sum of squares, runs test, residuals). During the curve fitting process, the inhibition constant was established as a global parameter. Therefore, the K_i values reported in the Results section represent the best fit value for respective data sets.

Results

Azide as a Cu(II)-Directed Ligand in Oxidized and Substrate-Reduced Amine Oxidases

The λ_{max} value for the LMCT band for the Cu(II)-N_3^- complex in PSAO was found to be 389 nm for PSAO ($\varepsilon_{389} \cong 3100\ M^{-1}cm^{-1}$), with a calculated K_d value of 53 ± 5 mM (Figure 40). Azide was found to bind to substrate reduced PSAO with the same affinity as oxidized enzyme [111]. Respective K_d values for other CuAOs appear in Table 7.

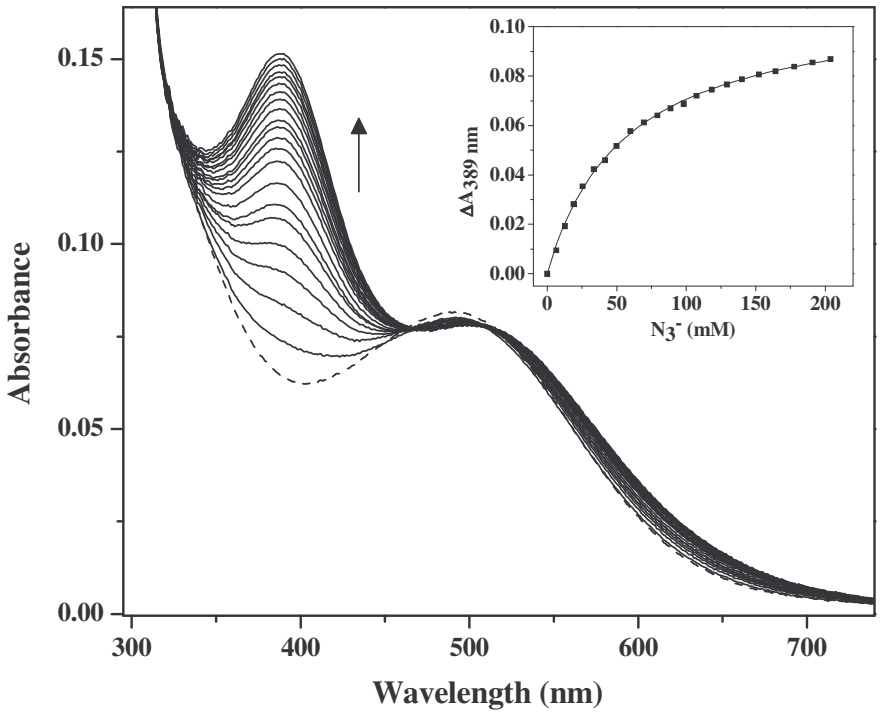

Figure 40: Azide coordination to Cu(II) in oxidized PSAO. Dashed spectrum (---) represents the wild-type protein prior to addition of azide. Inset depicts the change in absorbance of the LMCT band fit to a titration curve, yielding a K_d value for the Cu(II)-N_3^- complex (see text).

Kinetic Parameters

K_M and k_{cat} values for substrates amine and O_2 in the absence of inhibitors were generated through global model nonlinear regression analysis (GraphPad Prism) for each CuAO and are listed in Table 7. The values in Table 7 are in excellent agreement with the kinetic parameters generated by regression analysis using the Michaelis-Menten equation for control curves (Origin 7.0 software; data not shown).

Table 7: Properties of Copper Amine Oxidases

Enzyme	TPQ[a]	K_M (μM)		k_{cat} dimer (s^{-1})		K_d Cu(II)-N_3^- (mM)	
		Amine	O_2	Amine	O_2	Oxidized	Reduced
PSAO	1.8	424 ± 30[b]	46 ± 3	252 ± 3	308 ± 9	53 ± 5	59 ± 10[c]
rDAO[g]	1.4	26 ± 4[d]	14 ± 2	7.9 ± 0.2	4.0 ± 0.1	38 ± 3	ND
AGAO[h]	1.4	1.5 ± 0.2[e]	33 ± 2	44 ± 2	53 ± 2	213 ± 18	34 ± 5
PPLO	1.6	39 ± 2[f]	41 ± 2	11.2 ± 0.3	12.6 ± 0.3	153 ± 16[h]	87 ± 21

[a] Values are reported as TPQ content per dimer. [b] Amine substrate putrescine; 100 mM KPO_4, pH 7.2 at 30 °C with I = 540 mM (KCl). [c] Value reported in [111]. [d] Amine substrate putrescine; 50 mM HEPES, pH 7.2 at 37 °C with I = 250 mM (KCl). [e] Amine substrate β-phenylethylamine; 100 mM KPO_4, pH 7.2 at 30 °C with I = 440 mM (K_2SO_4). [f] Amine substrate benzylamine; 50 mM HEPES, pH 7.0 at 30 °C with I = 150 mM (KCl). ND is not determined. [g] Parameters were obtained by B.O. Elmore. [h] Parameters were obtained by G.A. Juda.

Azide Inhibition of the Reductive Half-Reaction

The effects of azide on the reductive half-reaction (Eq. 1) were determined by analyzing the kinetic parameters of each enzyme for a given amine substrate in the presence of increasing amounts of azide, at saturating O_2 levels. Nonlinear regression analysis revealed that a noncompetitive model best described the nature of azide's effects on amine oxidation for PSAO, PPLO, and AGAO, however, a competitive inhibition model best fit the data for rhDAO (Table 8). The effect of azide on amine oxidation for PSAO and PPLO is shown in Figures 41 and 43. Lineweaver-Burk replots of the nonlinear regression global fits (Figures 42 and 44) clearly show these lines converging on the x axis, as expected for noncompetitive inhibition [145].

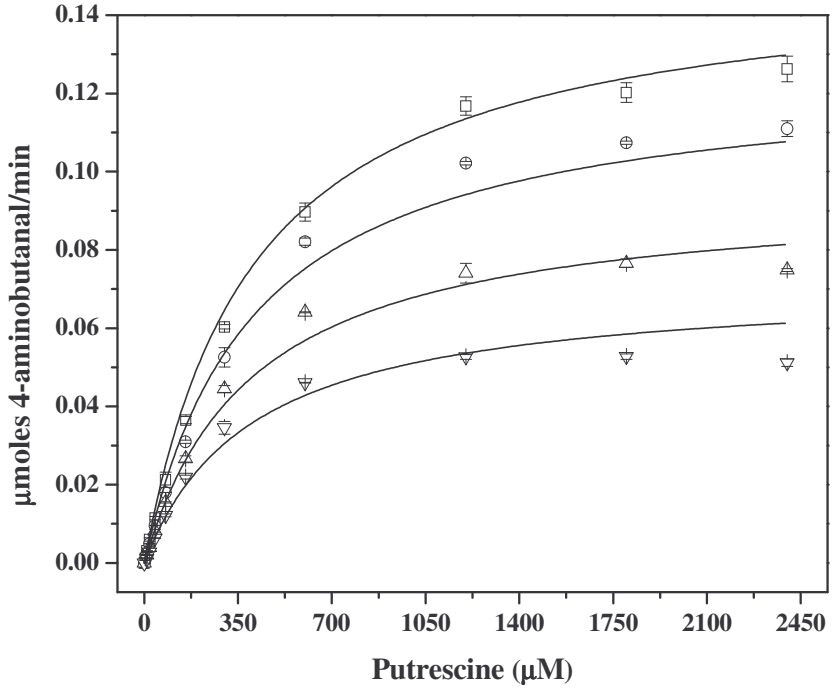

Figure 41: Azide inhibition of the reductive half reaction in PSAO. Experimental data curve fits obtained through global model nonlinear regression analysis. Data shown was collected in the presence of 0 (□), 46 (○), 133 (△), and 250 (▽) mM azide.

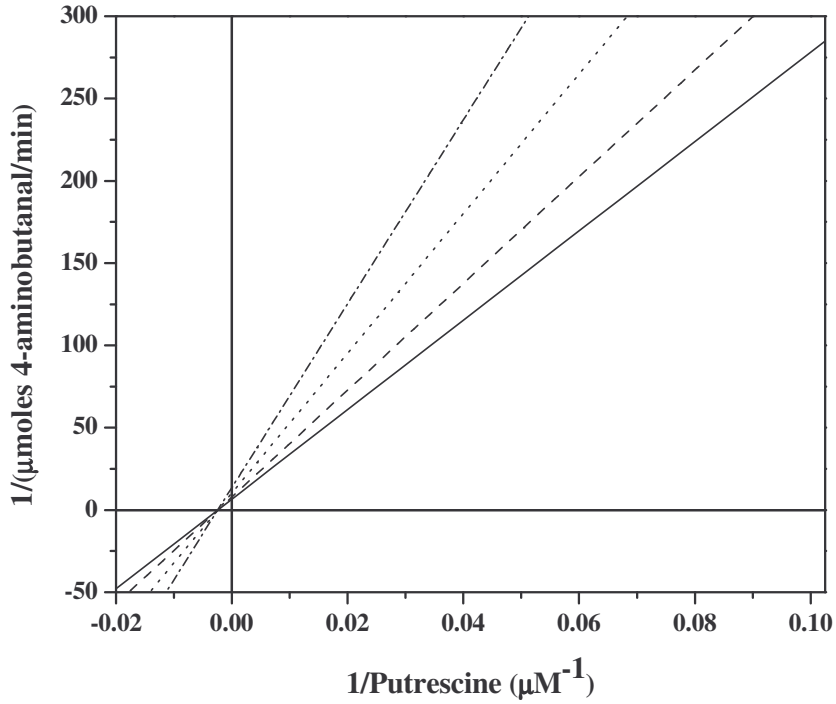

Figure 42: Lineweaver-Burk plot generated using the inverse of the hyperbolic fits in Figure 41, clearly illustrating the noncompetitive mode of inhibition. Respective lines correspond to 0 (—), 46 (- -), 133 (····), and 250 (-·-) mM azide.

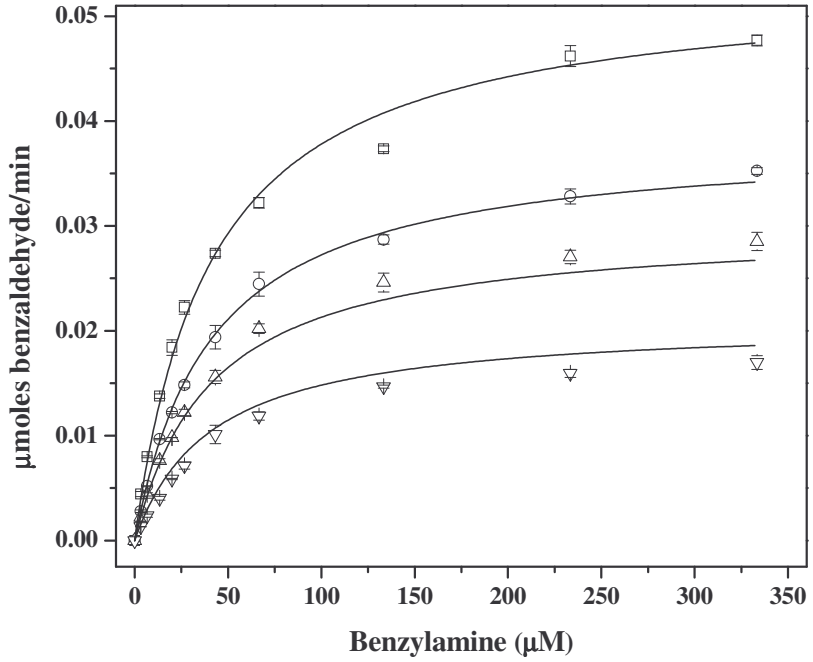

Figure 43: Azide inhibition of the reductive half reaction in PPLO. Experimental data curve fits obtained through global model nonlinear regression analysis. Data shown was collected in the presence of 0 (□), 10 (○), 20 (△), and 40 (▽) mM azide.

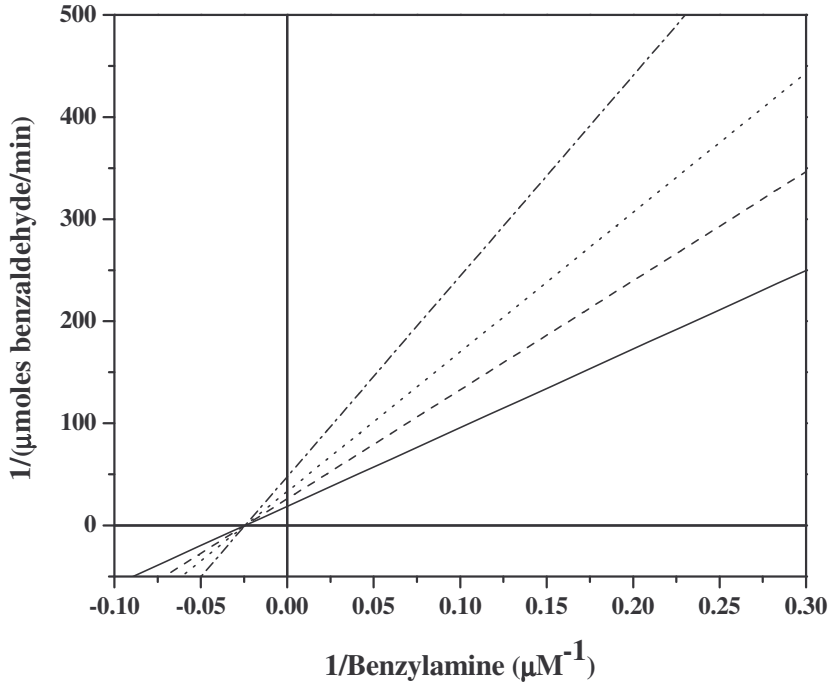

Figure 44: Lineweaver-Burk plot generated using the inverse of the hyperbolic fits in Figure 43, clearly illustrating the noncompetitive mode of inhibition. Respective lines correspond to 0 (—), 10 (- -), 20 (·····), and 40 (-·-) mM azide.

Azide Inhibition of the Oxidative Half-Reaction

The effects of azide on the oxidative half-reaction (Eq. 2) were determined by analyzing the kinetic parameters of each enzyme with saturating amine substrate (at least $10 \times K_M$) at a series of azide concentrations, while O_2 levels were varied from ~ 10 – 180 μM. Nonlinear regression analysis revealed that either competitive, noncompetitive, or mixed type inhibition models best described the nature of azide's effects on O_2 reduction, depending on the enzyme source (Table 8). Figure 45 shows azide's effects on O_2 reduction in PSAO. The Lineweaver-Burk representation of the nonlinear regression global fits for PSAO (Figure 46) clearly illustrate a competitive mode of inhibition. It should be noted that the K_i value of 31 ± 2 mM generated from the nonlinear regression analysis is in very good agreement with the experimentally determined K_d value for the Cu(II)-N_3^- complex in this enzyme (Tables 7 and 8). This result can readily be rationalized in terms of azide and substrate dioxygen directly competing for binding to copper during the oxidative half-reaction.

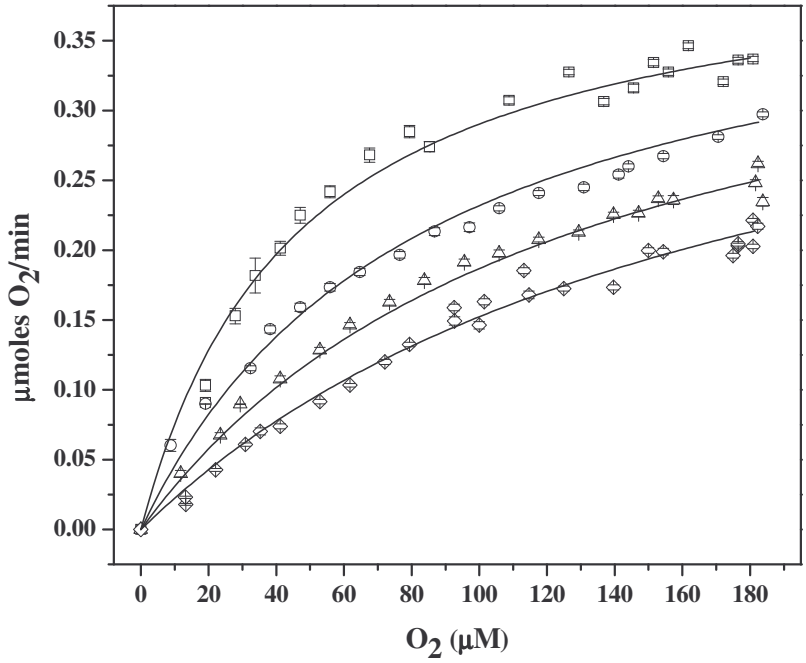

Figure 45: Azide inhibition of the oxidative half reaction in PSAO. Experimental data curve fits obtained through global model nonlinear regression analysis. Data shown was collected in the presence of 0 (□), 25 (○), 55 (△), and 90 (◇) mM azide.

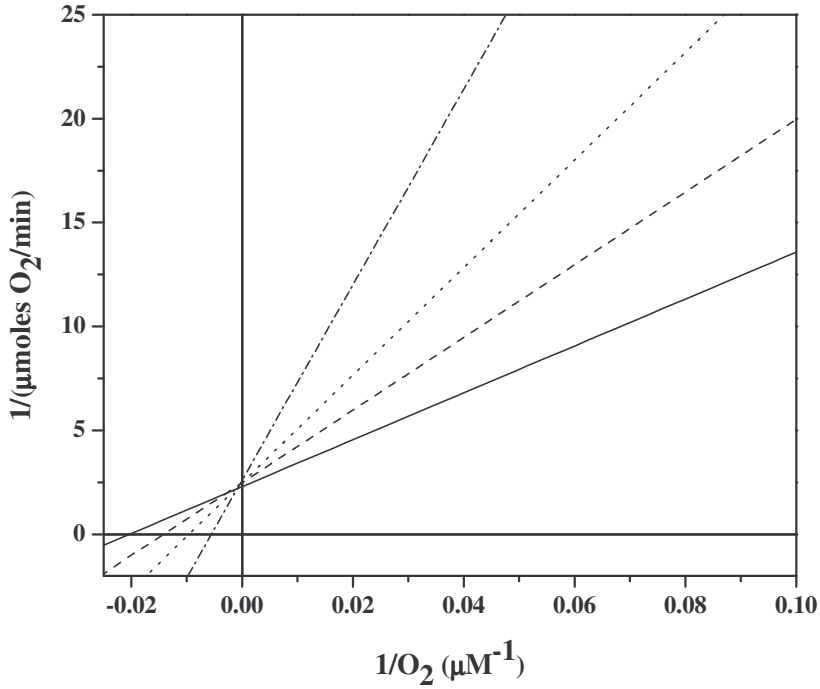

Figure 46: Lineweaver-Burk plot generated using the inverse of the hyperbolic fits in Figure 45, clearly illustrating the competitive mode of inhibition. Respective lines correspond to 0 (—), 25 (- -), 55 (····), and 90 (-·-) mM azide.

The effects of azide on O_2 reduction were also examined under non steady-state conditions where substrate putrescine was not saturating (1 mM; ~2 × K_M; Figure 47). Interestingly, azide was discovered to exhibit noncompetitive inhibition with respect to substrate O_2. Nonlinear regression analysis yielded a K_i value of 53 ± 3 mM (data not shown), although this value must be considered an approximate one as data were only collected at 0 mM and 25 mM azide levels. Regardless, this K_i value is in excellent agreement with the measured K_d value for the Cu(II)-N_3^- complex (Table 7). Additionally, $K_M(O_2)$ for PSAO was found to be dependent upon amine concentration, with lower amine concentrations (1 mM) corresponding to a higher binding affinity for dioxygen (K_M = 35 ± 3 μM), as previously reported for PSAO with the substrate tryptamine [196].

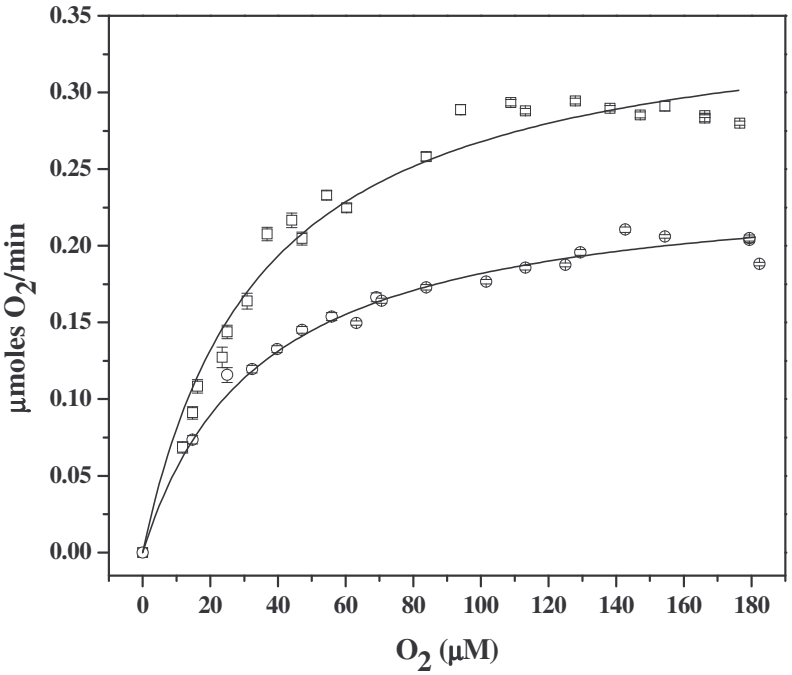

Figure 47: Azide inhibition of the oxidative half reaction in PSAO under non-steady state conditions. Experimental data curve fits obtained through global model nonlinear regression analysis. Data shown was collected in the presence of 0 (□) and 25 (○) mM azide.

In the case of PPLO (Figure 48), the global fitting analysis of the data revealed that a noncompetitive model of inhibition best describes the data at low azide concentrations (5 and 15 mM), with the mode of inhibition shifting to mixed type at higher azide concentrations (30 and 45 mM). The Lineweaver-Burk replot of the nonlinear regression global fits (Figure 49) clearly shows this shift, as the 0, 5, and 15 mM lines have a common x-intercept, whereas the 30 and 45 mM lines intercept the control off both axes.

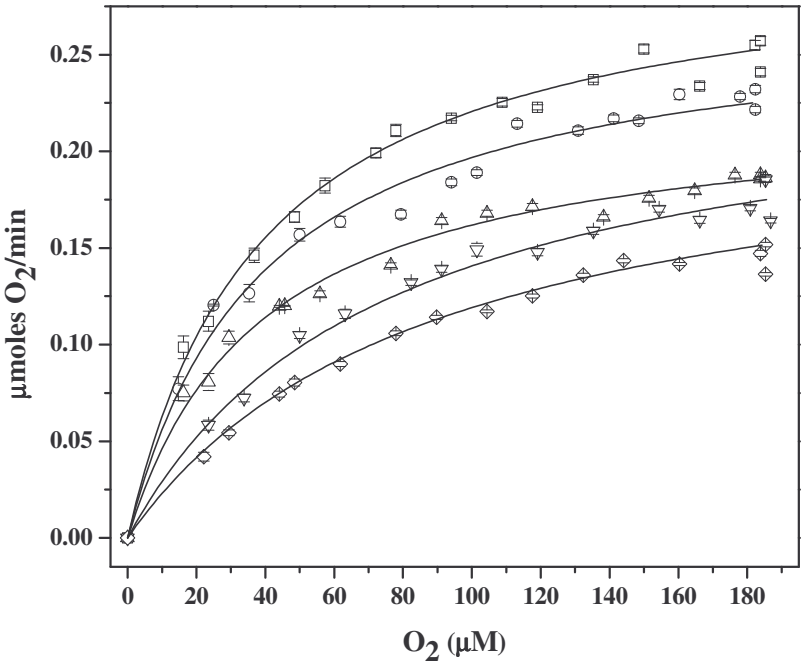

Figure 48: Azide inhibition of the oxidative half reaction in PPLO. Experimental data curve fits obtained through global model nonlinear regression analysis. Data shown was collected in the presence of 0 (□), 5 (○), 15 (△), 30 (▽), and 45 (◇) mM azide.

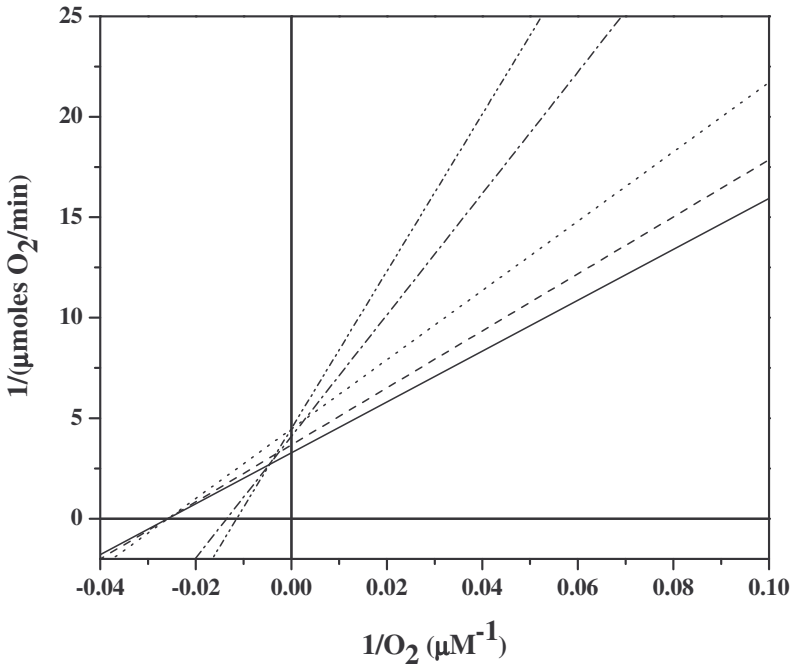

Figure 49: Lineweaver-Burk plot generated using the inverse of the hyperbolic fits in Figure 48, clearly illustrating the noncompetitive mode of inhibition at low azide levels and the partial competitive mode of inhibition at high azide levels. Respective lines correspond to 0 (—), 5 (– –), 15 (····), 30 (–··), and 45 (–···) mM azide.

Linear mixed-type inhibition is defined as a mixture of pure noncompetitive inhibition and partial competitive inhibition [145]. Consequently, neither a pure noncompetitive, pure competitive, nor a mixed type inhibition model adequately fit all the data curves shown in Figure 48. The fits displayed in the figure represent two inhibition models, with the 0, 5, and 15 mM curves being fit with a pure noncompetitive model (generating a K_i = 41 ± 2 mM), and the 30 and 45 mM curves being fit with a mixed-type model. When the 0, 30, and 45 mM curves are fit, values of K_i (23 ± 1 mM) and αK_i (112 ± 5 mM) are obtained, which are in very good agreement with the calculated K_i from the reductive half-reaction (26 ± 1 mM) and the K_d (87 ± 21 mM) for the Cu(II)-N_3^- complex in substrate reduced PPLO.

Table 8: Copper Amine Oxidase Azide Inhibition Parameters

Enzyme	Half Reaction	Mode of Inhibition	K_i (mM)
PSAO	Reductive	Noncompetitive	250 ± 18
-	Oxidative	Competitive	31 ± 2
rhDAO[a]	Reductive	Competitive	37 ± 8
-	Oxidative	Partial Competitive	92 ± 7
AGAO[b]	Reductive	Noncompetitive	18 ± 2
-	Oxidative	Noncompetitive	19 ± 1
PPLO	Reductive	Noncompetitive	26 ± 1
-	Oxidative	Partial Competitive	23 ± 1

[a] Data collected by B.O. Elmore. [b] Data collected by G.A. Juda

Discussion

The monodentate ligands azide and cyanide are known to displace the equatorial water ligand of Cu(II) in amine oxidases and inhibit both half-reactions (Eqs. 1 and 2) [98,111,197,198]. Despite the fact that these ligands have previously been examined for their effects upon CuAO catalysis in two select enzymes (pig plasma and *Hansenula polymorpha* amine oxidases), significant variations in the quality and reproducibility of the data have led to ambiguities in interpretation. As our results with cyanide show, systematic and direct comparisons among several CuAOs should be performed, as it has become increasingly clear that significant differences may exist in the interaction of CuAOs with these ligands [98,111,175]. In order to interpret the effects of azide on

CuAO mechanism, kinetic parameters were determined for both the reductive and oxidative half-reactions in the presence and absence of azide. Specifically, we wished to test the previously articulated hypothesis that azide competes with O_2 for binding to copper during enzymatic reoxidation. Owing to an intrinsic property of the amine oxidase Ping-Pong Bi Bi mechanism, the two half-reactions (i.e. substrate amine oxidation and substrate O_2 reduction) are kinetically independent [109,199-201]. In an attempt to cleanly dissect the effects of azide during each half-reaction, kinetic experiments were performed with variable concentrations of one substrate (either amine or O_2), while the other substrate was kept at saturating concentrations. The results summarized herein, in conjunction with those presented in reference [179], are part of the first comparative study that analyzes the effects of azide on both half-reactions of multiple amine oxidases (AGAO, PPLO, PSAO and rhDAO), including bacterial, yeast, plant, and mammalian enzymes.

Azide as a Cu(II)-Directed Ligand

Variations in the binding affinity of azide to Cu(II) among resting, oxidized CuAOs have been previously described [72,111-113,192,193]. The data herein support these findings as K_d values for Cu(II)-N_3^- complexes in the oxidized enzymes range from 38 – 213 mM (Table 7). In addition, it has been reported that the oxidation state of the quinone cofactor in some CuAOs may affect the affinity of azide for Cu(II). A marked increase in affinity of N_3^- for Cu(II) has been reported for APAO when TPQ is in the reduced aminoquinol state, relative to the oxidized state, however, no difference in affinity was noted between these two enzymatic states in PKAO, PPAO, or PSAO (Table

7) [111,113,114,192]. Results obtained for BPAO indicated a slightly higher binding affinity for azide in the resting form of the enzyme [112]. The results in Table 7 indicate that N_3^- binds to Cu(II) with higher affinity in the substrate-reduced forms of AGAO and PPLO, compared to the oxidized (resting) states. Moreover, the LMCT λ_{max} red shifts by ~ 42 nm in substrate-reduced AGAO relative to oxidized enzyme [179]. The shift in the energy of the LMCT transition suggests that the redox state of the TPQ cofactor perturbs the electronic structure of the Cu(II) center in AGAO.

Azide Inhibition of the Reductive Half-Reaction

The inhibition of PPAO by azide with respect to substrate amine has previously been described as uncompetitive [192,193], while inhibition patterns for BPAO have been reported as mixed at low amine concentrations with a shift to uncompetitive at higher substrate concentrations [112]. In this study, azide was discovered to exhibit noncompetitive inhibition of the reductive half-reaction, with one exception (Table 8). The result that azide acts as a competitive inhibitor in rhDAO with respect to substrate putrescine is novel among CuAOs. The most straightforward interpretation is that azide binding to copper in the free enzyme perturbs the active site in a way that prevents substrate amine binding. For example, azide binding to Cu(II) at the equatorial position could disrupt the active-site hydrogen bonding network, and thereby alter the orientation of the reactive TPQ C5 carbonyl, rendering it inaccessible to substrate amine. Hydrogen bonding has been shown to play an essential role in positioning the TPQ cofactor during both biogenesis and amine oxidation [81,83,202-204]. This hypothesis is further supported by the nearly identical values determined for the K_d (38 ± 3 mM) of the

Cu(II)-N_3^- complex in the free enzyme and the calculated K_i (37 ± 8 mM) for azide inhibition with respect to substrate putrescine.

In the case of PSAO, azide displays noncompetitive inhibition towards substrate amine (Figures 41 and 42). This indicates that azide binds randomly and reversibly to Cu(II) at different stages of catalysis independent of the binding of substrate. Current data show that azide binds to copper in the free enzyme (TPQ_{OX}) and the substrate reduced enzyme (TPQ_{AMQ}) with the same affinity (Table 7), therefore the noncompetitive nature of azide inhibition may simply represent azide complexing Cu(II) at these two stages of catalysis. Azide's inhibition of amine oxidation in PSAO with the relatively high K_i value of 250 ± 18 mM indicates that significant reduction in the velocity of the reductive half-reaction does not occur at the concentrations of azide used during the oxidative half-reaction experiments (see below). Thus, PSAO represents a favorable case for cleanly dissecting the effects of azide on the oxidative half-reaction.

The inhibition of AGAO and PPLO by azide with respect to substrate β-phenylethylamine and benzylamine, respectively, was also found to be noncompetitive (Figures 43 and 44). For AGAO, the determined inhibition constant of 18 ± 2 mM (Table 8) is significantly lower than the calculated K_d for the oxidized enzyme (213 ± 18 mM), but close to that of the substrate-reduced form (34 ± 5 mM) (Table 7). For PPLO the K_i of 26 ± 1 mM (Table 8) is significantly lower than the experimentally determined K_d values for the Cu(II)-N_3^- complex in both the oxidized and substrate-reduced forms of the enzyme (Table 7). Thus, the affinity of azide for Cu(II) may be higher in one of the three catalytic states for which this complex is not easily characterized (TPQ_{SSB}, TPQ_{PSB}, or TPQ_{IMQ}). Given the relatively potent noncompetitive nature of azide binding in AGAO

and PPLO, it can be expected that once azide levels approach or exceed K_i values (vs. substrate amine) *a substantial decrease in reaction velocity ($V_{max(i)}$) may result during the reductive half-reaction* of these enzymes. This subject is readdressed during the discussion of azide's effects on O_2 reduction in AGAO and PPLO.

Azide Inhibition of the Oxidative Half-Reaction

Considerable disagreement exists with regard to the interpretation of the effects of exogenous Cu(II) ligands on the oxidative half-reaction (Eq. 2). Two independent studies of PPAO concluded that azide was a competitive inhibitor with respect to substrate O_2, with calculated inhibition constants being consistent with measured K_d values for the Cu(II)-N_3^- complex [113,114]. These results implicated the copper site as having a direct role in O_2 activation. A subsequent study with HPAO found the inhibition by azide to be noncompetitive with respect to O_2 during the oxidative half-reaction [72]. The results of this latter study are viewed as consistent with the proposal that O_2 binds to an off-metal site in close proximity to TPQ prior to its reduction, with the initial electron transfer to O_2 coming directly from TPQ_{AMQ} (Figure 8) [59,72,89,91,106,109]. In HPAO, this hypothetical O_2 binding site is situated ~ 3 Å from TPQ and ~ 4.7 Å from the copper and is lined by the residues Y407, L425, and M639 [116]. Recently, we have experimentally identified a hydrophobic pocket in AGAO, PPLO, and PSAO by utilizing xenon as a probe for potential dioxygen-binding sites [116]. The crystal structures of these enzymes revealed one common xenon binding pocket in close proximity to the active site (~ 7 Å from Cu; ~ 9 Å from TPQ). Xenon was subsequently shown to bind in this exact site in BPAO [53]. It is important to note that the potential O_2 binding site identified in these

Xe-CuAO structures is distinct from the site previously proposed by Klinman *et al.* for BPAO and HPAO. While the experimental identification of a consensus Xe binding site does not rule out O_2 binding in the site proposed by Klinman *et al*. [109], it is clear that the most direct trajectory for O_2 from the observed Xe binding site towards the active site would involve initial close approach to the copper center (Figure 50). This hypothesis is supported by the results presented herein for the oxidative half-reaction in PSAO.

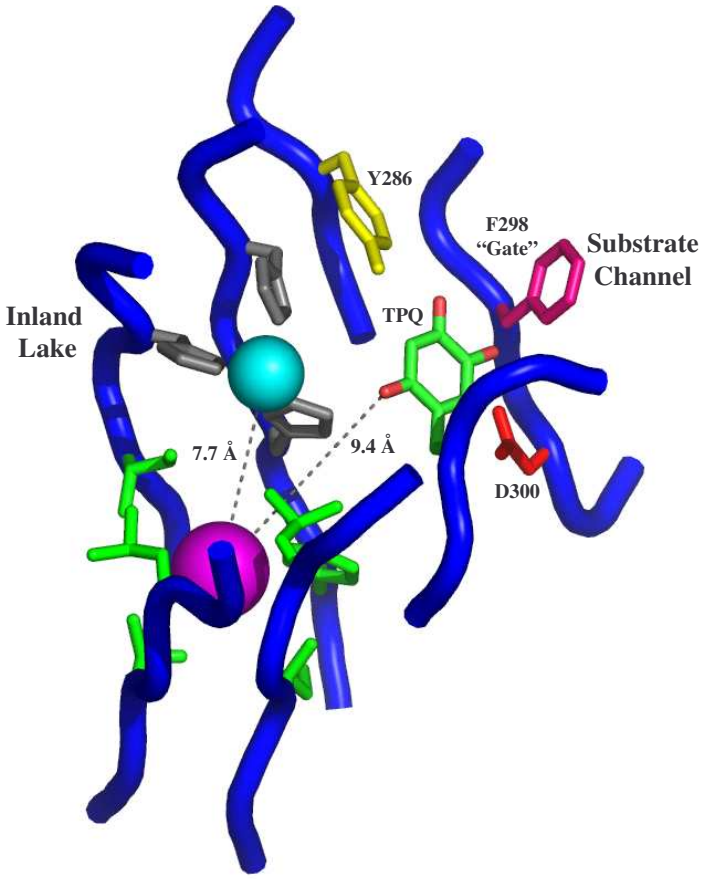

Figure 50: Xenon binding pocket in PSAO (1W2Z.pdb). Both Xe (purple) and Cu(II) (cyan) are represented as van der Waals spheres. The productive orientation of TPQ is shown colored by atom (oxygen, red; carbon, green). The copper ligands (H442, H444, H603; gray) and the residues forming the xenon binding pocket (I405, L407, Y446, I601, L616, T618; green) are not labeled for clarity. The approximate locations of the substrate channel and the inland lake are given (see [52]). Xenon to Cu(II) and xenon to TPQ(O2) distances are also shown (see [116]). Figure was generated using PyMOL (Delano, W.L. (2002) Delano Scientific, San Carlos, CA.).

Our results clearly show that azide exhibits competitive inhibition against substrate O_2 in PSAO with a K_i value of 31 ± 2 mM (Figures 45 and 46). This value is in very good agreement with the measured K_d value of 53 ± 5 mM for the Cu(II)-N_3^- complex in this enzyme (Figure 40). We believe these results are most consistent with mechanistic proposals placing Cu(I) on-pathway in PSAO, with the Cu(I)-TPQ_{SQ} moiety principally involved in O_2 activation (Figure 8, A → D). Despite the fact that azide binds Cu(II) and O_2 reacts with Cu(I), ligation of Cu(II) by azide should appear competitive towards O_2 for the following reasons: (1) Cu(II)-TPQ_{AMQ} is in direct equilibrium with Cu(I)-TPQ_{SQ} with an intramolecular electron transfer rate in PSAO of ~ 20,000 s^{-1} [87,104]; and (2) tetragonal Cu(II) complexes are known to display facile ligand substitution and therefore the reversible coordination by N_3^- should be rapid [112,198]. In addition, azide is known to stabilize Cu(II) in substrate-reduced CuAOs and has been found to bind to copper in reduced PSAO with the same affinity as in the oxidized enzyme (Table 7) [111]. It can be expected that during the oxidative half-reaction the binding of azide to Cu(II) shifts the Cu(II)-TPQ_{AMQ} ⇋ Cu(I)-TPQ_{SQ} equilibrium in favor of the former species, thereby preventing electron transfer from TPQ_{AMQ} to Cu(II), in a manner consistent with competitive inhibition. Further evidence of this equilibrium shift was observed during the azide titration of substrate-reduced AGAO, with rapid disappearance of the Cu(I)-TPQ_{SQ} bands occurring upon addition of azide [179].

PSAO is an excellent enzyme system for cleanly observing azide's effects on O_2 reduction, as the calculated K_i value for the noncompetitive inhibition of substrate amine oxidation by azide is ≈ 5 times greater than the affinity of azide for Cu(II) in either the

oxidized, resting state or the substrate-reduced TPQ_{AMQ} state (Table 7). This means that the reaction velocity ($V_{max(i)} \approx V_{max}$) during the reductive half-reaction is largely unaltered at the concentrations of azide used in the oxidative half-reaction experiments, even though at relatively high concentrations, azide may reduce the rates of one or more steps in the reductive half-reaction. Kinetics studies of PPAO provide a useful precedent [114]. In this case, azide was discovered to inhibit both the conversion of ES* $\rightarrow E_{red}$ and $E_{red} \rightarrow$ EO, with azide's effects primarily credited to the inhibition of $E_{red} \rightarrow$ EO through direct competition with O_2 [114]. Given our current understanding of the amine oxidase mechanism, these steps would correspond to C $\rightarrow$ D and [D $\leftrightharpoons$ E] $\rightarrow$ F in Figure 6. Azide exhibited competitive inhibition towards O_2 in PPAO at both non-saturating and saturating concentrations of amine substrate. This is not the case for PSAO, which displays noncompetitive inhibition towards O_2 at nonsaturating amine levels (Figure 47), and competitive inhibition at saturating amine concentrations (Figure 45). Our results show that for PSAO, saturating concentrations of amine overcome the kinetic effects of azide on the reductive half-reaction, such that azide exhibits clean competitive inhibition towards substrate O_2 in the oxidative half-reaction experiments.

Azide was found to exhibit mixed-type/partial competitive inhibition with respect to substrate O_2 in rhDAO. Given the competitive nature of azide inhibition towards amine oxidation, kinetic effects on the reductive half reaction could easily be overcome by using concentrations of amine in the oxidative half-reaction experiments that would cause $V_{max(i)} \approx V_{max}$ (77 times K_M). Therefore, the observed partial competitive mode of inhibition observed in regards to O_2 reduction can most easily be explained by azide

competing with O_2 for copper. However, further studies are required in order to confirm the reported K_i value (Table 8).

Azide was observed to exhibit noncompetitive inhibition with respect to O_2 in AGAO (Table 8). In PPLO, the inhibition shifts from noncompetitive at low azide levels (5 – 15 mM) to mixed-type at higher concentrations (30 – 45 mM) (Figures 48 and 49). In both these cases, K_i values for reductive and oxidative half-reactions are equivalent (Table 8), and are lower than measured K_d values for the Cu(II)-N_3^- complexes (Table 7). Given this observation, we expected that substantial inhibition in the rate of the reductive half-reaction may occur at the concentrations of azide used for the oxidative half-reaction experiments, and that this would complicate kinetic interpretation. This hypothesis was tested through theoretical curve simulations using the GraphPad Prism software program. By utilizing the equations provided by Cleland for a simple Ping-Pong Bi Bi system [205] with an inhibitor that reacts with free and substrate reduced enzyme only, simulations demonstrated that reaction rates would depend upon the magnitude of the K_i terms relative to each other and the inhibitor concentrations. Systematic variation of the K_i for the first half-reaction, relative to the K_i for the second half-reaction, reveals substantial effects on $V_{max(i)}$ for a family of theoretical V *versus* S curves (Figure 51). In fact, these effects on $V_{max(i)}$ could directly affect which inhibition model best fit the data. This is quite evident by examining the two sets of theoretical curves shown in Figure 51. For the set of red curves, a competitive inhibition model best describes the data, whereas a noncompetitive model best fits the set of blue curves. While these simulations do not exactly represent the kinetic behavior of amine oxidase inhibition by azide, which can be expected to be much more complex because azide may bind at multiple kinetic stages and

affect multiple rate constants, it does illustrate how the relative K_i's may influence the kinetic curves observed for the two half-reactions. Hence, it is quite possible that the noncompetitive mode of inhibition observed for azide in the oxidative half-reaction in AGAO and PPLO simply represents the relatively low K_i value for azide inhibition of the reductive half-reaction. In this context, the shift in the inhibition of PPLO by azide to mixed-type at higher azide levels can best be understood as the onset of partial competitive inhibition between azide and O_2 for copper. The reasonable agreement between αK_i (112 ± 5 mM) and the K_d (87 ± 21 mM) for the Cu(II)-N_3^- complex in substrate reduced PPLO supports this hypothesis. The fact that this behavior is not observed for AGAO is either consistent with the interpretation offered by Klinman for similar results with HPAO [72], or would be consistent with azide affecting multiple kinetic steps in the reductive half-reaction. At this time, the data do not permit us to distinguish between two possibilities: (1) inhibition by azide with respect to O_2 is intrinsically competitive in CuAOs, but that this effect cannot always be deconvolved experimentally from the effects of azide on the reductive half-reaction; or (2) CuAOs differ in some steps of their reoxidation mechanisms.

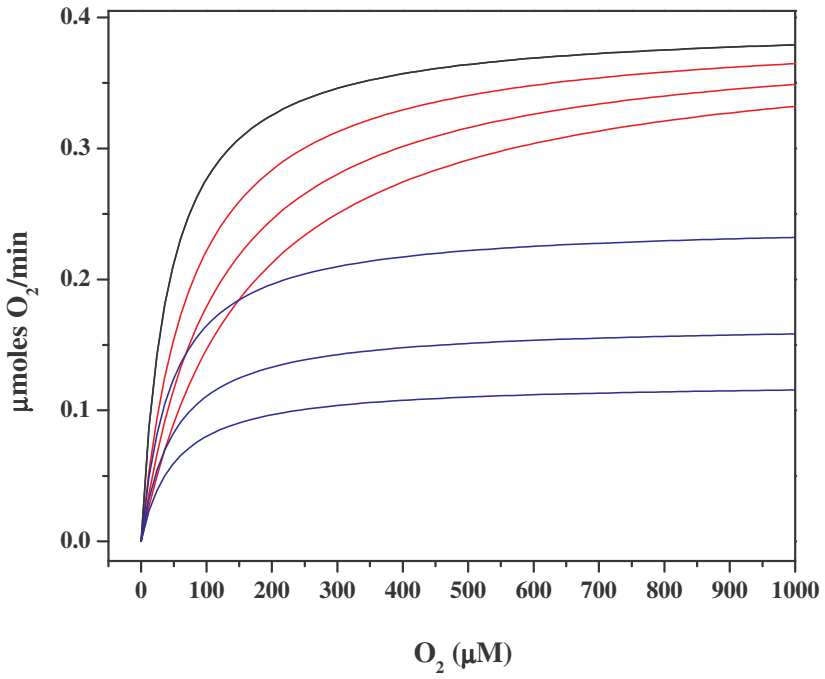

Figure 51: Theoretical curve simulations of the second half-reaction for a simple Ping-Pong Bi Bi system. The black curve is the control (inhibitor concentration is 0 mM) for both red and blue data sets, respectively. All kinetic parameters, including inhibitor concentrations, for both sets of theoretical curves were identical with the exception of the K_i value for the first half-reaction. The red curves were generated using a K_i value that was 100 times greater than the value used to generate the blue set of curves.

Mechanistic Conclusions

Although it is not possible to unambiguously determine the effects of azide on the oxidative half-reaction in AGAO and PPLO, it is worthwhile to address the mechanistic implications of the competitive nature of this inhibition in PSAO and PPAO, with regard to the different mechanistic proposals presented in the introduction. Competitive inhibition by azide in the oxidative half-reaction cannot readily be reconciled in terms of O_2 prebinding to the off-metal proteinaceous site proposed by Klinman and coworkers (Figure 8, A2), with subsequent electron transfer occurring directly from TPQ_{AMQ} to O_2.

However, if the recently identified xenon binding pocket in AGAO, BPAO, PPLO, and PSAO truly represents a transient O_2 binding site in these enzymes, then our results can be rationalized by the fact that migration of O_2 towards the active site would result in an initial close approach to copper, from which electron transfer should readily occur (Figure 8, A $\rightarrow$ B; Figure 50).

Kishishita *et al*. [92] consider their results both in terms of mechanisms in which copper reduction is not required (O_2 is reduced via the TPQ_{AMQ} with Cu(II) simply acting as a site for superoxide binding) and in which the Cu(I)-TPQ_{SQ} moiety is a catalytic intermediate. For the former mechanism, azide would exert competitive inhibition towards O_2 only if it affected the rate constant for superoxide binding to Cu(II) in a manner that would be experimentally detected as a rise in the apparent K_M for O_2, assuming that no other step becomes rate limiting in the presence of azide. This does not seem likely given the fact that both azide and superoxide are anions, and Cu(II) is known to undergo facile ligand substitution [112,198].

If PSAO and PPAO operated through the scheme proposed by Klinman and coworkers (Figure 8, A2 $\rightarrow$ D) [89], the most straightforward explanation for competitive inhibition is that azide coordination to copper perturbs the affinity of O_2 for the off-metal, hydrophobic dioxygen binding pocket as described in HPAO and BPAO [91,109]. In this context, it has been argued that the increased net charge at the metal center has a direct effect on the affinity of O_2 for this hydrophobic binding site, which was manifested as an increase in $K_M(O_2)$ in Co(II) substituted HPAO, relative to native HPAO in which Cu(II)-OH^- is believed to be present [107]. Given that azide binding to the copper center would result in the same net charge as copper bound hydroxide, it would seem that other factors

would need to be invoked to rationalize the reduced affinity of the hydrophobic pocket for O_2.

Conclusions

Despite the fact that azide ligand-substitution reactions have been previously used for the study of CuAO catalysis, no direct, systematic comparison of the reductive and oxidative half-reaction kinetics among multiple CuAOs has been performed. The work summarized above is the first comparative study aimed at analyzing azide's effects on each half-reaction for a series of CuAOs from bacterial, yeast, plant, and mammalian sources. At the time of writing, this work has been submitted for publication in the journal *Biochemistry* [179].

One issue complicating kinetic interpretation is that for several CuAOs, azide has varying affinity for Cu(II), depending on the redox state of the quinone cofactor. We have found that a comparative study of azide's effects on the reductive and oxidative half-reactions is essential to clearly interpret the inhibition results for each half-reaction. Not surprisingly, our results with PSAO illustrate the critical importance of maintaining steady-state conditions in one half-reaction of an enzyme operating through a Ping-Pong Bi Bi mechanism, while performing kinetic inhibition studies on the opposite half-reaction. Generally, this can be easily performed for enzyme systems in which the inhibitor of interest has an effect with respect to only one substrate, however, when an inhibitor induces substantial inhibition in both half-reactions, cleanly dissecting the effects of the inhibitor against only one substrate may be difficult. This is illustrated in

the cases of AGAO and PPLO for which azide is a potent noncompetitive inhibitor with respect to substrate amine.

Collectively, the competitive interaction of azide with respect to O_2 reported herein for PSAO and previously for PPAO [113,114] provides strong support for a direct interaction of dioxygen with the metal center during enzymatic reoxidation in these enzymes. This conclusion is most easily rationalized in terms of O_2 reacting with Cu(I)-TPQ_{SQ}, with azide stabilizing the Cu(II)-TPQ_{AMQ} species. Although data with rhDAO suggest the inhibition by azide with respect to O_2 is at least partially competitive, additional studies are warranted to establish the catalytic viability of Cu(I)-TPQ_{SQ} in this enzyme. We suspect a similar mechanism to be operative in AGAO and PPLO as well. Given the large body of evidence in support of a non-redox role of copper in HPAO, the data collectively suggest that copper amine oxidases from different sources may in fact utilize discrete mechanisms to reoxidize the reduced quinone species, despite the similarities of their active site structures in the resting state.

In the previous chapter, evidence for the catalytic viability of the TPQ_{SQ}-Cu(I) species in PSAO was provided [98]. Results conclusively showed that stabilization of Cu(I) by CN^- was the main source of catalytic inhibition, believed to result from the direct competition between CN^- and O_2 for Cu(I), which would prevent reoxidation of TPQ_{AMQ}. Taken collectively, the results presented for the monodentate ligands azide and cyanide provide support for the role of Cu(I) in O_2 reduction in PSAO (Figure 52).

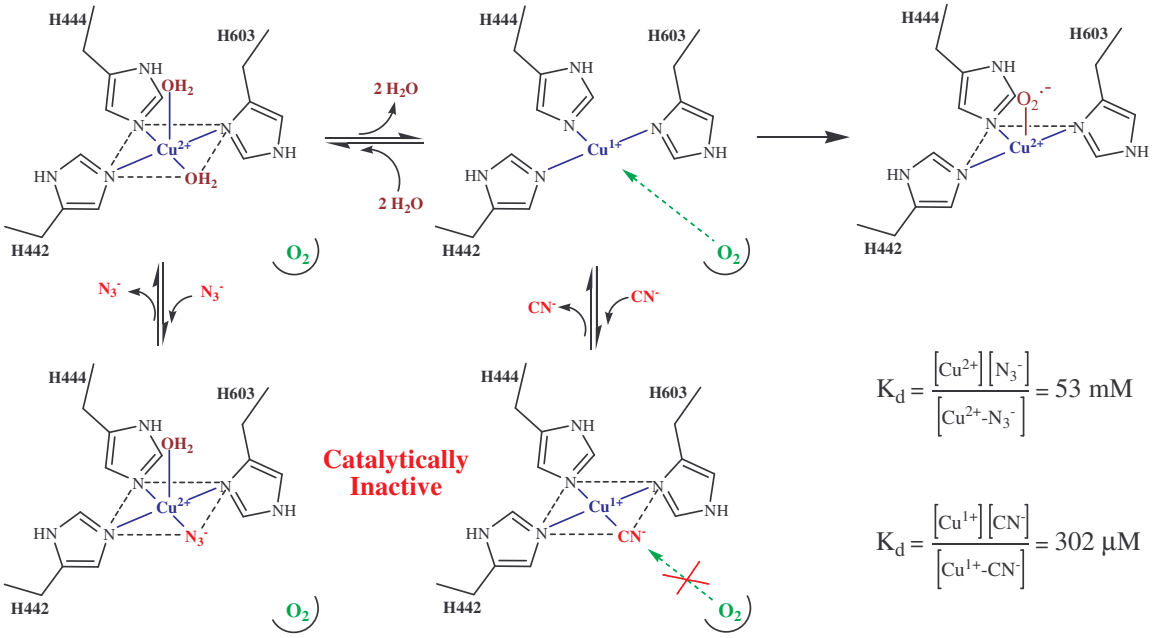

Figure 52: Azide and cyanide coordination during the oxidative half-reaction of PSAO. Top, left species represents Cu(II) coordination at the TPQ_{AMQ} stage and top, middle species represents Cu(I) coordination at the TPQ_{SQ} stage.

INTRAMOLECULAR ELECTRON TRANSFER RATE BETWEEN ACTIVE-SITE COPPER AND TPQ IN *Arthrobacter globiformis* AMINE OXIDASE

Introduction

The previous two chapters discussed the effects of the monodentate ligands cyanide and azide on amine oxidation and O_2 reduction, respectively, in PSAO [98,179]. The results of these studies provide strong, albeit indirect evidence, that the TPQ_{SQ}-Cu(I) moiety is a catalytically viable intermediate for this enzyme. Despite the conclusions for PSAO, the role of copper in O_2 reduction for other amine oxidase enzymes still needs to be explored. Significant variations exist in the behavior of these enzymes with substrate analogs, mechanism-based inhibitors, and monodentate copper ligands. All of these differences have been thoroughly addressed in previous chapters. One of the major themes born out of the studies presented in this thesis is that general mechanistic conclusions for all CuAOs cannot be drawn from studies on one enzyme. Previous studies have examined the role of copper during the oxidative half-reaction in the CuAO from *Hansenula polymorpha*, and used these results to draw conclusions for the entire CuAO family. This approach can foster the spread of improper and faulty conclusions in the literature, for which considerable implications exist regarding the role of copper in oxygen chemistry. In light of this, the role of copper in the oxidative half-reaction needs to be examined in several CuAOs before any ultimate conclusions can be made. The

final chapter of this thesis explores the catalytic viability of the TPQ_{SQ}-Cu(I) species in the enzyme AGAO.

The experimental disparities among CuAOs concerning the role of copper in O_2 reduction have been discussed throughout this thesis (see chapter 1 for a detailed synopsis). Figure 53 details the most likely mechanisms, which differ with respect to O_2 being reduced to $O_2^{\bullet-}$ by Cu(I) (**B** → **D**) or TPQ_{AMQ} (**B2** → **D2**). Briefly, given our discovery that TPQ_{SQ}-Cu(I) existed in several substrate-reduced CuAOs [87], we initially suggested that the first electron reduction of O_2 occurred by direct reaction with Cu(I) (Figure 53, **C**), resulting in a Cu(II) bound superoxide species (**B** → **D**) [87,104,105].

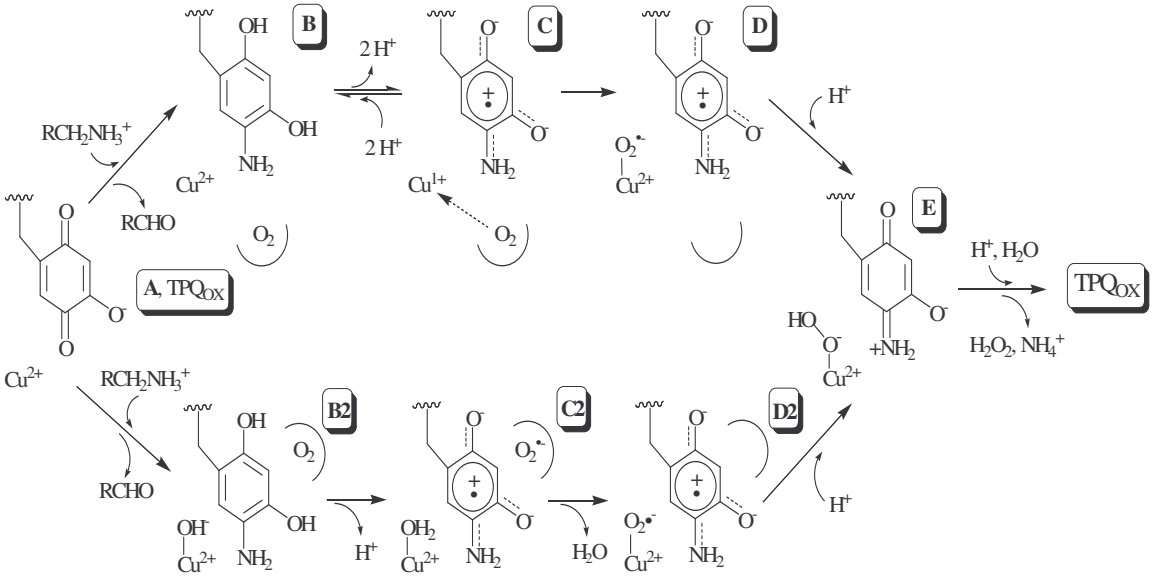

Figure 53: Proposed CuAO catalytic mechanism illustrating the two proposed pathways for cofactor reoxidation.

However, results obtained using the amine oxidase enzymes from *Hansenula polymorpha* (HPAO) and bovine plasma (BPAO) led to the proposal that Cu(II) reduction is not

essential for enzymatic reoxidation (Figure 53, **B2** → **D2**) [72,91,106,107]. These studies propose that O_2 binds in an off-metal hydrophobic pocket and the first electron transfer event to O_2 comes from TPQ_{AMQ} (**B2** → **C2**; rate limiting step). The superoxide anion that is generated then migrates to the Cu(II) center (**C2** → **D2**) [89].

Stopped-flow studies with the amine oxidase from the soil bacterium *Arthrobacter globiformis* (AGAO) showed that reduced enzyme reacted very rapidly with O_2 (< 1 ms), forming a Cu-peroxy species (λ_{max} = 410 nm). The results were consistent with either Cu(I)-TPQ_{SQ} or Cu(II)-TPQ_{AMQ} reacting rapidly with O_2, or with rapid $1e^-$ transfer from TPQ_{AMQ} to Cu(II). Formation of the charge delocalized, oxidized TPQ was proposed to be the rate-determining step in the oxidative half-reaction of wild-type AGAO [119]. In marked contrast to the reports on HPAO [106,107], Co(II) and Ni(II) reconstituted forms of AGAO had K_M values for amine and O_2 substrates that were essentially identical to the native enzyme; however, k_{cat} values for Co(II)- and Ni(II)-AGAO were ~ 1 sec^{-1}, as compared to 110 sec^{-1} for Cu(II)-AGAO [92].

Metal substituted AGAO and HPAO differ in two decisive aspects: (1) compared to other metal ion substituted enzymes, the Co(II) forms display the most activity in both AGAO and HPAO, but the levels of recovery vary substantially (2% in AGAO and 19% in HPAO, relative to the native copper enzymes); (2) the major cause of the reduced activity in HPAO was the large increase in K_M for O_2, whereas it is the substantial decrease in k_{cat} in AGAO, with $K_M(O_2)$ remaining unchanged. X-ray crystal structures of Co(II)- and Ni(II)-AGAO established that the hydrogen-bonding network in the active site was preserved [92]. Rate constants for reoxidation (measured by decay of the

TPQ_{AMQ}) were 0.18 s^{-1} and 0.17 s^{-1} for Co(II)-and Ni(II)-AGAO, respectively, *and conclusively show that the initial reaction with O_2 is substantially slower in the metal substituted enzymes*. The drastic reductions in k_{obs} rates in metal-substituted AGAOs were attributed to the reaction between TPQ_{AMQ} and O_2 becoming rate-limiting. Conversely, the rate acceleration of the initial reaction of substrate-reduced enzyme with O_2 observed for the native copper enzyme was regarded as consistent with the participation of a reactive Cu(I) semiquinone, but cannot be regarded as conclusive. Kishishita *et al*. present two possible reoxidation mechanisms [92]. In the first case, O_2 is proposed to receive an electron directly from the TPQ_{AMQ} species, with copper's role being restricted to the binding of superoxide and the facilitation of the second electron transfer event. The second case supports the catalytic viability of Cu(II) reduction, implicating the Cu(I)-TPQ_{SQ} species as an intermediate [92]. Taken collectively, it is clear that additional kinetics and spectroscopic experiments of structurally characterized CuAOs is necessary to clearly delineate the role of copper during the oxidative half-reaction.

Along these lines, we set out to measure the electron transfer rate between TPQ_{AMQ} and Cu(II) in AGAO. Given the significance of the unresolved mechanistic question regarding copper's potential redox role, and in light of the kinetic characteristics now clearly understood for wild-type and metal-substituted forms of AGAO [92], we felt that determining k_{ET} for this enzyme would help assess the possible role of the Cu(I)-TPQ_{SQ} moiety in AGAO catalysis. In order for the Cu(I)-TPQ_{SQ} species to be a viable intermediate, one critical criterion must be met: $k_{ET} \geq k_{cat}$. Previous studies from our laboratory have conclusively shown that this is the case for amine oxidase enzymes from

pea seedlings (PSAO) [104] and *Arthobacter* P1 (APAO) [105]. This chapter details the pH dependence of kinetic activity, the pH and temperature dependence of K_{eq}, and the temperature jump relaxation measurements for the internal redox equilibrium TPQ_{AMQ}-Cu(II) ⇋ TPQ_{SQ}-Cu(I) in AGAO.

Materials and Methods

Enzyme Purification and Isolation

AGAO was purified as described previously [163]. I am indebted to Kimberly M. Hilmer and Kristina Okonski for purifying the AGAO used in temperature jump experiments, and Gregory A. Juda, Wes Paul, and Laura Wheeler for purifying the AGAO used for EPR experiments.

Protein concentrations were calculated using the extinction coefficient at 280 nm as previously reported [138], and using an extinction coefficient of 2,500 $M^{-1}cm^{-1}$ for TPQ [89], and 1.4 titrateable TPQs per dimer [163]. All experiments for AGAO were carried out in 100 mM potassium phosphate buffer.

Kinetic Characterization

The rate of β-phenylethylamine oxidation by AGAO was monitored using a horseradish peroxidase (HRP)-ABTS (2,2'-azino-bis(3-ethyl)benzthiazoline-6-sulfonic acid) coupled assay. The peroxidase catalyzed reduction of H_2O_2 to H_2O is coupled to the $1e^-$ oxidation of ABTS, forming a metastable radical cation with λ_{max} of 414 nm, and

ε_{414} = 24,600 $M^{-1}cm^{-1}$ [141]. Kinetics were run at pH 6.2, 7.2, and 8.2 in 0.1 M potassium phosphate buffer at 30 °C.

Kinetic analysis was initiated by addition of substrate amine to enzyme and buffer mixtures under magnetic stirring. Initial rate data was then linearly fit. Assays were most often run in triplicate, sometimes duplicate, at a particular substrate concentration, and then averaged. Enzyme kinetic curves of velocity versus substrate concentration were fit with the Michaelis-Menten equation using Origin 7.0 software (Microcal, MA, USA). Error bars on each plot represent the standard deviation of the rate at a particular substrate concentration. Data were collected on a Hewlett-Packard 8453 diode-array spectrophotometer equipped with a thermostatted cell chamber connected to an Endocal RTE-5 circulating water bath.

Due to the fact that the ABTS radical cation becomes more unstable as pH increases [206], a control experiment was performed at pH 8.2 with known, varying amounts of H_2O_2 in order to estimate rate of degradation. Approximately 15% degradation occurred within 2 minutes. In order to completely minimize the effects of radical cation decay at pH 8.2 during kinetic measurements, the linear rate of data acquisition time was limited to the first 10 seconds of the assay. Furthermore, an ε_{414} of the radical was obtained at this pH for comparative purposes, and was calculated to be ~ 27300 $M^{-1}cm^{-1}$.

Spectroscopic Characterization

Samples were made anaerobic by purging with Ar gas passed through a vanadium bubbler, HCO_3, H_2O setup [180] for 3 hours. A catalase (~300 units), glucose (3.4 M),

glucose oxidase (6 mg/ml) solution [135] was added to the temperature jump protein samples to ensure that anaerobic conditions were maintained throughout experimentation. Protein samples were respectively reduced with ~ 5 fold excess (over active sites) benzylamine or β-phenylethylamine at either pH 6.2, 7.2, or 8.2. UV and visible absorption data at various temperature and pH values were acquired on a Cary 6000i UV/vis/NIR spectrophotometer (Varian, Australia) connected to a Cary dual cell Peltier accessory.

Temperature jumps of ~ 1.8 °C in a 5-mm cell were performed between 30 – 32 °C as described previously [104,105]. Protein samples were 40 μM in concentration. The change in light intensity at 468 nm was analyzed and data from 9 jumps were averaged for each kinetic trace, allowing time for temperature equilibration between jumps. For a control experiment, three temperature jumps on oxidized AGAO were performed, and no relaxation process was detected. Data were initially fit using an On-Line Systems (Athens, GA) kinetics package. For comparative purposes, kinetic traces were fit with a first order exponential equation using Origin 7.0 software (Microcal, MA, USA), yielding k_{obs} rates which were in good agreement with those generated with the On-Line Systems program.

Room temperature (24.2 – 26.2 °C) EPR spectra of AGAO at pH 6.2, 7.2, and 8.2 were collected on a Bruker EMX, X-band spectrometer. All spectra were obtained using a quartz flat cell (Wilmad, NJ). Oxidized and substrate reduced samples at a single pH value were run immediately following one another. Anaerobic AGAO was reduced with benzylamine and transferred to the flat cell in an anaerobic glove bag and the flat cell was

then appropriately sealed. A buffer spectrum was collected in the flat cell at the identical conditions of the respective enzyme samples and subsequently subtracted from each spectrum. Protein concentrations ranged between 190 – 250 μM, and benzylamine concentrations ranged from 2.1 – 3.0 mM, which corresponds to roughly a 5 fold excess of substrate amine over active site concentration. Experimental conditions were: frequency, 9.746 GHz (pH 6.2 and 7.2) and 9.783 GHz (pH 8.2); power, 6.35 mW (pH 6.2 and 7.2) and 10.06 mW (pH 8.2); modulation amplitude, 18 G. Peak areas obtained from the integration of the first hyperfine features in oxidized and substrate-reduced samples obtained under identical conditions were compared to determine the amount of Cu(II) reduction, as previously described [87,207].

In order to calculate k_{ET} values from K_{eq} (~ 25 °C) and k_{obs} (~ 30 °C) measurements, K_{eq} values for the TPQ_{AMQ}-Cu(II) ⇋ TPQ_{SQ}-Cu(I) equilibrium had to be determined at the same respective temperatures that were used to determine k_{obs}. The measured K_{eq} values were used to calculate ε_{468} for the semiquinone moiety at each pH value, assuming that ε_{468} was independent of temperature. The values obtained were 3600 $M^{-1}cm^{-1}$ at pH 6.2, 4500 $M^{-1}cm^{-1}$ at pH 7.2, and 4700 $M^{-1}cm^{-1}$ at pH 8.2. This allowed for the creation of van't Hoff plots at each pH value (data not shown; see [208]), which enabled the calculation of K_{eq} at the exact temperatures used in the temperature jump experiments.

Results

pH Effects on Kinetic Activity

As shown in Figure 54, β-phenylethylamine oxidation displays typical Michaelis-Menten behavior at pH 6.2 and pH 7.2. The K_M for β-phenylethylamine at these two pH values is unchanged, although k_{cat} is decreased at the more acidic pH (Table 9). Oxidation of β-phenylethylamine at pH 8.2 shows simple substrate inhibition (Figure 54), whereby an inactive, ternary enzyme-substrate-substrate complex forms [209]. The K_M value is seen to increase slightly, and the projected k_{cat} value is within error of that observed at pH 7.2 (Table 9). The data are in good agreement with the initial pH activity profile published with AGAO [142].

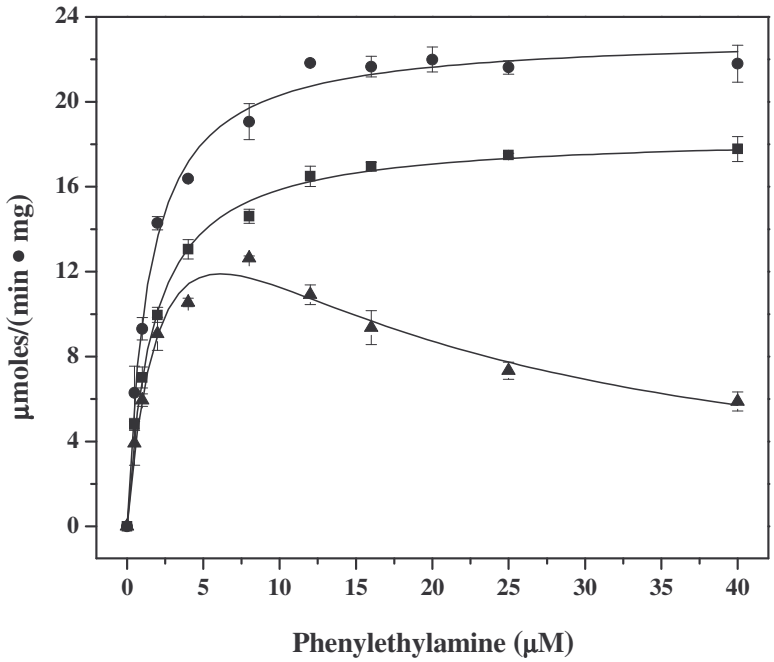

Figure 54: AGAO catalytic activity at pH 6.2 (■), 7.2 (●), and 8.2 (▲). Data at pH 6.2 and 7.2 were fit with the Michaelis-Menten equation, while pH 8.2 data were fit with a model of simple substrate inhibition [209] using Origin 7.0 software (Microcal, MA, USA).

Table 9: AGAO Kinetic Parameters for β-Phenylethylamine

pH	Temperature	K_M (μM)	k_{cat} (s^{-1})
6.2[a]	30 °C	1.6 ± 0.1	43 ± 1
7.2[a]	30 °C	1.4 ± 0.1	55 ± 1
8.2[b]	30 °C	2.6 ± 0.6	52 ± 7

[a] Kinetic constants obtained from the Michaelis-Menten equation. [b] Kinetic constants obtained from a model of simple substrate inhibition [209], thus accounting for the larger error associated with these values.

Temperature and pH Effects on the TPQ_{AMQ}-Cu(II) ⇋ TPQ_{SQ}-Cu(I) Internal Redox Equilibrium

Anaerobically reduced CuAOs are characterized by an internal electron-transfer equilibrium between the TPQ_{AMQ}-Cu(II) and the TPQ_{SQ}-Cu(I) moieties, with the magnitude of K_{eq} dependent upon enzyme source [87]. TPQ_{SQ} displays a unique absorbance spectrum with λ_{max} values at ~ 360, 440, and 470 nm [87,92,104,105,210], while TPQ_{AMQ} has a λ_{max} ~ 310 nm, with a featureless absorbance spectrum in the visible region [91,92,97,105]. Consequently, effects of temperature and pH can be readily determined by monitoring changes in the characteristic electronic spectrum of the TPQ_{SQ}.

Temperature effects on the redox equilibrium have been well documented, with higher temperatures favoring the TPQ_{SQ} moiety [104,105,210]. The same effect was observed for AGAO, as temperature was increased from 25 °C to 37 °C (Figure 55). In terms of pH, Figure 56 clearly shows that the spectral features of the TPQ_{SQ} moiety

become more intense as pH becomes more basic, indicating that the equilibrium shifts to the right under these conditions (Figure 53, **B** ⇋ **C**). However, this does not appear to be the case for either ECAO or LSAO, which show maximum TPQ_{SQ} formation near pH 7, with the equilibrium shifting to TPQ_{AMQ} at acidic and alkaline pH values [121,211]. The active site structural or chemical basis for these differences is unclear at this time.

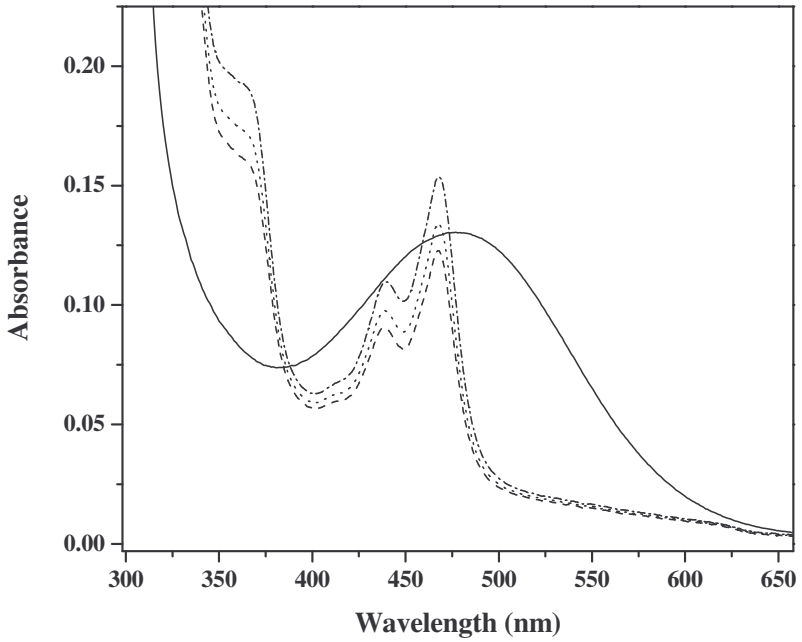

Figure 55: Temperature effects on the TPQ_{AMQ}-Cu(II) ⇋ TPQ_{SQ}-Cu(I) equilibrium in AGAO. Oxidized AGAO, (—); reduced AGAO, 25 °C (– –), 30 °C (····), and 37 °C (–·–). Spectra were recorded at pH 7.2 at a protein concentration of 50 μM.

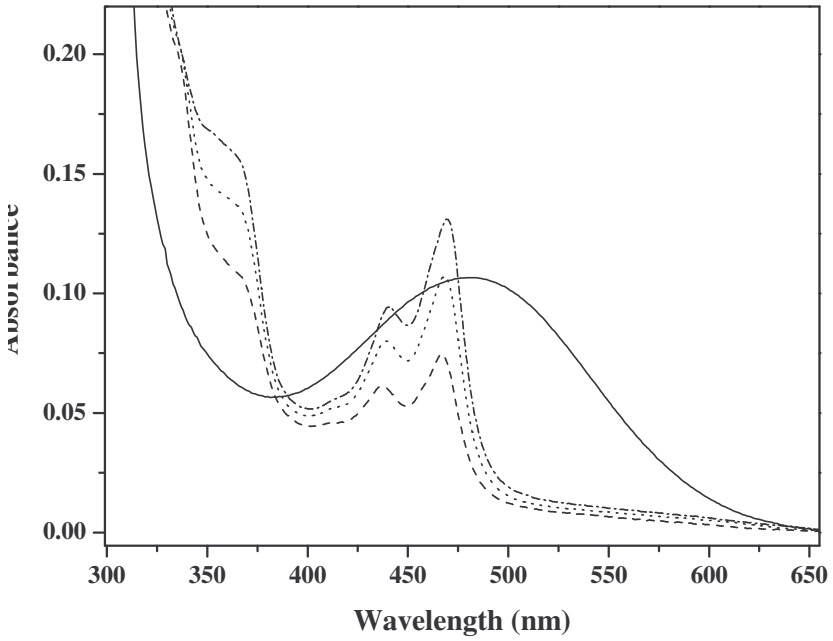

Figure 56: pH effects on the TPQ_{AMQ}-Cu(II) ⇋ TPQ_{SQ}-Cu(I) equilibrium in AGAO. Oxidized AGAO, pH 7.2 (—); reduced AGAO, pH 6.2 (- - -), pH 7.2 (·····), and pH 8.2 (-·-·-). Spectra were recorded at 30 °C at a protein concentration of 41 μM.

pH Effects on k_{obs} and K_{eq}

As mentioned previously, in order for the TPQ_{SQ}-Cu(I) species to be considered a catalytically viable intermediate, the electron transfer rate (k_{ET}) between TPQ_{AMQ} and Cu(II) must be greater than or equal to k_{cat}. In order to calculate k_{ET} and make this comparison, two additional experiments are needed. The first determines k_{obs} through temperature jump measurements, while the second determines K_{eq} through EPR experiments. Figures 57 and 58 illustrate the increase in the amount of TPQ_{SQ} following temperature jump experiments, as measured through a decrease in transmitted light intensity at 468 nm, as a function of pH. Collectively, the fits to the relaxation data were all accurately described by a single-exponential equation. Within experimental error, no difference in k_{obs} was observed between the nature of the amine substrate (benzylamine

or β-phenylethylamine) used to reduce the enzyme, or between rates obtained at pH 6.2 and 7.2 (Table 10). However, a significant reduction in k_{obs} occurs at pH 8.2. This is readily apparent by inspection of the temperature jump traces shown in Figures 57 (pH 7.2) and 58 (pH 8.2). The pH dependence of k_{obs} contrasts with our previous observations with APAO, which conclusively showed that k_{obs} was independent of *both* the pH and the nature of the amine used to reduce the enzyme [105].

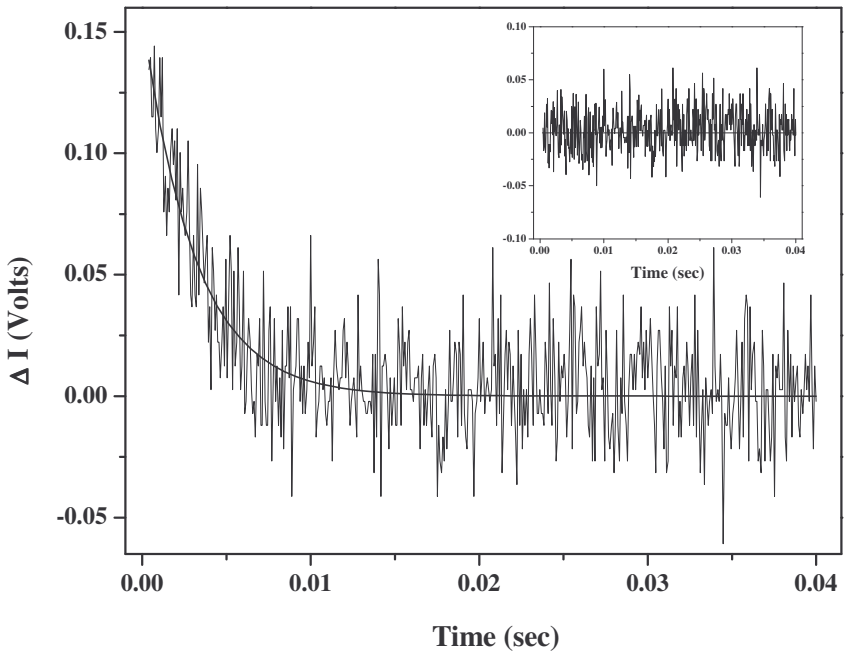

Figure 57: Relaxation behavior of β-phenylethylamine reduced AGAO at pH 7.2 following a 1.8 °C temperature jump. The change in intensity (ΔI) relates to transmittance, therefore a decrease in intensity corresponds to an absorbance increase. Inset shows the residuals associated with the single exponential fit.

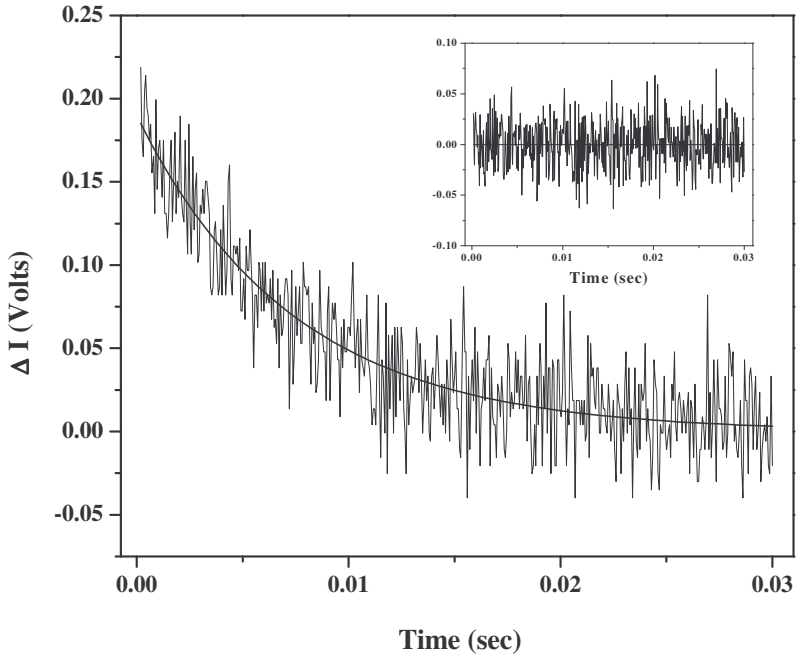

Figure 58: Relaxation behavior of β-phenylethylamine reduced AGAO at pH 8.2 following a 1.8 °C temperature jump. The change in intensity (ΔI) relates to transmittance, therefore a decrease in intensity corresponds to an absorbance increase. Inset shows the residuals associated with the single exponential fit.

Table 10: Kinetic Parameters for the Internal Redox Equilibrium TPQ_{AMQ}-Cu(II) ⇋ TPQ_{SQ}-Cu(I) in AGAO

pH	Substrate	k_{obs} (s^{-1})	K_{eq} [e]	k_{ET} (s^{-1}) [f]
6.2	PEA	310 ± 27 [a]	0.58	114 ± 14
7.2	PEA	325 ± 21 [b]	0.81	145 ± 13
7.2	BNZ	358 ± 24 [c]	0.77	156 ± 15
8.2	PEA	136 ± 5 [d]	0.96	67 ± 4

[a] Data collected at 30.5 °C. [b] Data collected at 32 °C. [c] Data collected at 30.7 °C. [d] Data collected at 30 °C. [e] Respective values for K_{eq} correspond to the temperatures reported for k_{obs}, as calculated from van't Hoff plots (see text), using 1.4 TPQs/dimer [163]. [f] The reported k_{ET} error values assume that the error in k_1 and k_{-1} is equally shared.

The amount of Cu(II) reduction in substrate reduced AGAO at various pH values was determined through integration of the first hyperfine feature in the EPR spectrum (data not shown), as based on the demonstration that the area of the Cu(II) $M_I = -3/2$ hyperfine line in the first derivative EPR spectrum is proportional to the intensity of the entire Cu(II) signal [87,207]. Spectra were obtained under identical conditions for oxidized and substrate reduced AGAO at pH 6.2, 7.2, and 8.2 (Figure 59), respectively. Careful comparisons of the peak area for the reduced sample to the peak area for the fully oxidized sample (Origin 7.0 software; Microcal, MA, USA) yielded K_{eq} values for the TPQ_{AMQ}-Cu(II) $\leftrightharpoons$ TPQ_{SQ}-Cu(I) equilibrium at the various pH values tested. K_{eq} for the redox equilibrium in AGAO, calculated from quantifying the EPR signals, steadily increases as pH becomes more basic (Table 10), as expected from the spectroscopic data shown in Figure 56. For comparative purposes, double integration of the complete Cu(II) signal in oxidized and substrate reduced spectra was performed (Origin 7.0 software, data not shown). Following the mathematical subtraction of the sharp g ~ 2 signal attributed to the TPQ_{SQ} radical [87], calculation of K_{eq} from the areas of oxidized and substrate reduced spectra provided reasonable agreement with the values obtained from single integration of the first hyperfine feature.

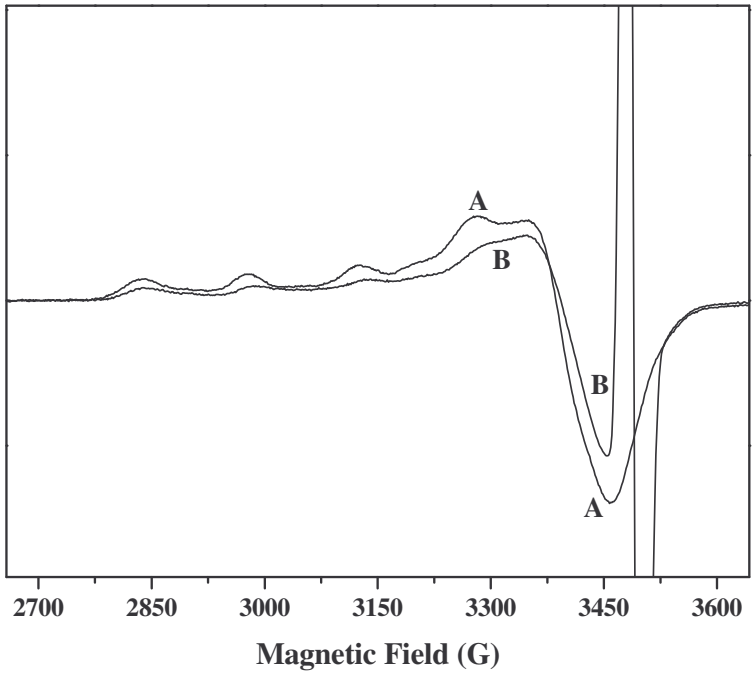

Figure 59: Room temperature EPR spectra of oxidized (A) and substrate reduced (B) AGAO at pH 8.2.

Calculation of the Forward Electron-Transfer Rate Constant

For reversible, first order reactions, k_{obs} is the sum of the forward and reverse rate constants. Therefore, in the case of the internal redox equilibrium TPQ_{AMQ}-Cu(II) ⇋ TPQ_{SQ}-Cu(I), the forward rate constant k_1 is equivalent to k_{ET}, and k_{obs} can be expressed as $k_{ET} + k_{-1}$. Likewise, K_{eq} for this equilibrium can be expressed as k_{ET}/k_{-1}. Combining this information yields k_{ET} values for the electron transfer from TPQ_{AMQ} to Cu(II), as shown in Table 10. The electron transfer rate is seen to be, within the limits of experimental uncertainty, equivalent at pH 6.2 and 7.2, while the rate at pH 8.2 is calculated to be about half of that observed for pH 6.2 and 7.2. Despite this observation, k_{ET} exceeds k_{cat} at each pH value (Tables 9 and 10). Interestingly, these results clearly

show that while formation of the TPQ_{SQ}-Cu(I) moiety is favored at basic pH (Figure 56 and Table 10), the electron transfer rate from TPQ_{AMQ} to Cu(II) is reduced.

Discussion

As discussed in detail above, the principal unresolved question regarding the mechanism(s) of CuAOs is the role of copper in enzyme reoxidation. Figure 53 details the most likely mechanisms, which differ with respect to O_2 being reduced to $O_2^{\bullet-}$ by Cu(I) (**B** $\rightarrow$ **D**) or TPQ_{AMQ} (**B2** $\rightarrow$ **D2**). In order for the former mechanism to be considered viable, it must be shown that k_{ET} between TPQ_{AMQ} and Cu(II) is sufficiently rapid to place the TPQ_{SQ}-Cu(I) moiety on pathway ($k_{ET} \geq k_{cat}$). Previously, our laboratory showed that k_{ET} was $\approx 20{,}000\ s^{-1}$ in PSAO [104] and $\approx 60 - 75\ s^{-1}$ in APAO [105]. While substantially different from one another, k_{ET} was significantly faster than k_{cat} for the preferred amine substrates of these enzymes, indicating that the TPQ_{SQ}-Cu(I) moiety may be a catalytic intermediate in each case. Given the detailed kinetic characterization of wild-type and metal-substituted forms of AGAO [92,119], this enzyme is an attractive candidate for measurement of the $TPQ_{AMQ} \rightarrow$ Cu(II) electron transfer rate. At the time of writing, this work has been submitted for publication in the journal *Biochemistry* [212].

The results presented herein establish that k_{ET} is greater than k_{cat} at all three pH values tested (Tables 9 and 10), thereby permitting TPQ_{SQ}-Cu(I) to be a viable catalytic intermediate during enzymatic reoxidation in AGAO. The data indicate that k_{ET} is

approximately equivalent at pH 6.2 and 7.2, being ≈ 2 – 2.5 times k_{cat} for these respective pH values [212]. At pH 8.2, however, k_{ET} decreases by a factor of two, becoming comparable to k_{cat}. This result is intriguing in light of the observation that the TPQ_{AMQ}-Cu(II) ⇋ TPQ_{SQ}-Cu(I) equilibrium shifts to the right at basic pH (Figure 56). Thus, the increase in K_{eq} for the aminoquinol ⇋ semiquinone equilibrium under basic conditions, is not sufficient to offset the decrease in k_{obs}. This result reflects a reduction in either k_{ET}, k_{-1}, or both. The reverse rate constant k_{-1} was found to be ≈ 200 s^{-1} at both pH 6.2 and 7.2, but decreased to ≈ 69 s^{-1} at pH 8.2. Thus, both forward and reverse rate constants are affected at pH 8.2 [212].

More generally, k_{ET} for reduced AGAO and APAO are quite similar, but dramatically slower than the rate in PSAO [104,105]. Comparison of EXAFS data for several oxidized and reduced CuAOs provided evidence that the Cu(I) centers in CuAOs are three-coordinate with N,O donor ligands [182]. EXAFS analysis suggested that either one of the histidine ligands was lost, or that the disorder of the Cu(I)-His bond lengths increases significantly upon Cu(II) reduction. The coordination environment of Cu(I) is then expected to be composed of three histidine imidazoles or two histidine imidazoles and a water molecule. Yet, for two imidazole simulations, PSAO is the only enzyme that does not show an increase in the disorder among the Cu(I)-His bond lengths [182]. It may be coincidental that PSAO also displays the fastest k_{ET} value, or these data may indicate that disorder among the remaining Cu(I)-His ligands in certain CuAOs influences the reorganizational energy and k_{ET} [212].

Potential Significance of the Decreased k_{ET} at pH 8.2

It is worth considering the origin of the decrease in k_{ET} at pH 8.2, especially since no such decrease was observed in APAO [105]. The observation that both the forward and reverse rate constants are slowed at basic pH may indicate that electron transfer to Cu(II) is coupled to proton transfer (Figure 53, **B** ⇋ **C**). Measuring k_{obs} in D_2O would directly test this hypothesis. The slower k_{ET} determined for pH 8.2 may also implicate a role of metal bound hydroxide during reoxidation, given the pK_a value of 7.5 for Cu(II)-H_2O [213]. Therefore, the Cu(II)-OH^- species would be more prevalent at basic pH (Figure 53, **B2**), and hydroxide would be expected to stabilize Cu(II). Moreover, as this alternate mechanism invokes electron transfer to O_2 concomitant with proton transfer from the resulting TPQ_{SQ} to Cu(II)-OH^- (**B2** → **C2**), it is also possible that the protonation state of the cofactor semiquinone contributes to the decrease in k_{ET}. The reduced electron transfer rate could also arise from an alternate ionization state of the amine functionality in TPQ_{AMQ}, which may be more thermodynamically stable. However, this does not seem likely, as available evidence suggests that only the neutral form of TPQ_{AMQ} is formed upon substrate reduction in AGAO [92], BPAO [91,214], ECAO [115], and HPAO [97]. Based on the pK_as of neutral aromatic primary amines (neutral aniline ⇆ amide anion; $pK_a \approx 35$), ionization of this group in the aminoquinol is unlikely to have any influence in the pH range we are examining.

Is TPQ_{SQ}-Cu(I) on Pathway During Enzymatic Reoxidation?

As mentioned above, the calculated rates at pH 6.2, 7.2, and 8.2 for electron transfer from TPQ_{AMQ} to Cu(II) meet the first required criterion ($k_{ET} \geq k_{cat}$) for TPQ_{SQ}-Cu(I) being a viable intermediate during reoxidation in AGAO. This result should be considered in the context of previous studies of the reoxidation of wild-type AGAO [119]. $k_{obs} \geq 1000\ s^{-1}$ for the reaction of substrate reduced, wild-type AGAO with O_2, as measured by the rapid loss in the absorbance features of the TPQ_{SQ} moiety [119]. Following the disappearance of these features, slower rates of 51 – 64 s^{-1} (from 0 – 20 ms) were measured at both pH 7.3 and 8.2 for formation of the protonated (340 nm) and deprotonated (310 nm) iminoquinone forms of TPQ, respectively. Hirota *et al.* concluded that *both* the TPQ_{AMQ} and TPQ_{SQ} moieties reacted rapidly with O_2 (despite the observation that significant absorbance in the 300 – 400 nm region remains), with the concomitant formation of a Cu-peroxy species and the protonated and deprotonated forms of TPQ_{IMQ}. Formation of the oxidized, charge delocalized TPQ_{OX} was determined to be the rate limiting step of the oxidative half-reaction. In stark contrast to the copper containing enzyme, k_{obs} values for the reaction of substrate reduced Co(II)- and Ni(II)-AGAO were measured to be $\approx 0.18\ s^{-1}$ and $0.17\ s^{-1}$, respectively [92]. These drastically reduced rates in metal-substituted AGAOs were attributed to the reaction between TPQ_{AMQ} and O_2 becoming rate-limiting.

Although the stopped-flow and temperature jump experiments were conducted at different temperatures (5 °C and 30 °C, respectively), it is possible that some of the kinetic events observed by Hirota *et al*. [119] represent electron transfer from TPQ_{AMQ} to

Cu(II). From the van't Hoff plots at pH 7.2 and 8.2 (data not shown), K_{eq} at 5 °C is calculated to be 0.3 and 0.32, respectively. If we assume that k_{obs} is relatively temperature independent over this range, then our measured values for k_{obs} at pH 7.2 and 8.2 (Table 10), yield rates of 75 ± 6 s^{-1} and 33 ± 2 s^{-1} for k_{ET} at these respective pH values. The reported rates of formation at 310 and 340 nm [119] for pH 8.2 (51 ± 7 and 52 ± 7 s^{-1}) and pH 7.3 (64 ± 7 and 58 ± 7 s^{-1}) are in reasonable agreement with these k_{ET} values. Therefore, provided the assumption that k_{obs} is relatively temperature independent is approximately correct, the findings reported by Hirota *et al*. may be consistent with the participation of the TPQ_{SQ}-Cu(I) intermediate in catalysis. For this to be the case, the initial rapid disappearance of the TPQ_{SQ} absorbance features that occurs upon addition of O_2 must represent the reaction of the available TPQ_{SQ}-Cu(I) with O_2, forming TPQ_{IMQ} and the Cu(II) bound hydroperoxide (Figure 53, **C** → **E**). This is a reasonable presumption supported by the extremely rapid binding of dioxygen to certain Cu(I) model complexes [103], and the precedence for the reactivity of three-coordinate Cu(I) sites with dioxygen in copper-containing metalloproteins [100-102]. The slower rates of formation at 310 and 340 nm over the next 20 ms would then represent electron transfer from the remaining TPQ_{AMQ} to Cu(II) at rates ≈ k_{ET}, followed by the rapid reaction of O_2 with Cu(I).

The slight disparity between k_{obs} and estimated k_{ET} values for pH 7.2 and 8.2 at 5 °C may simply reflect the difficulty in determining rate constants from very subtle absorbance changes in the 300 – 350 nm region, especially in light of the fact that TPQ_{SQ}, TPQ_{AMQ}, and TPQ_{IMQ} all absorb in this region, and reactions involving these species may

occur throughout the time course of the oxidative half-reaction. More specifically, both the TPQ_{AMQ} and the deprotonated TPQ_{IMQ} absorb at 310 nm [119]. Thus, if Cu(I) is indeed involved in O_2 reduction, then the process of obtaining accurate rate constants for the decay and formation of these two species becomes very difficult, as the absorbance changes at 310 nm would be expected to be minimal until most of the TPQ_{AMQ} is converted to TPQ_{SQ}. Regardless, it is very clear that a more careful analysis of the absorbance changes accompanying reaction of reduced AGAO with O_2, coupled with the determination of the temperature dependence of k_{obs}, are required in order to confirm or rule out the role of TPQ_{SQ}-Cu(I) in the reduction of O_2 in this enzyme.

Conclusions

As summarized herein, the kinetics of O_2 reduction in AGAO vary dramatically depending upon the type of metal present in the active site. In the case of Co(II)- and Ni(II)-substituted AGAO enzymes, the initial reaction between TPQ_{AMQ} and O_2 becomes rate-limiting. For wild-type, Cu(II) containing AGAO, the initial reaction between O_2 and the substrate reduced enzyme occurs quite rapidly with a $k_{obs} \geq 1000\ s^{-1}$. The determination of k_{ET} at three pH values, coupled with the published kinetics data for reoxidation in AGAO, has allowed us to directly probe the role of the TPQ_{SQ}-Cu(I) moiety in the reduction of O_2. The results presented above conclusively show that k_{ET} is greater than k_{cat} at the three pH values tested, thereby permitting TPQ_{SQ}-Cu(I) to be a viable catalytic intermediate during enzymatic reoxidation in AGAO [212]. Yet, in light of the measured $k_{obs} \geq 1000\ s^{-1}$ for reaction of substrate reduced AGAO with O_2, no

definitive conclusions concerning the role of Cu(I) in O_2 reduction can be drawn at this time. Thus, it is apparent that this issue will only be resolved by more thorough analysis of the spectral changes (including k_{obs} values for the intermediates) that occur upon reaction of reduced AGAO with O_2 at variable pH and temperature values.

CONCLUDING REMARKS

Mammalian copper-containing amine oxidases have long been referred to as semicarbazide-sensitive amine oxidases (SSAOs), due to their sensitivity to the small molecule inhibitor semicarbazide. SSAOs have been detected or described in numerous mammalian tissues and are implicated in the pharmacology and toxicology of biogenic and exogenous amines and their oxidation products. Levels of SSAO activity are upregulated in several pathological states including diabetes mellitus, congestive heart failure, hepatic cirrhosis, uremia, and Alzheimer's disease. Given this observation, the recent identification that a protein mediating L-selectin dependent lymphocyte adhesion to endothelial cells (human vascular adhesion protein; HVAP) was a copper amine oxidase led to an increased interest in CuAOs. Furthermore, we were the first group to overexpress and purify a recombinant mammalian copper-containing amine oxidase (human diamine oxidase; rhDAO). Kinetics studies revealed that histamine, 1-methylhistamine, and agmatine were the preferred substrates for rhDAO, suggesting that hDAO could play a central role in the metabolism of these biogenic amines. These results collectively speak towards the fact that the role of CuAOs in higher organisms is just beginning to be understood.

Further justification for structural and mechanistic studies of CuAOs comes from the observation that numerous inhibitors of amine oxidases and amine metabolism have shown promising antileukemic, antitumor, antifungal, and antiprotozoal activity. For example, pentamidine and related diamidines are front line therapeutics in the treatment of *Pneumocystis carinii* pneumonia (PCP) and other types of fungal or protozoal infections in

immunosuppressed patients, such as those with AIDS. We recently discovered that pentamidine is an extremely potent inhibitor of both rhDAO and HVAP, thus supporting the hypothesis that some of the deleterious side effects of pentamidine administration may be related to its inhibition of these copper amine oxidases. There is increasing interest in the discovery of potent and selective SSAO inhibitors as anti-inflammatory agents. Numerous CuAO inhibitors have been screened against SSAO, but are either unselective or relatively weak. Together with the results presented in this thesis, the data provide a foundation for correlating the interactions of amine oxidases with inhibitors to therapeutic applications and toxicities. Results from such studies may ultimately facilitate the design of more effective and less toxic anti-bacterial, anti-fungal, and anti-protozoal pharmaceuticals.

Along these lines, one of the major goals of my thesis project was to understand and define the molecular factors which control substrate specificity and recognition, as well as inhibitor selectivity, among CuAOs. The work described in Chapter 2 of this thesis was the first published study to demonstrate practical selectivity of mechanism-based inhibitors among CuAOs from bacterial, yeast, plant, and mammalian sources. Furthermore, this was the first evidence that illustrated how distinctions among the active sites were directly responsible for differentiating the chemical interactions between the inhibitors and selected enzymes. These studies indicated that factors such as the dimensions and shape of the substrate channel and binding pocket play a key role in determining inhibitor selectivity. Moreover, the remarkable distinctions between the CuAOs from bacterial (AGAO) and plant (PSAO) sources with the 4-(aryloxy)-2-butynamine family of compounds provided the first example of a substrate analog that

could serve as a potent mechanism-based inhibitor for one CuAO and a substrate for another. This difference was discovered to arise from the presence of a hydrophobic pocket in the active site channel of AGAO, initially discovered from computer modeling studies. The degree of inhibitor potency was dictated by the extent of van der Waals' interactions formed among respective substituent groups on each compound with the amino acids comprising the hydrophobic pocket. Residues in the hydrophobic pocket were subsequently shown to interact with other inhibitor compounds structurally unrelated to the 4-(aryloxy)-2-butynamine family. Thus, it is apparent that the hydrophobic binding pocket in AGAO plays a crucial role in determining inhibitor potency for a broad range of amine analogs.

In a broader context, the development of selective copper amine oxidase inhibitors takes on an elevated sense of importance due to the fact that certain compounds can react with both CuAOs and monoamine oxidase (MAO) enzymes. Evidence for this cross-reactivity was given in Chapter 3, where the antidepressant MAO-directed inhibitor tranylcypromine (TCP, drug name Parnate) was shown to inhibit CuAOs from both bacterial (AGAO) and mammalian (BPAO and EPAO) sources. Inhibition of AGAO by TCP resulted in formation of a substrate Schiff base complex. Bound TCP could only be removed upon chemical displacement with either a substrate or a substrate analog, suggesting that TCP has very high affinity for the active site of AGAO. Structural characterization of the AGAO-TCP complex through X-ray crystallography revealed that the phenyl substituent of TCP was cradled by the aforementioned hydrophobic pocket. It is quite possible that the phenyl group forms π–stacking interactions with some of the

aromatic residues in this pocket, which confers the observed stability to the AGAO-TCP Schiff base complex.

The ability of certain compounds like TCP to react with both CuAOs and MAOs arises because both these enzyme families carry out the same overall chemistry ($RCH_2NH_2 \rightarrow RCHO$). These enzymes do, however, utilize very distinct mechanisms to carry out the oxidation of primary amines. Accordingly, amine compounds capable of effecting a transamination-specific irreversible modification should inactivate only the quinone-dependent copper amine oxidase family. This realization led to the development of a class of compounds (3-aryl-3-pyrrolines) which were discovered to selectively inhibit only the copper containing amine oxidase family, while acting as pure substrates for MAO-B. Resonance Raman analysis on the inactivated enzyme suggested a mechanism involving conversion of the quinone cofactor to a reduced pyrrolylated form that cannot be reoxidized to the starting quinone. Cofactor pyrrolylation corresponds to mechanism-based inactivation with a partition ratio of zero, and as such, 3-aryl-3-pyrrolines should be considered as excellent probes for evaluating the physiological functions of these enzymes and may even have therapeutic potential as selective inhibitors. Discovering potent and selective mechanism-based inhibitors of human CuAOs continues to be a focus of study in our laboratory. In collaboration with Dr. Lawrence Sayre (CWRU), we continue to screen potential inhibitors, including several new diamine analogs, against rhDAO and HVAP.

In addition to the studies aimed at understanding the molecular factors governing substrate and inhibitor binding in CuAOs, a goal of this thesis was to probe the role of copper during enzymatic reoxidation. Two mechanistic proposals have been put forth,

whereby O_2 is reduced to $O_2^{\bullet-}$ by either Cu(I) or TPQ_{AMQ}. In order to investigate these two possibilities, binding and inhibition studies of PSAO were performed with the monodentate copper ligands cyanide and azide. PSAO was chosen for such studies because it is the most catalytically efficient copper amine oxidase enzyme, and it forms the most semiquinone under standard conditions (i.e. this enzyme has the largest K_{eq} value for the TPQ_{AMQ}-Cu(II) ⇆ TPQ_{SQ}-Cu(I) equilibrium). Chapter 4 provides the first direct evidence for cyanohydrin derivatization of the TPQ cofactor in PSAO and presents a general mechanism of CuAO inhibition by cyanide. Stabilization of Cu(I) by CN^- appears to act as the dominant mode of inhibition, presumably acting in direct competition with O_2 for binding to Cu(I), thereby preventing reoxidation of the reduced enzyme. Support for this conclusion comes from the greater similarity between the K_i value for inhibition of substrate amine and the K_d for the Cu(I)-CN^- complex, relative to the K_d for the Cu(II)-CN^- complex, thereby suggesting that the Cu(I)-TPQ_{SQ} moiety is likely a catalytically competent intermediate in PSAO.

The results of inhibition by azide (Chapter 5) are substantially more complex, and must be interpreted in terms of azide's affects upon each half-reaction (amine oxidation and O_2 reduction). PSAO is an excellent enzyme system for cleanly observing azide's effects on O_2 reduction, as the calculated K_i value for the noncompetitive inhibition of substrate amine oxidation by azide is ≈ 5 times greater than the affinity of azide for Cu(II) in either the oxidized, resting state or the substrate-reduced TPQ_{AMQ} state. This means that the reaction velocity ($V_{max(i)} \approx V_{max}$) during the reductive half-reaction is largely unaltered at the concentrations of azide used in the oxidative half-reaction experiments. The results clearly show that azide exhibits competitive inhibition against

substrate O_2 in PSAO with a K_i value that is in very good agreement with the measured K_d value for the Cu(II)-N_3^- complex. These results are most consistent with the mechanistic proposal placing Cu(I) on-pathway in PSAO, with the Cu(I)-TPQ_{SQ} moiety principally involved in O_2 activation.

In PPLO, inhibition by azide shifts from noncompetitive at low azide levels to mixed-type at higher concentrations. In this case, K_i values for reductive and oxidative half-reactions are equivalent and are lower than measured K_d values for the Cu(II)-N_3^- complexes. Given this observation, it is quite possible that substantial inhibition in the rate of the reductive half-reaction is induced at the concentrations of azide used for the oxidative half-reaction experiments, thereby abolishing the kinetic independence of each half-reaction. Therefore, the noncompetitive mode of inhibition observed for azide in the oxidative half-reaction in PPLO may simply represent the relatively low K_i value for azide inhibition of the reductive half-reaction. This same argument can be made for AGAO. In this context, the shift in the inhibition to mixed-type at higher azide levels for PPLO can best be understood as the onset of partial competitive inhibition between azide and O_2 for copper. The reasonable agreement between αK_i and the K_d for the Cu(II)-N_3^- complex in substrate reduced PPLO supports this hypothesis. At this time, the data do not permit us to distinguish between two possibilities: (1) inhibition by azide with respect to O_2 is intrinsically competitive in CuAOs, but that this effect cannot always be deconvolved experimentally from the effects of azide on the reductive half-reaction; or (2) CuAOs differ in some steps of their reoxidation mechanisms.

Although it is likely that copper plays a redox role during catalysis in all CuAOs, especially in light of the similarities in their resting state active site structures, definitive

proof of whether initial electron transfer to dioxygen originates from TPQ_{AMQ} or Cu(I) in PPLO and AGAO remains elusive. Taken collectively, the above results certainly indicate that additional kinetics and spectroscopic experiments are needed to clearly delineate the role of copper during the oxidative half-reaction. Along these lines, the electron transfer rate (k_{ET}) between TPQ_{AMQ} and Cu(II) was determined in AGAO. In order for the Cu(I)-TPQ_{SQ} species to be considered a catalytic intermediate, k_{ET} must be greater than or equal to k_{cat}. The results presented in Chapter 6 establish that k_{ET} is greater than k_{cat} at all three pH values tested, thereby permitting TPQ_{SQ}-Cu(I) to be a viable catalytic intermediate during enzymatic reoxidation in AGAO. A more definitive conclusion can not be made at this time, however, because k_{ET} is ~ 10 times slower than the measured $k_{obs} \geq 1000\ s^{-1}$ for reaction of substrate reduced AGAO with O_2. If k_{obs} for the intramolecular electron transfer event is relatively independent of temperature over the range studied (5 °C to 30 °C), then these rate differences can be reconciled. The faster rate would implicate reaction of available TPQ_{SQ}-Cu(I) with O_2, while the slower rate would then represent electron transfer from the remaining TPQ_{AMQ} to Cu(II) at rates $\approx k_{ET}$, followed by the rapid reaction of O_2 with Cu(I). It is clear that the role of TPQ_{SQ}-Cu(I) in the reduction of O_2 in AGAO will only be resolved by a more careful determination of the rate constants associated with the reaction of reduced AGAO with O_2, coupled with the determination of the temperature dependence of k_{obs}. These experiments will be conducted in the near future.

As illustrated by the results with cyanide and azide, the intriguing differences in the magnitude of k_{ET}, the dependence of k_{ET} on pH, and the strikingly different outcomes of metal ion substitution in AGAO and HPAO, it is now evident that general mechanistic

conclusions cannot be drawn based on the results from a single CuAO. This is especially true when considering that the fundamental difference between the proposed reoxidation mechanisms described previously could very well be a subtle one concerning the timing between the initial electron transfer event and the migration of O_2 from its initial binding site to the copper ion. Thorough kinetic, spectroscopic, and structural studies are needed, including further structural analysis of metal-substituted enzymes, in order to confidently determine the reoxidation mechanism. Furthermore, the issues become more complex if CuAOs from different sources indeed utilize distinct mechanisms of cofactor reoxidation.

REFERENCES CITED

1. Binda C, Mattevi A, Edmondson DE (2002) J. Biol. Chem. 277:23973-23976.

2. Knowles PF, Dooley DM (1994) Amine Oxidases, In: *Metal Ions in Biological Systems*. Singel, H and Singel, A (eds) Marcel Dekker, Inc., New York, pp 361-403.

3. McIntire WS, Hartmann C (1993) Copper-Containing Amine Oxidases, In: *Principles and Applications of Quinoproteins.* Davidson, VL (eds) Marcel Dekker, Inc., New York, pp 97-171.

4. Janes SM, Klinman JP (1995) Methods Enzymol. 258:20-34.

5. Tanizawa K (1995) J. Biochem. (Tokyo) 118:671-678.

6. Okeley NM, van der Donk WA (2000) Chemistry and Biology 7:159-171.

7. Ostermeier C, Harrenga A, Ermler U, Michel H (1997) Proc. Natl. Acad. Sci. USA 94:10547-10553.

8. Das TK, Pecoraro C, Tomson FL, Gennis RB, Rousseau DL (1998) Biochemistry 37:14471-14476.

9. Janes SM, Mu D, Wemmer D, Smith AJ, Kaur S, Maltby D, Burlingame AL, Klinman JP (1990) Science 248:981-987.

10. Cai D, Klinman JP (1994) J. Biol. Chem. 269:32039-32042.

11. Matsuzaki R, Fukui T, Sato H, Ozaki Y, Tanizawa K (1994) FEBS Lett 351:360-364.

12. Ruggiero CE, Smith JA, Tanizawa K, Dooley DM (1997) Biochemistry 36:1953-1959.

13. Bollinger JA, Brown DE, Dooley DM (2005) Biochemistry 44:11708-11714.

14. Pearson AR, Jones LH, Higgins LA, Ashcroft AE, Wilmot CM, Davidson VL (2003) Biochemistry 42:3224-3230.

15. Satoh A, Kim JK, Miyahara I, Devreese B, Vandenberghe I, Hacisalihoglu A, Okajima T, Kuroda S, Adachi O, Duine JA, Van Beeumen J, Tanizawa K, Hirotsu K (2002) J. Biol. Chem. 277:2830-2834

16. Wilce MCJ, Dooley DM, Freeman HC, Guss JM, Matsunami H, McIntire WS, Ruggiero CE, Tanizawa K, Yamaguchi H (1997) Biochemistry 36:16116-16133.

17. Carter SR, McGuirl MA, Brown DE, Dooley DM (1994) J. Inorg. Biochem. 56:127-141.

18. Elmore B, Bollinger JA, Dooley DM (2002) J. Biol. Inorg. Chem. 7:565-579.

19. McGuirl MA, McCahon CD, McKeown KA, Dooley DM (1994) Plant Physiol. 106:1205-1211.

20. Green J, Haywood GW, Large PJ (1983) Biochem. J. 211:481-493.

21. Elmore, B0 (2002) *Characterization of Recombinant Human Kidney Diamine Oxidase and Equine Plasma Amine Oxidase*, PhD Thesis, Montana State University, Bozeman, MT.

22. Kumagai, H ,Yamada, H (2000) *Structure and Function of Amine Oxidases*. Mondovi, B (eds) CRC Press, Boca Raton, Florida.

23. Bachrach, U, Heimer, Y (1985) *The Physiology of Polyamines*. Bachrach, U, Heimer, Y (eds) CRC Press, Boca Raton, Florida.

24. Seiler N (2000) Neurochem. Res. 25:471-490.

25. Nilsson BO (1999) Inflamm. Res. 48:509-515.

26. Grillo MA, Colombatto S (2004) Amino Acids 26:345-351.

27. Satriano J (2004) Amino Acids 26:321-329.

28. Satriano J, Schwartz D, Ishizuka S, Lortie MJ, Thomson SC, Gabbai F, Kelly CJ, Blantz RC (2001) J. Cell Physiol. 188:313-320.

29. Rangachari PK (1992) Am. J. Physiol. 262:G1-13.

30. Gupta MK, Gupta P, Rezai F (2001) Clin. Cardiol. 24:258-259.

31. Schmidt WU, Sattler J, Hesterberg R, Röher HD, Zoedler T, Sitter H, Lorenz W (1990) Agents Actions 30:267-270.

32. Tang AW (2003) Am. Fam. Physician 68:1325-1332.

33. Vermillion DL, Huizinga JD, Riddell RH, Collins SM (1993) Gastroenterology 104:1692-1699.

34. Haddock RC, Mack P, Fogerty FJ, Baenziger NL (1987) J. Biol. Chem. 262:10220-10228.

35. High A, Prior T, Bell RA, Rangachari PK (1999) J. Pharmacol. Exp. Ther. 288:490-501.

36. Girard B, Otterness DM, Wood TC, Honchel R, Wieben ED, Weinshilboum RM (1994) Mol. Pharmacol. 45:461-468.

37. Gitomer WL, Tipton KF (1986) Biochem. J. 233:669-676.

38. Tahara A, Nishibori M, Ohtsuka A, Sawada K, Sakiyama J, Saeki K (2000) J. Histochem. Cytochem. 48:943-954.

39. Lyles GA (1996) Int. J. Biochem. Cell Biol. 28:259-274.

40. Langford SD, Trent MB, Balakumaran A, Boor PJ (1999) Toxicol. Appl. Pharmacol. 155:237-244.

41. Matyus P, Dajka-Halasz B, Foldi A, Haider N, Barlocco D, Magyar K (2004) Curr. Med. Chem. 11:1285-1298.

42. O'Sullivan J, Unzeta M, Healy J, O'Sullivan MI, Davey G, Tipton KF (2004) Neurotoxicology 25:303-315.

43. Yu PH, Wright S, Fan EH, Lun ZR, Gubisne-Harberle D (2003) Biochim. Biophys. Acta 1647:193-199.

44. Kamsler A, Segal M (2004) Mol. Neurobiol. 29:167-178.

45. Enrique-Tarancon G, Castan I, Morin N, Marti L, Abella A, Camps M, Casamitjana R, Palacin M, Testar X, Degerman E, Carpene C, Zorzano A (2000) Biochem. J. 350(Pt 1):171-180.

46. Jaakkola K, Jalkanen S, Kaunismaki K, Vanttinen E, Saukko P, Alanen K, Kallajoki M, Voipio-Pulkki LM, Salmi M (2000) J. Am. Coll. Cardiol. 36:122-129.

47. Jaakkola K, Nikula T, Holopainen R, Vahasilta T, Matikainen MT, Laukkanen ML, Huupponen R, Halkola L, Nieminen L, Hiltunen J, Parviainen S, Clark MR, Knuuti J, Savunen T, Kaapa P, Voipio-Pulkki LM, Jalkanen S (2000) Am. J. Pathol. 157:463-471.

48. Stolen CM, Marttila-Ichihara F, Koskinen K, Yegutkin GG, Turja R, Bono P, Skurnik M, Hanninen A, Jalkanen S, Salmi M (2005) Immunity 22:105-115.

49. Kumar V, Dooley DM, Freeman HC, Guss JM, Harvey I, McGuirl MA, Wilce MCJ, Zubak VM (1996) Structure 4:943-955.

50. Li RB, Klinman JP, Mathews FS (1998) Structure 6:293-307.

51. Parsons MR, Convery MA, Wilmot CM, Yadav KDS, Blakeley V, Corner AS, Phillips SEV, McPherson MJ, Knowles PF (1995) Structure 3:1171-1184.

52. Duff AP, Cohen AE, Ellis PJ, Kuchar J.A., Langley DB, Shepard EM, Dooley DM, Freeman HC, Guss JM (2003) Biochemistry 42:15148-15157.

53. Lunelli M, Di Paolo ML, Biadene M, Calderone V, Battistutta R, Scarpa M, Rigo A, Zanotti G (2005) J. Mol. Biol. 346:991-1004.

54. Jakobsson E, Nilsson J, Ogg D, Kleywegt GJ (2005) Acta Crystallogr. D Biol. Crystallogr. 61:1550-1562.

55. Dove JE, Klinman JP (2001) Adv. Protein Chem. 58:141-174.

56. Dawkes HC, Phillips SEV (2001) Curr. Opin. Struct. Biol. 11:666-673.

57. Halcrow, M, Phillips, S, Knowles, P (2000) Amine Oxidases and Galactose Oxidase, In: *Subcellular Biochemistry*. Holzenburg, A. and Scrutton, N (eds) Kluwer Academic/Plenum Publishers, New York, pp 183-231.

58. Wilmot CM, Murray JM, Alton G, Parsons MR, Convery MA, Blakeley V, Corner AS, Palcic MM, Knowles PF, McPherson MJ, Phillips SEV (1997) Biochemistry 36:1608-1620.

59. Chen ZW, Schwartz B, Williams NK, Li RB, Klinman JP, Mathews FS (2000) Biochemistry 39:9709-9717.

60. Salminen TA, Smith DJ, Jalkanen S, Johnson MS (1998) Protein Eng. 11:1195-1204.

61. Zhang XP, McIntire WS (1996) Gene 179:279-286.

62. Shepard EM, Smith J, Elmore B, Kuchar J.A., Sayre LM, Dooley DM (2002) Eur. J. Biochem. 269:3645-3658.

63. O'Connell KM, Langley DB, Shepard EM, Duff AP, Jeon HB, Sun G, Freeman HC, Guss JM, Sayre LM, Dooley DM (2004) Biochemistry 43:10965-10978.

64. Di Paolo ML, Stevanato R, Corazza A, Vianello F, Lunelli L, Scarpa M, Rigo A (2003) Biochem. J. 371:549-556.

65. Equi AM, Brown AM, Cooper A, Ner SK, Watson AB, Robins DJ (1991) Tetrahedron 47:507-518.

66. Brown DE, McGuirl MA, Dooley DM, Janes SM, Mu D, Klinman JP (1991) J. Biol. Chem. 266:4049-4051.

67. Ruggiero CE, Dooley DM (1999) Biochemistry 38:2892-2898.

68. Okajima T, Kishishita S, Chiu YC, Murakawa T, Kim M, Yamaguchi H, Hirota S, Kuroda S, Tanizawa K (2005) Biochemistry 44:12041-12048.

69. Kim M, Okajima T, Kishishita S, Yoshimura M, Kawamori A, Tanizawa K, Yamaguchi H (2002) Nature Struct. Biol. 9:591-596.

70. Dove JE, Schwartz B, Williams NK, Klinman JP (2000) Biochemistry 39:3690-3698.

71. Schwartz B, Dove JE, Klinman JP (2000) Biochemistry 39:3699-3707.

72. Schwartz B, Olgin AK, Klinman JP (2001) Biochemistry 40:2954-2963.

73. Brazeau BJ, Johnson BJ, Wilmot CM (2004) Arch Biochem Biophys 428:22-31.

74. DuBois JL, Klinman JP (2005) Biochemistry 44:11381-11388.

75. Prabhakar R, Siegbahn PEM (2004) J. Amer. Chem. Soc. 126:3996-4006.

76. Matsunami H, Okajima T, Hirota S, Yamaguchi H, Hori H, Kuroda S, Tanizawa K (2004) Biochemistry 43:2178-2187.

77. Nakamura N, Matsuzaki R, Choi YH, Tanizawa K, Sanders-Loehr J (1996) J. Biol. Chem. 271:4718-4724.

78. Samuels NM, Klinman JP (2005) Biochemistry 44:14308-14317.

79. Kryatov SV, Mohanraj BS, Tarasov VV, Kryatova OP, Rybak-Akimova EV, Nuthakki B, Rusling JF, Staples RJ, Nazarenko AY (2002) Inorg. Chem. 41:923-930.

80. Choi YH, Matsuzaki R, Suzuki S, Tanizawa K (1996) J. Biol. Chem. 271:22598-22603

81. Schwartz B, Green EL, Sanders-Loehr J, Klinman JP (1998) Biochemistry 37:16591-16600.

82. Hevel JM, Mills SA, Klinman JP (1999) Biochemistry 38:3683-3693.

83. Murray JM, Kurtis CR, Tambyrajah W, Saysell CG, Wilmot CM, Parsons MR, Phillips SEV, Knowles PF, McPherson MJ (2001) Biochemistry 40:12808-12818.

84. Shepard EM, Juda GA, Dooley DM (2006) NIH Grant GM 27659.

85. Kuchar J, Dooley D (2001) J. Inorg. Biochem. 83:193-204.

86. Murray JM, Saysell CG, Wilmot CM, Tambyrajah WS, Jaeger J, Knowles PF, Phillips SEV, McPherson MJ (1999) Biochemistry 38:8217-8227.

87. Dooley DM, McGuirl MA, Brown DE, Turowski PN, McIntire WS, Knowles PF (1991) Nature 349:262-264.

88. Mure M, Klinman JP (1995) J. Am. Chem. Soc. 117:8707-8718.

89. Mure M, Mills SA, Klinman JP (2002) Biochemistry 41:9269-9278.

90. Medda R, Padiglia A, Pedersen JZ, Rotilio G, Finazzi-Agro A, Floris G (1995) Biochemistry 34:16375-16381.

91. Su QJ, Klinman JP (1998) Biochemistry 37:12513-12525.

92. Kishishita S, Okajima T, Kim M, Yamaguchi H, Hirota S, Suzuki S, Kuroda S, Tanizawa K, Mure M (2003) J. Amer. Chem. Soc. 125:1041-1055.

93. Mills SA, Klinman JP (2000) J. Amer. Chem. Soc. 122:9897-9904.

94. Coleman AA, Scaman CH, Kang YJ, Palcic MM (1991) J. Biol. Chem. 266:6795-6800.

95. Alton G, Taher TH, Beever RJ, Palcic MM (1995) Arch. Biochem. Biophys. 316:353-361.

96. Uchida M, Ohtani A, Kohyama N, Okajima T, Tanizawa K, Yamamoto Y (2003) Biosci. Biotechnol. Biochem. 67:2664-2667.

97. Plastino J, Green EL, Sanders-Loehr J, Klinman JP (1999) Biochemistry 38:8204-8216.

98. Shepard EM, Juda GA, Ling KQ, Sayre LM, Dooley DM (2004) J. Biol. Inorg. Chem. 9:256-268.

99. Ho, RYN, Liebman, JF, Valentine, JS (1995) Overview of the Energetics and Reactivity of Oxygen, In: *Active Oxygen in Chemistry.* Foote, C. S., Valentine, JS, Greenberg, A, and Liebman, JF (eds) Blackie Academic and Professional, New York, pp 1-23.

100. Murthy, NN, Karlin, KD (1995) *Mechanistic Bioinorganic Chemistry*, (Thorp, H.H., Pecoraro, V.L., Eds.), pp 165-193, Amer. Chem. Soc., Washington D.C.

101. Karlin, KD, Tyekl'ar, Z (1993) *Bioinorganic Chemistry of Copper*. Chapman & Hall, New York.

102. Whittaker JW (1999) Essays Biochem 34:155-172.

103. Fry HC, Scaltrito DV, Karlin KD, Meyer GJ (2003) J. Am. Chem. Soc. 125:11866-11871.

104. Turowski PN, McGuirl MA, Dooley DM (1993) J. Biol. Chem. 268:17680-17682.

105. Dooley DM, Brown DE (1996) J. Biol. Inorg. Chem. 1:205-209.

106. Mills SA, Klinman JP (2000) J. Amer. Chem. Soc. 122:9897-9904.

107. Mills SA, Goto Y, Su QJ, Plastino J, Klinman JP (2002) Biochemistry 41:10577-10584.

108. Prabhakar R, Siegbahn PEM, Minaev BF (2003) Biochim. Biophys. Acta Protein Struct. Mol. Enzymol. 1647:173-178.

109. Goto Y, Klinman JP (2002) Biochemistry 41:13637-13643.

110. Dooley DM, Golnik KC (1983) J. Biol. Chem. 258:4245-4248.

111. McGuirl MA, Brown DE, Dooley DM (1997) J. Biol. Inorg. Chem. 2:336-343.

112. Dooley DM, Cote CE (1985) Inorg. Chem. 24:3996-4000.

113. Barker R, Boden N, Cayley G, Charleton SC, Henson R, Holmes MC, Kelly ID, Knowles PF (1979) Biochem. J. 177:289-302.

114. Olsson B, Olsson J, Pettersson G (1978) Eur. J. Biochem. 87:1-8.

115. Wilmot CM, Hajdu J, McPherson MJ, Knowles PF, Phillips SEV (1999) Science 286:1724-1728.

116. Duff AP, Trambaiolo DM, Cohen AE, Ellis PJ, Juda GA, Shepard EM, Langley DB, Dooley DM, Freeman HC, Guss JM (2004) J. Mol. Biol. 344:599-607.

117. Schoenborn BP, Watson HC, Kendrew JC (1965) Nature 207:28-30.

118. Cai DY, Williams NK, Klinman JP (1997) J. Biol. Chem. 272:19277-19281.

119. Hirota S, Iwamoto T, Kishishita S, Okajima T, Yamauchi O, Tanizawa K (2001) Biochemistry 40:15789-15796.

120. Padiglia A, Medda R, Pedersen JZ, Finazzi-Agro A, Lorrai A, Murgia B, Floris G (1999) J Biol. Inorg. Chem. 4:608-613.

121. Medda R, Padiglia A, Bellelli A, Sarti P, Santanche S, Agro AF, Floris G (1998) Biochem. J. 332:431-437.

122. Abeles RH, Maycock AL (1976) Accounts Chem. Res. 8:313-319.

123. Neumann R, Hevey R, Abeles RH (1975) J. Biol. Chem. 250:6362-6367.

124. Hevey RC, Babson J, Maycock AL, Abeles RH (1973) J. Am. Chem. Soc. 95:6125-6127.

125. Tang SS, Simpson DE, Kagan HM (1984) J. Biol. Chem. 259:975-979.

126. Kumagai H, Uchida H, Yamada H (1979) J. Biol. Chem. 254:10913-10919.

127. Medda R, Padiglia A, Pedersen JZ, Agro AF, Rotilio G, Floris G (1997) Biochemistry 36:2595-2602.

128. Pino R, Lyles GA (1997) Vopr. Med. Khim. 43:537-547.

129. Blicharski JR, Lyles GA (1990) J. Neural. Transm. Suppl. 32:337-339.

130. Yu PH, Davis BA, Boulton AA (1995) Adv. Exp. Med. Biol. 363:17-23.

131. Abeles RH, Tashjian AH, Jr. (1975) Biochem. Pharmacol. 24:307-308.

132. Boulton AA, Davis BA, Durden DA, Dyck LE, Juorio AV, Li XM, Paterson IA, Yu PH (1997) Drug Dev. Res. 42:150-156.

133. Sayre LM, Wang F, Lee Y, Huang H, Greenaway FT, He Z, Lightning A, Kagan HM (1994) *Biochemistry of Vitamin B6 and PQQ*. Birkhauser Verlag, Basel, Switzerland.

134. Jeon HB (2000) *Synthesis and Evaluation of Mechanism-Based Inhibitors of Copper-Containing Amine Oxidases*, PhD Thesis, Case Western Reserve University, Cleveland, OH.

135. Janes SM, Klinman JP (1991) Biochemistry 30:4599-4605.

136. Dove JE, Smith AJ, Kuchar J, Brown DE, Dooley DM, Klinman JP (1996) FEBS Lett. 398:231-234.

137. Moenne-Loccoz P, Nakamura N, Steinebach V, Duine JA, Mure M, Klinman JP, Sanders-Loehr J (1995) Biochemistry 34:7020-7026.

138. Tanizawa K, Matsuzaki R, Shimizu E, Yorifuji T, Fukui T (1994) Biochem. Biophys. Res. Commun. 199:1096-1102.

139. Suzuki S, Sakurai T, Nakahara A, Manabe T, Okuyama T (1983) Biochemistry 22:1630-1635.

140. Tabor CW, Tabor H, Rosenthal SM (1954) J. Biol. Chem. 208:645-661.

141. Szutowicz A, Kobes RD, Orsulak PJ (1984) Anal. Biochem. 138:86-94.

142. Shimizu E, Ohta K, Takayama S, Kitagaki Y, Tanizawa K, Yorifuji T (1997) Biosci. Biotechnol. Biochem. 61:501-505.

143. Holt A, Sharman DF, Baker GB, Palcic MM (1997) Anal. Biochem. 244:384-392.

144. Fluckiger R, Paz MA, Gallop PM (1995) Methods Enzymol. 258:140-149.

145. Segel, IH (1975) *Enzyme Kinetics: Behavior and Analysis of Rapid Equilibrium and Steady-State Enzyme Systems*. John Wiley and Sons, New York, New York.

146. Silverman, R.B. (1988) *Mechanism-Based Enzyme Inactivation: Chemistry and Enzymology*. CRC Press, Inc, Boca Raton, Florida.

147. McGaughey G, Gagne M, Rappe A (1998) J. Biol. Chem. 273:15458-15463.

148. Tur SS, Lerch K (1988) FEBS Lett. 238:74-76.

149. Battersby AR, Staunton J, Klinman J, Summers MC (1979) FEBS Lett. 99:297-298.

150. Frebort I, Pec P, Luhova L, Matsushita K, Toyama H, Adachi O (1994) Eur. J. Biochem. 225:959-965.

151. Frebort I, Sebela M, Svendsen I, Hirota S, Endo M, Yamauchi O, Bellelli A, Lemr K, Pec P (2000) Eur. J. Biochem. 267:1423-1433.

152. Matsuzaki R, Tanizawa K (1998) Biochemistry 37:13947-13957.

153. Lee Y, Shepard EM, Smith J, Dooley DM, Sayre LM (2001) Biochemistry 40:822-829.

154. Contakes SM, Juda GA, Langley DB, Halpern-Manners NW, Duff AP, Dunn AR, Gray HB, Dooley DM, Guss JM, Freeman HC (2005) Proc. Natl. Acad. Sci. USA 102:13451-13456.

155. Youdim MB, Finberg JP (1991) Biochem. Pharmacol. 41:155-162.

156. Weber-Grandke H, Hahn G, Mutschler E, Mohrke W, Langguth P, Spahn-Langguth H (1993) Br. J. Clin. Pharmac. 36:363-365.

157. Mallinger AG, Himmelhoch JM, Thase ME, Edwards DJ, Knopf S (1990) J. Clin. Psychopharmacol. 10:176-183.

158. Paech C, Salach JI, Singer TP (1979) Suicide Inactivation of Monoamine Oxidase by trans-Phenylcyclopropylamine, In: *Monoamine Oxidase: Structure, Function, and Altered Functions*. Singer TP, Von Korff RW, Murphy DL (eds) Academic Press, New York.

159. Moises HW, Beckmann H (1981) J. Neural. Transm. 50:185-192.

160. Horn AS, Snyder SH (1972) J. Pharmacol. Exp. Ther. 180:523-530.

161. Roh JH, Suzuki H, Azakami H, Yamashita M, Murooka Y, Kumagai H (1994) Biosci. Biotechnol. Biochem. 58:1652-1656.

162. Wilmot CM, Saysell CG, Blessington A, Conn DA, Kurtis CR, McPherson MJ, Knowles PF, Phillips SE (2004) FEBS Lett. 576:301-305.

163. Juda GA, Bollinger JA, Dooley DM (2001) Protein Express. Purif. 22:455-461.

164. Saysell CG, Tambyrajah WS, Murray JM, Wilmot CM, Phillips SEV, McPherson MJ, Knowles PF (2002) Biochem. J. 365:809-816.

165. Lee Y, Ling KQ, Lu XL, Silverman RB, Shepard EM, Dooley DM, Sayre LM (2002) J. Amer. Chem. Soc. 124:12135-12143.

166. Lin-Vien D, Colthup N, Fateley W, Grasselli J (1991) *The Handbook of Infrared and Raman Characteristic Frequencies of Organic Molecules*. Academic Press, Boston.

167. Nakamura N, Moenne-Loccoz P, Tanizawa K, Mure M, Suzuki S, Klinman JP, Sanders-Loehr J (1997) Biochemistry 36:11479-11486.

168. Lord RC, Yu NT (1970) J. Mol. Biol. 50:509-524.

169. Hacisalihoglu A, Jongejan A, Jongejan JA, Duine J (2000) J. Mol. Catal. B: Enz. 11:81-88.

170. Coleman AA, Hindsgaul O, Palcic MM (1989) J. Biol. Chem. 264:19500-19505.

171. Fitzgerald DH, Tipton KF, Lyles GA (1998) J. Neural. Transm. Suppl. 52:259-264.

172. Fitzgerald DH, Tipton KF (2002) J. Neural. Transm. 109:251-265.

173. Lee YH, Huang H, Sayre LM (1996) J. Am. Chem. Soc. 118:7241-7242.

174. Shepard EM, Heggem H, Juda GA, Dooley DM (2003) Biochim. Biophys. Acta Protein Struct. Mol. Enzymol. 1647:252-259.

175. He Z, Zou Y, Greenaway FT (1995) Arch. Biochem. Biophys. 319:185-195.

176. Steinebach V, De Vries S, Duine JA (1996) J. Biol. Chem. 271:5580-5588.

177. Imanaga, Y (1989) Investigations on the Active Site of Glucose Dehydrogenase from *Pseudomonas fluorescens*, In: *PQQ and Quinoproteins*. Jongejan, JA, Duine JA (eds) Kluwer Academic Publishers, Boston, MA.

178. Finazzi-Agro A, Rinaldi A, Floris G, Rotilio G (1984) FEBS Lett. 176:378-380.

179. Juda GA, Shepard EM, Elmore B0, Dooley DM (2006) Biochemistry (submitted).

180. Meites L, Meites T (1948) Anal. Chem. 20:984-985.

181. Dooley DM, McGuirl MA, Peisach J, McCracken J (1987) FEBS Lett. 214:274-278.

182. Dooley DM, Scott RA, Knowles PF, Colangelo CM, McGuirl MA, Brown DE (1998) J. Am. Chem. Soc. 120:2599-2605.

183. Castellano FN, He Z, Greenaway FT (1993) Biochim. Biophys. Acta. Gen. Subj. 1157:162-166.

184. Green EL, Nakamura N, Dooley DM, Klinman JP, Sanders-Loehr J (2002) Biochemistry 41:687-696.

185. Dooley DM, Cote CE, McGuirl MA, Bates JL, Perkins JB, Moog RS, Singh I, Knowles PF, McIntire WS (1989) Copper-PQQ Interactions in Amine Oxidases, In: *PQQ and Quinoproteins*. Jongejan, JA, and Duine, JA (eds) Kluwer Academic Publishers Dordrecht, pp 307-316.

186. Dooley DM, McIntire WS, McGuirl MA, Cote CE, Bates JL (1990) J. Am. Chem. Soc. 112:2782-2789.

187. Agostinelli E, De Matteis G, Sinibaldi A, Mondovi B, Morpurgo L (1997) Biochem. J. 324:497-501.

188. De Matteis G, Agostinelli E, Mondovi B, Morpurgo L (1999) J. Biol. Inorg. Chem. 4:348-353.

189. Segel, IH (1976) *Biochemical Calculations 2nd Edition*. John Wiley & Sons, New York, NY.

190. Douglas, B, McDaniel, D, Alexander, J (1994) *Concepts and Models of Inorganic Chemistry 3rd Edition*, John Wiley and Sons, Inc., New York, NY.

191. Padiglia A, Medda R, Bellelli A, Agostinelli E, Morpurgo L, Mondovi B, Finazzi-Agrò A, Floris G (2001) Eur. J. Inorg. Chem. 1:35-42.

192. Lindstrom A, Olsson B, Pettersson G (1974) Eur. J. Biochem. 48:237-243.

193. Dooley DM, Cote CE, Golnik KC (1984) J. Mol. Catal. 23:243-253.

194. Kuchar J.A. (2001) *Cloning, Sequence Analysis, and Characterization of the "Lysyl Oxidase" from Pichia pastoris*, PhD. thesis, Montana State University, Bozeman, MT.

195. Ortiz de Montellano PR, David SK, Ator MA, Tew D (1988) Biochemistry 27:5470-5476.

196. Yamasaki EF, Swindell R, Reed DJ (1970) Biochemistry 9:1206-1210.

197. Dooley DM, McGuirl MA (1986) Inorg. Chim. Acta. 123:231-236.

198. Dooley DM, McGuirl MA, Cote CE, Knowles PF, Singh I, Spiller M, Brown RD, Koenig SH (1991) J. Amer. Chem. Soc. 113:754-761.

199. Oi S, Inamasu M, Yasunobu KT (1970) Biochemistry 9:3378-3383.

200. Nordlie, R (1982) Kinetic Examination of Enzyme Mechanisms Involving Branched Reaction Pathways-A Detailed Consideration of Multifunctional Glucose-6-phosphatase, In: *Methods and Enzymology*. Purich DL (ed), pp 319-323, Academic Press, New York.

201. Webb BC, Todhunter JA, Purich DL (1976) Arch. Biochem. Biophys. 173:282-292.

202. Cai DY, Dove J, Nakamura N, Sanders-Loehr J, Klinman JP (1997) Biochemistry 36:11472-11478.

203. Mure M, Brown DE, Saysell C, Rogers MS, Wilmot CM, Kurtis CR, McPherson MJ, Phillips SE, Knowles PF, Dooley DM (2005) Biochemistry 44:1568-1582.

204. Mure M, Kurtis CR, Brown DE, Rogers MS, Tambyrajah WS, Saysell C, Wilmot CM, Phillips SE, Knowles PF, Dooley DM, McPherson MJ (2005) Biochemistry 44:1583-1594.

205. Cleland WW (1963) Biochimica et Biophsica Acta 67:173-187.

206. McCoy-Messer J, Bateman RC (1993) BioTechniques 15:270-273.

207. Vanngard, T. (1967) *Magnetic Resonance in Biological Systems*. Ehrenberg A, Malmstrom BG, and Vanngard T (eds) pp 213-219, Pergamon, Oxford.

208. Dooley DM, McGuirl MA (1986) Inorg. Chem. 25:1261-1264.

209. Cleland, W. W. (1979) Substrate Inhibition, In *Enzyme Kinetics and Mechanism*. Purich DL (ed) pp 500-513, Academic Press, New York.

210. Medda R, Padiglia A, Bellelli A, Pedersen JZ, Agro AF, Floris G (1999) FEBS Lett. 453:1-5.

211. Steinebach V, De Vries S, Duine JA (1996) J. Biol. Chem. 271:5580-5588.

212. Shepard EM, Dooley DM (2006) Biochemistry (submitted).

213. Huheey, J. E. (1972) *Inorganic Chemistry, Principles of Structure and Reactivity*, Harper and Row, New York.

214. Hartmann C, Brzovic P, Klinman JP (1993) Biochemistry 32:2234-2241.